USAAMRDL-TR-75-8

IMPROVED ULTRASONIC FUEL MASS FLOWMETER FOR ARMY AIRCRAFT ENGINE DIAGNOSTICS

PANAMETRICS, INC.
221 Crescent Street
Waltham, Mass. 02154

June 1975

Final Report for Period March 1974 - December 1974

Prepared for

EUSTIS DIRECTORATE
U. S. ARMY AIR MOBILITY RESEARCH AND DEVELOPMENT LABORATORY
Fort Eustis, Va. 23604

EUSTIS DIRECTORATE POSITION STATEMENT

The Eustis Directorate of the U. S. Army Air Mobility Research and Development Laboratory is conducting a series of efforts directed at advancing the state of the art of aircraft engine sensors. These are in support of efforts associated with improving the capability of diagnosing the condition and determining the health of Army aircraft engines.

This contract was awarded to conduct work on solving the key technical problems identified as a result of the previous Contract DAAJ02-71-C-0061. Work included the design, fabrication, and laboratory testing of an improved ultrasonic mass fuel flowmeter.

The conclusions presented herein are generally agreed with by the Eustis Directorate.

The technical monitor of this contract was Mr. G. William Hogg, Military Operations Technology Division.

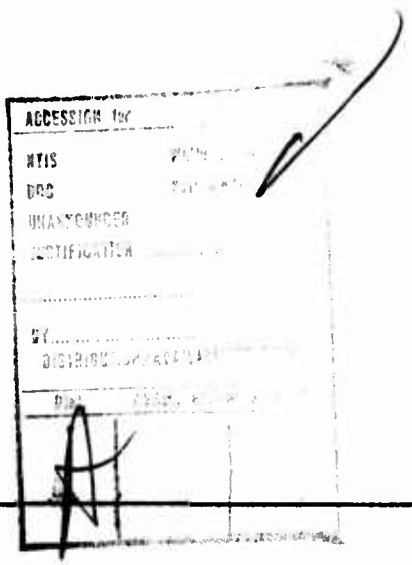

Unclassified

SECURITY CLASSIFICATION OF THIS PAGE (When Data Entered)

REPORT DOCUMENTATION PAGE

READ INSTRUCTIONS BEFORE COMPLETING FORM

1. REPORT NUMBER: USAAMRDL TR-75-8
2. GOVT ACCESSION NO.
3. RECIPIENT'S CATALOG NUMBER

4. TITLE (and Subtitle): IMPROVED ULTRASONIC FUEL MASS FLOWMETER FOR ARMY AIRCRAFT ENGINE DIAGNOSTICS.

5. TYPE OF REPORT & PERIOD COVERED: Final Technical Report. 22 Mar-21 Dec 74

6. PERFORMING ORG. REPORT NUMBER

7. AUTHOR(s): Norman E. Pedersen, Lawrence C. Lynnworth, James E. Bradshaw

8. CONTRACT OR GRANT NUMBER(s): DAAJ02-73-C-0054 NEW

9. PERFORMING ORGANIZATION NAME AND ADDRESS
Panametrics, Inc.
221 Crescent Street
Waltham, Massachusetts 02154

10. PROGRAM ELEMENT, PROJECT, TASK AREA & WORK UNIT NUMBERS: 1F163204DB38

11. CONTROLLING OFFICE NAME AND ADDRESS
Eustis Directorate, U. S. Army Air Mobility Research and Development Laboratory
Fort Eustis, Virginia 23604

12. REPORT DATE: June 75

13. NUMBER OF PAGES: 236

14. MONITORING AGENCY NAME & ADDRESS (if different from Controlling Office)

15. SECURITY CLASS. (of this report): Unclassified

15a. DECLASSIFICATION/DOWNGRADING SCHEDULE

16. DA-1-F-163204-DB-38

16. DISTRIBUTION STATEMENT (of this Report)

Approved for public release; distribution unlimited.

17. DISTRIBUTION STATEMENT (of the abstract entered in Block 20, if different from Report)

18. SUPPLEMENTARY NOTES

19. KEY WORDS (Continue on reverse side if necessary and identify by block number)

Acoustics, Area-Averaging Flowmeter, Densitometer, Flow Profile, Flow Velocimeter, Flowmeter, Fuel Flowmeter, Instrumentation, Mach Number, Mass Flowmeter, Ultrasonics

20. ABSTRACT (Continue on reverse side if necessary and identify by block number)

An advanced prototype ultrasonic flowmeter system was designed, fabricated, and tested at fuel flow rates from below 100 lb/hr up to 6000 lb/hr at temperatures from 50 to 115°F and in the Reynolds number range from below 1000 to above 30,000. In order to reduce errors due to flow profile to a small fraction of 1% of full scale, and to avoid the need for a profile-dependent "meter constant" despite operation over laminar, transitional and turbulent flow regimes, a rectangular flow channel was provided (cont'd)

DD FORM 1 JAN 73 1473 EDITION OF 1 NOV 65 IS OBSOLETE

Unclassified

SECURITY CLASSIFICATION OF THIS PAGE (When Data Entered)

403 420.

in which the flow was obliquely interrogated over its complete cross section by a square-enveloped ultrasonic beam. The cell included screens for minimizing eddies at the transducer ports, gradual circular to rectangular pipe transitions, flushing means, and a bleed port. Flow related parameters were measured by ~~means of a novel approach~~ utilizing a fully coherent electronic system which operated synchronously from a 5-MHz crystal controlled oscillator. The transmitted waveform was generated by means of synchronously gating the output of the 5-MHz oscillator for a 50-microsecond interval at a 2-kHz repetition rate. Upstream and downstream common-path transmissions were consecutive and spaced 250 microseconds apart. Independent measurements were made of the phase difference between the upstream and downstream 5-MHz spectral components of the received waveforms and the phase sum of the 2-kHz modulation components of these waveforms. These two independent measurements were combined to yield the Mach number v/c and v, where v = flow velocity and c = sound speed. High signal-to-noise ratio was achieved by means of narrowband receivers and fully coherent detection, thereby providing distinct advantages in precision and stability over conventional flowmetering techniques which utilize broadband pulses. One cell configuration contained an ultrasonic reflectometer which generated a pair of echoes. The echo amplitudes were processed to yield the fuel's characteristic impedance ρc, where ρ = density. The product of the v/c and ρc terms is ρv, which equals the mass flow rate $\dot{M}$. In a second cell, presently the preferred configuration, ρ was measured downstream of the velocimeter region in a serial branch by a standard capacitance-type densitometer. $\dot{M}$ then was determined as the ρv product. The flowmeter was programmed to perform such computations digitally. In six independent JP-4 calibration tests at 50, 75 and 100°F, and using the second cell and the corresponding formulation $\dot{M} = \rho v$, the maximum average deviation from linearity was 0.2% of full scale, while the mean of the average deviations was 0.13% of full scale. With respect to reproducibility, the maximum average deviation was 0.25% of full scale, while the mean of the average deviations was 0.2% of full scale. These test results demonstrated that the calibrated ρv system consisting of an ultrasonic flow velocimeter and a capacitance-type densitometer could measure $\dot{M}$ to within $\pm$ 1% of range for the fuels JP-4 and JP-5 and the conditions of interest. With appropriate modification, the system could be used to measure dynamic volumetric and mass flow rates. Response time, presently several seconds, could be reduced to the range 10 to 100 milliseconds.

PREFACE

The continuing encouragement of G. W. Hogg and B. Poteate of USAAMRDL is appreciated. Transducer fabrication at Panametrics was assisted by R. E. Fisher, J. H. Fowler, K. A. Fowler, D. R. Patch, J. D. Bennett and R. S. Seferian. Helpful discussions with Dr. E. H. Carnevale were conducted throughout the program. Flow cell fabrication was assisted by W. Dougherty of Dougherty Tool Company (electric discharge machining of rectilinear channels) and G. Iozzo of Braze-All (screen soldering). Dr. J. Pedersen assisted with the data reduction. The excellent cooperation of Avco-Lycoming personnel is sincerely appreciated, particularly J. Balcher, J. I. Black (now at J. I. Black and Associates, Consulting Engineers) and R. Hohenberg (now at Mechanical Technology, Inc.). The contributions of B. B. Chick and Dr. G. Peterson of Matec are also acknowledged, relative to the echo comparator instrument that they designed and fabricated. The cooperation of D. E. Stuart of Simmonds Precision, concerning their densitometer, is acknowledged. Dr. George Wallis of P. R. Mallory & Co., Inc. provided considerable help during our joint evaluation of field-assisted bonding methods for ρc probes.

TABLE OF CONTENTS

LIST OF ILLUSTRATIONS

LIST OF ILLUSTRATIONS (cont'd)

LIST OF ILLUSTRATIONS (cont'd)

LIST OF ILLUSTRATIONS (cont'd)

LIST OF ILLUSTRATIONS (cont'd)

LIST OF ILLUSTRATIONS (cont'd)

LIST OF TABLES

LIST OF TABLES (cont'd)

INTRODUCTION

This introductory section includes paragraphs on the need for a mass flowmeter, results of the previous program, approaches to solve specific problems, and a summary of work accomplished in the present program.

NEED FOR MASS FLOWMETER

Before proposing that the present program be conducted, we felt it was necessary to first determine whether or not an industry-wide need existed for a diagnostic meter to measure the mass flow rate $\dot{M}$ for aviation fuels. Therefore, we supplemented information available in the literature by contacting instrumentation and control engineers at AiResearch, Avco, General Electric and Pratt & Whitney (Table 1). Of ten engineers interviewed, eight expressed a definite need for $\dot{M}$ measurements for engine diagnostics and/or control. One of the two objectors presented the view that since engine efficiencies and fuel heating values vary by several percent, thrust cannot be controlled accurately enough from $\dot{M}$ alone. However, it was acknowledged that (a) $\dot{M}$ might be the correct parameter to base control on, in future electronic-computer-controlled engines; and (b) $\ddot{M}$, the time rate of change in $\dot{M}$, could be an important control parameter in fuel scheduling, to avoid undesirable transients. ($\ddot{M}$ = fuel density times acceleration.) Another objector felt that rpm, pressure and temperature were more important than $\dot{M}$, for control. However, this individual felt that a diagnostic need might become apparent during the development and testing of the T700 engine. Some other individuals placed emphasis either on diagnostics or on control, depending on their own primary responsibilities. Several indicated the need for $\dot{M}$ data in both disciplines. A response time of about 10 ms apparently would satisfy all those surveyed. An engineer concerned with large engines such as GE's CF6, which develops a thrust of 40,000 lb and which burns fuel at the rate of nearly 20,000 lb/hr on takeoff, pointed out that a demonstration of our proposed flowmeter in the 2000 lb/hr range would be valuable, and of course would be applicable to many "smaller" engines such as GE's J85 or other helicopter engines.

Discussions showed that military applications are generally more severe than commercial. The military situation is more likely to include fuel mixtures or fuel substitutions, and contaminants. Engineers are apparently reluctant to run tests with contaminated fuel flowing through new turbine flowmeters, because of the bearing wear and maintenance problems. Instead, older, less accurate flowmeters are often used. Clearly, an accurate ultrasonic mass flowmeter would be useful in such tests.

TABLE 1. SUMMARY OF SURVEYED MANUFACTURERS' REQUIREMENTS FOR MASS FLOWMETERS FOR AVIATION FUELS

Source	Fuels	$\dot{M}$ (lb/hr)	Accuracy (%)	Fuel Temp (^{o}F)	Fuel Pressure (psi)	Diagnostics	Control
1	Jet fuels + Avgas	200-3000	1/2	-65 to +250	2000	X	X
2	JP-4, 5, 8, Avgas, CITE, DF 1, 2, Iso-octane	50-2000 50-5000	1/2 1/2	-65 to +160 +50 to +115	1000 100	X	X
3	JP-4, 5, Jet A DF's	20,000	1/2 2	+32 to +100 -65 to +160	1000	X	X
4	JP-4, 5	25 to 28,000 $\ddot{M}$	$\leq$ 1/2	+40 to +90	50	X	X
5	JP-3, 4, 5, 7, 8; 7808 Oil	500 to 100,000	1/2	+60 to +300	200	X	X

Table 1 also shows that there is some interest in $\dot{M}$ ranging below 50 lb/hr, and considerable interest up to 5000 lb/hr. Again, for larger engines, $\dot{M}$ ranges over 25,000 lb/hr, with some requirements as high as 100,000 lb/hr. In most engines, the range of $\dot{M}$ does not exceed about 25:1. For example, the GE T700 engine burns about 100 to 2500 lb/hr of JP-4 or JP-5.

Regarding fuel temperature, ground testing diagnostics, if carried out in Alaska or desert sun, approach the limits of the present temperature span, -65°F and +160°F. High altitude (~30,000 ft) generates the minimum temperature limit. The maximum temperature requirement depends partly on the engine and application, on the meter location, and on heat-up after engine turnoff, in the absence of cooling by fuel flow. Thus, a 250°F requirement may be applicable in some instances.

In most diagnostic testing, the fuel is known. Also, a manual check on density and temperature may not be objectionable. Besides the diagnostic need in ground testing, Edwards Air Force Base and other sources have indicated a need in flight testing. Here, in the development and evaluation of new engines, flight test data is telemetered to the ground.

Fuel pressure is often below 100 psi, but can be $\gtrsim$ 1000 psi, depending on meter location, and so a 2000-psi capability is desired.

The accuracy requirement is generally felt to be about 0.5%; but it was pointed out that for some control applications, this might be relaxed to 2% in the interests of reliability, simplicity, small size and light weight.

Lastly, we should briefly indicate the diagnostic need for an adequate mass flowmeter, based on our own experiences in conducting calibration and contamination tests at Avco-Lycoming. In calibration tests the available turbine flowmeters individually covered $\dot{M}$ ranges of only 10:1. They had to be calibrated on the particular fuel used in the test. That is, on switching from JP-4 to JP-5, they had to be recalibrated. Even on a given fuel, changes in fuel temperature (density) required the turbine flowmeter reading to be multiplied by a density ratio correction factor. In contaminant tests, lifetimes of turbine flowmeters are usually less than about 10 hours.

It seemed reasonable that the basic ultrasonic approach of the previous program could be extended to linearly respond to an $\dot{M}$ range of 50 to 5000 lb/hr, could operate from -65 to +160°F and at pressures to 2000 psi, and could respond in 10 ms. We therefore proposed a program which generally retained the positive features of the earlier approach, but did not retain the negative elements.

RESULTS OF PREVIOUS PROGRAM

Reviewing the previous program,[1] five major results may be identified:

- A new ultrasonic transmission flow velocimeter technique for continuously measuring v/c^2 was demonstrated. This technique was believed to inherently offer the best accuracy consistent with fast response, 20 ms, of any ultrasonic approach demonstrated so far. Operation up to 5000 lb/hr was demonstrated.

- A new ultrasonic reflection densitometer technique for measuring ρc was demonstrated on liquids ranging in density from 0.7 to 1.6 g/cm^3.

- A new weighted-area-averaging method was demonstrated on water, Avgas-100, JP-4, JP-5 and a contaminated solvent, for interrogating 100% of the flowing liquid's square cross section using a rectangularly collimated plane wave. This method potentially offers linearity and accuracy essentially independent of Reynolds number or flow profile.

- Using a cell design containing nonintrusive transducers and no rotating parts, endurance of over 100 hours was demonstrated using a test fluid flowing at ~1900 lb/hr and contaminated essentially in conformance with military specifications for flow measuring instruments.

- A new ultrasonic mass flowmeter was built, consisting of a flow velocimeter (v/c^2), a densitometer (ρc) and a time intervalometer ($\tau \sim 1/c$). The combination of these outputs has been shown to yield an output voltage approximately proportional to the mass flow rate $\dot{M}$ over specified ranges.

It was concluded that a refinement of the new technology demonstrated in the previous program should result in an ultrasonic mass flowmeter capable of meeting current U. S. Army requirements for diagnostics, and, ultimately, engine control.

Our approach to overcoming the remaining problems is summarized next.

APPROACHES TO SOLVE SPECIFIC PROBLEMS

Three key problems were to be solved in the present program:

(1) Improve the accuracy to $\pm$ 1% at 2000 lb/hr, 5% at minimum flow (50 lb/hr).

(2) Eliminate the effects due to temperature-dependence of impedance of transducers used in the flow velocimeter.

(3) Avoid nonlinearity at high flow velocities.

We approached these problems as follows:

(1) Accuracy

We wanted to retain the advantages of continuous wave as demonstrated in the previous program, and yet avoid the stringent requirements on impedance matching associated with phase coding with single transmitter/receiver transducers on each side of the acoustic path. This led us to select the synchronous radio frequency burst method described later. The phase difference of the 5-MHz carrier is measured after heterodyning. Additionally, the system measures the sum of upstream and downstream transit times at 2 kHz, which is the pulse repetition frequency. This eliminates the previous requirement for a separate time intervalometer. Further, this data is processed to yield the Mach No., v/c, which, when multiplied by the ρc term, yields a product proportional to $\dot{M}$, the mass flow rate. $\dot{M}$ can also be determined as the product of v and ρ.

In the general ρc subsystem under study, where assumptions about specific fuel type or specific ρ-c-T (density-sound speed-temperature) correlations cannot be made, we chose to measure the echo amplitudes of a nearly-symmetrical ρc reflectometer probe using a manufacturer-modified version of their standard commercial instrument. The instrument, called an Echo Comparator, resolves echo amplitudes to 0.01 dB, or 0.1%, which is adequate for the present purposes. After some modification, its thermal stability appeared to be reasonable. The ρc probe, however, appeared to be considerably more sensitive to temperature, with drift attributed to coupling or adherence changes in the bond layers between the transducer and the buffer rods. Several bonding methods were evaluated, but an adequate solution has not yet been demonstrated.

As of this writing, it appears that some additional development work is still required to reduce ρc errors to a fraction of 1% over the temperature and time-scale ranges anticipated for the system. Specific approaches for accomplishing this are discussed in Appendix C, based on either reflection or transmission coefficient principles, and utilizing existing electronic equipment, or a new adaptation of the narrowband concepts used in the flow velocimeter. On the other hand, a satisfactory densitometer alternative has been identified for JP-4 and JP-5. This alternative is based on the ρ-dependence of the fuel's dielectric constant, and the required equipment is commercially available.

(2) Transducer Improvements

By choosing an rf burst mode referred to in paragraph (1) wherein the pulses are interlaced, each transducer still functions as transmitter and receiver, but now these two functions are separated in time by 250μs. Therefore, the stringent requirements on transducer impedance remaining constant could be relaxed considerably, without sacrificing electrical isolation between transmitter and receiver.

Additionally, partly as a result of other related transducer activities, we departed from a conventional tungsten-loaded-epoxy transducer backing and chose a graphite backing instead. The acoustic impedance of graphite is relatively insensitive to temperature, and the differential thermal expansion between the ceramic transducer element and graphite is relatively small. Therefore, a more stable, reliable thin epoxy bond between the two can be achieved. Such bonds have successfully withstood thermal cycling tests from liquid nitrogen temperature, about -200°C, up to boiling water temperature, +100°C.

(3) Linearity

Analysis of test data obtained in the first contract led us to conclude that the observed departures from linearity were due mainly to eddies generated in the 45° transducer recesses, and due secondarily to eddies generated at the abrupt inlet transition of the cell.

After comparing several alternatives, we chose to install a corrosion-resistant 40-mesh screen over each transducer recess, to maintain a substantially continuous wall, as far as the flow was concerned. Next, we designed a circular-to-rectangular inlet transition pipe.

Test and calibration data obtained in June and December 1974 showed that the nonlinearity previously observed at high flow rates was eliminated.

SUMMARY OF WORK ACCOMPLISHED

1. Panametrics furnished the personnel, material, equipment, and facilities to perform experimental, developmental and research work to design, fabricate, and test an ultrasonic mass flowmeter for use on Army aircraft gas turbine engines. The redesigned flowmeter was based on the flowmeter design previously designed by us under Contract No. DAAJ02-71-C-0061.[1]

2. We performed work directed toward attaining the following objectives as related to the ultrasonic mass flowmeter:

a. The flowmeter was designed to operate over the temperature range of -65°F to +160°F (-54°C to +71°C).

b. The flowmeter was designed to measure fuel flow over the range of 50 pounds per hour to over 4,000 pounds per hour. $\dot{M}$ was to be determined as the product of flow velocity and density-related terms.

c. The transducer cell was to have no moving parts associated with the $\dot{M}$ measurement per se. However, manually operated valves are included as part of a contaminant-flushing branch.

d. The transducer cell was to contain no significant pressure-dropping restrictions or obstructions in the flow path.

e. The transducer cell was to be sized and configured so as to be adaptable for mounting on Army aircraft gas turbine engines.

3. The work accomplished may be further understood by considering the following three tasks:

a. Task I - Design Optimization:

(1) In this initial task we optimized the previous ultrasonic mass flowmeter to combine the parametric measurements of a velocimeter, a densitometer, and a time intervalometer, such that the output is in direct proportion to mass flow rate. It turned out that the time intervalometer function could be accomplished within the velocimeter, without the need for a separate instrument.

(2) In this effort we addressed the problems associated with transducer ports and the inlet transition. We optimized the design of the transducer cell so as to eliminate the undesirable effects associated with stationary eddies and nonlaminar flow. Specifically, we used screens along the flow channel walls, a gradual inlet transition, and a mixer just upstream of the v measuring region. (The need for the mixer is not yet fully established.)

(3) We optimized the velocimeter design so as to eliminate the undesirable effects associated with temperature variations by eliminating the coded cw approach in favor of an interlaced coherent burst approach. Despite encouraging results in our attempts to eliminate thermal effects in the ρc system, we finally interrupted this activity in favor of a standard capacitance type densitometer. This densitometer, as described in a 1974 publication by Stuart,[2] provides adequate ρ accuracy for

JP-4 and JP-5 over the full temperature range of interest. This densitometer, or even other standard densitometer alternatives, can be installed downstream of the v-measuring region in a serial or parallel branch.

b. Task II - Fabrication:

(1) We fabricated one mass flowmeter system based on the optimized design developed under Task I. The mass flowmeter system included a velocimeter, a densitometer, a signal processor containing programmed calculator chips to automatically and digitally compute mass flow rate and other terms of interest.

(2) The transducer portion of the flowmeter system, which was on the fuel line containing the fuel being metered, was designed and fabricated to withstand the thermo-mechanical environment of an Army aircraft gas turbine engine installation. This was verified by thermal and vibration tests.

c. Task III - Tests:

(1) We conducted verification tests on the velocimeter and densitometer, including long term stability and drift tests.

(2) We conducted preliminary calibration tests and endurance tests, using water flowing at rates up to 4000 lb/hr at room temperature.

(3) We tested the ρc densitometer probe from cryogenic levels up to boiling water temperature under no-flow conditions.

(4) We conducted calibration tests, but not contaminant tests. The calibration tests used JP-4 and diesel fuel I VVF 800. The tests were conducted at room temperature and at higher and lower temperatures (i. e., 50, 75, 100, 115^{o}F) over the mass flow rate range of 50 to 6000 lb/hr.

(5) Vibration tests were conducted on the ρc probe, the transducers, and a test block containing a screen soldered along the flow channel sidewall, generally in accordance with MIL-F-5009D. No significant detrimental effects were observed.

THEORY OF OPERATION

BASIC EQUATIONS

The flow measuring system used in this effort differs from conventional ultrasonic flowmetering systems. Many conventional systems use a dual "sing-around" technique, in which a series of pulses is transmitted in first one direction (e. g. , upstream) and then in the opposite direction (downstream). The repetition rate of the pulses in a given direction is predominantly determined by the transit time across the fluid medium: When a pulse is received, this causes the next pulse to be transmitted in the same direction. The repetition rate thus becomes essentially the reciprocal of the transit time. Neglecting second-order effects, the equations appropriate to a conventional system associated with a flow cell similar to that shown in Fig. 1, are

$$f_1 = \frac{1}{T_1} = \frac{1}{D} \sin\theta \, (c + v \cos\theta) \tag{1}$$

$$f_2 = \frac{1}{T_2} = \frac{1}{D} \sin\theta \, (c - v \cos\theta) \tag{2}$$

The frequency difference is measured, giving

$$f_1 - f_2 = 2v \frac{\sin\theta \cos\theta}{D} = \frac{v}{D} \sin 2\theta \tag{3}$$

where v = flow velocity, c = sound speed, D = pathlength across the fluid perpendicular to the pipe axis, and θ = angle of transmission relative to the pipe axis. The main difficulty with this type of system is that the frequency difference, $f_1 - f_2$, is very small indeed. As can be seen by adding Eqs. (1) and (2) and noting that $v << c$, we see that

$$\frac{f_1 - f_2}{f_1} \simeq \frac{v}{c} \tag{4}$$

If, for example, D = 1", $\theta = 45^\circ$, and c = 5000 ft/sec, we have from Eqs. (1) or (2), $f_1 \simeq f_2 \simeq 21$ kHz, and from Eq. (3), for v = 1 ft/sec, $f_1 - f_2 =$ 12 Hz. If the system is to have a resolution of, say, 0. 01 ft/sec, from Eq. (4) we see that the resolution of the frequency difference must be ~0. 12 Hz, with the basic sing-around frequency on the order of 20 kHz, which means that each of the sing-around oscillators must be stable to within a few parts per million.

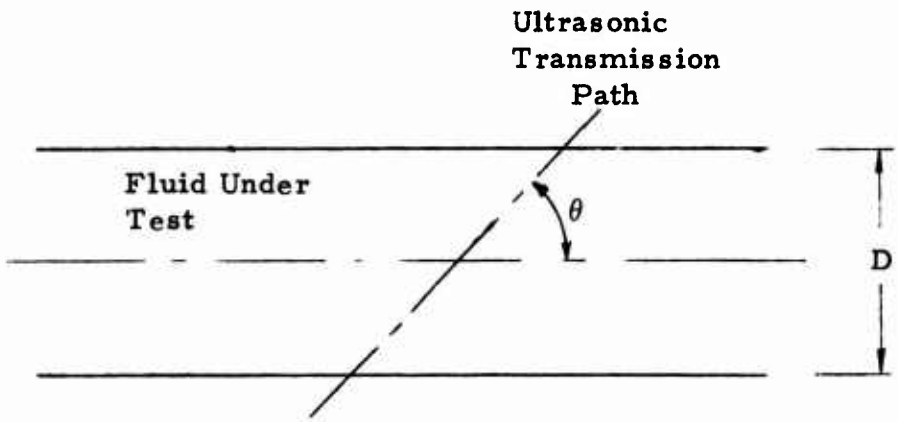

Figure 1. Basic Geometry.

In terms of time resolution, it can easily be shown (assuming a 45^{o} path) that each pulsed oscillator must have a basic resolving time of $\delta T \leqq (D/c^2)\,\delta v$. If, as before, $\delta v = 0.01$ ft/sec, D = 1" and $c = 5 \times 10^3$ ft/sec, we find that $\delta T \leqq 3.3 \times 10^{-11}$ sec = 33 picoseconds. This is, of course, a very heavy burden upon the electronics. Another way of stating the problem is to note that the required average phase stability of each individual oscillator (for $\delta v = 0.01$ ft/sec, D = 1", c = 5000 ft/sec) would be $\sim 2 \times 10^{-6} \times 360^{o}/2\pi = 1.1 \times 10^{-4}$ electrical degrees.

In addition to the above problem in precision, one is also confronted with a situation where the higher the required precision, the longer must be the measurement time. In the above example, a measurement time on the order of 8.3 seconds would be required. If the pipe diameter is increased, the measurement time increases, as can be seen from Eq. (3). For example, for a 10" pipe, 83 seconds would be required to resolve the flow velocity to within .01 ft/sec.

Many of the above problems have been eliminated in the present measuring technique. Rather than measure one quantity to extremely high accuracy, as in conventional ultrasonic flowmeters, the present system utilizes two measurements, $(T_1 - T_2)$ and $(T_1 + T_2)$, each of which need be accurate to only a relative precision on the order of the overall required instrumental precision. (Measurement of the latter term, $T_1 + T_2$, may be thought of as accomplishing the objective associated with the separate time intervalometer of the previous contract.)

It was shown above that the time differential between the upstream and downstream transits must be resolved to a small fraction of a nanosecond. This can most easily and reliably be accomplished to high accuracy by means of a phase measurement between two high-frequency sine waves of the same fixed frequency.

The mathematical theory of operation of the system is straightforward and is given below.

The phase shifts, ϕ_1 and ϕ_2, of the (fixed frequency) upstream and downstream waves, respectively, are given below:

$$\phi_1 = 2\pi f_o T_1 = \frac{2\pi f_o D}{\sin\theta} \frac{1}{c - v\cos\theta} \tag{5}$$

$$\phi_2 = 2\pi f_o T_2 = \frac{2\pi f_o D}{\sin\theta} \frac{1}{c + v\cos\theta} \tag{6}$$

where f_o = 5 MHz (the high-frequency component). The phase difference $(\phi_1 - \phi_2)$ is

$$\phi_1 - \phi_2 = \frac{4\pi f_o D}{\sin\theta} \frac{v\cos\theta}{c^2 - v^2\cos^2\theta} \tag{7}$$

The frequency f_o is chosen so that when $v = v_{max}$ the phase difference approaches but does not exceed 180^o.

The high-frequency (f_o) carrier wave is actually modulated by a rectangular pulse having a width of 50 microseconds and a repetition rate of 2 kHz. The phase shifts of the fundamental frequencies (2 kHz) of the modulation waveforms are similarly given by

$$\psi_1 = 2\pi f_m T_1 = \frac{2\pi f_m D}{\sin\theta} \frac{1}{c - v\cos\theta} \tag{8}$$

$$\psi_2 = 2\pi f_m T_2 = \frac{2\pi f_m D}{\sin\theta} \frac{1}{c + v\cos\theta} \tag{9}$$

The sum of these phase shifts $(\psi_1 + \psi_2)$ is

$$\psi_1 + \psi_2 = \frac{4\pi f_m D}{\sin\theta} \frac{c}{c^2 - v^2\cos^2\theta} \tag{10}$$

We next divide Eq. (7) by Eq. (10):

$$\frac{\phi_1 - \phi_2}{\psi_1 + \psi_2} = \left(\frac{f_o}{f_m}\right)\left(\frac{v}{c}\right)\cos\theta \tag{11}$$

The output of the reflectometer densitometer is proportional to (ρc), where ρ = fluid density. Multiplying Eq. (11) by this factor yields

$$\left(\frac{\phi_1 - \phi_2}{\psi_1 + \psi_2}\right) \rho c = \left(\frac{f_o}{f_m}\right)(\rho v\cos\theta) = \left(\frac{f_o}{f_m}\right)\dot{M}\cos\theta \tag{12}$$

where $\dot{M}$ is the mass flow rate of fluid down the pipe. Note that scale factors have been omitted and $\dot{M}$ is normalized per unit area.

Also, if we divide Eq. (11) by $(\psi_1 + \psi_2)$, we obtain

$$\frac{\phi_1 - \phi_2}{(\psi_1 + \psi_2)^2} = v \left(\frac{f_o}{f_m^2}\right) \frac{\sin\theta \cos\theta}{4\pi D} \left[1 - \left(\frac{v}{c}\right)^2 \cos^2\theta\right] \tag{13}$$

Noting that, even under the most extreme flow conditions, $(v/c)^2 <<< 1$, we can simplify (13):

$$\frac{\phi_1 - \phi_2}{(\psi_1 + \psi_2)^2} \doteq v \left(\frac{f_o}{f_m^2}\right) \frac{\sin\theta \cos\theta}{4\pi D} \tag{14}$$

Thus, in addition to mass flow rate, we can also obtain an output proportional to flow velocity v. This v, in turn, can be multiplied by ρ, the output of a densitometer of more conventional design, which measures ρ alone, not ρc. The product of v and ρ is $\dot{M}$.

Let us next investigate the required precision to which the various quantities must be measured. Three "independent" quantities are measured. Let us consider the case when these three are $(\phi_1 - \phi_2)$, $(\psi_1 + \psi_2)$, (ρc).

In the case of the $\dot{M}$ determination

$$\left|\frac{\delta \dot{M}}{\dot{M}}\right| = \left|\frac{\delta (\phi_1 - \phi_2)}{(\phi_1 - \phi_2)}\right| + \left|\frac{\delta (\psi_1 + \psi_2)}{(\psi_1 + \psi_2)}\right| + \left|\frac{\delta (\rho c)}{(\rho c)}\right| \tag{15}$$

where the magnitudes of the various relative errors are added to take into account the worst case. Thus, if we wish to obtain a 0.6% worst-case error in $\dot{M}$, the relative errors of each of the measured quantities should be kept below ~0.2%.

In the case of the velocity determination (Eq. (14)),

$$\left|\frac{\delta v}{v}\right| = \left|\frac{\delta (\phi_1 - \phi_2)}{(\phi_1 - \phi_2)}\right| + 2 \left|\frac{\delta (\psi_1 + \psi_2)}{(\psi_1 + \psi_2)}\right| \tag{16}$$

It should be noted that we have no frequency stability problems here, since the fundamental frequency, f_o, is fixed and is derived from a crystal oscillator. The fundamental modulating frequency, f_m, is derived by dividing down from f_o = 5 MHz by exactly 2500 to give exactly 2 kHz.

Since these frequencies are fixed, narrowband receivers can be used, thereby providing extremely high signal-to-noise ratio, while operating the transmitter at only a few volts peak-to-peak.

From the above, it can be seen that, by means of independently (and unambiguously) measuring two quantities ($\Delta\phi$ and $\psi_1 + \psi_2$), instead of the single quantity (Δf) of conventional systems, the required measurement precision can be significantly relaxed, and also the response time of the instrument can, if need be, be made very short without greatly sacrificing measurement precision.

The entire system is digitally synchronized to the 5-MHz crystal-controlled clock oscillator, including the digital phase measuring units. As will be shown, the $T_1 - T_2$ and $T_1 + T_2$ outputs are actually a series of pulses which are accumulated over the period of time required for the electronic computations of v/c, v, and $\dot{M}$ to be made. Upon completion of a given set of computations, the stored pulse counts are fed to the calculator and a new set of computations is begun, while at the same time new $(T_1 - T_2)$ and $(T_1 + T_2)$ data is being collected for the next computation. The (ρc) data is fed to the calculator chip in BCD format. The digital computations are presently being made with the Mostek 5012 and 5013 calculator chips. Several seconds are required to compute $\dot{M}$. This time can be decreased substantially, if necessary, to ~1 millisecond by using high-speed (and higher cost) digital computing elements or, with some sacrifice in computing accuracy, by using high-quality analog components.

DETAILED DESCRIPTION OF SYSTEM ELEMENTS

As can be seen from the foregoing, the complete ultrasonic mass flowmeter system consists of the following subsystems:

(1) A flow sensor in which the flow-related parameters are measured.

(2) A densitometer which measures the density-dependent acoustic impedance, or, alternatively, a densitometer which measures ρ.

(3) A computing system which combines the outputs of (1) and (2) to provide mass flow rate and flow velocity, as well as intermediate quantities such as v/c^2 and v/c.

The flow cell used in most of this program may be denoted the (v/c) times ρc cell, to contrast it with the ρ times v cell used at the end of the program, and which used a dielectric-constant-type densitometer. The (v/c) times (ρc) or (v/c) (ρc) cell included a body, an inlet, an outlet, two transducers for the flow velocity measurement, and a densitometer probe

for the ρc measurement (Figs. 2-4). It was fabricated principally of stainless steel 304, for corrosion resistance, and to permit inlet and outlet transitions to be welded to it. The rectilinear channels, 1/2" x 1" for flow, and 1/2" x 1/2" for ultrasound, were produced by electric discharge machining. Transducers communicate over a 3" path at 45° to the flow axis, essentially uniformly interrogating a full cross section to provide area-averaging independent of profile. (Appendix B contains construction details, shows alternative designs, and includes background information on the need for accommodating various flow profiles.)

The v/c times ρc cell design principally differs from its predecessor of the previous contract as follows. (1) Cell material is stainless steel. (2) Screens are soldered along sidewalls to minimize eddy effects near transducer recesses. (3) The inlet gradually transitions from circular to rectangular, to further minimize eddies. (4) Sight ports are included, with line-of-sight being orthogonal to line-of-sound. (5) Transducers are backed by graphite, for thermal immunity. (6) The ρc densitometer probe, instead of being stepped, is nearly symmetrical (suggestion of N. E. Pedersen) and may be separated from the "flow velocimeter" portion of the cell. (7) Flushing and gas bleed ports are provided to allow entrapped air to be released, and to allow prompt clearing out of the transducer cavities and screens, should they eventually fill with contaminant particles. (8) Space is available for installing a Kenics static mixer upstream of the v measuring region. (This mixer was used in the December tests.)

The flow parameter electronic measurement system provides two separate outputs. The first is the phase difference between the 5-MHz components of the upstream and the downstream waveforms, while the second output is the sum of the upstream and the downstream transit times. These transit times are determined by independently measuring the phase shifts of the low-frequency (2-kHz) components of the modulation waveform associated with the upstream and the downstream waves. These waveforms are identical but are shifted in time with respect to each other. The basic waveform is a 5-MHz cw wave, modulated by a 50-μs rectangular pulse having a repetition rate of 2 kHz (500 microseconds between pulses). The upstream and downstream transmissions are shifted by 250 μs but are otherwise identical. The transit time across the fluid medium is approximately 50 microseconds. Figure 5 is a diagram showing the modulation waveforms and the timing sequence for upstream and downstream transmission and reception.

The transmitted waveforms can be described mathematically as a cw wave (the 5 MHz) modulated by a Fourier series representing the repetitive pulse:

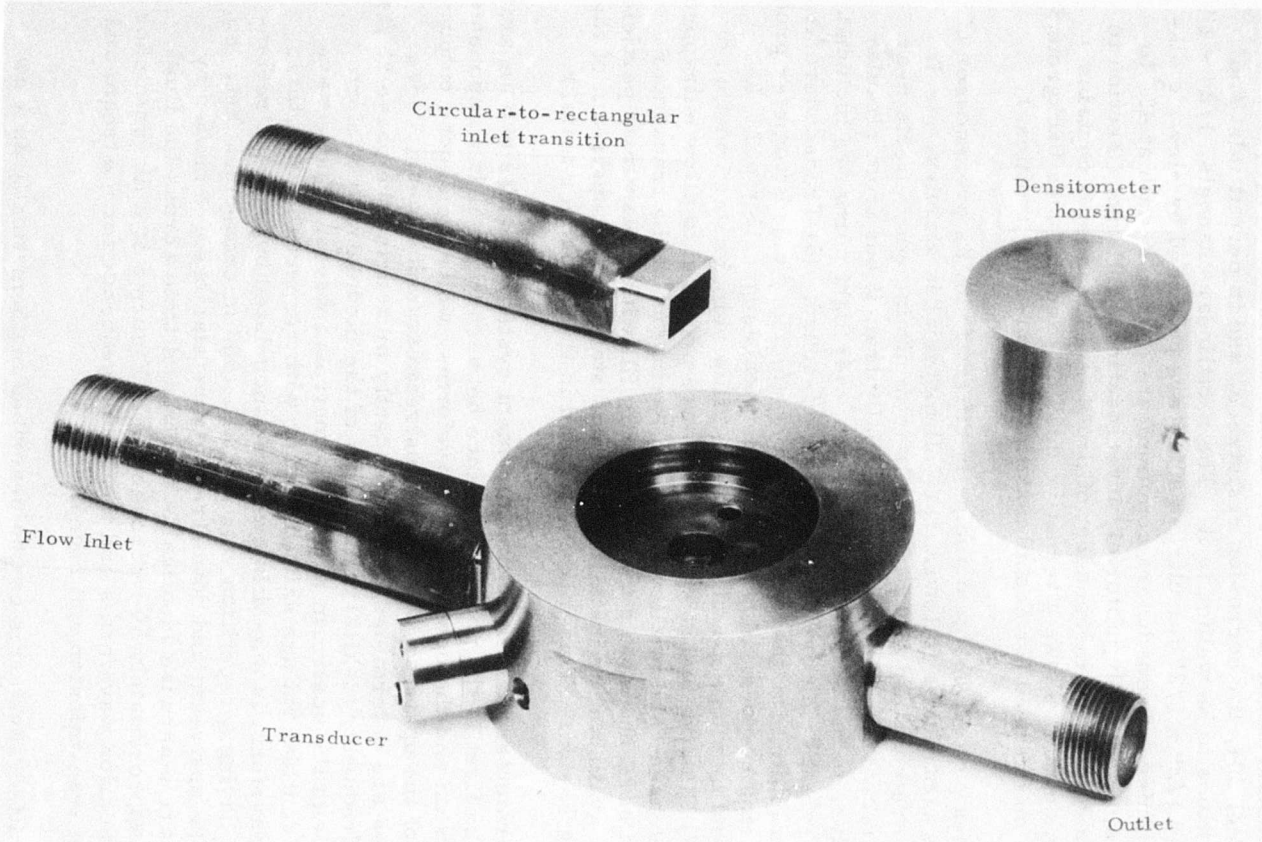

Figure 2. Mass Flowmeter Cell Fabricated of Stainless Steel.

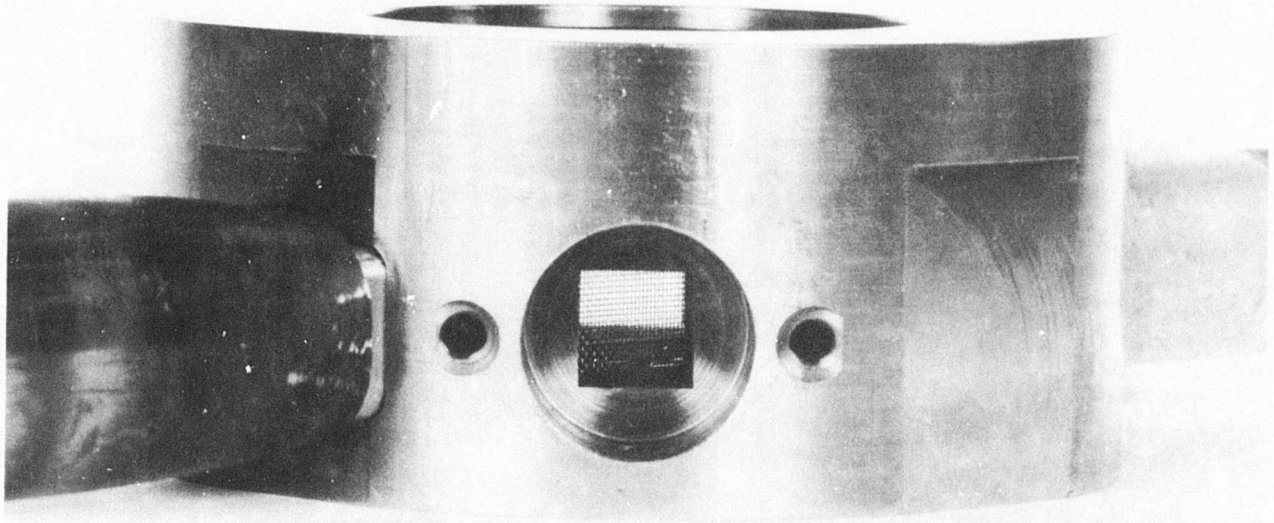

Figure 3. View Through Transducer Port. Screen is Soldered Along Sidewall of Flow Channel to Reduce Eddies in Measuring Region. Screen is 40-Mesh Nickel, Having Wire Diameter of 0.13 mm (0.005 in.).

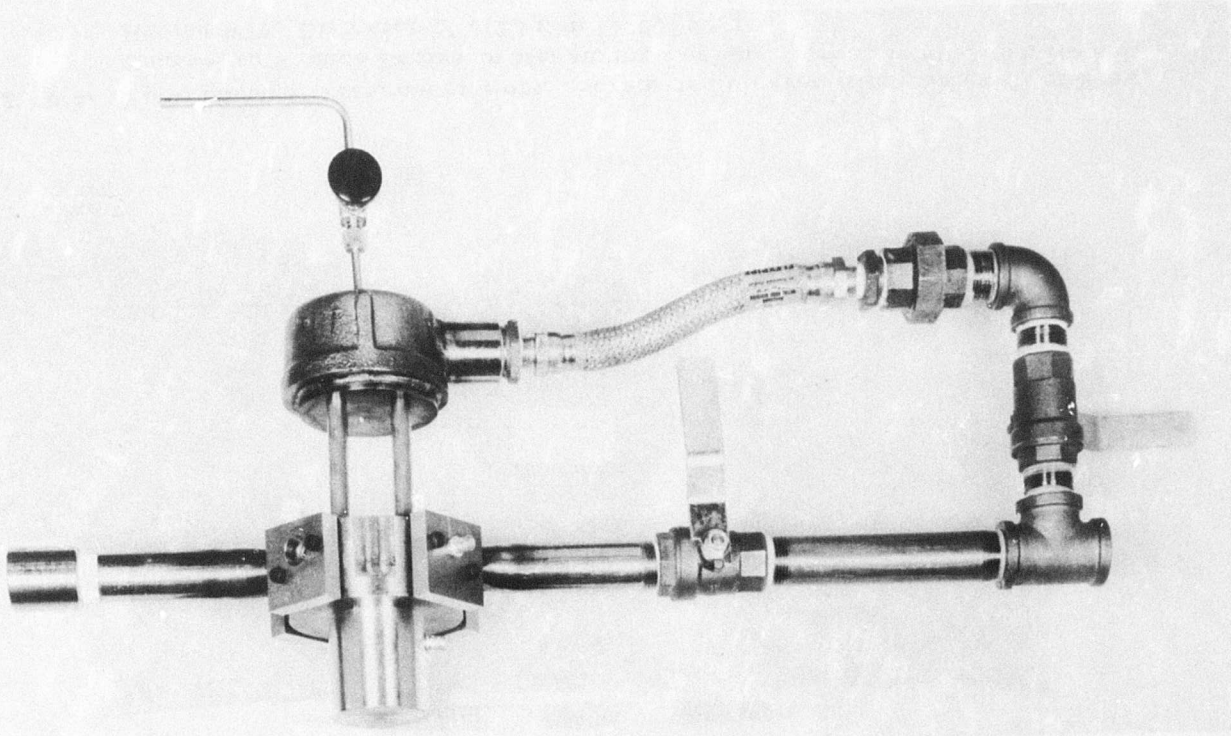

Figure 4. $\dot{M}$ Flow Cell Used in Calibration Tests at Avco-Lycoming June and December 1974. Cell Consists of Stainless Steel Body, Velocimeter Transducer Pair, Housed ρ c Densitometer, Sight Ports, Screens, Inlet and Outlet Transition Pipes, Flushing and Vent System. Additionally, in Tests Conducted During December, a Static Mixer Was Installed Just Upstream of the Measuring Region, and a Capacitance-Type Densitometer Was Installed Downstream.

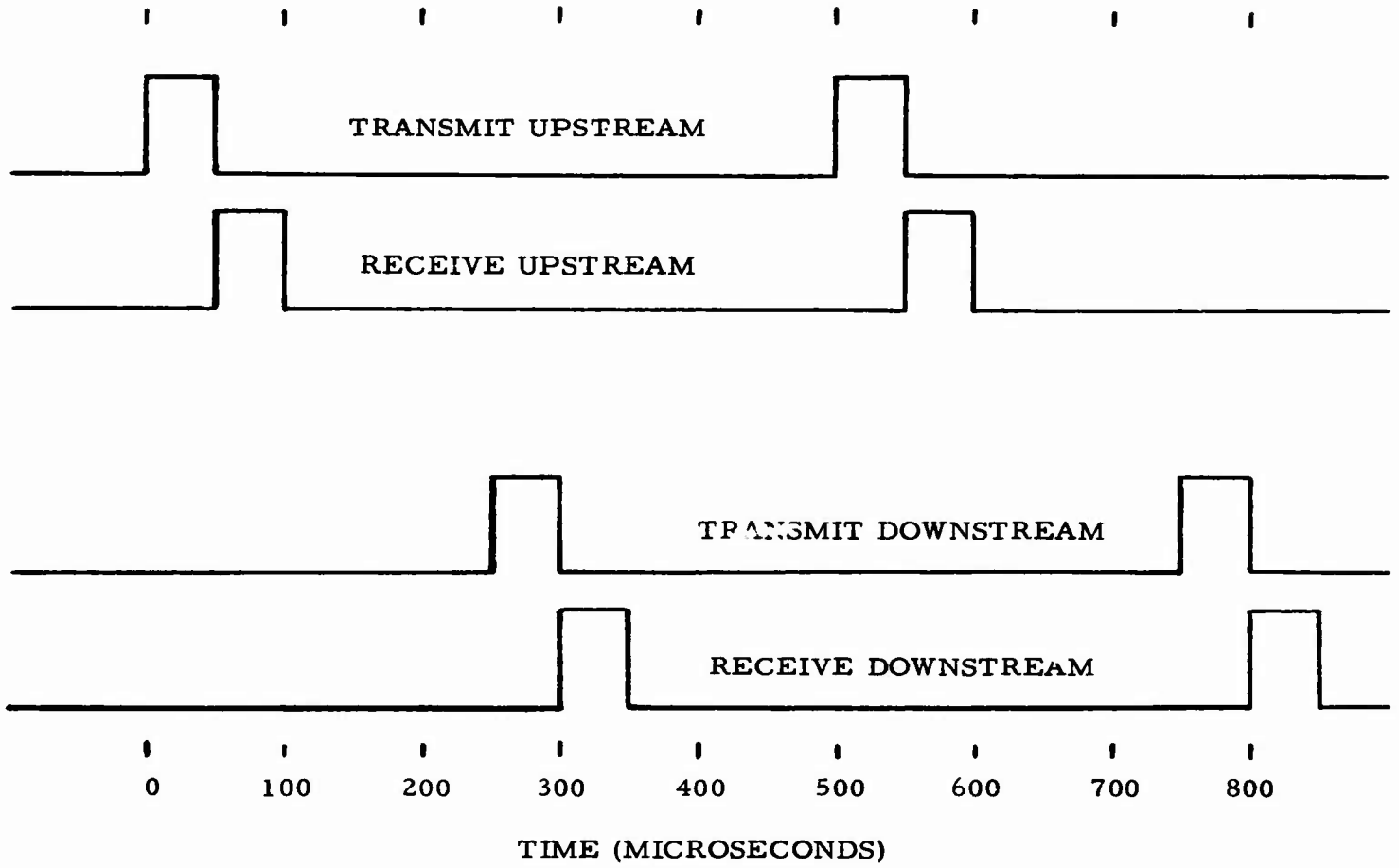

Figure 5. Modulation Waveforms and Timing Sequence.

$$s = \sin \omega_o t \sum_{N=0}^{\infty} A_N \sin (N \omega_m t + \alpha_N) \qquad (17)$$

Noting that the modulation waveform is positive or zero, depending upon whether transmission is occurring or is not occurring, it is obvious that $A_o > 0$. This is true because the time integral of the modulation waveform is positive, and A_o is the only term in the series which does not integrate to zero.

From the above we see that there will be a 5-MHz component in the received spectrum which, with appropriate filtering, can be recovered. Also, if the received wave is amplitude detected and the resultant is passed through a narrowband 2-kHz filter, the fundamental frequency of the modulation waveform can be recovered.

If the 5-MHz components of the upstream and downstream waves are each recovered as described above, and are compared in phase, an accurate measure of the transit time difference between upstream and downstream waves is obtained. Also, the phases of the 2-kHz fundamentals of the upstream and downstream modulations are independently and unambiguously measured relative to a 2-kHz reference wave. These phases are then added to give the sum of the upstream and downstream transit times. Thus, the flow parameter measurement system provides the following two outputs: $(T_2 - T_1)$ and $(T_2 + T_1)$. A block diagram of this system is given in Fig. 6. Referring to this figure, the system's operation will now be described.

A 5-MHz crystal-controlled oscillator provides the overall system synchronization, as well as the carrier wave to be transmitted. The output of this oscillator is divided by 2500 and serves to trigger two 50 microsecond gates, which then modulate the 5-MHz cw waveform. The gates are sequentially operated 250 microseconds apart, the overall duty cycle being 500 microseconds. The switching logic operates analog solid-state switches which serve to alternately connect the upstream and downstream transducers to their respective transmitter or receiver as required.

Each of the receivers employs a common broadband input stage, at the output of which the signal is split into two channels: the high-frequency and low-frequency channels.

The operation of each high-frequency receiver channel is as follows. After a stage of isolation, the broadband received waveform is fed to a narrowband 5-MHz crystal filter of the bandpass type. The filter

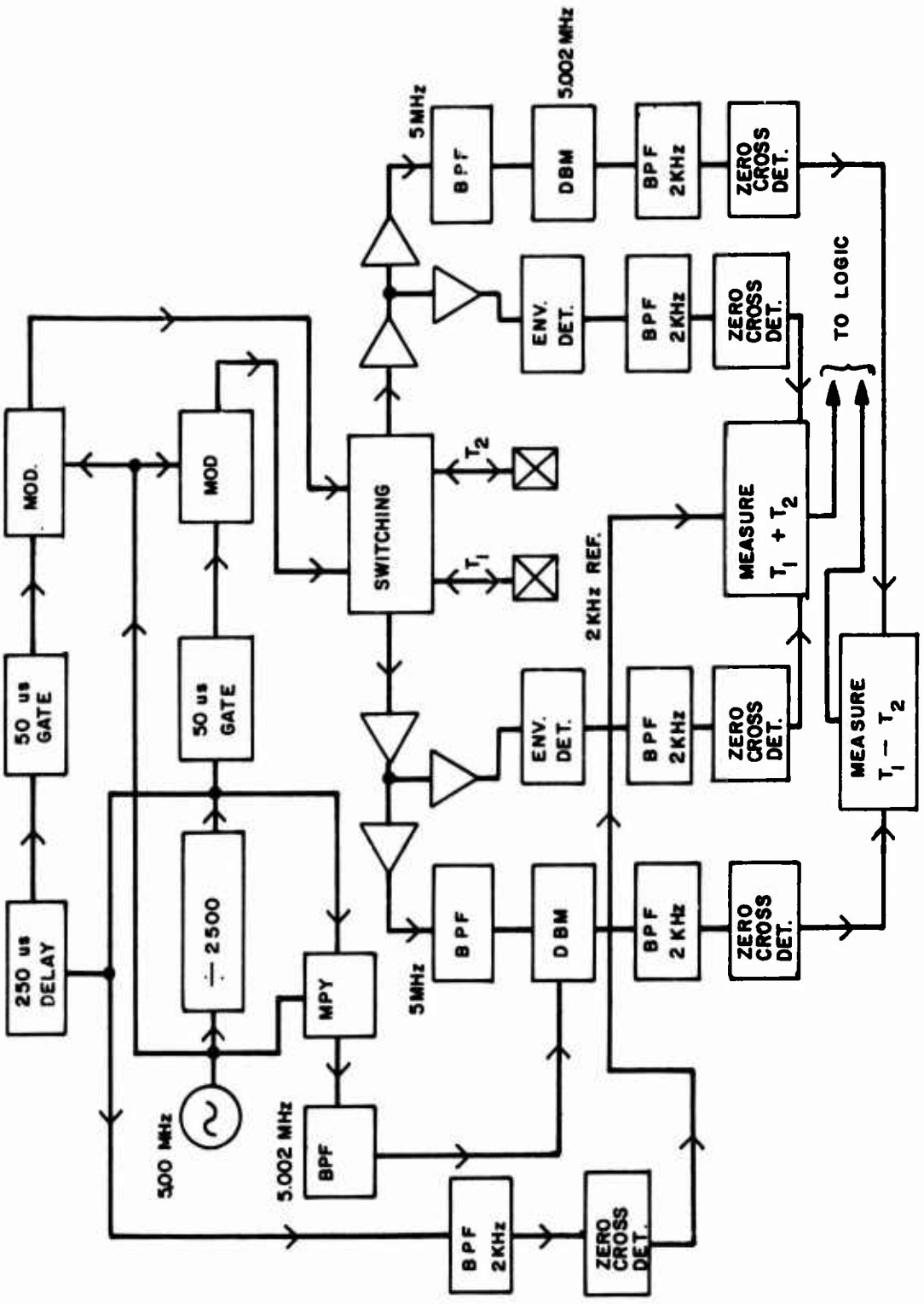

Figure 6. System Block Diagram.

characteristics are such as to reject each of the 2-kHz modulation spectral lines by more than 70 dB. Thus, the filter output is a 5-MHz cw wave. A coherent "local oscillator" frequency of 5.002-MHz is derived by means of mixing the 5-MHz oscillator output with the (5-MHz/2500) = 2-kHz signal, and (by means of a crystal filter) passing only the 5.002-MHz component. This is then mixed with the 5-MHz crystal filter output to produce a 2-kHz i.f. wave which, after bandpassing in an active analog filter, is converted to a square wave by means of a zero cross detector. The phase shift of this square wave is equal to the phase shift of the 5-MHz component of the waveform transmitted across the fluid path.

The operation of the 2-kHz portion of each receiver is straightforward. After a stage of isolation, the received waveform is amplitude detected and passed into a narrowband 2-kHz active analog bandpass filter. The filter output is then fed to a zero cross detector, which produces a square wave at its output. The phase shift of this square wave corresponds to the shift in phase of the 2-kHz modulation component of the waveform transmitted across the fluid path.

The difference in transit time, $T_1 - T_2$, is, of course, very small and must be resolved to a fraction of a nanosecond. This is done by means of measuring the time of coincidence of the two 5-MHz-derived 2-kHz square waves. Let the time of flight upstream and downstream be represented by $T + \Delta t$ and $T - \Delta t$, respectively. A 180° phase shift between these square waves results for $\Delta t = 100$ nanoseconds. The actual $T_1 - T_2$ measurement consists of counting the number of 5-MHz pulses which occur within the coincidence time. Thus, each half cycle is divided into 2500/2 = 1250 parts. Thus, the phase difference can be measured to ~0.14 degree, which results in an instrumental time differential measurement precision of 0.08 nanosecond,* or 80 picoseconds. Actually, since, during the measurement period, small flow fluctuations result in slight transit time variations, interpolation automatically takes place, and the resolution is really better than 0.08 nanosecond.

The quantity $T_1 + T_2$ is measured by counting the number of 5-MHz pulses during the coincidence between each modulation-derived 2-kHz square wave and a reference 2-kHz square wave, and adding each count. (This accomplishes the time intervalometer function.) These pulse sequences, as well as the pulse sequences from the $T_1 - T_2$ measurement, are fed to counters in the flow calculator, which will be described in the following section.

*As mentioned later in this report, a measurement technique was devised which cancels differences in propagation delay and phase shift variations of the two 5-MHz crystal filters by means of systematically reversing the upstream and downstream transducer connections.

Figures 7-9 illustrate the flowmeter electronic system.

FLOW CALCULATOR

The purpose of this subsystem is to compute flow velocity v and mass flow rate $\dot{M}$, and to provide a digital display of these. Other quantities which can be read out are v/c^2, v/c, ρc, and $T_1 + T_2$, where c = sound speed, ρ = fluid density, and $T_1 + T_2$ = sum of upstream and downstream transit times.

The calculator section makes the above computations from previously accumulated data and, as the calculation proceeds, simultaneously collects updated data for the next computation. Thus, both the computational and the storage functions operate continuously, rather than consecutively.

A block diagram of the calculator section is shown in Fig. 10. Four inputs are provided. Two of these (the $\phi_1 - \phi_2$ and $\psi_1 + \psi_2$ inputs) accept the pulse sequences from the flow parameter measurement section. These two sets of pulse trains are counted by means of a pair of 10^8 BCD counters. The data necessary for the ρc calculation, namely, KA - LB and KA + LB, are analog voltages and are fed to two analog-to-digital converters. (As explained in Ref. 1 and Appendix C, A and B are echo amplitudes generated with the ρc probe, and K and L are null-balancing constants.) Upon completion of a computation, the contents of the A/D converters are fed to separate registers, and the counters are reset (and begin new counts). The register outputs are fed via a data buss to the calculator, which utilizes the Mostek 5012 and 5013 calculator chips. The control function is provided by a programmable read-only memory. The outputs of the calculator are selectively read out (by means of a multiposition switch) on a 12-digit LED panel display.

The overall cycle time of the calculator is presently several seconds. As mentioned earlier, this time could be shortened to about one second by means of more efficient programming, or to less than 100 ms through the use of one of the new microcomputer assemblies. At some reduction in accuracy, the computations could also be performed by means of integrated circuit analog computing elements.

The outputs of the calculator are presently unscaled. We can think of the Avco/Lycoming tests as the means of experimentally determining the scale factor.

The flow calculator can also be programmed to compute $\dot{M}$ from products proportional or related algebraically to vc (for a given fuel) or from v and

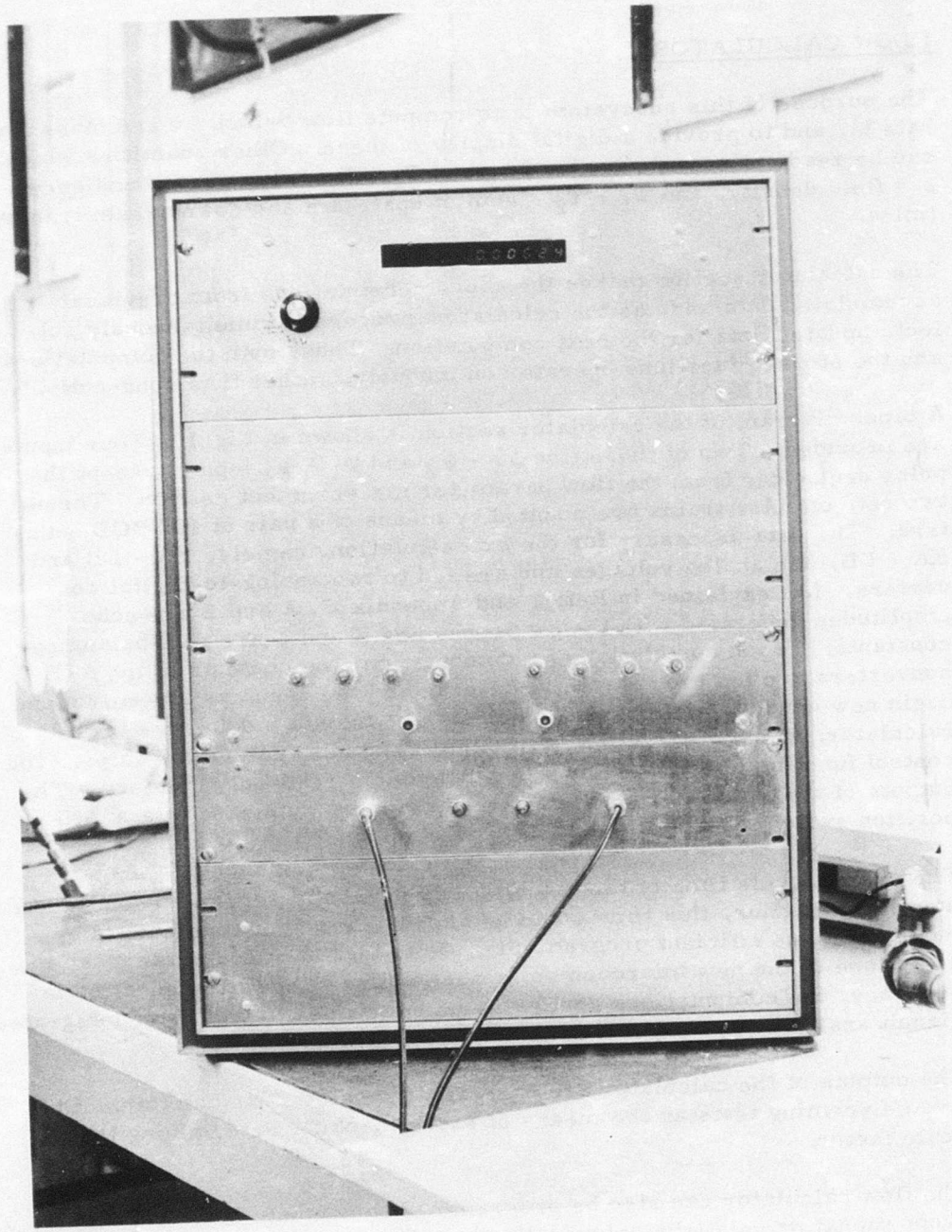

Figure 7. Front View of Flowmeter Electronics Assembly.

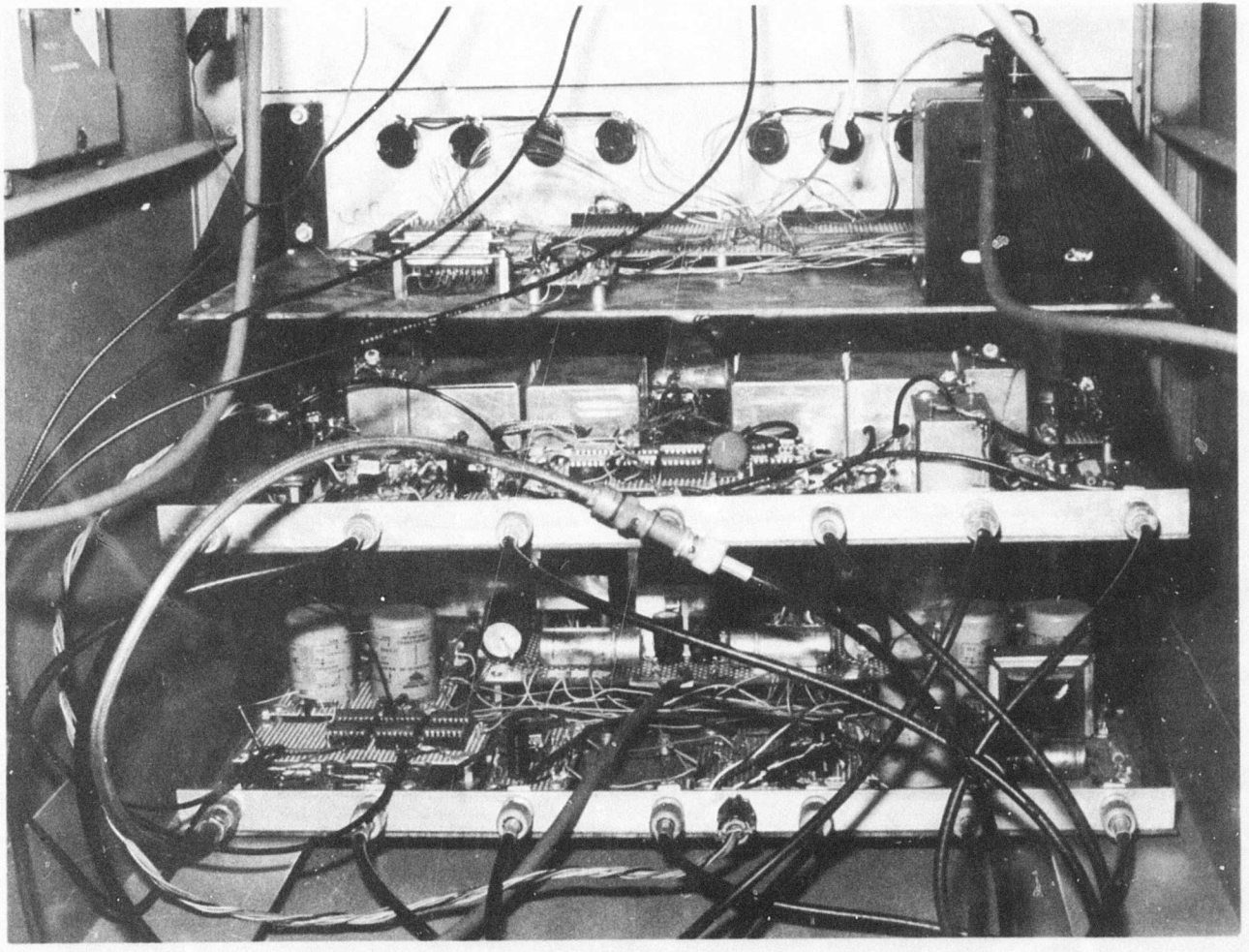

Figure 8. Analog Portion of Flowmeter Electronics.

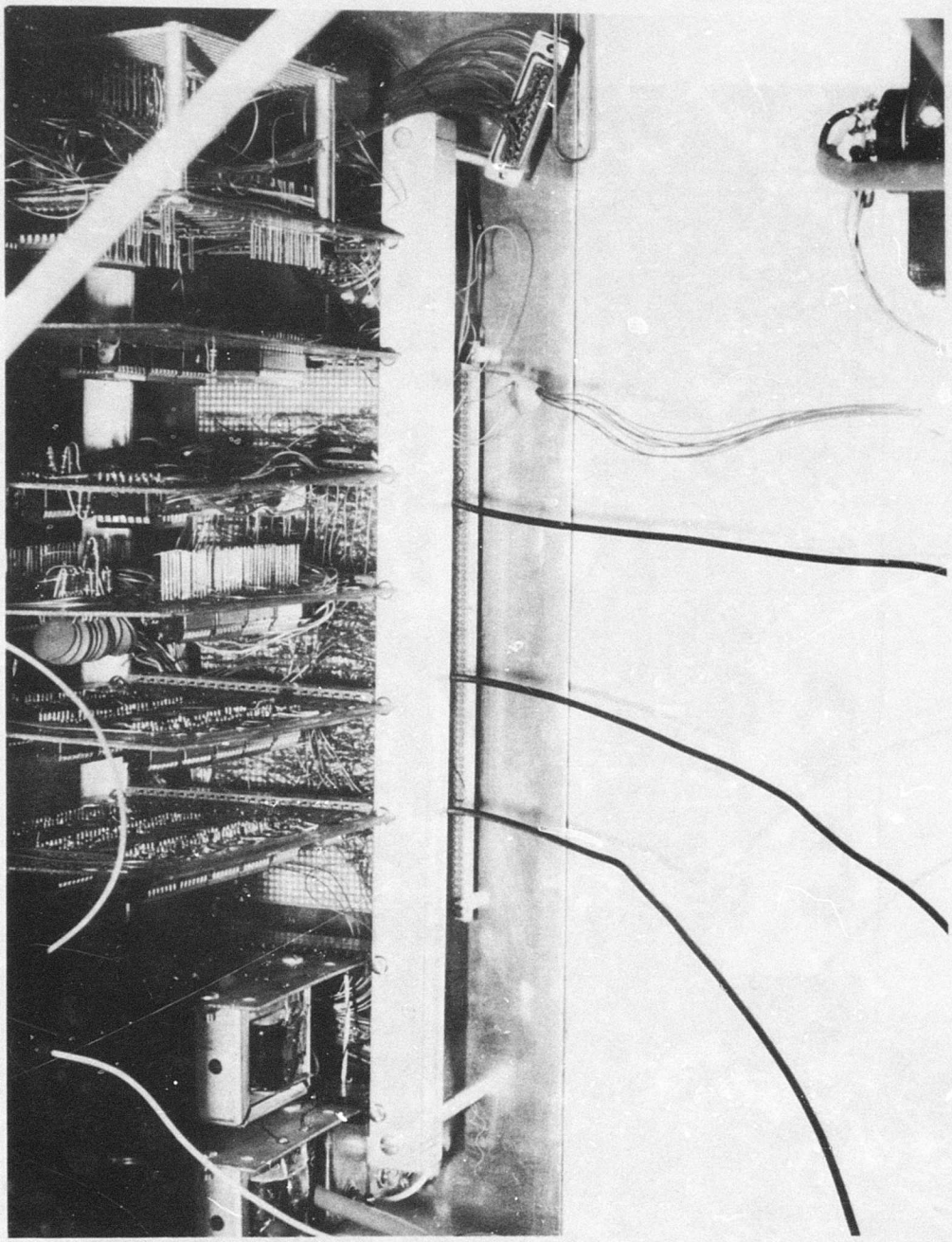

Figure 9. Digital Portion of Flowmeter Electronics.

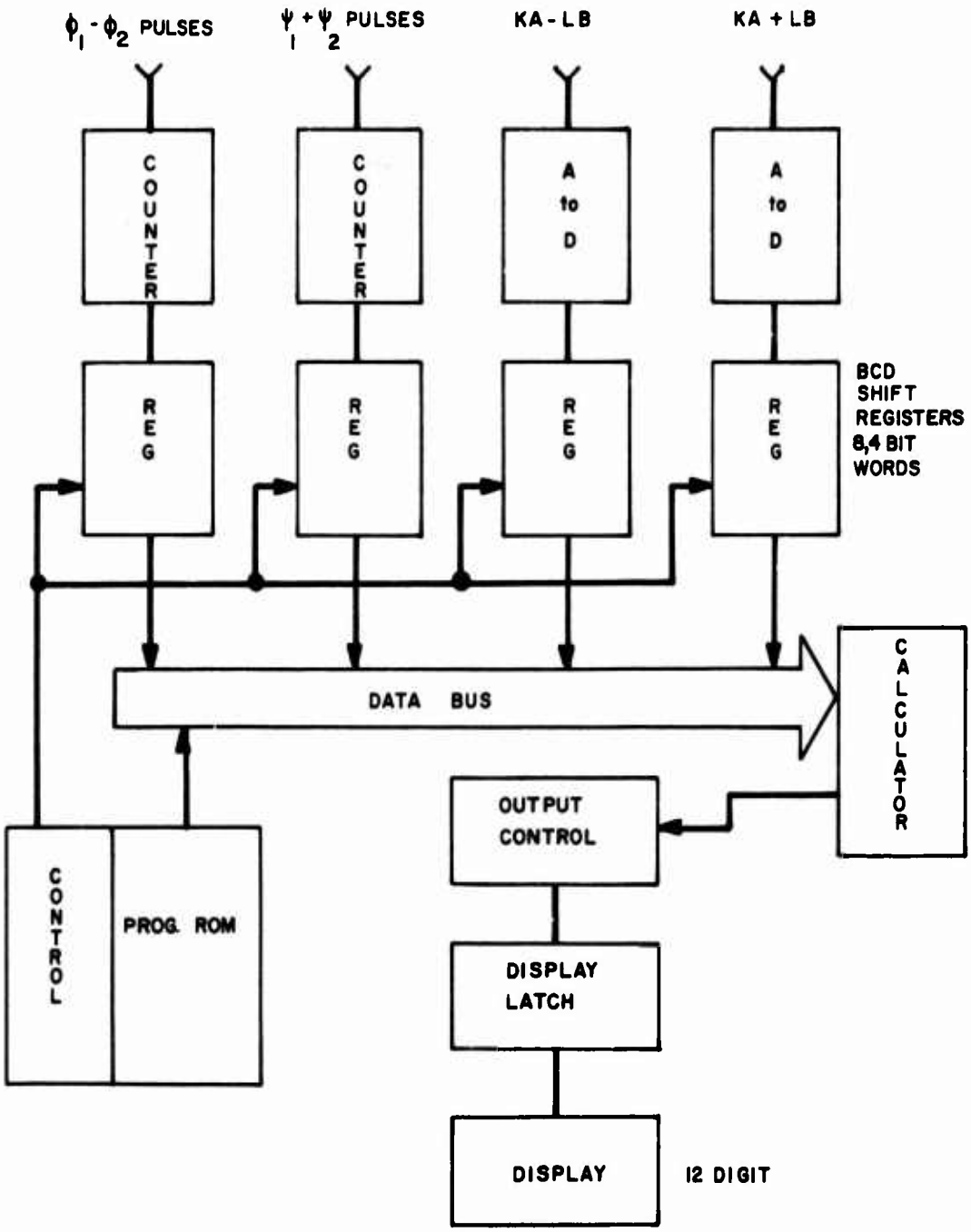

Figure 10. Flow Calculator.

Note: The KA-LB and KA+LB inputs are not used in flow velocity measurements.

independent density data ($\dot{M} = \rho v$). Density is measured directly by devices such as ITT-Barton's resonant vane densitometer or Simmonds Precision's dielectric constant densitometer. Despite their intrusiveness, such devices appear to have sufficient resistance against clogging, and sufficiently low pressure drop, as to be potentially usable with the ultrasonic flow velocimeter in some instances. To avoid the 0.1 to < 10 psi pressure drop that may be associated with intrusive densitometers installed in series, one can install the densitometer in a parallel branch through which the flow velocity is < 1 ft/s, thereby assuring that the pressure drop will be negligibly small (Fig. 11). In addition to the above resonance and dielectric types, nuclear densitometers utilizing one or two energy levels may also be applicable in some cases. These, too, are commercially available (e.g., Tyco). For completeness, these alternatives to the $(v/c)(\rho c)$ formulation are indicated here.

THERMAL EFFECTS

Appendix E analyzes the effects of temperature on the acoustic properties of the fuels, on the cell dimensions and integrity, on the transducers used in the velocimeter, on the transducers and coupling interfaces used in the ρc densitometer, and on the fused silica buffer rods used in the ρc probe. Appendix E includes an analysis of refraction and "acoustic short circuit" (a term denoting the early arrival of metal-borne waves which interfere with the measurement of fuel-borne waves). These analyses support the present choice of retaining the oblique fixed-angle interrogation path formed by 45° channel recesses (but with the addition of screens soldered along the flow channel sidewalls). One potential alternative to the fixed incidence angle screened channel was a solid wedge installed in the 45° channel recesses. However, its use was discounted in the present cell, because of the refraction complications.

Some of the analysis of Appendix E applies not only to the "wetted transducer" concept used in the present program, but also to nonwetted clamp-on or externally mounted transducers.

In a few instances, Appendix E includes test results to indicate performance of specific flow cell, transducer or ρc probe components at the temperatures of liquid nitrogen and boiling water, essentially -200°C and +100°C. These particular temperatures, while beyond the contractual limits of -54°C to +71°C, were selected for some tests, because of the simplicity of attaining them experimentally and because they illustrate performance beyond minimum requirements.

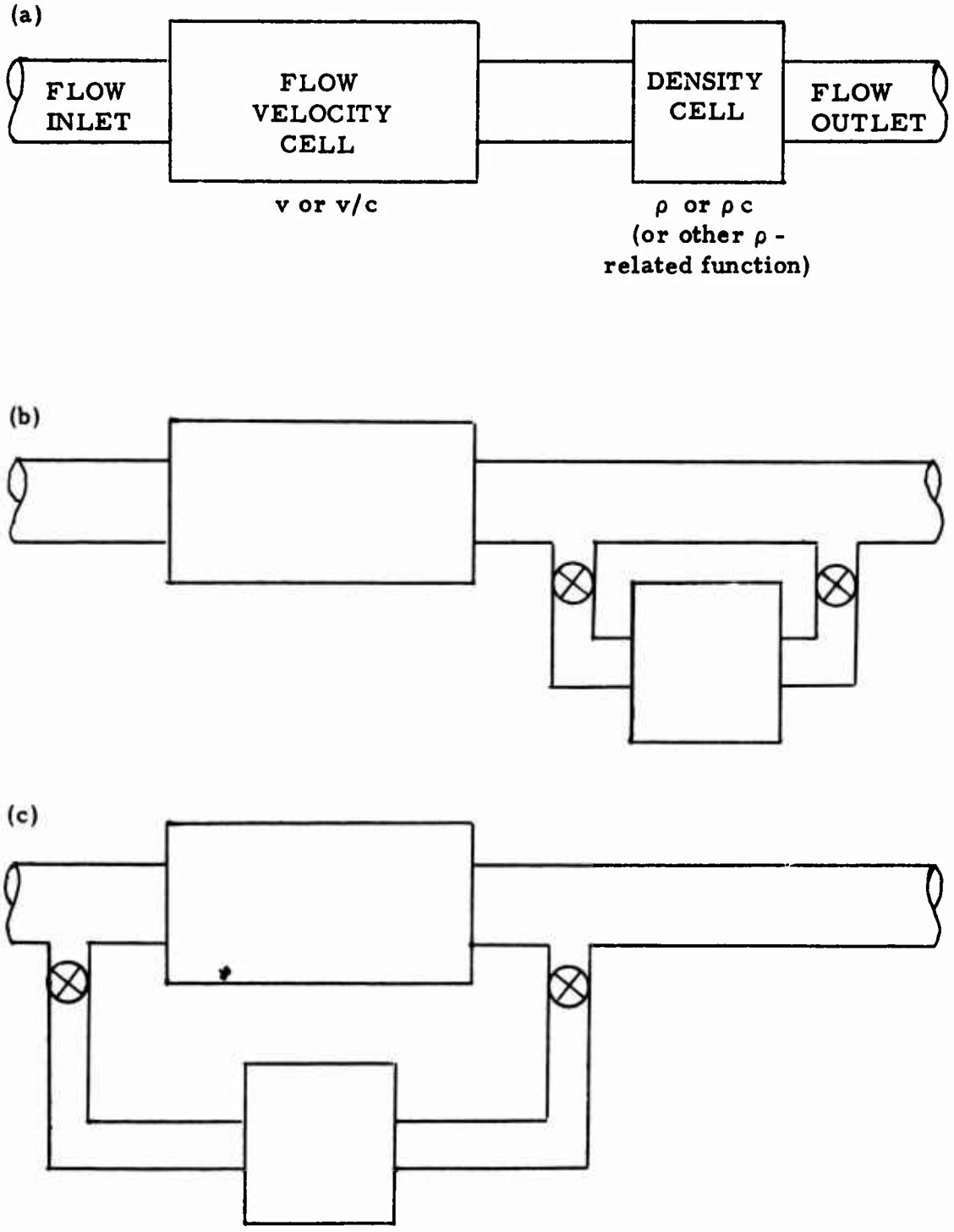

Figure 11. Branch Concept for Densitometry. (a) Density Cell in Series, Downstream. (b) Density Cell in Parallel Branch, Downstream. (c) Density Cell Branch in Parallel With Flow Velocity Cell.

TEST RESULTS

IN-HOUSE TESTS OF FLOWMETER

In order to determine that the overall system was operating properly, it was necessary to conduct a series of semiquantitative tests which were to be conducted prior to the calibration tests at Avco/Lycoming. These preliminary tests consisted of determination of (1) repeatability, (2) zero drift, and (3) long-term stability.

The lack of an in-house calibrated flow loop precluded a highly quantitative preliminary test program. However, it was determined that, in the short term, nearly identical flow conditions could be reproduced by consecutively valving off the flow to zero and then fully opening a gate valve. Of course, creation of the zero flow condition is a trivial matter. Since we could not depend upon precise long-term repeatability of a particular flow rate, the long-term stability measurement was really a measurement of zero drift over periods of ~16 hours.

These tests were most useful in that they revealed two mechanical problems. The first related to the fact that the transducers were sealed to the faces of the mechanical housing by means of O-rings. Changes in pressure gave rise to slight shifts in the angular positions of the transducers, which, in turn, caused slight changes in the high-frequency phase difference. The second problem was more difficult to overcome in a truly positive way: A system of vent tubes (described elsewhere in this report) was installed, which made it possible to bleed both transducer cavities, and also to reverse flush the cavities. This arrangement made it possible not only to eliminate any air bubbles from the cavities, but also to clean the cavities and screens by means of alternate forward and reverse flushing.

After the annoying problems described above were taken care of, the repeatability and short-term zero drift of the system were consistently on the order of 0.1% to 0.2% of full scale. However, the long-term zero drift of the system was on the order of 1%, which is, of course, unacceptable. Because of this latter situation, a measurement procedure was developed which virtually negates zero drifts occurring over periods greater than one minute.* The observed zero drift is due to very slight and nonidentical thermally induced phase differences in the RF sections of the two receivers. By means of making two consecutive flow measurements, the latter with the transducer connections reversed, then adding

*The technique can be electronically implemented and, when this is done, will eliminate zero drift for periods greater than a few seconds.

the two measurements and dividing by 2, the effect is negated. The reason is that a relative phase lead for one set of connections remains a relative phase lead for reversed transducer connections. The flow induced relative phase, however, reverses when the two transducer connections are reversed. The procedure is mathematically illustrated below:

Suppose we have an upstream phase of α_1 and a downstream phase of α_2, and that the phase shifts in receivers 1 and 2 are β_1 and β_2, respectively. Since the system measures only the magnitude of the phase shift, the first measurement, M_1, is

$$M_1 = |(\alpha_1 + \beta_1) - (\alpha_2 + \beta_2)| \tag{18}$$

Next, reversing the transducer connections, we perform a second measurement, M_2:

$$M_2 = |(\alpha_2 + \beta_1) - (\alpha_1 + \beta_2)| \tag{19}$$

Now, as long as $|\alpha_2 - \alpha_1| > |\beta_2 - \beta_1|$, and assuming flow in the positive direction (e.g., $\alpha_1 > \alpha_2$),

$$M = M_1 + M_2 = (\alpha_1 - \alpha_2) + (\beta_1 - \beta_2) + (\alpha_1 - \alpha_2) + (\beta_2 - \beta_1) \tag{20}$$

$$\frac{1}{2} M = (\alpha_1 - \alpha_2) \tag{21}$$

Thus, as long as the magnitude of the zero drift is smaller than the absolute value of the flow measurement in the absence of zero drift (~1% of full scale), the zero drift is eliminated by this procedure.

The above technique was extensively and successfully tested in the Panametrics laboratory prior to the calibration tests at Avco/Lycoming.

CALIBRATION TESTS AT AVCO/LYCOMING, JUNE 1974

The purpose of these tests was to determine the linearity and reproducibility of the volumetric flowmeter, and of the overall mass flowmeter. As previously mentioned, for purposes of analysis and diagnostics, a multiplicity of output readings was provided. These readings are listed below:

(a) v/c^2. This quantity is proportional to the phase difference between the 5-MHz components of the upstream and downstream waves.

(b) $(T_1 + T_2)$. This is the sum of the upstream and downstream transit times and is derived from the sum of the phases of the 2-kHz components of the upstream and downstream transmitted waveforms. Note that $(T_1 + T_2)$ is proportional to the reciprocal of the sound speed.

(c) v/c. The ratio of fluid velocity to sound speed is obtained by dividing (v/c^2) by $(T_1 + T_2)$.

(d) ρc. The product of fluid density and sound speed is the acoustic impedance, and is the output quantity of the ρc densitometer.

(e) $(v/c)(\rho c) = \dot{M}$. This is the mass flow rate, which is the quantity of greatest interest in the program.*

(f) v. The fluid velocity is computed by means of dividing (v/c^2) by $(T_1 + T_2)^2$.

As previously discussed, the various outputs were recorded in the normal and reversed transducer connection conditions, and the average value of each reading was computed as a part of the data analysis.

Flow measurements were made using a Cox calibration test stand as the $\dot{M}$ standard at the Avco/Lycoming flow calibration laboratory. The two fuels used were JP-4 and marine diesel fuel, I VVF 800. Measurements were made on each fuel at room temperature ($75^{\circ}F$) and at elevated temperature ($\sim 115^{\circ}F$).

The equipment was set up and checked out on the morning of June 19. JP-4 measurements were made on the afternoon of June 19 and on June 20, and diesel fuel measurements were made on June 21. In all, four JP-4 runs and two diesel fuel runs were made. Unfortunately, a fluid leakage problem and a cracked fused silica buffer rod in the (ρc) unit prevented measurement of (ρc) in the first three JP-4 runs.

The raw data for each of the six runs is given in Appendix A. Note that the "a" and "b" of each point represent the normal and reversed transducer connection configurations, while "av" denotes the average of the "a" and "b" measurements. Note also that the column labeled $(v/c)(\rho c)$

*Due to a minor programming problem involving scale factor, this quantity was not directly read out, but was computed subsequent to the data runs by means of directly multiplying outputs (c) and (d) above. Note that no loss of accuracy was incurred because of this.

was subsequently computed as the product of (v/c) and (ρ c), and that $\dot{M}$ is the mass flow rate measured by Avco.

Analysis of the data proceeded as follows: First, the data for a given column were plotted as a function of $\dot{M}$. The best straight-line fit (through the origin) was drawn for each plot, and the slope was computed. Then the percentage of deviation of each data point was computed (1) as a percentage of reading and (2) as a percentage of full scale (which we have taken to be 4000 lb/hr). These are listed with subscripts "lin" and "max", respectively. The results of these computations are given in Tables 2 through 7, in which the average deviation was computed as % of full scale for each quantity in each run. Any points having deviations greater than the statistical limit of error were next excluded and the average deviation recomputed.*

The experimental data, in both tabular and graphical form, are presented for all six runs in Appendix A. At this point two experimentally observed facts should be mentioned:

First, it was found that the positive peak of the 2-kHz reference wave (used to measure T_1 and T_2) was running saturated. Since this wave is fed to a zero cross detector, one might suppose that this would be of no consequence. However, since capacitive coupling into the zero cross detector was used, a change in amplitude of this reference wave would result in a slight shift of the zero point as seen by the zero cross detector. This effect is additive, since we are measuring (T_1 + T_2).**

Secondly, it was noted that on two of the data runs (#3 and #5) an abnormal departure from linearity was observed for mass flow rates below ~500 lb/hr, e.g., for laminar flow at ~10% of full scale.† Observation of the flowing fuel through the sight port revealed visible, wavy striations in the flow. The results of this inhomogeneity can be seen in the graphs of Appendix A.

---

*Such deviations were rare and were generally found to be isolated to only one of the several measured quantities for a given $\dot{M}$. Thus, it is reasonable to conclude that these are reading errors.

**This problem has been corrected since the return of the equipment to the Panametrics laboratory.

†Use of a Kenics "Static Mixer" apparently eliminated this nonlinearity in the December tests. Alternatively, one could use a flow cell dimensioned for a particular flow range to minimize departures from linearity.

TABLE 2. RUN #1 - JP-4 FUEL, ANALYSIS

Point #	M	v/c Slope = 0.000375 $(v/c)_{max}$ = 1.50000			v/c^2 Slope = 2.05435 $(v/c^2)_{max}$ = 8217		
		v/c	$\frac{\Delta(v/c)}{(v/c)_{lin}}$ (%)	$\frac{\Delta(v/c)}{(v/c)_{max}}$ (%)	v/c^2	$\frac{\Delta(v/c^2)}{(v/c^2)_{lin}}$ (%)	$\frac{\Delta(v/c^2)}{(v/c^2)_{max}}$ (%)
1	4692	1.738	-1.25	-1.47	9596	-0.45	-0.52
2	3884	1.453	-0.28	-0.27	7985	0.075	0.073
11	3176	1.170	-1.76	-1.40	6438	-1.32	-1.05
3	3159	1.178	-0.59	-0.47	6490	0	0
4	2492	0.9512	1.81	1.13	5114	-0.098	-0.061
5	1955	0.7334	0.04	0.02	4031.5	0.39	0.19
6	1416	0.5360	0.94	0.33	2936	0.93	0.33
7	855.5	0.3332	3.87	0.83	1819	3.53	0.76
8	446.6	0.1840	9.85	1.10	970.5	5.78	0.65
9	211.1	0.0988	24.7	1.31	478.2	10.3	0.54
10	38.82	0.0211	44.5	0.43	100.1	25.5	0.25
				a. d. = 0.80%			a. d. = 0.40%

TABLE 2 - Continued

Point #	$\dot{M}$	v (Slope = 0.6905, $(v)_{max}$ = 2762)	$\frac{\Delta(v)}{(v)_{lin}}$ (%)	$\frac{\Delta(v)}{(v)_{max}}$
1	4692	3193	-1.45	-1.70
2	3884	2674	-0.295	-0.290
11	3176	2143	-2.28	-1.81
3	3159	2225	2.02	1.59
4	2492	1710	-0.639	-0.398
5	1955	1348	-0.148	-0.205
6	1416	987.6	1.01	0.358
7	855.5	613.9	3.89	0.833
8	446.6	345.8	12.1	1.35
9	211.1	205.6	41.0	2.16
10	38.82	44.2	64.9	0.630
				a.d. = 1.03%

TABLE 3. RUN #2 - JP-4 FUEL, ANALYSIS

Point #	$\dot{M}$	v/c Slope = 0.0003726 $(v/c)_{max}$ = 1.490			v/c^2 Slope = 2.15909 $(v/c^2)_{max}$ = 8636		
		v/c	$\frac{\Delta(v/c)}{(v/c)_{lin}}$ (%)	$\frac{\Delta(v/c)}{(v/c)_{max}}$ (%)	v/c^2	$\frac{\Delta(v/c^2)}{(v/c^2)_{lin}}$ (%)	$\frac{\Delta(v/c^2)}{(v/c^2)_{max}}$ (%)
10	4396	1.630	-0.49	-0.54	9398	-0.98	-1.08
11	4299	1.606	0.25	0.27	9286	0.04	0.05
9	3993	1.477	-0.74	-0.74	8527	-1.09	-1.09
12	3679	1.372	0.07	0.07	7978	0.44	0.41
8	3557	1.308	-1.28	-1.14	7531	-1.93	-1.71
13	3347	1.246	-0.08	-0.07	7262	0.50	0.42
7	3114	1.150	-0.86	-0.67	6696	-0.40	-0.31
14	2794	1.040	-0.10	-0.07	6034	0.033	0.023
6	2603	0.9757	-0.60	0.39	5662	0.75	0.49
15	2253	0.8343	-0.62	-0.35	4882	0.37	0.21
5	1965	0.7456	1.83	0.90	4318	1.77	0.87
16	1725	0.6370	-0.89	-0.38	3738	0.38	0.16
4	1546.4	0.5838	1.32	0.51	3446	3.20	1.24
17	1338	0.4899	-1.73	-0.58	2898	0.31	0.10
3	1023.9	0.3838	0.60	0.15	2306	4.30	1.10
18	775.5	0.2196	-24.0	-4.66	1728	3.23	0.63
2	614.7	0.2419	5.63	0.87	1433	7.99	1.23
1	221.8	0.1078	30.5	1.69	548.8	14.6	0.81
				a.d. = 0.78%			a.d. = 0.66%

TABLE 3 - Continued

Point #	$\dot{M}$	v	$\frac{\Delta(v)}{(v)_{lin}}$ (%)	$\frac{\Delta(v)}{(v)_{max}}$ (%)
		v Slope = 0.6455 $(v)_{max}$ = 2582		
10	4396	2842	0.176	0.192
11	4299	2730	-1.62	-1.74
9	3993	2580	0.116	0.116
12	3679	2384	0.379	0.349
8	3557	2282	-0.610	-0.542
13	3347	2156	-0.185	-0.155
7	3114	1990	-1.0	-0.775
14	2794	1805	0.109	0.007
6	2603	1695	0.890	0.581
15	2253	1442	-0.825	-0.465
5	1965	1300	2.5	1.24
16	1725	1097	-1.44	-0.620
4	1546.4	991.2	-0.67	-0.259
17	1338	834.6	-3.47	-1.16
3	1023.9	649.7	-1.6	-0.434
18	775.5	493.0	-1.52	-0.294
2	614.7	394.2	-0.66	-0.101
1	221.8	21[illegible].5	49	2.69
				a. d. = 0.53% after omitting Pt. #1, which is > SLE

TABLE 4. RUN #3 - JP-4 FUEL, ANALYSIS

Point #	$\dot{M}$	v/c Slope = 0.000339, $(v/c)_{max}$ = 1.357			v/c^2 Slope = 1.9375, $(v/c^2)_{max}$ = 7750		
		v/c	$\frac{\Delta(v/c)}{(v/c)_{lin}}$ (%)	$\frac{\Delta(v/c)}{(v/c)_{max}}$ (%)	v/c^2	$\frac{\Delta(v/c^2)}{(v/c^2)_{lin}}$ (%)	$\frac{\Delta(v/c^2)}{(v/c^2)_{max}}$ (%)
10	4474	1.517	0.20	0.22	8621.5	-0.53	-0.59
9	3728	1.264	0.48	0.44	7146	-1.07	-0.99
8	2939	0.9963	0.29	0.21	5663.5	-0.53	-0.39
7	2397	0.8126	0	0	4638	-0.13	-0.08
6	1786	0.6055	-0.66	-0.30	3463.5	+0.12	0.05
5	1301	0.4410	-1.56	-0.52	2596	2.98	0.97
4	712	0.2414	-5.81	-1.10	1431.5	3.77	0.67
3	512.1	0.1736	12.7	-1.86	1066	7.44	0.95
1	314.2	0.1065	-26.0	-2.76	715.8	17.6	1.38
11	171.5	0.0581	-5.99	-0.27	347.75	4.66	0.20
2	147.8	0.0501	-29.4	-1.54	341.5	19.2	0.71
				a. d. = 0.84%			a. d. = 0.63%

TABLE 4 - Continued

Point #	$\dot{M}$	v (Slope = 0.60185, $(v)_{max}$ = 2407)	$\frac{\Delta(v)}{(v)_{lin}}$ (%)	$\frac{\Delta(v)}{(v)_{max}}$
10	4474	2685	-0.297	-0.332
9	3728	2229	-0.557	-0.623
8	2939	1757	-0.678	-0.499
7	2397	1438	-0.347	-0.208
6	1786	1084	0.837	0.374
5	1301	817.2	4.37	1.42
5	712	464.2	8.33	1.48
3	512.1	373.8	21.3	2.72
1	314.2	294.4	55.7	4.38
11	171.5	146.6	42.7	1.80
2	147.8	147.5	65.7	2.43
				a.d. = 1.48%

TABLE 5. RUN #4 - JP-4 FUEL, ANALYSIS

Point #	M	v/c Slope = 0.000336 $(v/c)_{max}$ = 1.344			v/c^2 Slope = 1.9079 $(v/c^2)_{max}$ = 7631.6		
		v/c	$\frac{\Delta(v/c)}{(v/c)_{lin}}$ (%)	$\frac{\Delta(v/c)}{(v/c)_{max}}$ (%)	v/c^2	$\frac{\Delta(v/c^2)}{(v/c^2)_{lin}}$ (%)	$\frac{\Delta(v/c^2)}{(v/c^2)_{max}}$ (%)
10	3976	1.336	0	0	7576	-0.13	-0.13
9	3364	1.129	-0.09	-0.07	6408	-0.16	-0.13
8	2679	0.9030	0.32	0.22	5122	-0.22	-0.14
7	1951	0.6599	0.67	0.33	3741	0.51	0.25
6	1416	0.4820	1.30	0.46	2746	1.63	0.58
5	897.8	0.3101	2.78	0.63	1760	2.74	0.62
4	612.9	0.2158	4.81	0.74	1224	4.70	0.72
3	243.9	0.0891	8.66	0.53	505.4	8.62	0.53
2	99.9	0.0367	9.23	0.23	205.8	7.97	0.20
1	34.14	0.0153	33.0	0.28	85.0	30.6	0.26
				a.d. = 0.35%			a.d. = 0.36%

TABLE 5 - Continued

Point #	$\dot{M}$	v Slope = 0.6079 $(v)_{max}$ = 2432			ρv Slope = 0.3718×10^{-4} $(\rho v)_{max}$ = 148.72×10^{-3}		
		v	$\frac{\Delta(v)}{(v)_{lin}}$ (%)	$\frac{\Delta(v)}{(v)_{max}}$ (%)	ρv	$\frac{\Delta(\rho v)}{(\rho v)_{lin}}$ (%)	$\frac{\Delta(\rho v)}{(\rho v)_{max}}$ (%)
10	3976	2368	2.03	2.01	148.3×10^{-3}	0.318	0.316
9	3364	1946	-4.84	-4.07	125.32	0.200	0.168
8	2679	1600	-1.78	-1.19	100.25	-0.643	-0.430
7	1951	1168	-1.52	-0.740	73.32	-1.08	-0.524
6	1416	852.0	-1.02	-0.362	53.55	-1.71	-0.605
5	897.8	547.3	0.275	0.062	34.42	-3.12	-0.699
4	612.9	381.4	2.36	0.362	23.95	-5.09	-0.780
3	243.9	157.2	6.00	0.366	9.893	-9.10	-0.555
2	99.9	67.1	10.5	0.263	4.079	-9.83	-0.245
1	34.14	26.4	27.5	0.234	1.694	-33.49	-0.286
				a. d. $\pm$ 0.62% after omitting Pt. #9, which is > SLE			a. d. = 0.46%

TABLE 6. RUN #5 - JP-4 FUEL, ANALYSIS

T=110-115°F		v/c Slope = 0.0003077 $(v/c)_{max}$ = 1.2308			v/c^2 Slope = 1.713 $(v/c^2)_{max}$ = 6852		
Point #	$\dot{M}$	v/c	$\frac{\Delta(v/c)}{(v/c)_{lin}}$ (%)	$\frac{\Delta(v/c)}{(v/c)_{max}}$ (%)	v/c^2	$\frac{\Delta(v/c^2)}{(v/c^2)_{lin}}$ (%)	$\frac{\Delta(v/c^2)}{(v/c^2)_{max}}$ (%)
1	5524	1.693	-0.41	-0.56	9382	-0.86	-1.18
2	4977	1.539	0.52	0.65	8552	0.30	0.38
3	4269	1.309	-0.38	-0.41	7312	-0.01	-0.02
4	3773	1.142	-1.64	-1.54	6356	-1.66	-1.56
5	3171	0.9865	1.11	0.88	5512	1.47	1.17
6	2512	0.7704	-0.32	-0.20	4360	1.32	0.83
7	2023	0.6300	1.22	1.62	3550	2.45	1.24
8	1769	0.4401	-19.1	-8.47	2508	-17.2	-7.62
9	1409	0.4447	2.58	0.91	2484	2.90	1.02
10	834	0.2758	7.48	1.56	1504	5.25	1.10
11	480	0.1661	12.5	1.50	857.2	4.26	0.51
12	238	0.1070	46.2	2.75	480.0	17.7	1.06
13	148	0.0786	72.7	2.69	264.2	4.22	1.56
14	78	0.1026	327.5	6.39	189.6	41.9	8.17
				a.d. = 1.59% after omitting Pt. #7, which is > SLE			a.d. = 1.48% after omitting Pt. #14, which is > SLE

TABLE 6 - Continued

T = 110-115°F		v Slope = 0.5645 $(v)_{max}$ = 2258			ρ v Slope = 0.39216×10^{-4} $(\rho v)_{max}$ = 156.86×10^{-3}		
Point #	$\dot{M}$	v	$\frac{\Delta(v)}{(v)_{lin}}$ (%)	$\frac{\Delta(v)}{(v)_{max}}$	ρ v	$\frac{\Delta(\rho v)}{(\rho v)_{lin}}$ (%)	$\frac{\Delta(\rho v)}{(\rho v)_{max}}$ (%)
1	5524	3072	-1.475	-2.04	218.2×10^{-3}	0.739	0.102
2	4977	2793	-0.605	-0.753	198.8	1.84	2.29
3	4269	2364	-1.908	-2.04	169.1	1.02	1.08
4	3773	2061	-3.24	-3.06	147.9	-0.068	-0.064
5	3171	1792	0.112	0.088	127.7	2.65	2.10
6	2512	1377	-2.89	-1.82	99.84	1.35	0.848
7	2023	1141	-0.087	-0.44	81.77	3.08	1.56
8	1769	780.2	-21.87	-9.68	57.21	-17.53	-7.75
9	1409	818.6	2.92	1.03	57.94	4.87	1.71
10	834	526.2	11.77	2.45	36.02	10.12	2.11
11	480	321.6	18.69	2.24	21.73	15.5	1.86
12	238	260.9	94.1	5.60	14.03	50.4	3.00
13	148	176.0	110.6	4.09	10.31	77.8	2.88
14	78	63.46	44.13	0.860	13.50	341	6.66
				a.d. = 2.56%			a.d. = 2.43%

TABLE 7. RUN #6 - JP-4 FUEL, ANALYSIS

$T = 76^{\circ}F$		v/c Slope = 0.0002844 $(v/c)_{max}$ = 1.1376			v/c^2 Slope = 1.4844 $(v/c^2)_{max}$ = 5836.6		
Point #	$\dot{M}$	v/c	$\frac{\Delta(v/c)}{(v/c)_{lin}}$ (%)	$\frac{\Delta(v/c)}{(v/c)_{max}}$ (%)	v/c^2	$\frac{\Delta(v/c)^2}{(v/c^2)_{lin}}$ (%)	$\frac{\Delta(v/c)^2}{(v/c^2)_{max}}$ (%)
1	6585	1.870	-0.16	-0.26	9602	-1.77	-2.91
2	5754	1.627	-0.55	-0.79	8422	-1.39	-2.00
3	4975	1.408	-0.50	-0.62	7308	-1.04	-1.30
4	4647	1.316	-0.45	-0.53	6842	2.15	2.42
5	4074	1.160	0.09	0.09	6042	-0.08	-0.08
6	3359	0.9616	0.66	0.55	5012	0.52	0.44
7	2046	0.5994	3.01	1.54	3110	2.40	1.23
8	1277	0.3784	4.18	1.34	1984	4.64	1.48
9	894	0.2698	6.10	1.36	1406	5.95	1.33
10	439	0.1372	9.85	1.08	713.8	9.53	1.05
11	305	0.0955	10.2	0.77	496.8	9.74	0.74
12	47	0.0159	18.7	0.22	85.0	21.8	0.26
				a.d. = 0.76%			a.d. = 1.27%

TABLE 7 - Continued

T = 76°F		v Slope = 0.5645 $(v)_{max}$ = 2258			ρv Slope = 0.39216×10^{-4} $(\rho v)_{max}$ = 156.86×10^{-3}		
Point #	$\dot{M}$	v	$\frac{\Delta(v)}{(v)_{lin}}$ (%)	$\frac{\Delta(v)}{(v)_{max}}$ (%)	ρv	$\frac{\Delta(\rho v)}{(\rho v)_{lin}}$ (%)	$\frac{\Delta(\rho v)}{(\rho v)_{max}}$ (%)
1	6585	3652	-1.78	-2.92	254.1×10^{-3}	-1.59	-2.61
2	5754	3176	-2.25	-3.23	221.1	-2.04	-2.93
3	4975	2672	-4.88	-6.07	191.2	-2.00	-2.49
4	4647	2560	-2.44	-2.83	178.4	-2.13	-2.42
5	4074	2248	-2.26	-2.30	157.4	-1.50	-1.53
6	3359	1863	-1.74	-1.46	130.5	-0.911	-0.765
7	2046	1164	0.779	0.399	81.22	1.22	0.625
8	1277	729.3	1.15	0.368	51.27	2.38	0.759
9	894	515.8	2.20	0.492	36.56	4.28	0.956
10	439	264.7	6.78	0.744	18.59	7.06	0.873
11	305	184.6	7.20	0.549	12.95	8.28	0.631
12	47	30.6	15.3	0.180	2.15	16.82	0.198
				a.d. = 1.80%			a.d. = 1.40%

It should also be noted that the range gates of the two receivers were adjusted between Run 1 and Run 2. This precludes legitimate comparison of the absolute slopes between Run 1 and the subsequent runs. However, the internal consistency of the various runs is not affected.

Referring to Table 8, we see that the average deviation (% of full scale) of the various measured quantities has a tendency to increase from v/c^2 to v/c to v. The reason for this is attributed to the slight asymmetric saturation of the 2-kHz reference wave, as noted above. During precalibration tests at Panametrics (when this wave was not saturated) it was noted that the readout of $(T_1 + T_2)$ remained stable to within better than 0.1% under constant temperature conditions. Therefore, we would expect that the basic linearities for v/c^2 would prevail for v/c and v for an unsaturated reference wave.

Note also in Table 8 that the deviations from linearity appear to be two to three times higher in the case of diesel fuel than in the case of JP-4. We do not have an explanation for this, but we regard the basic linearity of the v/c^2 data of the JP-4 runs to represent the inherent precision of the velocity dependent portion of the flowmeter.

Since the density vs. temperature characteristic of the JP-4 and diesel fuel samples used in these tests was provided by Avco, and since one can directly compare the slopes of the $\left(\frac{v}{c}\right)(\rho c) = \dot{M}_{meas}$ vs. $\dot{M}$ curves, it is possible to make a number of run-to-run comparisons. Specifically, we will take into account temperature-dependent density change and compare the modified slopes of fluid velocity vs. $\dot{M}$ for Runs 2, 3, 4, 5 and 6. We will also directly compare the slopes of $\dot{M}_{meas}$ vs. $\dot{M}$ for Runs 4 and 5-6. In these comparisons, we will arbitrarily use Run 4 as the reference run.

The following data are needed for the comparisons:

$$\text{JP-4} \begin{cases} \rho(-80^{\circ}\text{F}) = 0.836 \text{ gm/cc} \\ \rho(240^{\circ}\text{F}) = 0.692 \end{cases}$$

$$\text{Marine Diesel I VVF 800} \begin{cases} \rho(76^{\circ}\text{F}) = 0.830 \text{ gm/cc} \\ \rho(113^{\circ}\text{F}) = 0.823 \end{cases}$$

TABLE 8. AVERAGE DEVIATIONS (% OF FULL SCALE)

Run #	Fuel and Temperature	v/c^2 (%)	v/c (%)	v (%)	ρv (%)
1	JP-4 75°F	0.40	0.80	1.03	-
2	JP-4 100-103°F	0.66	0.78	0.53	-
3	JP-4 75°F	0.63	0.84	1.48	-
4	JP-4 75°F	0.36	0.35	0.62	0.46
5	Deisel 110-115°F	1.48	1.59	2.56	2.43
6	Deisel 75°F	1.27	0.76	1.80	1.40

Data taken at Avco/Lycoming, June 19-21, 1974.
All data plotted vs. $\dot{M}$ ($\pm$ 0.2%) as measured by Avco.

Using the above data, we find that the temperature dependences of the densities are

$$\frac{1}{\rho}\frac{\partial \rho}{\partial T} = \begin{cases} \text{JP-4:} & -\ 0.06\%\ \text{Deg F}^{-1} \\ \text{Diesel:} & -\ 0.23\%\ \text{Deg F}^{-1} \end{cases}$$

Applying the above velocity vs. $\dot{M}$ slopes as computed in Appendix A, we have the following direct comparisons among the runs:

Run #	Slope deviation (%)	
2	+4.5	Run 4 used as standard
3	-1.0	
5	+0.2	
6	+1.1	

Next, we directly compare the slope of the combined 5 and 6 with Run 4. Even though the fuels are different, the $\dot{M}$ curves should agree. Inspection of the curves of $(v/c)(\rho c)$ vs. $\dot{M}$ for Runs 4, 5 and 6 (Appendix A) for $\dot{M}$ = 4000 lb/hr shows:

Run 4 (JP-4): $\left(\frac{v}{c}\right)(\rho c) = 148$

Runs 5 and 6 (Diesel): $\left(\frac{v}{c}\right)(\rho c) = 155$

The ratio of the above values is 0.955. Thus, the two runs agree to within 4.5%.

It is interesting to inspect the curves of Runs 5 and 6 as follows: First, referring to v/c^2 vs. $\dot{M}$, note the large difference in slopes between the elevated temperature (5) curve and the room temperature (6) curve. Next, inspecting the v/c vs. $\dot{M}$ curves, we see that the slopes are much closer. Next, inspecting the $(v/c)(\rho c)$ vs. $\dot{M}$ curve, we see that the slopes coincide much more closely. This shows that the system is compensating for the temperature difference between the 5 and 6 runs. Also, note that the slopes essentially coincide in the case of v vs. $\dot{M}$. The reason for this is that the fractional sound speed variation of the diesel fuel is -1.73×10^{-3} deg F^{-1}, while the density dependence on temperature is only -2.29×10^{-4} deg F^{-1}. This fact, however, does not suggest that the (ρc) unit was not performing an important correction. This correction is directly seen in comparing the (v/c) vs. $\dot{M}$ curves of Runs 5 and 6,

and noting that the difference in (ρ c) alone brought the two (v/c) curves into coincidence.*

CALIBRATION TESTS AT AVCO/LYCOMING DECEMBER 1974

In this section, we present the results of a series of tests run at Avco/ Lycoming on December 17-18, 1974. The tests were run on JP-4 fuel at three basic temperatures. These were 50°F, 72°F, and 101°F. Two separate and independent data runs were made at each basic temperature in order to obtain numerical estimates of the precision of the flowmeter. The basic data were taken in a manner identical to that used during the June 1974 tests.

The numerical data taken during these tests are presented in both numerical and graphical form in Appendix A. The analysis presented in this section is based entirely upon these numerical data.

As mentioned in the Conclusions, the (ρ c) data exhibited drift substantially in excess of that required for a final instrument. It was, therefore, decided that the density data to be used would be the best available under the circumstances. This was obtained with the hydrometer which is permanently installed in the Cox test stand at Avco. In addition, an uncalibrated Simmonds densitometer was obtained on loan from Simmonds Precision Instrument Corporation, Vergennes, Vermont, and data was taken on this during all tests in order to obtain a measure of its stability and reproducibility as a potential candidate for use in a final prototype unit.

As was noted in the case of the June 1974 tests, two of the six runs exhibited a slight nonlinearity at very low flow rates. In these (December) tests, a Kenics "Static Mixer" (see Fig. B-9) was incorporated immediately upstream of the flow cell. As can be seen from inspection of the data plots in Appendix A, no such nonlinearities were observed in the December test results.

*Based on subsequent saturation tests and analyses of the densitometer, it appears that the excellent stability of the echo comparator ρ c electronics, ~0.1%, observed during these isothermal calibration tests may have been obtained as a tradeoff with linearity. Such a tradeoff could account for the 4.5% slope difference between Run 4 and Runs 5 and 6 mentioned on the previous page. Nonlinear response could also account for the observed difference of a few percentage points between calculated and measured ρ c change in individual fuels tested at Avco during fuel heating and cooling cycles.

The Avco measurements were done under the direct supervision of Mr. Joseph Balcher, who participated in all phases of the tests. The quantities measured by Avco were mass flow rate $\dot{M}$ (lb/hr), density ρ (gm/cc), and temperature (deg F).

The Panametrics measurements were readings of the digital display on the front panel of the flowmeter electronics package. The units of these measurements are machine units, as was the case in the June 1974 tests. The quantities measured were v/c^2, v/c, v, $T_1 + T_2$, and V_s, where v = fluid velocity, c = sound velocity, T_1 and T_2 are the upstream and downstream transit times, and V_s = Simmonds densitometer output (volts). As in the June tests, two readings were taken for each test point, one of these corresponding to reversed transducer leads. As already shown, the average of these produces a result which eliminates residual instrumental zero offset.

ANALYSIS OF DATA FROM FIELD TEST #2

As mentioned above, two separate data runs were made for each of the temperatures (~50°F, ~70°F, and ~100°F). The two data runs corresponding to a given temperature were <u>not</u> run simultaneously. If two such runs are taken together, included in the scatter of data will be such effects as mechanical and thermal hysteresis as well as a potential long term electronic drift. Thus, the data can be analyzed in three ways:

(a) Linearity. This is expressed as the average or standard deviation, expressed as % of full scale, of the data points of a given run, from the best least squares straight-line fit.

(b) Precision. The average or standard deviation from the least squares linear fit of the data points of two separate data runs gives a good measure of the precision of the flow measuring system for a given T.

(c) Temperature effects. The average or standard deviation from the least squares linear fit of the data points of all data points would give a measure of the precision, including fluid temperature effects. However, if a definite trend in the deviation is observed, the precision index computed in this manner would be artificially high. Instead, if such a trend were observed, a temperature-dependent coefficient should be introduced for the purpose of eliminating the effect of fluid temperature on precision.

(d) Accuracy. Since the velocity data were taken as a function of quantitative $\dot{M}$ and ρ measurements, the potential accuracy of the system would be essentially the same as the precision discussed in (b) above.

One is nearly always limited by the amount of experimental data in the specification of precision indices. In this series of tests, sixty-five separate values of $\dot{M}$ were run. Although we would, of course, like to see much more data, we believe that this number of independent measurements constitutes a good base on which to base estimates of linearity, precision and temperature dependence.

ANALYSIS OF INDIVIDUAL DATA RUNS

Each of the six data runs was analyzed by means of computing the average deviation* from the best linear least squares fit to the data. Since fluid velocity is the basic quantity measured by the instrument, we have normalized the Avco measured $\dot{M}$ by the product of the Avco measured ρ and the known cross-sectional area A = 1/2 in.^{2} of the flow cell, to give units of ft/sec. These are given in Tables 9 through 14 and are the standards against which v(exp) is measured in machine units. From these two columns, the best linear fit is obtained. Then, the value of velocity in machine units is computed for a perfect fit. This we denote by v(calc). The difference Δv = v(exp) - v(calc) is then computed. Next, $|\Delta v|$ is given as a percent of full scale. These results appear in the right-hand column. Finally, the average deviation (a. d.) is computed for each individual data run. These values appear at the bottom of each table. Note that the density (specific gravity units) and temperature (^{o}F) are given at the top of each table.

The significant result of these analyses is that the average deviations from linearity are very small: 0.15%, 0.10%, 0.10%, 0.14%, 0.13% and 0.18% for Runs 1 through 6, respectively.

ANALYSIS OF PAIRS OF RUNS

As mentioned earlier, two separate data runs were made at each temperature. The time sequence of these is given below:

Run #	Temperature (^{o}F)	Time
1	75	December 17, a.m.
2	101	December 17, p.m.
3	51	December 18, a.m.
4	72	December 18, a.m.
5	50	December 18, p.m.
6	102	December 18, p.m.

*Note that the standard deviation is equal to the average deviation, multiplied by the factor 1.25.

TABLE 9. RUN #1 - JP-4 FUEL, ANALYSIS
$o = 0.756$
$T = 75^{o}F$

Point #	$\dot{M}/\rho A$ (ft/sec)	v (exp)	v (calc)	Δv $(v_{exp} - v_{calc})$	$\frac{\lvert \Delta v \rvert}{v_{max}}$ (%)
1	7.879	3193	3185	8.0	0.25
2	6.787	2742	2745	-3.0	0.09
3	5.904	2382	2389	-7.0	0.22
4	5.067	2058	2052	6.0	0.19
5	4.266	1724	1730	-6.0	0.19
6	3.409	1384	1384	0.0	0.00
7	2.532	1032	1031	1.0	0.03
8	1.724	698.8	705.4	-6.6	0.21
9	0.8846	366.5	367.4	-0.9	0.03
10	0.4269	181.0	183.0	-2.0	0.06
11	0.1980	101.3	90.9	10.4	0.33

Data taken at Avco/Lycoming, December 17, 1974 a.m.

Average deviation = 0.15%

TABLE 10. RUN #2 - JP-4 FUEL, ANALYSIS
ρ = 0.744
T = 101°F

Point #	$\dot{M}/\rho A$ (ft/sec)	v (exp)	v (calc)	Δv $(v_{exp}-v_{calc})$	$\frac{\lvert\Delta v\rvert}{v_{max}}$ (%)
1	7.635	3058	3062	-4.0	0.13
2	6.803	2731	2729	2.0	0.07
3	6.236	2506	2502	4.0	0.13
4	5.531	2220	2221	-1.0	0.03
5	5.067	2038	2035	3.0	0.10
6	4.289	1728	1724	4.0	0.13
7	3.541	1418	1425	-7.0	0.23
8	2.551	1025	1029	-4.0	0.13
9	1.977	801.6	799.4	2.2	0.07
10	1.175	477.4	478.5	-1.1	0.04
11	0.6151	256.9	254.6	2.3	0.08

Data taken at Avco/Lycoming, December 17, 1974 p.m.

Average deviation = 0.10%

TABLE 11. RUN #3 - JP-4 FUEL, ANALYSIS
ρ = 0.766
T = 51.5°F

Point #	$\dot{M}/\rho A$ (ft/sec)	v (exp)	v (calc)	Δv $(v_{exp}-v_{calc})$	$\frac{\lvert \Delta v \rvert}{v_{max}}$ (%)
1	8.364	3422	3420	2.0	0.06
2	7.534	3086	3081	5.0	0.15
3	6.572	2685	2689	-4.0	0.12
4	5.708	2332	2337	-5.0	0.15
5	4.749	1946	1946	0.0	0.00
6	3.870	1586	1588	-2.0	0.06
7	2.935	1212	1206	6.0	0.18
8	2.031	835.6	837.9	-2.3	0.07
9	1.165	481.0	484.7	-3.7	0.11
10	0.5566	235.0	236.6	-1.6	0.05
11	0.2769	128.4	122.6	5.8	0.17

Data taken at Avco/Lycoming, December 18, 1974 a.m.

Average deviation = 0.10%

TABLE 12. RUN #4 - JP-4 FUEL, ANALYSIS
ρ = 0.758
T = 72.5°F

Point #	$\dot{M}/\rho A$ (ft/sec)	v (exp)	v (calc)	Δv $(v_{exp}-v_{calc})$	$\frac{\lvert\Delta v\rvert}{v_{max}}$ (%)
1	7.971	3220	3222	-2.0	0.06
2	6.237	2898	2895	3.0	0.09
3	6.237	2536	2524	12.0	0.37
4	5.421	2188	2194	-6.0	0.19
5	4.603	1858	1865	-7.0	0.22
6	3.859	1561	1565	-4.0	0.12
7	3.144	1278	1277	1.0	0.03
8	2.049	834.5	835.6	-1.1	0.03
9	1.166	482.1	479.7	2.4	0.07
10	0.4570	189.8	193.9	-4.1	0.13
11	0.2498	116.8	110.4	6.4	0.20

Data taken at Avco/Lycoming, December 18, 1974 a.m.

Average deviation = 0.14%

TABLE 13. RUN #5 - JP-4 FUEL, ANALYSIS
ρ = 0.767
T = 50°F

Point #	$\dot{M}/\rho A$ (ft/sec)	v (exp)	v (calc)	Δv ($v_{exp}-v_{calc}$)	$\frac{\lvert\Delta v\rvert}{v_{max}}$ (%)
1	8.389	3398	3398	0.0	0.00
2	7.740	3138	3136	2.0	0.06
3	6.827	2766	2768	-2.0	0.06
4	5.950	2413	2414	-1.0	0.03
5	5.099	2062	2071	-9.0	0.26
6	4.114	1678	1673	5.0	0.15
7	3.159	1298	1288	10.0	0.29
8	2.234	918.3	914.4	3.9	0.11
9	1.317	531.5	544.7	-13.2	0.39
10	0.8240	345.4	345.6	-0.2	0.01
11	0.5422	235.8	231.9	3.9	0.11

Data taken at Avco/Lycoming, December 18, 1974 p.m.

Average deviation = 0.13%

TABLE 14. RUN #6 - JP-4 FUEL, ANALYSIS
ρ = 0.744 (adjusted)
T = 102°F

Point #	$\dot{M}/\rho A$ (ft/sec)	v (exp)	v (calc)	Δv (v_{exp}-v_{calc})	$\frlvert\Delta v\frrvert / v_{max}$ (%)
1	6.998	2790	2798	-8.0	0.29
2	6.238	2492	2493	-1.0	0.04
3	5.507	2204	2200	4.0	0.14
4	4.811	1930	1922	8.0	0.29
5	4.033	1612	1610	2.0	0.07
6	3.259	1296	1300	-4.0	0.14
7	2.477	996.5	986.8	9.7	0.35
8	1.721	676.8	684.0	-7.2	0.26
9	0.9539	372.0	376.7	-4.7	0.17
10	0.5955	234.4	233.1	1.3	0.05

Data taken at Avco/Lycoming, December 18, 1974 p.m.

Average deviation = 0.18%

Due to the fact that no two runs at a given temperature were made consecutively, if we analyze the composite results of each set of runs at the same temperature, we can obtain a good measure of the precision of the flowmeter. This has been done and the results are given in Tables 15, 16 and 17. The method of analysis is identical to that used for the individual runs, except that the combined data of two runs is used in each analysis.

The significant result of these analyses is that the average deviations from the best linear fit are 0.25%, 0.14% and 0.21% for Runs 3 and 5, 1 and 4 and 2 and 6, respectively.

It should be noted that, since the Avco density measurement is subject to a possible maximum error of $\pm$ 0.2%, it is best to take the measured density at the median temperature (75°F), at which ρ = 0.756 gm/cc, and to then correct the readings at 50° and 101° if necessary. This can be done because the slope of the JP-4 density vs. temperature characteristic curve is well known by Avco to be -0.0004 gm/cc per deg F. Thus, when analyzing two or more sets of data, it was not necessary to include the potential errors of multiple measurements of density. As it turned out, it was necessary to correct only one of the density readings. This was the density measurement of Run 6, in which the measured density was 0.746 gm/cc and the corrected density was 0.744 gm/cc. This correction was not necessary when analyzing the individual runs for linearity, since the measured density was a constant for each run. It was, however, necessary to use the correction in the composite analysis of all six runs, which we next describe.

COMPOSITE ANALYSIS OF THE SIX RUNS

Next, in order to include the effects of variable fluid temperature, we analyzed the combination of all six data runs. The same analysis procedures were used as in the foregoing cases. As mentioned above, density was corrected on the basis of ρ (75°F) = 0.756 gm/cc and $\partial \rho / \partial T$ = 0.0004 gm/cc per deg F.

The significant results of this analysis were: (a) the average deviation was 0.32% and (b) a definite temperature-dependent trend is observed. Notice that the sign of Δv, given in Table 18, is very predominantly positive for the low temperature data, is mixed for the room temperature data, and is very predominantly negative in the case of the high temperature data. This is, of course, a very small effect, since the average deviation for the six-run composite analysis is only about 0.1% greater than the mean of the average deviations of the runs taken two at a time. However, this dependence can be measured in more extensive tests over a considerably wider temperature range, and the final instrument can be

TABLE 15. RUNS #3 AND #5 - JP-4 FUEL, COMPOSITE ANALYSIS
$T_5 = 50^{\circ}F$
$T_3 = 51.5^{\circ}F$

$\dot{M}/\rho A$ (ft/sec)	v (exp)	v (calc)	Δv $(v_{exp}-v_{calc})$	$\frac{\lvert \Delta v \rvert}{v_{max}}$ (%)
8.364	3422	3403	19.0	0.56
7.534	3086	3067	19.0	0.56
6.572	2685	2676	9.0	0.26
5.708	2332	2326	6.0	0.18
4.749	1946	1937	9.0	0.26
3.870	1586	1581	5.0	0.15
2.935	1212	1202	10.0	0.29
2.031	835.6	835.2	0.4	0.01
1.165	481.0	484.0	-3.0	0.09
0.5566	235.0	237.3	-2.3	0.07
0.2769	128.4	123.9	4.5	0.13
8.389	3398	3413	-15.0	0.44
7.740	3138	3150	-12.0	0.35
6.827	2766	2780	-14.0	0.41
5.950	2413	2424	-11.0	0.32
5.099	2062	2079	-17.0	0.50
4.114	1678	1680	-2.0	0.06
3.159	1298	1293	5.0	0.15
2.234	918.3	917.3	1.0	0.03
1.317	531.5	545.8	-14.3	0.42
0.8240	345.4	345.7	-0.3	0.02
0.5422	235.8	231.5	4.3	0.13

TABLE 16. RUNS #4 AND #1 - JP-4 FUEL, COMPOSITE ANALYSIS
T_4 = 75°F
T_1 = 72.5°F

$\dot{M}/\rho A$ (ft/sec)	v (exp)	v (calc)	Δv $(v_{exp}-v_{calc})$	$\frac{\lvert \Delta v \rvert}{v_{max}}$ (%)
7.971	3220	3222	-2.0	0.06
7.160	2898	2895	3.0	0.09
6.237	2536	2523	-13.0	0.40
5.421	2188	2195	-7.0	0.22
4.603	1858	1865	-7.0	0.22
3.859	1561	1565	-4.0	0.12
3.144	1278	1277	1.0	0.03
2.049	834.5	836.2	1.7	0.05
1.166	482.1	480.4	1.7	0.05
0.4570	189.8	194.7	-4.9	0.15
0.2498	116.8	111.2	5.6	0.17
7.879	3193	3185	8.0	0.25
6.789	2742	2745	-3.0	0.09
5.904	2382	2389	-7.0	0.22
5.067	2058	2052	6.0	0.19
4.266	1724	1729	-5.0	0.16
3.409	1384	1384	0.0	0.00
2.532	1032	1031	1.0	0.03
1.724	698.8	705.0	-6.2	0.19
0.8846	366.5	367.0	-0.5	0.02
0.4269	181.0	182.6	-1.6	0.05
0.1980	101.3	90.4	10.9	0.34

TABLE 17. RUNS #2 AND #6 - JP-4 FUEL, COMPOSITE ANALYSIS
ρ_6 adjusted to 0.744
T_2 = 101°F
T_6 = 102°F

$\dot{M}/\rho A$ (ft/sec)	v (exp)	v (calc)	Δv ($v_{exp}-v_{calc}$)	$\frac{\lvert\Delta v\rvert}{v_{max}}$ (%)
7.635	3058	3059	-1.0	0.03
6.803	2731	2725	6.0	0.20
6.236	2506	2498	8.0	0.26
5.531	2220	2216	4.0	0.13
5.067	2038	2030	8.0	0.26
4.289	1728	1719	9.0	0.29
3.541	1418	1419	-1.0	0.03
2.551	1025	1023	2.0	0.07
1.977	801.6	792.8	8.8	0.29
1.175	477.4	471.5	5.9	0.19
0.615	256.9	247.2	9.7	0.32
6.998	2790	2803	-13.0	0.42
6.238	2492	2499	-7.0	0.23
5.507	2204	2206	-2.0	0.07
4.811	1930	1927	3.0	0.10
4.033	1612	1616	-4.0	0.13
3.259	1296	1306	-10.0	0.33
2.477	996.5	992.9	3.6	0.12
1.721	676.8	690.1	-13.3	0.43
0.9539	372.0	382.9	-10.9	0.36
0.5955	234.4	239.4	-5.0	0.16

TABLE 18. RUNS #1 THROUGH #6 - JP-4 FUEL, COMPOSITE ANALYSIS
All ρ's adjusted to ρ = 0.756 for T = 75°F
using $\Delta\rho$ = 0.0004/deg F

T (°F)	$\dot{M}/\rho A$ (ft/sec)	v (exp)	v (calc)	Δv ($v_{exp}-v_{calc}$)	$\frac{\lvert\Delta v\rvert}{v_{max}}$ (%)
	8.400	3398	3395	3.0	0.09
	7.751	3138	3133	5.0	0.15
	6.836	2766	2764	2.0	0.06
	5.598	2413	2410	3.0	0.09
	5.105	2062	2066	-4.0	0.12
	4.119	1678	1668	10.0	0.29
	3.164	1298	1283	15.0	0.44
	2.236	918.3	908.5	9.8	0.29
50°	1.320	531.5	538.9	-7.4	0.22
(Run 5)	0.8252	345.4	339.3	6.1	0.18
	0.5428	235.8	225.5	10.3	0.30
	8.372	3422	3383	39.0	1.15
	7.539	3086	3047	39.0	1.15
	6.577	2685	2659	26.0	0.77
	5.713	2332	2311	21.0	0.62
	4.753	1946	1924	22.0	0.65
	3.873	1586	1569	17.0	0.50
	2.937	1212	1191	21.0	0.62
	2.032	835.6	826.3	9.3	0.27
	1.166	481.0	476.7	2.3	0.07
51.5°	0.5571	235.0	231.2	3.8	0.11
(Run 3)	0.2771	128.4	118.3	10.1	0.30
72.5°	7.982	3220	3226	-6.0	0.18
(Run 4)	7.169	2898	2898	0.0	0.00

TABLE 18 - Continued

T (°F)	$\dot{M}/\rho A$ (ft/sec)	v (exp)	v (calc)	Δv ($v_{exp}-v_{calc}$)	$\frac{\lvert\Delta v\rvert}{v_{max}}$ (%)
	6.245	2536	2525	11.0	0.32
	5.427	2188	2196	- 8.0	0.24
	4.610	1858	1866	- 8.0	0.24
	3.864	1561	1564	- 3.0	0.09
	3.147	1278	1276	2.0	0.06
	2.052	834.5	834.1	0.4	0.01
	1.168	482.1	477.5	4.6	0.14
72.5°	0.4576	189.8	191.1	- 1.3	0.04
(Run 4)	0.2500	116.8	107.3	9.5	0.28
	7.879	3198	3184	9.0	0.26
	6.789	2742	2744	- 2.0	0.06
	5.904	2382	2388	- 6.0	0.18
	5.067	2058	2050	8.0	0.24
	4.266	1724	1727	- 3.0	0.09
	3.409	1384	1381	3.0	0.09
	2.532	1032	1028	4.0	0.12
	1.724	698.8	701.7	2.9	0.09
	0.8846	366.5	363.3	3.2	0.09
75°	0.4269	181.0	178.7	2.3	0.07
(Run 1)	0.1980	101.3	86.4	14.9	0.44
	7.620	3058	3080	-22.0	0.65
	6.789	2731	2745	-14.0	0.41
	6.222	2506	2516	-10.0	0.29
	5.519	2220	2233	-13.0	0.38
101°	5.057	2038	2046	- 8.0	0.24
(Run 2)	4.280	1728	1733	- 5.0	0.15

TABLE 18 - Continued

T (°F)	$\dot{M}/\rho A$ (ft/sec)	v (exp)	v (calc)	Δv (v_{exp}-v_{calc})	$\frac{\Delta v}{v_{max}}$ (%)
	3.534	1418	1432	-14.0	0.41
	2.545	1025	1033	- 8.0	0.24
	1.974	801.6	802.5	- .9	0.03
101°	1.173	477.4	479.5	- 2.1	0.06
(Run 2)	0.6137	256.9	254.0	2.9	0.08
	6.987	2790	2825	-35.0	-1.03
	6.228	2492	2519	-27.0	0.80
	5.498	2204	2224	-20.0	0.59
	4.803	1930	1944	-14.0	0.41
	4.025	1612	1630	-18.0	0.53
	3.254	1296	1319	-23.0	0.68
	2.473	996.5	1004	- 7.6	0.22
	1.718	676.8	699.7	-22.9	0.67
102°	0.9524	372.0	390.7	-18.7	0.55
(Run 6)	0.5945	234.4	246.3	-11.9	0.35

Data taken at Avco/Lycoming, December 17, 18, 1974.

Average deviation = 0.32%

calibrated so that any such temperature dependence need not affect the measurement accuracy.

SUMMARY OF RESULTS

The analytical results of the December Avco/Lycoming tests are summarized in Table 19. Although these have been individually discussed above, it is of interest to inspect them in one table and to note how the average deviations (a. d. 's) vary from run to run and among the composites. The mean of the average deviations for the individual run analyses is 0. 13%; the mean of the average deviations of the three analyses of runs taken in pairs is 0. 20%; and the average deviation for all six runs taken together is 0. 32%. It appears as though the precision of the velocity measuring instrument can be given by an average deviation of about $\pm$0. 2%, which corresponds to a standard deviation of $\pm$0. 25%. The observed temperature dependence of the overall composite analysis indicates that a final instrument should be calibrated over a reasonably wide range of temperatures.

The Simmonds densitometer, although uncalibrated, demonstrated remarkable stability and reproducibility. This can be seen from the V_s data of Appendix A. Using the approximate formula (given by Simmonds)

$$\rho\,(\mathrm{gm/cc}) \simeq 0.71\,(1 + V_s/15) \qquad (22)$$

where V_s = output of densitometer in volts, the stability of the densitometer is exceptionally good. Using the above formula, and taking the extremes of the V_s data for Runs 3 and 5 combined, the variation in indicated density is 0. 1% from ρ_{max} to ρ_{min}. A similar calculation for Runs 1 and 4 gives a 0. 2% overall indicated density variation, while Runs 2 and 6 give an indicated density range of 0. 1%. Although the density computed from the above (rule of thumb) equation differs from the corresponding Avco value by about one percent, a calibrated Simmonds densitometer should be considered as the prime candidate for an alternative means of providing fluid density for the final mass flowmeter system. Simmonds has made extensive measurements on JP-4 fuel over a wide range of temperatures and mixtures. As a result of these measurements, Simmonds states* that the errors associated with their densitometer are conservatively within a 2σ value of 0. 5%, which is equivalent to an average deviation of 0. 2%. Although the Simmonds instrument might not be used in the main fuel line, it could be used in a bypass line, in which only a small

*Discussions between N. Pedersen and D. Stuart of Simmonds Precision Instrument Corporation.

TABLE 19. SUMMARY OF RESULTS

Run #	Temperature (°F)	Average Deviation of $\frac{\lvert \Delta v \rvert}{v_{max}}$ (% of full scale)	Standard Deviation $\frac{\lvert \Delta v \rvert}{v_{max}}$ (%) of full scale)
1	72.5	0.15	0.19
2	101	0.10	0.13
3	51.5	0.10	0.13
4	75	0.14	0.18
5	50	0.13	0.16
6	102	0.18	0.22
3 and 5	51.5 and 50	0.25	0.31
4 and 1	75 and 72.5	0.14	0.18
2 and 6	101 and 102	0.21	0.26
1, 2, 3, 4, 5 and 6	50 through 102	0.32	0.40

fraction of the total flow would take place* the temperature of the fluid in the bypass could be monitored and, if necessary, a small correction could be supplied to be utilized in the final $\dot{M}$ computation.

VIBRATION TESTS

Referring to Fig. 4, the components considered most likely to fail in a vibration test were the transducers, the ρc densitometer probe and the soldered screen.

A test plate was designed and fabricated, upon which the above components were mounted. Then, on July 5, 1974, a vibration test was conducted by Associated Testing Laboratories, Inc., Burlington, Massachusetts. The test generally followed MIL-E-5009D. Test levels were:

5 to 14 Hz	0.5 in. double amplitude
14 to 150 Hz	$\pm$ 5 g's
150 to 500 Hz	$\pm$ 20 g's

Also, one 15-minute logarithmic sweep (5-500-5 Hz) was performed in each mutually perpendicular plane. No resonances were noted.

From these observations, it was concluded that the items tested can withstand the vibration environment specified.

*Note that the bypass line would not be in parallel with the flow cell, but would preferably be downstream relative to the flow cell.

CONCLUSIONS

A mass flowmeter system has been designed, fabricated, and tested for fuel flows in excess of 4000 lb/hr. Two separate test series were run. The first test runs were made in June 1974, while the second were made in December 1974. The overall results of the June Avco/Lycoming tests show that, for JP-4 fuel, velocimeter linearity of better than 1% and reproducibility from one day to the next on the order of $\pm$ 1% of full scale have been achieved. During the tests, it was observed that the $(T_1 + T_2)$ portion of the measurement was operating under nonideal conditions. The problem was subsequently corrected, and it was anticipated that the linearity and reproducibility of the v and v/c results would be consistently within 0.5% in future tests. This was expected to be confirmed in the second series of calibration tests to be conducted.

The second series of tests at Avco/Lycoming, run on JP-4 in December 1974, did in fact confirm the above predictions. The six individual velocity data runs showed average deviations of less than 0.2% of full scale, while the mean of the average deviations was 0.13%. The average deviation associated with measurement precision was 0.25% or less, while the mean of these average deviations was 0.2%. The data were taken over a temperature range of ~50°F to ~100°F. When all the runs were analyzed together, it was found that the average deviation for the six run composite was 0.32%. Thus, one can reasonably conclude that a slight fuel temperature effect is present and gives a deviation from linearity of ~0.2% per 100°F. This can be taken into account in the final instrumental calibration and should not be considered to be a measurement error.

The instrumentation required to perform the v and v/c measurements has been demonstrated to be stable and reliable over many hundreds of hours of operation. There is no doubt that a reliable and accurate flowmeter can be fabricated. Also, the area-averaging technique, utilizing a 1" x 1/2" rectangular duct with screened ports and gradual inlet transition, has been demonstrated to provide linear phase shift as a function of flow velocity over a 50:1 range of flow, including the laminar, transitional, and turbulent flow regimes. Departures from linearity have not been observed except in some cases at unmixed flows less than 10% of full scale.

Although significant improvements have been made in reduction of the voltage drift of the ρc densitometer, random output variations on the order of a few percent are still observed. Work is still proceeding to improve the stability of the ρc measurement to the required $\pm$ 0.5% or better. At this writing, the evidence indicates that most of the presently observed output variations are due to instabilities in the probe. Corrective procedures are now being implemented, and include a potentially

improved separated probe design. The construction of a prototype mass flowmeter, however, need not be dependent upon successful operation of the $(\rho c)(v/c) = \dot{M}$ measurement mode. A number of commercially available densitometers exist, including the Simmonds Precision capacitance-type instrument, whose stability we measured. Such a densitometer could be installed in the line as indicated in Fig. 11, and the product ρv could be directly computed. At this time, it appears that this latter approach is to be preferred over the $(\rho c)(v/c)$ approach.

We conclude that this $\dot{M} = \rho v$ approach could determine the mass flow rate of fuels such as JP-4, JP-5 or their mixtures with a precision (standard deviation) of better than 1% of full scale, over the full flow range, temperature, vibration and contamination parameters of interest in this program. The measuring equipment normally operates with no moving parts, would introduce no significant pressure drop, and would respond linearly and rapidly (response time ~1 s) to mass flow rate in diagnostic engine tests. Response time could be reduced to the millisecond range (~10 to 100 ms) for control purposes, by using high-speed analog or digital components in the electronic portion of the mass flowmeter system. Thus, not only steady-state mass flow rate, but also dynamic (transient or pulsating) flow could be measured.

LITERATURE CITED

1. L. C. Lynnworth and N. E. Pedersen, USAAMRDL TR 72-66 (Jan. 1973); Proc. IEEE Ultrasonics Symp. 81-84 (1972), IEEE Cat. No. 72 CHO 708-8 SU.

2. D. E. Stuart, in: R. B. Dowdell, Ed. Flow - Its Measurement and Control in Science and Industry ISA (1974), pp. 695-700.

3. J. Kritz, ISA Proc. 10 Part 2, 55-16-3, pp. 1-6 (1955); Instruments and Automation 28, 1912-1913 (Nov. 1955); J. L. McShane, pp. 897-913, in Ref. 2.

4. R. C. Swengel, U. S. Patent No. 2, 746, 291 (May 22, 1956).

5. L. A. Petermann, U. S. Patent No. 2, 874, 568 (Feb. 24, 1959).

6. S. G. Fisher and P. G. Spink, Modern Developments in Flow Measurement, C. G. Clayton, Ed., Peregrinus Ltd. (1972), pp. 139-159.

7. N. Suzuki, H. Nakabori and M. Yamamoto, pp. 115-138, in Ref. 6.

8. B. Pfau, Chemie-Ingenieur-Technik 42 (17), 1103-1109 (Sept. 1970).

9. W. C. Haase, W. S. Foletta and J. D. Meindl, Proc. IEEE Ultrasonics Symp. 81-85 (1973), Cat. No. 73 CHO 807-8 SU.

10. F. Noble, Rev. Sci. Instrum. 39 (9) 1327 (Sept. 1968).

11. M. K. Bevir, J. Fluid Mechanics 43 (Part 3) 577-590 (Sept. 16, 1970).

12. A. C. Haacke, pp. 735-743, in Ref. 2.

13. Q. C. Turtle, U. S. Patent No. 3, 788, 140 (Jan. 29, 1974).

14. L. C. Lynnworth, IEEE Trans-Sonics and Ultrasonics SU-22 (2), pp. 71-101 (March 1975).

15. N. E. Pedersen and L. C. Lynnworth, NASA CR-112313(R) (June 1973); Proc. IEEE Ultrasonics Symp. 178-181 (1973), IEEE Cat. No. 73 CHO 807-8 SU.

16. E. P. Papadakis, J. Acoust. Soc. Amer. 40 863-876 (1966); L. C. Lynnworth, E. P. Papadakis and W. W. Rea, AMMRC CTR 74-20, p. 163 (April 1974); E. P. Papadakis, K. A. Fowler and L. C. Lynnworth, J. Acoust. Soc. Amer. 53 (5) 1336-1343 (1973).

17. J. T. Krause, C. R. Kurkjian, D. A. Pinnow and E. A. Sigety, Appl. Phys. Letters 17 (9) 367-368 (Nov. 1, 1970).

18. L. C. Lynnworth, Area Averaging Ultrasonic Flowmeters, U. S. Patent Application No. 402,363 (filed Oct. 1, 1973). See also, L. C. Lynnworth, C. A. Carey and N. E. Pedersen, AEDC-TR-74-77 (Oct. 1974).

19. J. Nikuradse, Ph.D. Thesis, Göttingen (1926).

20. H. Schlichting, Boundary Layer Theory, Pergamon Press Ltd., London (1955).

21. Anon. (EDO Corp.), Chem. Engineering, p. 54 (Nov. 25, 1974).

22. G. G. Twidle et al, Ultrasonics 10 (5), 197-199 (Sept. 1972); National Phys. Lab. (Teddington) Mar. Sci. Rpt. 3-71 (Oct. 1971).

23. D. F. White, A. E. Rodely and C. L. McMurtrie, pp. 967-974, and H. Yamasaki and M. Rubin, in: R. B. Dowdell, Ed., Flow - Its Measurement and Control in Science and Industry, ISA (1974).

24. J. Coulthard, Ultrasonics 11 (2) 83-88 (March 1973).

25. K. H. Ong and M. S. Beck, "Slurry Flow Velocity, Concentration and Particle Size Measurement Using Flow Noise and Correlation Techniques", presented at the Int'l. Symp. on New Concepts and Systems in Measurement and Control in the Pulp and Paper Industry, Hollingbourne, Kent, U. K., sponsored by Inst. of Meas't. and Control and British Paper and Board Industry Federation (Oct. 9-10, 1974).

26. H. J. McSkimin and P. Andreatch, Jr., J. Acoust. Soc. Amer. 49 (3) Part 2, 713-722 (March 1971).

27. J. M. Benson, 549-554; T. B. Morrow and S. J. Kline, 555-562; G. B. Lim and C. A. Sleicher, 563-577, in Ref. 2.

28. L. C. Lynnworth and D. R. Patch, MTRSA 10 (8) Cover, 6-11 (Aug. 1970); L. C. Lynnworth, D. R. Patch and E. H. Carnevale, U. S. Patent No. 3,636,754 (Jan. 25, 1972); L. C. Lynnworth and E. H. Carnevale, 715-732, in H. H. Plumb, Ed., Temperature - Its Measurement and Control in Science and Industry, ISA (1972).

29. L. C. Lynnworth, U. S. Patent No. 3,538,750 (Nov. 10, 1970).

30. D. J. Hayes, M. D. Rechtin and A. R. Hilton, Proc. IEEE Ultrasonics Symp. 502-505 (1974), IEEE Cat. No. 74 CHO 896-1 SU.

31. Scientific Apparatus Makers Assoc., SAMA Standard PMC 20.1-1973 (endorsed by ISA) (1973).

32. J. T. Malone and D. K. Whirlow, U. S. Patent No. 3,564,912 (Feb. 23, 1971).

33. M. J. Golis, Materials Evaluation 32 (9), 46A-47A (Sept. 1974).

34. L. E. Kinsler and A. R. Frey, Fundamentals of Acoustics, Second Ed., Wiley, New York, N. Y. (1962), pp. 136-139.

35. G. Canella, Brit. J. NDT 16 (6), 179-182 (Nov. 1974).

APPENDIX A
TEST DATA TAKEN AT AVCO/LYCOMING

In this appendix, we present the data taken at Avco/Lycoming during two series of Calibration Tests. These were run in June 1974 and in December 1974.

Since the December results are the more significant, these are presented first. The data presented in the tables consist of points such as 2a, 2b, and 2av. This nomenclature corresponds to normal and reversed transducer connections, and the average of the two readings, respectively. The following quantities were read from the digital panel display of the flowmeter: v/c^2, $T_1 + T_2$, v/c and v. Numerically, these data are in machine units. The output of the Simmonds densitometer, V_s, was also recorded. The temperature, T, and mass flow rate, $\dot{M}$, were measured by the Avco team. The flow data, v/c^2, v/c, and v, are also presented in graphical form in the accompanying graphs. In the flow velocity graphs, the flow rate $\dot{M}$ has been normalized by the factor ρA to give flow rate in ft/sec, where ρ = Avco measured fluid density and A = cross-sectional area of flow cell (=1/2 in.^{2}).

Since the data were taken at varying temperatures, this normalization permits easier comparison among the runs. For convenience, another set of graphs, namely, ρv vs. $\dot{M}$ is also provided.

TABLE A-1. RUN #1 - JP-4 FUEL
DENSITY ρ = 0.756

Point #	T (^{o}F)	V_s (volts)	v/c^2	$T_1 + T_2$	v/c	v	$\dot{M}$ (lb/hr)
1a		1.187	9310	5388	1.715	3185	
1b		1.188	9321	5388	1.714	3201	
1av		1.188	9316	5388	1.714	3193	4648
2a		1.175	8080	5388	1.486	2765	
2b		1.175	7937	5384	1.460	2719	
2av		1.175	8004	5386	1.473	2742	4004
3a	72	1.174	7030	5380	1.291	2395	
3b		1.173	6924	5380	1.275	2368	
3av		1.174	6977	5380	1.283	2382	3483
4a		1.172	6033	5382	1.110	2062	
4b		1.172	6005	5383	1.104	2053	
4av		1.172	6019	5382	1.107	2058	2989
5a	73	1.171	5021	5382	0.9232	1715	
5b		1.171	5073	5380	0.9349	1732	
5av		1.171	5047	5381	0.9290	1724	2517
6a	73	1.170	4002	5380	0.7395	1369	
6b		1.169	4088	5382	0.7518	1398	
6av		1.170	4045	5381	0.7456	1384	2011
7a		1.168	3000	5382	0.5520	1023	
7b		1.167	3033	5384	0.5618	1042	
7av		1.168	3016	5383	0.5569	1032	1494

TABLE A-1 - Continued

Point #	T (^{o}F)	V_s (volts)	v/c^2	$T_1 + T_2$	v/c	v	$\dot{M}$ (lb/hr)
8a	73	1.166	2004	5380	0.3667	683.1	
8b		1.165	2093	5380	0.3856	714.6	
8av		1.166	2048	5380	0.3762	698.8	1017
9a		1.164	1007	5380	0.1869	346.7	
9b		1.162	1149	5394	0.2075	386.3	
9av		1.163	1078	5387	0.1972	366.5	521.9
10a	73	1.160	486	5398	0.0916	173.3	
10b		1.159	551.5	5398	0.1011	188.7	
10av		1.160	518.8	5398	0.0964	181.0	251.8
11a	74	1.154	248.6	5292	0.0452	86.8	
11b		1.153	337.9	5012	0.0622	115.8	
11av		1.154	293.2	5152	0.0537	101.3	116.8

Data taken at Avco/Lycoming, December 17, 1974, p.m.

TABLE A-2. RUN #2 - JP-4 FUEL
DENSITY ρ = 0.744

Point #	T (^{o}F)	V_s (volts)	v/c^2	$T_1 + T_2$	v/c	v	$\dot{M}$ (lb/hr)
1a	101.5	0.865	9870	5680	1.721	3034	
1b		0.864	9987	5687	1.750	3083	
1av		0.864	9928	5684	1.736	3058	4433
2a	101	0.863	8782	5684	1.534	2697	
2b		0.862	8987	5680	1.572	2765	
2av		0.862	8884	5682	1.553	2731	3950
3a	101	0.862	8053	5685	1.404	2471	
3b		0.861	8282	5680	1.448	2540	
3av		0.862	8168	5682	1.426	2506	3620
4a	101	0.860	7093	5684	1.236	2173	
4b		0.859	7362	5681	1.290	2267	
4av		0.860	7228	5683	1.263	2220	3211
5a	101	0.858	6464	5684	1.130	1984	
5b		0.858	6812	5681	1.187	2091	
5av		0.858	6638	5683	1.158	2038	2942
6a	101	0.858	5439	5684	0.9516	1671	
6b		0.857	5787	5682	1.009	1784	
6av		0.858	5613	5683	0.9803	1728	2490
7a	101	0.857	4459	5694	0.7776	1367	
7b		0.857	4805	5682	0.8370	1470	
7av		0.857	4632	5688	0.8073	1418	2056

TABLE A-2 - Continued

Point #	T (°F)	V_s (volts)	v/c^2	$T_1 + T_2$	v/c	v	$\dot{M}$ (lb/hr)
8a	101.5	0.857	3172	5698	0.5567	970.7	
8b		0.856	3521	5680	0.6151	1079	
8av		0.856	3346	5689	0.5859	1025	1481
9a	101.5	0.856	2412	5698	0.4209	749.2	
9b		0.855	2785	5680	0.4865	853.9	
9av		0.856	2598	5689	0.4537	801.6	1148
10a	102	0.855	1412	5686	0.2482	436.6	
10b		0.854	1696	5684	0.2930	518.2	
10av		0.854	1554	5685	0.2706	477.4	6822
11a	102	0.855	692	5682	0.1215	213.2	
11b		0.855	982	5680	0.1705	300.6	
11av		0.855	837	5681	0.1460	256.9	357.1

Data taken at Avco/Lycoming, December 17, 1974, p.m.

TABLE A-3. RUN #3 - JP-4 FUEL
DENSITY ρ = 0.766

Point #	T (^{o}F)	V_s (volts)	v/c^2	$T_1 + T_2$	v/c	v	$\dot{M}$ (lb/hr)
1a	51.5	1.386	9430	5172	1.805	3486	
1b		1.386	9052	5170	1.738	3358	
1av		1.386	9241	5171	1.772	3422	5000
2a		1.387	8504	5170	1.624	3145	
2b		1.387	8167	5170	1.564	3026	
2av		1.387	8336	5170	1.594	3086	4503
3a	51.5	1.388	7385	5172	1.417	2740	
3b		1.388	7085	5170	1.360	2630	
3av		1.388	7235	5171	1.388	2685	3928
4a	51	1.388	6442	5170	1.232	2388	
4b		1.388	6153	5172	1.179	2276	
4av		1.388	6298	5171	1.206	2332	3412
5a	51	1.389	5395	5174	1.035	2001	
5b		1.389	5100	5178	.9819	1891	
5av		1.389	5248	5176	1.008	1946	2839
6a	51	1.390	4397	5170	0.8454	1629	
6b		1.390	4181	5171	0.8003	1543	
6av		1.390	4289	5170	0.8228	1586	2313
7a	51	1.391	3370	5174	0.6450	1247	
7b		1.391	3163	5178	0.6094	1177	
7av		1.391	3266	5176	0.6272	1212	1754

TABLE A-3 - Continued

Point #	T (°F)	V_s (volts)	v/c^2	$T_1 + T_2$	v/c	v	$\dot{M}$ (lb/hr)
8a	50.5	1.391	2366	5178	0.4527	876	
8b		1.391	2157	5178	0.4127	795.3	
8av		1.391	2262	5178	0.4327	835.6	1214
9a	50.5	1.390	1418	5171	0.2732	514.8	
9b		1.389	1218	5172	0.2310	447.2	
9av		1.390	1318	5172	0.2521	481.0	696.3
10a	51	1.384	747	5174	0.1444	282.8	
10b		1.384	493.1	5170	0.1003	187.2	
10av		1.384	620	5172	0.1224	235.0	332.7
11a	51	1.378	460.3	5170	0.0954	191.7	
11b		1.377	196.4	5180	0.0369	65.0	
11av		1.378	328.4	5175	0.0662	128.4	165.5

Data taken at Avco/Lycoming, December 18, 1974, a.m.

TABLE A-4. RUN #4 - JP-4 FUEL
DENSITY ρ = 0.758

Point #	T (^{o}F)	V_s (volts)	v/c^2	$T_1 + T_2$	v/c	v	$\dot{M}$ (lb/hr)
1a	72.5	1.160	9635	5380	1.772	3281	
1b		1.160	9248	5380	1.704	3158	
1av		1.160	9442	5380	1.738	3220	4715
2a	72.5	1.161	8627	5380	1.587	2952	
2b		1.161	8303	5384	1.526	2845	
2av		1.161	8465	5382	1.556	2898	4235
3a	72.5	1.161	7610	5382	1.397	2594	
3b		1.160	7217	5390	1.326	2479	
3av		1.160	7414	5386	1.362	2536	3689
4a	72.5	1.160	6564	5380	1.210	2239	
4b		1.159	6290	5390	1.154	2137	
4av		1.160	6427	5385	1.182	2188	3206
5a	72.5	1.160	5582	5380	1.030	1904	
5b			5336	5384	0.9816	1811	
5av		1.160	5459	5382	1.0058	1858	2723
6a	72.5	1.160	4705	5382	0.8666	1608	
6b			4432	5380	0.8143	1514	
6av		1.160	4568	5381	0.8404	1561	2282
7a	72.5	1.160	3859	5382	0.7107	1320	
7b		1.160	3600	5380	0.6623	1237	
7av		1.160	3730	5381	0.6865	1278	1859

TABLE A-4 - Continued

Point #	T (^{o}F)	V_s (volts)	v/c^2	$T_1 + T_2$	v/c	v	$\dot{M}$ (lb/hr)
8a	72.5	1.161	2574	5380	0.4744	881.0	
8b			2341	5380	0.4265	788.0	
8av		1.161	2458	5380	0.4504	834.5	1212
9a	72.5	1.161	1563	5384	0.2832	526.7	
9b			1318	5386	0.2423	437.5	
9av		1.161	1440	5385	0.2628	482.1	689.7
10a	72.5	1.160	699.4	5382	0.1326	246.0	
10b		1.159	395.5	5380	0.0726	133.7	
10av		1.160	547.4	5381	0.1026	189.8	270.3
11a	72.5	1.158	521.6	5382	0.0972	180.1	
11b		1.158	160.6	5390	0.0295	53.5	
11av		1.158	341.1	5386	0.0634	116.8	147.7

Data taken at Avco/Lycoming, December 18, 1974, a.m.

TABLE A-5. RUN #5 - JP-4 FUEL
DENSITY ρ = 0.767

Point #	T (^{o}F)	V_s (volts)	v/c^2	$T_1 + T_2$	v/c	v	$\dot{M}$ (lb/hr)
1a	50	1.403	9396	5160	1.801	3493	
1b		1.403	8897	5174	1.704	3304	
1av		1.403	9146	5167	1.752	3398	5021
2a	50	1.403	8699	5160	1.667	3229	
2b		1.403	8190	5170	1.572	3048	
2av		1.403	8444	5165	1.620	3138	4633
3a	50	1.403	7694	5162	1.475	2858	
3b			7193	5174	1.380	2673	
3av		1.403	7444	5168	1.428	2766	4086
4a	50	1.404	6745	5162	1.293	2504	
4b		1.404	6256	5174	1.201	2322	
4av		1.404	6500	5168	1.247	2413	3561
5a	50	1.405	5758	5160	1.104	2137	
5b			5343	5164	1.028	1988	
5av		1.405	5550	5162	1.066	2062	3052
6a	50	1.405	4733	5161	0.9084	1764	
6b			4293	5160	0.8244	1592	
6av		1.405	4513	5160	0.8664	1678	2462
7a	50	1.405	3716	5161	0.7120	1380	
7b			3274	5162	0.6277	1216	
7av		1.405	3495	5162	0.6698	1298	1891

TABLE A-5 - Continued

Point #	T (^{o}F)	V_s (volts)	v/c^2	$T_1 + T_2$	v/c	v	$\dot{M}$ (lb/hr)
8a	50		2686	5162	0.5156	1000	
8b		1.406	2258	5161	0.4337	836.6	
8av		1.406	2472	5162	0.4746	918.3	1337
9a	50	1.405	1685	5162	0.3245	623.0	
9b			1181	5164	0.2277	440.0	
9av		1.405	1433	5163	0.2761	531.5	788.8
10a	50	1.402	1215	5160	0.2332	450.7	
10b			657	5174	0.1244	240.2	
10av		1.402	936	5167	0.1788	345.4	493.2
11a	50	1.399	893	5172	0.1737	333.5	
11b			347.8	5170	0.0692	138.0	
11av		1.399	620.4	5171	0.1214	233.8	324.5

Data taken at Avco/Lycoming, December 18, 1974, p. m.

TABLE A-6. RUN #6 - JP-4 FUEL
DENSITY ρ = 0.746

Point #	T (^{o}F)	V_s (volts)	v/c^2	$T_1 + T_2$	v/c	v	$\dot{M}$ (lb/hr)
1a	101.5	0.865	9507	5700	1.653	2891	
1b		0.865	8807	5702	1.530	2689	
1av		0.865	9157	5701	1.592	2790	4063
2a	101.5	0.866	8479	5704	1.472	2582	
2b			7871	5701	1.370	2401	
2av		0.866	8175	5702	1.421	2492	3622
3a	102	0.866	7510	5704	1.308	2290	
3b			6960	5700	1.205	2119	
3av		0.866	7235	5702	1.256	2204	3197
4a	101.5	0.866	6612	5704	1.148	2010	
4b			6064	5700	1.056	1851	
4av		0.866	6338	5702	1.102	1930	2793
5a	101.5	0.866	5583	5700	0.9698	1690	
5b			5046	5703	0.8781	1534	
5av		0.866	5314	5702	0.9240	1612	2341
6a	101.5	0.867	4542	5707	0.7883	1383	
6b			4001	5700	0.6948	1210	
6av		0.867	4272	5704	0.7416	1296	1892
7a	101.5		3579	5702	0.6218	1092	
7b			2933	5702	0.5130	901.0	
7av		0.867	3256	5702	0.5674	996.5	1438

TABLE A-6 - Continued

Point #	T (^{o}F)	V_s (volts)	v/c^2	$T_1 + T_2$	v/c	v	$\dot{M}$ (lb/hr)
8a	101.7	0.867	2532	5709	0.4413	776.7	
8b			1893	5702	0.3296	576.8	
8av		0.867	2212	5706	0.3854	676.8	999.1
9a	101.75	0.869	1557	5697	0.2738	476.9	
9b			887.6	5700	0.1519	267.0	
9av		0.869	1222.3	5698	0.2128	372.0	553.8
10a	101.75		1069	5693	0.1865	326.0	
10b		0.866	469.4	5699	0.0832	142.9	
10av		0.866	769.2	5696	0.1348	234.4	345.7
11a							
11b							
11av							

Data taken at Avco/Lycoming, December 18, 1974, p.m.

TABLE A-7. RUN #1 - JP-4 FUEL

Point #	T (^{o}F)	v/c^2	$T_1 + T_2$	v/c	v	$\dot{M}$ (lb/hr)
1a	75	9556	5412	1.749	3261	
1b		9635	5530	1.728	3125	
1av		9596	5471	1.738	3193	4692
2a	75	8015	5470	1.447	2651	
2b		7956	5422	1.459	2697	
2av		7985	5446	1.453	2674	3884
3a	75	6530	5482	1.180	2149	
3b		6451	5432	1.177	2302	
3av		6490	5457	1.178	2225	3159
4a	75	5084	5448	0.968	1701	
4b		5144	5460	0.9347	1719	
4av		5114	5454	0.9514	1710	2492
5a	75	4031	5468	0.7322	1342	
5b		4032	5436	0.7346	1353	
5av		4031.5	5452	0.7334	1348	1955
6a	75	2923	5442	0.5330	979.6	
6b		2948	5430	0.5390	995.6	
6av		2936	5436	0.5360	987.6	1416
7a	75	1782	5431	0.3257	600.4	
7b		1856	5408	0.3407	627.4	
7av		1819	5420	0.3332	613.9	855.5

TABLE A-7 - Continued

Point #	T (^{o}F)	v/c^2	$T_1 + T_2$	v/c	v	$\dot{M}$ (lb/hr)
8a	75	1025	5324	0.1967	369.3	
8b		916.0	5300	0.1712	322.4	
8av		970.5	5312	0.1840	345.9	446.6
9a	75	443.1	4923	0.0908	187.9	
9b		513.3	4750	0.1068	223.2	
9av		478.2	4836	0.0988	205.6	211.1
10a	75	136.4	4890	0.0290	57.4	
10b		63.85	4853	0.0131	30.9	
10av		100.1	4872	0.0211	44.2	38.82
11a	75	6461	5458	1.172	2137	
11b		6416	5456	1.168	2149	
11av		6438	5457	1.170	2143	3176

Data taken at Avco/Lycoming, June 19, 1974.

TABLE A-8. RUN #2 - JP-4 FUEL

Point #	T (^{o}F)	v/c^2	$T_1 + T_2$	v/c	v	$\dot{M}$ (lb/hr)
1a	103	587.5	5006	0.1143	214.9	
1b		510.1	5011	0.1012	210.1	
1av		548.8	5008	0.1078	212.5	221.8
2a	103	1421	5825	0.2327	375.7	
2b		1445	5810	0.2511	412.7	
2av		1433	5818	0.2419	394.2	614.7
3a	103	2402	5820	0.3881	641.9	
3b		2210	5730	0.3796	657.5	
3av		2306	5775	0.3838	649.7	1023.9
4a	102.5	3479	5731	0.5745	962.4	
4b		3414	5718	0.5932	1020	
4av		3446	5724	0.5838	991.2	1546.4
5a	102	4294	5741	0.7433	1296	
5b		4343	5732	0.7478	1304	
5av		4318	5736	0.7456	1300	1965
6a	101.5	5752	5802	0.9848	1694	
6b		5572	5747	0.9666	1696	
6av		5662	5774	0.9757	1695	2603
7a	101.5	6624	5759	1.141	1970	
7b		6768	5800	1.158	2011	
7av		6696	5780	1.150	1990	3114

TABLE A-8 - Continued

Point #	T (^{o}F)	v/c^2	$T_1 + T_2$	v/c	v	$\dot{M}$ (lb/hr)
8a	101	7627	5743	1.322	2303	
8b		7435	5708	1.293	2260	
8av		7531	5726	1.308	2282	3557
9a	101	8478	5720	1.469	2562	
9b		8576	5732	1.485	2599	
9av		8527	5726	1.477	2580	3993
10a	100.5	9457	5745	1.633	2837	
10b		9340	5734	1.627	2848	
10av		9398	5740	1.630	2842	4396
11a	100	9211	5691	1.602	2670	
11b		9360	5776	1.609	2789	
11av		9286	4734	1.606	2730	4299
12a	100	8069	5802	1.383	2394	
12b		7888	5764	1.360	2375	
12av		7978	5783	1.372	2384	3679
13a	100	7157	5773	1.231	2132	
13b		7367	5789	1.262	2180	
13av		7262	5781	1.246	2156	3347
14a	100	6131	5787	1.054	1831	
14b		5936	5761	1.025	1779	
14av		6034	5774	1.040	1805	2794

TABLE A-8 - Continued

Point #	T (^{o}F)	v/c^2	$T_1 + T_2$	v/c	v	$\dot{M}$ (lb/hr)
15a	100	4785	5770	0.8205	1418	
15b		4978	5818	0.8481	1467	
15av		4882	5794	0.8343	1442	2253
16a	100	3829	5839	0.6510	1113	
16b		3647	5799	0.6231	1081	
16av		3738	5819	0.6370	1097	1725
17a	100	2823	5835	0.4796	815.3	
17b		2974	5892	0.5002	853.8	
17av		2898	5864	0.4899	834.6	1338
18a	100	1781	5887	0.3010	507.8	
18b		1675	5892	0.2821	478.3	
18av		1728	5890	0.2196	493.0	775.5

Data taken at Avco/Lycoming, June 20, 1974, a.m.

TABLE A-9. RUN #3 - JP-4 FUEL

Point #	T (°F)	v/c^2	$T_1 + T_2$	v/c	v	$\dot{M}$ (lb/hr)
1a	75	681	5065	0.1360	283.1	
1b		750.6	5006	0.1521	305.8	
1av		715.8	5035.5	0.1440	294.4	314.2
2a	75	387	4393	0.0803	165.7	
2b		296	4730	0.0617	129.3	
2av		341.5	4561.5	0.0710	147.5	147.8
3a	75	1036	5327	0.1922	358.5	
3b		1096	5356	0.2053	389.2	
3av		1066	5341.5	0.1988	373.8	512.1
4a	75	1495	5532	0.2673	482.6	
4b		1368	5540	0.2453	445.8	
4av		1431.5	5536	0.2563	464.2	712
5a	75	2499	5597	0.4227	789.0	
5b		2693	5610	0.4732	845.5	
5av		2596	5603.5	0.4480	817.2	1301
6a	75	3565	5641	0.6262	1107	
6b		3362	5623	0.5928	1060	
6av		3463.5	5632	0.6095	1084	1786
7a	75	4511	5633	0.7933	1411	
7b		4765	5675	0.8319	1465	
7av		4638	5654	0.8126	1438	2397

TABLE A-9 - Continued

Point #	T (°F)	v/c^2	$T_1 + T_2$	v/c	v	$\dot{M}$ (lb/hr)
8a	75	5802	5686	1.012	1777	
8b		5525	5630	0.9749	1737	
8av		5663.5	5658	0.9934	1757	2939
9a	75	7070	5624	1.246	2214	
9b		7222	5677	1.271	2244	
9av		7146	5650.5	1.258	2229	3728
10a	75	8694	5672	1.520	2679	
10b		8549	5616	1.509	2691	
10av		8621.5	5644	1.514	2685	4474
11a	75	400	5660	0.0703	129.0	
11b		295.5	5646	0.0534	164.2	
11av		347.75	5653	0.0618	146.6	171.5

Data taken at Avco/Lycoming, June 20, 1974, p.m.

TABLE A-10. RUN #4 - JP-4 FUEL

Point #	T (^{o}F)	v/c^2	$T_1 + T_2$	v/c	ρc	v	$\dot{M}$ (lb/hr)	v/c (ρc) x 10^3
1a	75	117.3	5572	0.0208	0.11107	35.7	34.14	2.310
1b		52.8	5493	0.0097	0.11109	17.1		1.078
1av		85.0	5532	0.0153	0.11108	26.4		1.694
2a	75	196.9	5623	0.0349	0.1112	63.1	99.9	3.881
2b		214.8	5626	0.0385	0.1111	71.1		4.277
2av		205.8	5624	0.0367	0.1112	67.1		4.079
3a	75	510.4	5639	0.0903	0.1110	160.4	243.9	10.023
3b		500.5	5640	0.0878	0.1112	154.1		9.763
3av		505.4	5640	0.0891	0.1111	157.2		9.893
4a	75	1212	5657	0.2125	0.1110	374.9	612.9	23.59
4b		1235	5666	0.2190	0.1110	388.0		24.31
4av		1224	5662	0.2158	0.1110	381.4		23.95
5a	75	1785	5663	0.3130	0.1110	550.5	897.8	34.74
5b		1735	5643	0.3072	0.1110	544.1		34.10
5av		1760	5653	0.3101	0.1110	547.3		34.42
6a	75	2714	5649	0.4748	0.1110	840.8	1416	52.70
6b		2779	5666	0.4892	0.1112	863.3		54.40
6av		2746	5658	0.4820	0.1111	852.0		53.55
7a	75	3821	5666	0.6701	0.1112	1182	1951	74.52
7b		3661	5638	0.6496	0.1110	1154		72.11
7av		3741	5652	0.6599	0.1111	1168		73.32

TABLE A-10 - Continued

Point #	T (^{o}F)	v/c^2	$T_1 + T_2$	v/c	ρc	v	$\dot{M}$ (lb/hr)	v/c (ρ c) x 10^3
8a	75	5044	5634	0.8874	0.1110	1575	2679	98.50
8b		5200	5657	0.9186	0.1110	1626		102.00
8av		5122	5646	0.9030	0.1110	1600		100.25
9a	75	6511	5661	1.149	0.1110	1921	3364	127.54
9b		6306	5632	1.109	0.1110	1970		123.10
9av		6408	5646	1.129	0.1110	1946		125.32
10a	75	7505	5642	1.319	0.1110	2342	3976	146.41
10b		7648	5655	1.353	0.1110	2393		150.18
10av		7576	5648	1.336	0.1110	2368		148.30

Data taken at Avco/Lycoming, June 20, 1974, p. m.

TABLE A-11. RUN #5 - MARINE DIESEL FUEL I VVF 800

Point #	T (^{o}F)	v/c^2	$T_1 + T_2$	v/c	ρc	v	$\dot{M}$ (lb/hr)
1a	111	9410	5510	1.692	0.1289	3083	
1b		9354	5510	1.694	0.1289	3062	
1av		9382	5510	1.693	0.1289	3072	5524
2a	110.5	8581	5470	1.557	0.1291	2834	
2b		8523	5603	1.521	0.1293	2752	
2av		8552	5536	1.539	0.1292	2793	4977
3a	110	7391	5498	1.308	0.1292	2346	
3b		7233	5510	1.310	0.1292	2383	
3av		7312	5504	1.309	0.1292	2364	4269
4a	110	6420	5550	1.146	0.1295	2075	
4b		6292	5569	1.138	0.1295	2047	
4av		6356	5560	1.142	0.1295	2061	3773
5a	109.5	5439	5552	0.9743	0.1295	1755	
5b		5584	5540	0.9987	0.1294	1828	
5av		5512	5546	0.9865	0.1294	1792	3171
6a	108	4425	5612	0.7807	0.1296	1384	
6b		4296	5606	0.7600	0.1297	1370	
6av		4360	5609	0.7704	0.1296	1377	2512
7a	108	3428	5552	0.6123	0.1299	1108	
7b		3673	5520	0.6478	0.1297	1174	
7av		3550	5536	0.6300	0.1298	1141	2023

TABLE A-11 - Continued

Point #	T (^{o}F)	v/c^2	$T_1 + T_2$	v/c	ρc	v	$\dot{M}$ (lb/hr)
8a	106	2644	5644	0.4537	0.1300	806.3	
8b		2372	5583	0.4265	0.1301	754.0	
8av		2508	5614	0.4401	0.1300	780.2	1769
9a	105	2334	5530	0.4193	0.1303	759.0	
9b		2634	5520	0.4701	0.1304	878.3	
9av		2484	5525	0.4447	0.1303	818.6	1409
10a	105	1638	5429	0.2959	0.1306	575.9	
10b		1371	5388	0.2556	0.1307	476.4	
10av		1504	5408	0.2738	0.1306	526.2	834
11a	104	728.7	4920	0.1416	0.1309	276.1	
11b		985.7	5119	0.1906	0.1308	367.2	
11av		857.2	5020	0.1661	0.1308	321.6	480
12a	103	564.2	4493	0.1223	0.1311	305.5	
12b		395.8	4140	0.0917	0.1311	216.3	
12av		480.0	4316	0.1070	0.1311	260.9	238
13a		209.5	3252	0.0778	0.1312	121.2	
13b		319.0	2498	0.0793	0.1313	230.8	
13av		264.2	3375	0.0786	0.1312	176.0	148
14a	102	169.3	1712	0.09508	0.1316	484.3	
14b		210.0	1713	0.1102	0.1316	78.5	
14av		189.6	1712	0.1026	0.1316	634.6	78

Data taken at Avco/Lycoming, June 21, 1974.

TABLE A-12. RUN #6 - MARINE DIESEL FUEL I VVF 800

Point #	T (^oF)	v/c^2	$T_1 + T_2$	v/c	ρc	v	$\dot{M}$ (lb/hr)
1a	76	9583	5159	1.848	0.1359	3585	
1b		9622	5090	1.892	0.1359	3718	
1av		9602	5124	1.870	0.1359	3652	6585
2a	76	8463	5101	1.641	0.1359	3208	
2b		8381	5161	1.613	0.1359	3144	
2av		8422	5131	1.627	0.1359	3176	5754
3a	76	7307	5167	1.404	0.1359	2574	
3b		7310	5118	1.412	0.1357	2769	
3av		7308	5142	1.408	0.1358	2672	4975
4a	76	6878	5132	1.329	0.1357	2591	
4b		6906	5172	1.303	0.1356	2529	
4av		6842	5152	1.316	0.1356	2560	4647
5a	75	6007	5179	1.149	0.1357	2217	
5b		6076	5151	1.171	0.1357	2278	
5av		6042	5165	1.160	0.1357	2248	4074
6a	75	5047	5150	0.9713	0.1357	1884	
6b		4976	5187	0.9519	0.1357	1842	
6av		5012	5168	0.9616	0.1357	1863	3359
7a	75	3055	5175	0.5868	0.1355	1130	
7b		3166	5129	0.6121	0.1355	1197	
7av		3110	5152	0.5994	0.1355	1164	2046

TABLE A-12 - Continued

Point #	T (°F)	v/c^2	$T_1 + T_2$	v/c	ρc	v	$\dot{M}$ (lb/hr)
8a	75	2051	5170	0.3929	0.1355	759.4	
8b		1916	5217	0.3639	0.1355	699.2	
8av		1984	5194	0.3784	0.1355	729.3	1277
9a	75	1332	5182	0.2549	0.1355	492.0	
9b		1481	5149	0.2848	0.1355	539.5	
9av		1406	5166	0.2698	0.1355	515.8	894
10a	75	793.1	5172	0.1524	0.1355	294.4	
10b		634.6	5180	0.1221	0.1355	235.0	
10av		713.8	5176	0.1372	0.1355	264.7	439
11a	75	420.2	5160	0.0810	0.1355	156.7	
11b		573.3	5150	0.1100	0.1357	212.6	
11av		496.8	5155	0.0955	0.1356	184.6	305
12a	75	160.8	5012	0.0300	0.1355	57.4	
12b		9.1	5038	0.0018	0.1355	3.8	
12av		85.0	5025	0.0159	0.1355	30.6	47

Data taken at Avco/Lycoming, June 21, 1974.

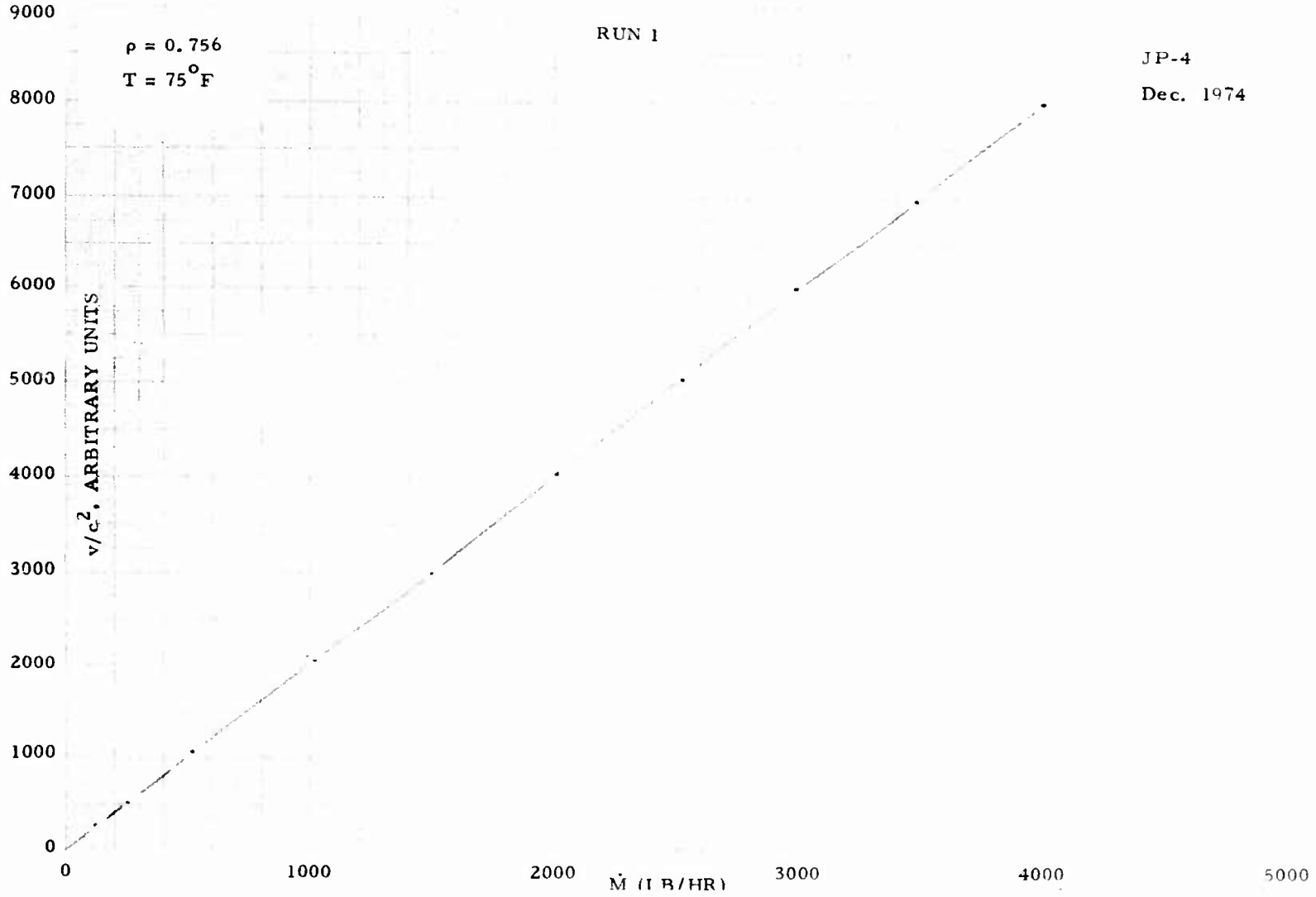

Figure A-1. v/c^2 Versus $\dot{M}$.

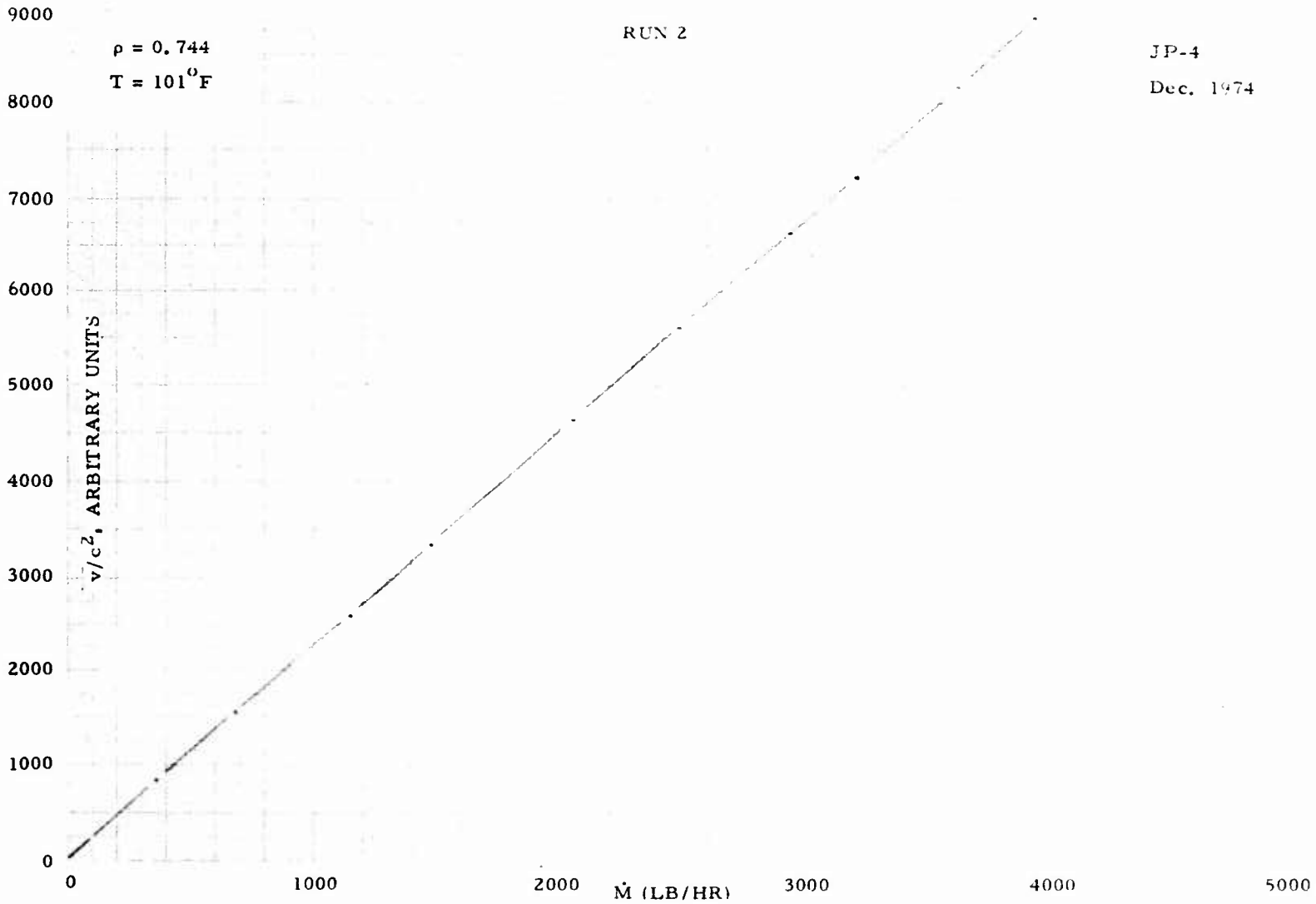

Figure A-2. v/c^2 Versus $\dot{M}$.

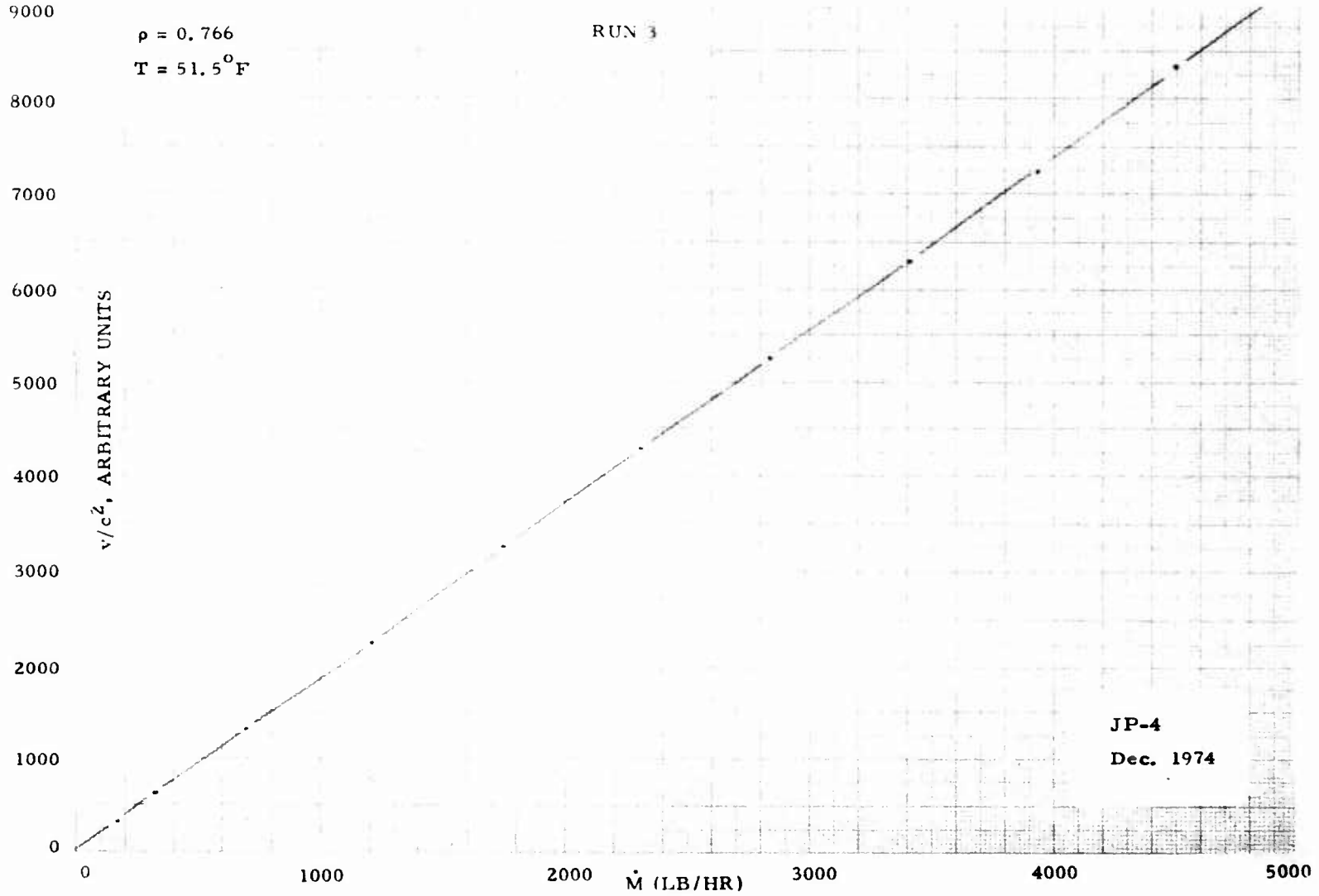

Figure A-3. v/c^2 Versus $\dot{M}$.

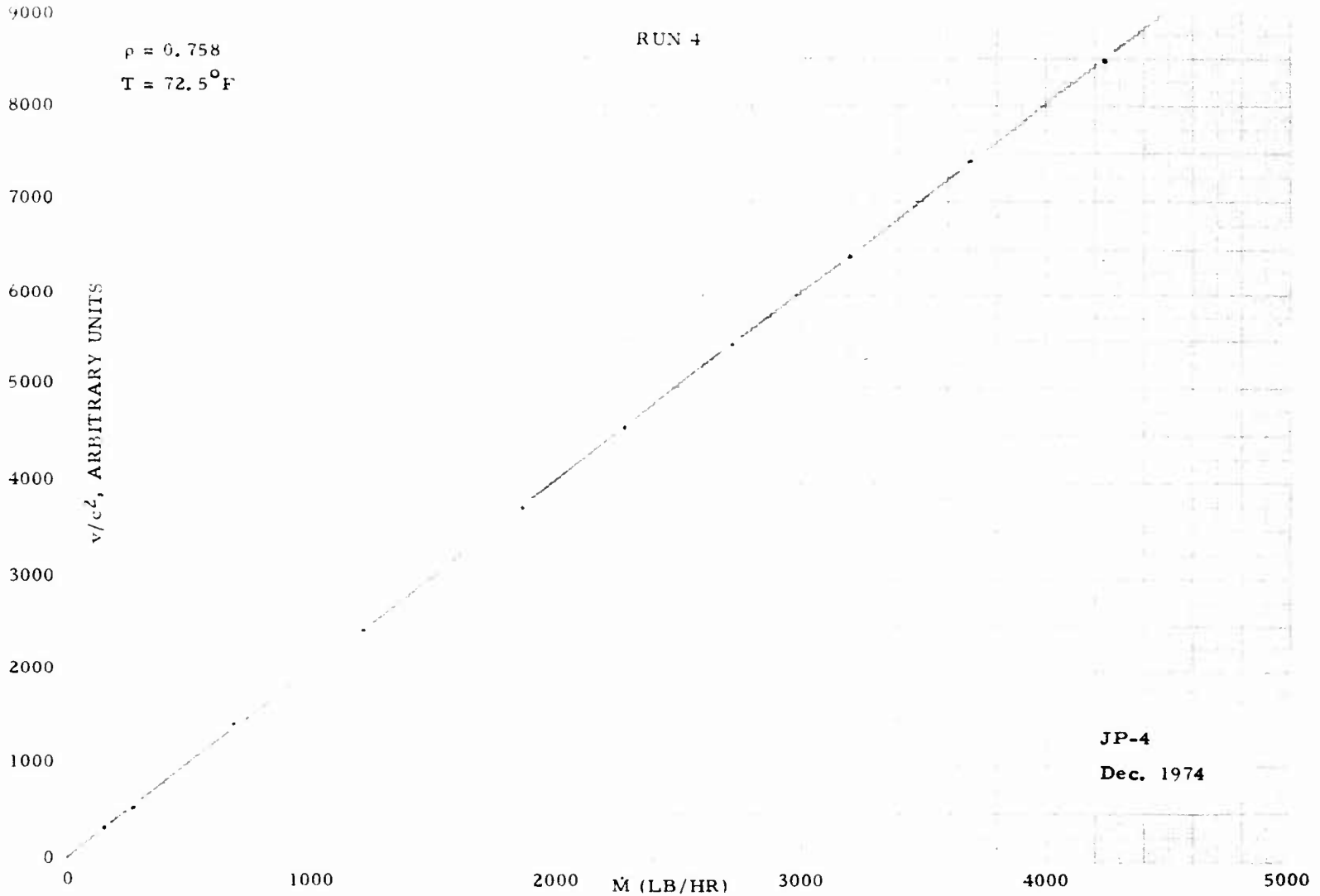

Figure A-4. v/c^2 Versus $\dot{M}$.

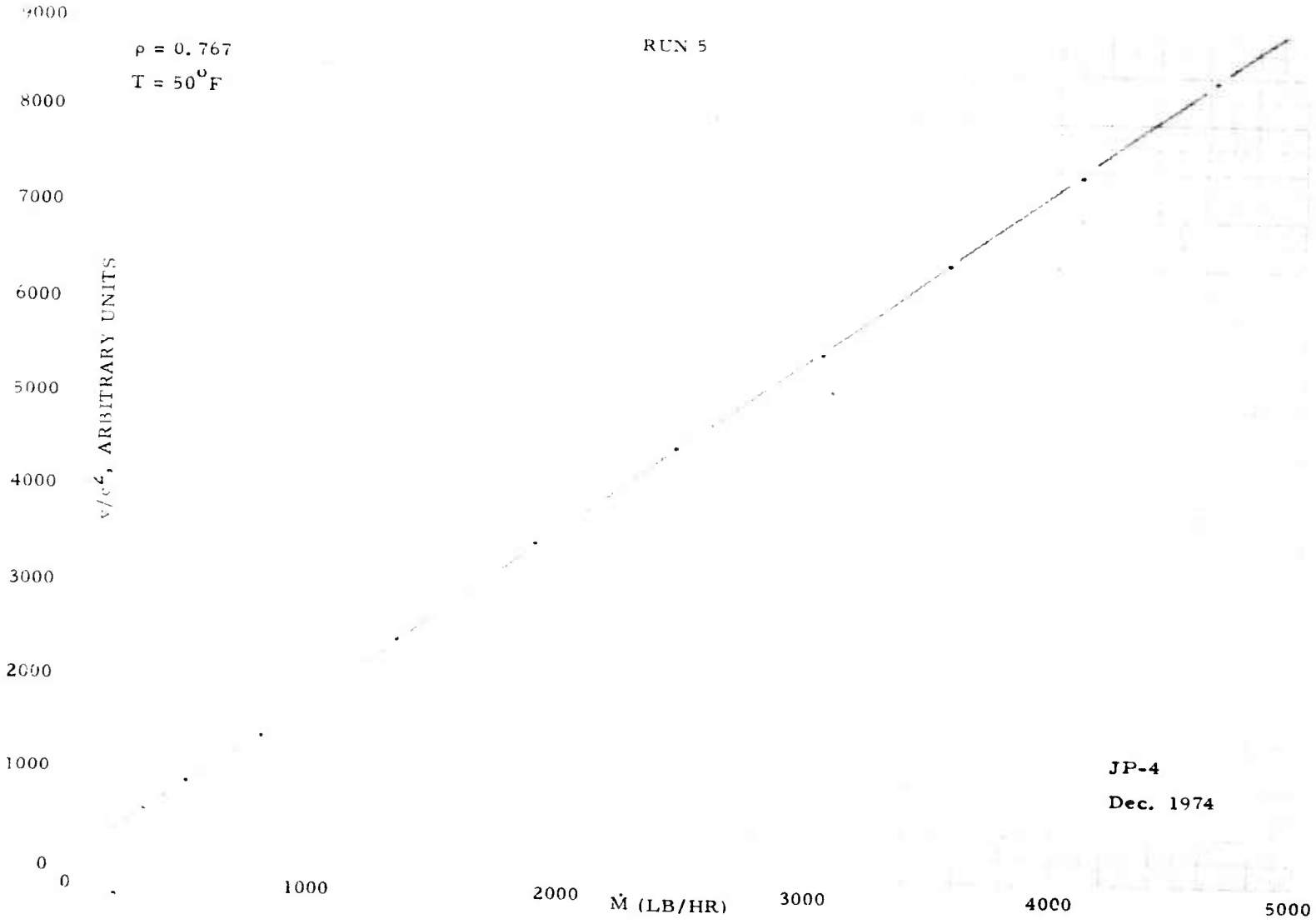

Figure A-5. v/c^2 Versus $\dot{M}$.

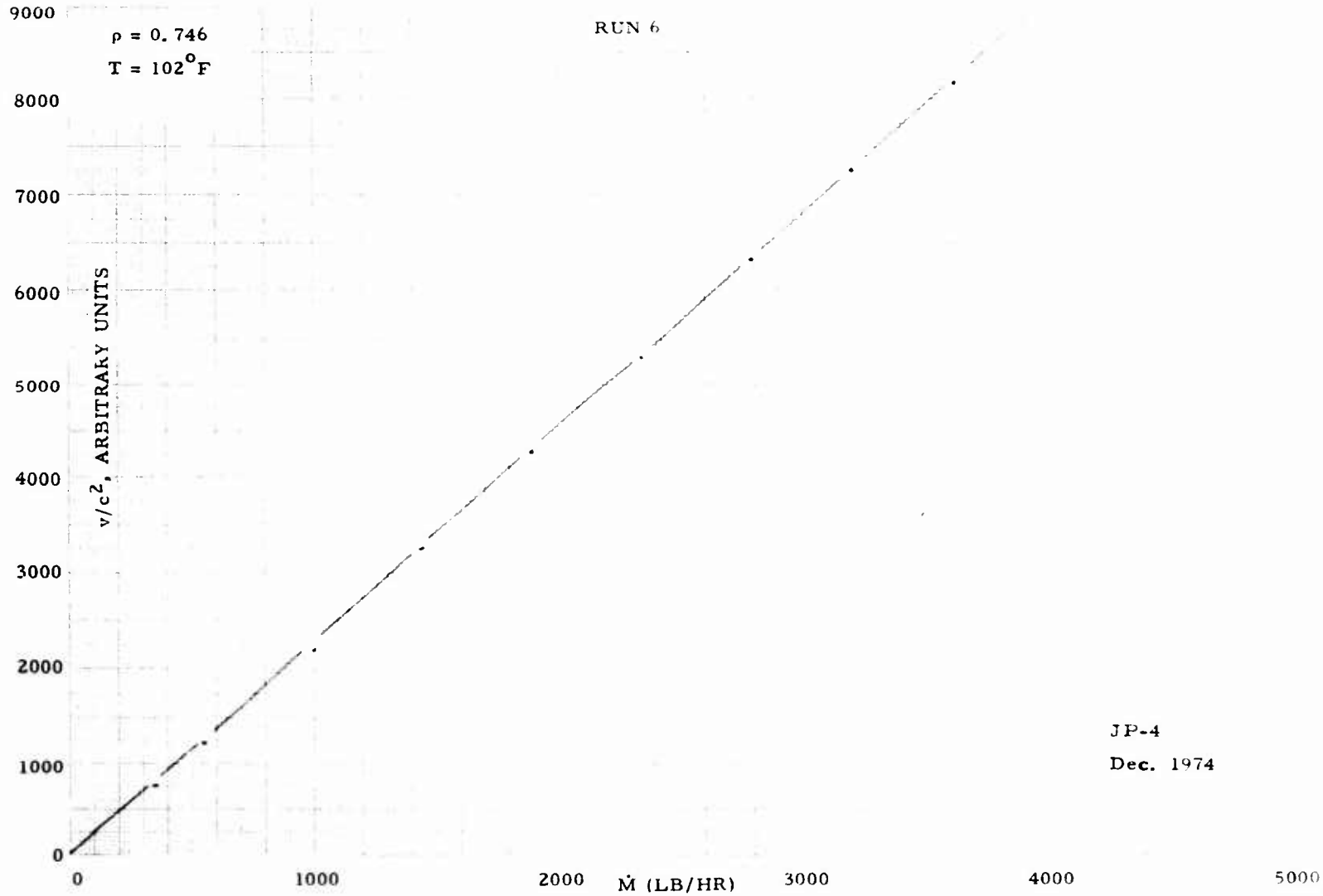

Figure A-6. v/c^2 Versus $\dot{M}$.

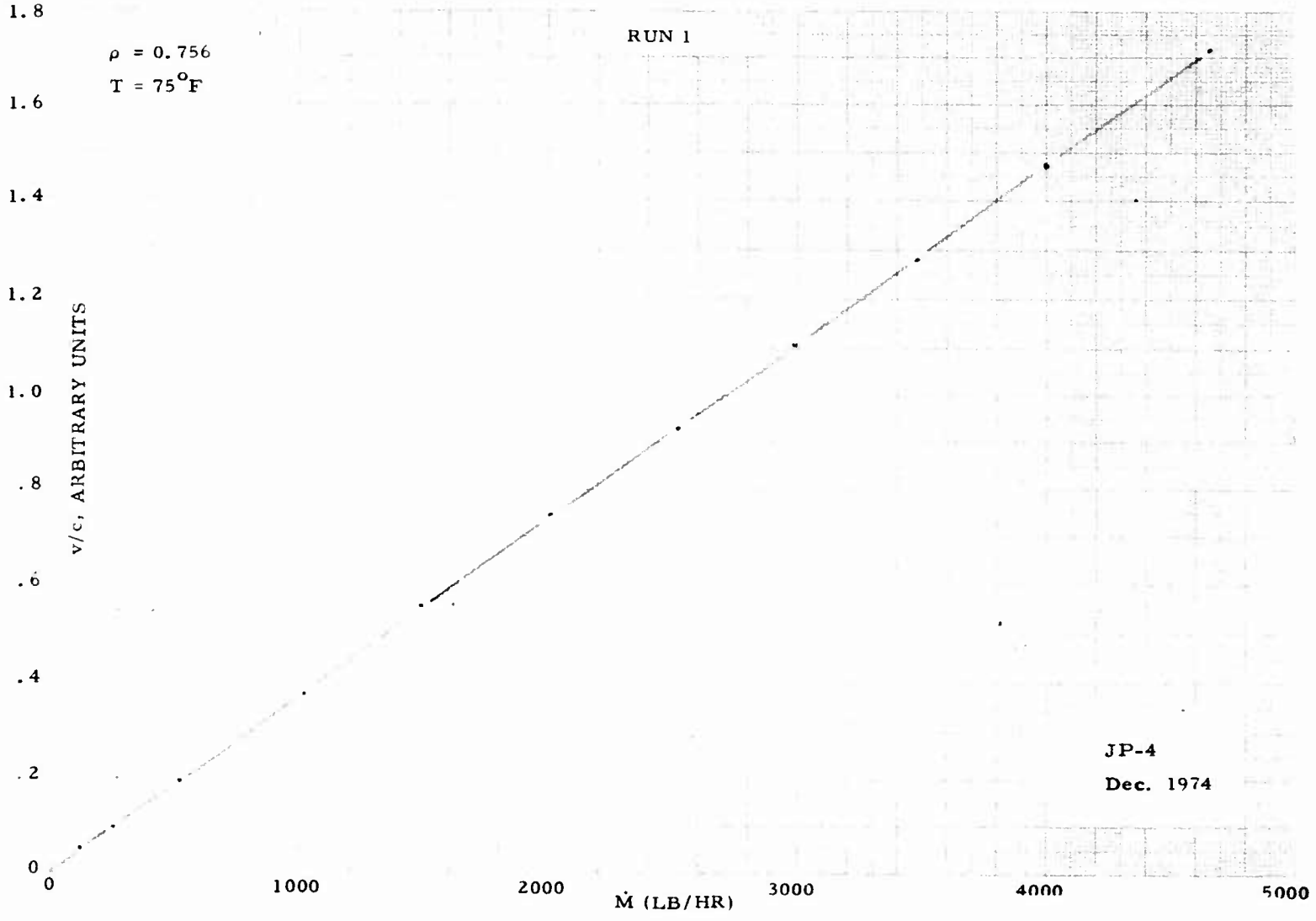

Figure A-7. v/c Versus Ṁ.

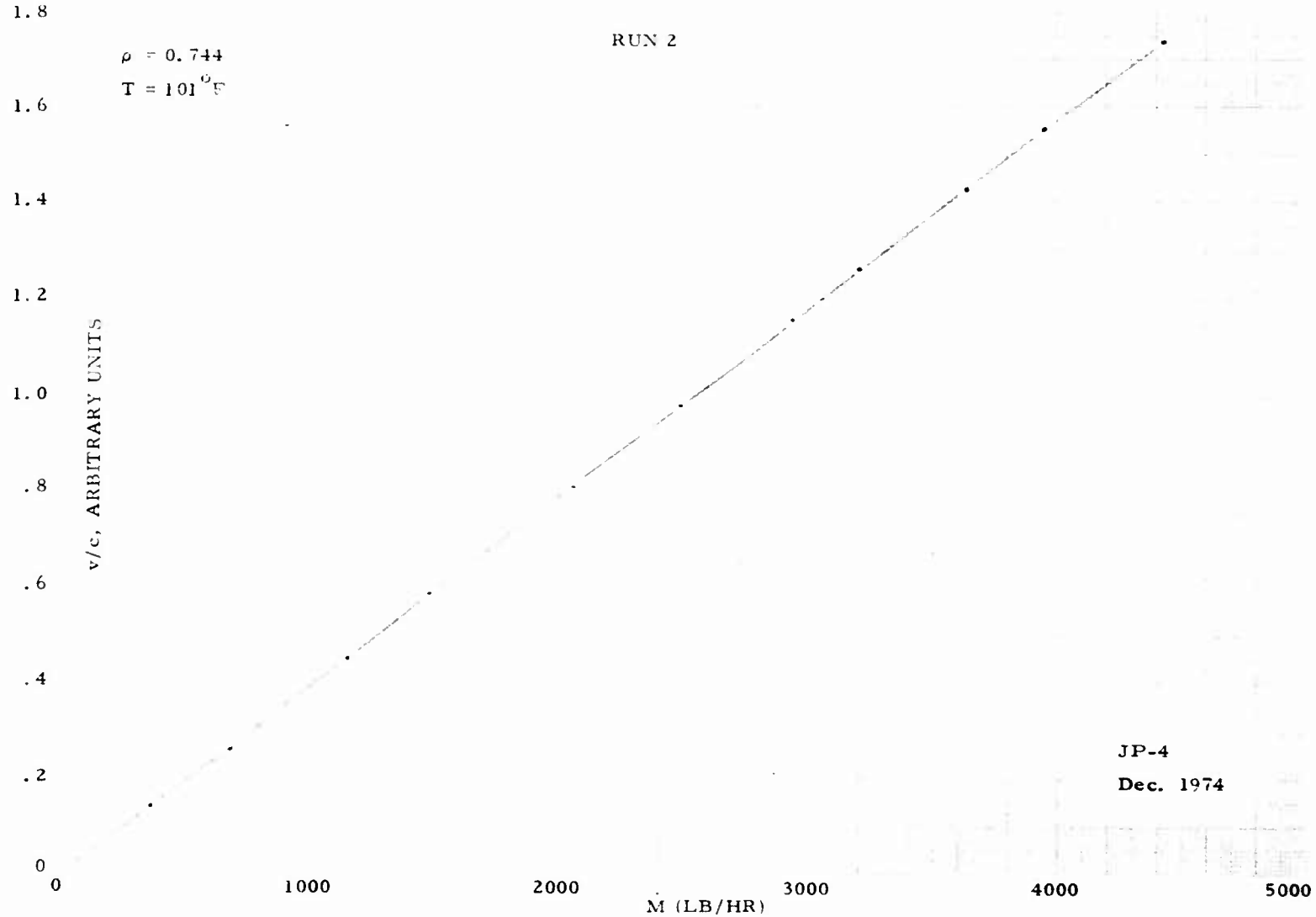

Figure A-8. v/c Versus $\dot{M}$.

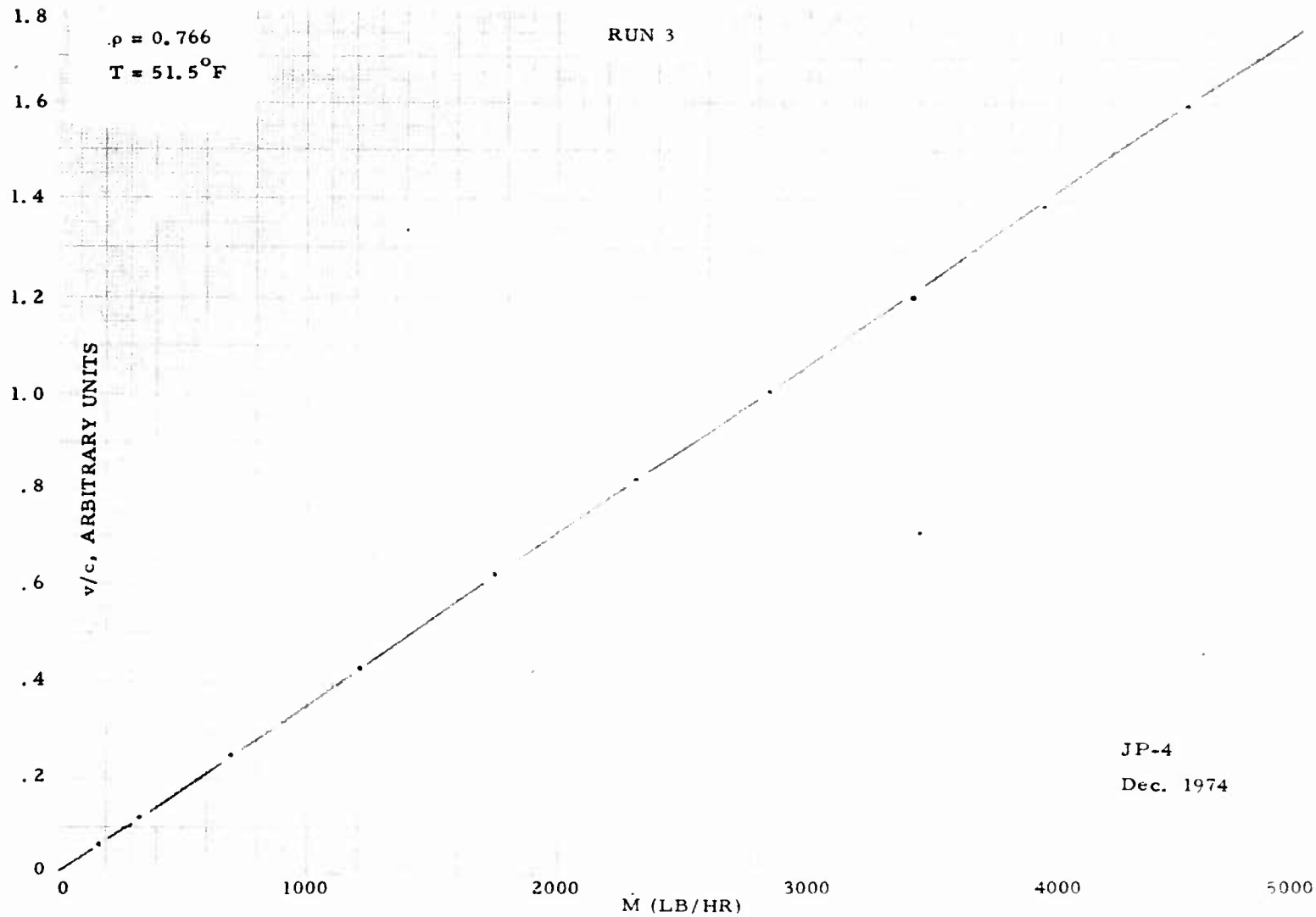

Figure A-9. v/c Versus $\dot{M}$.

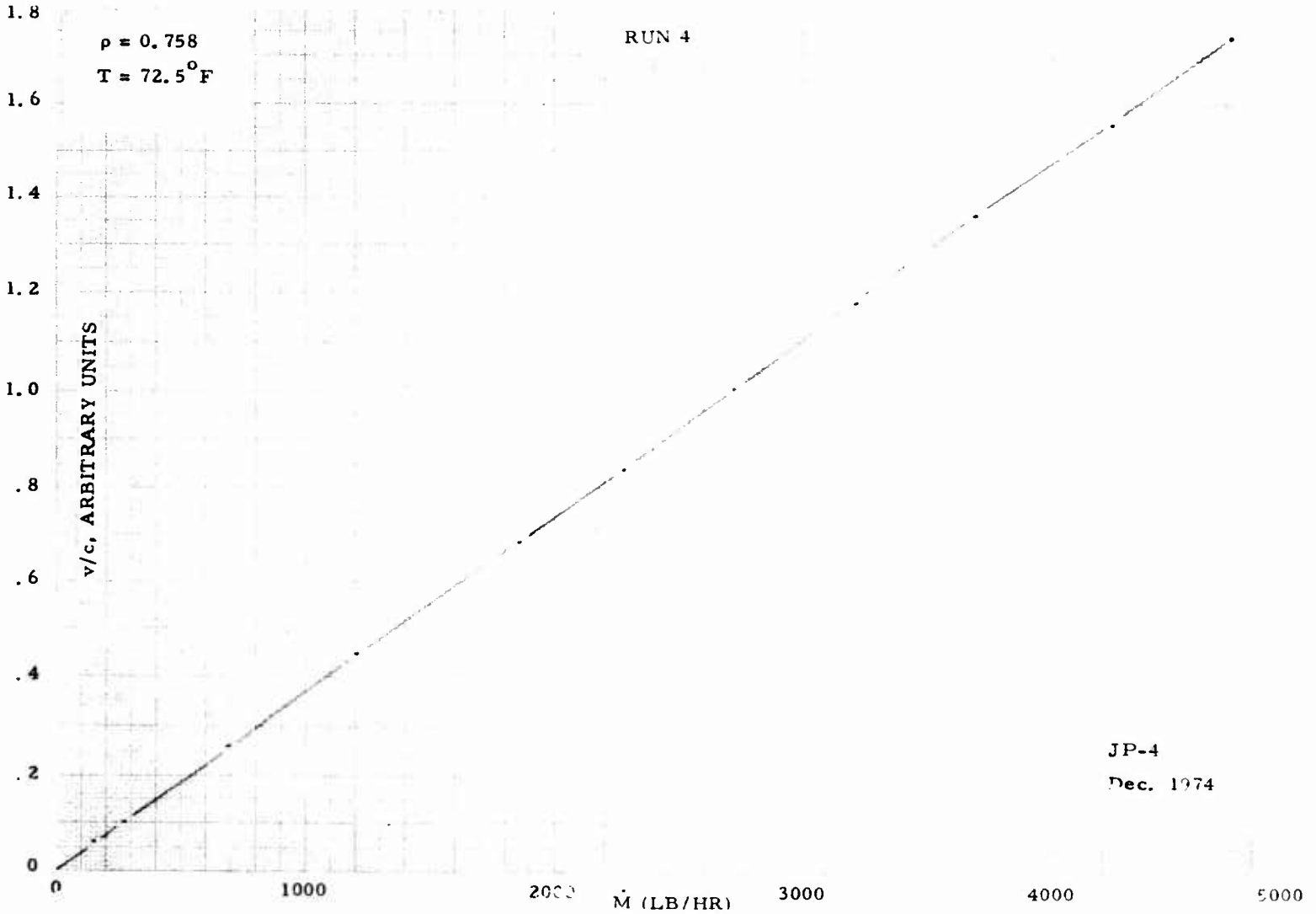

Figure A-10. v/c Versus $\dot{M}$.

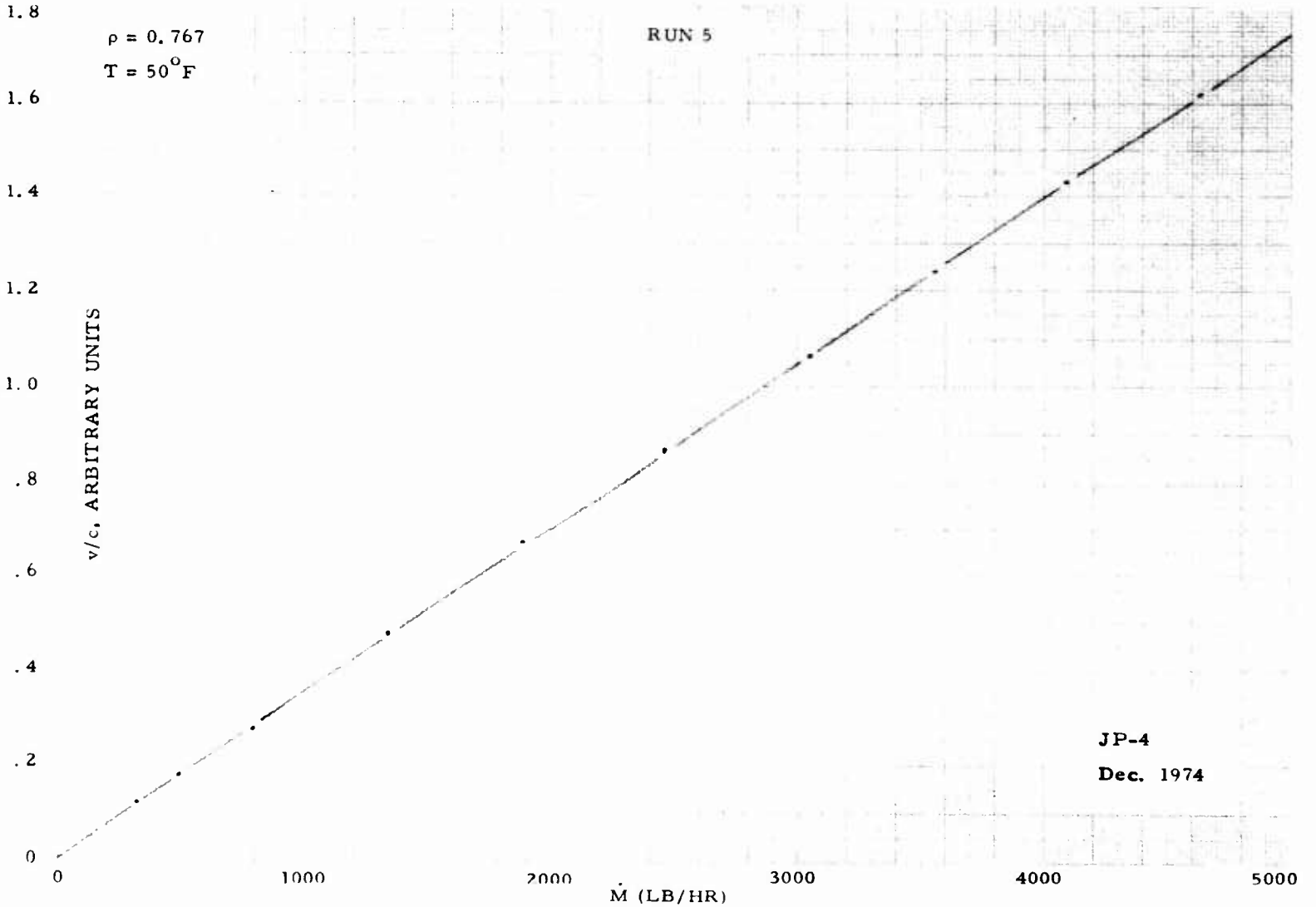

Figure A-11. v/c Versus Ṁ.

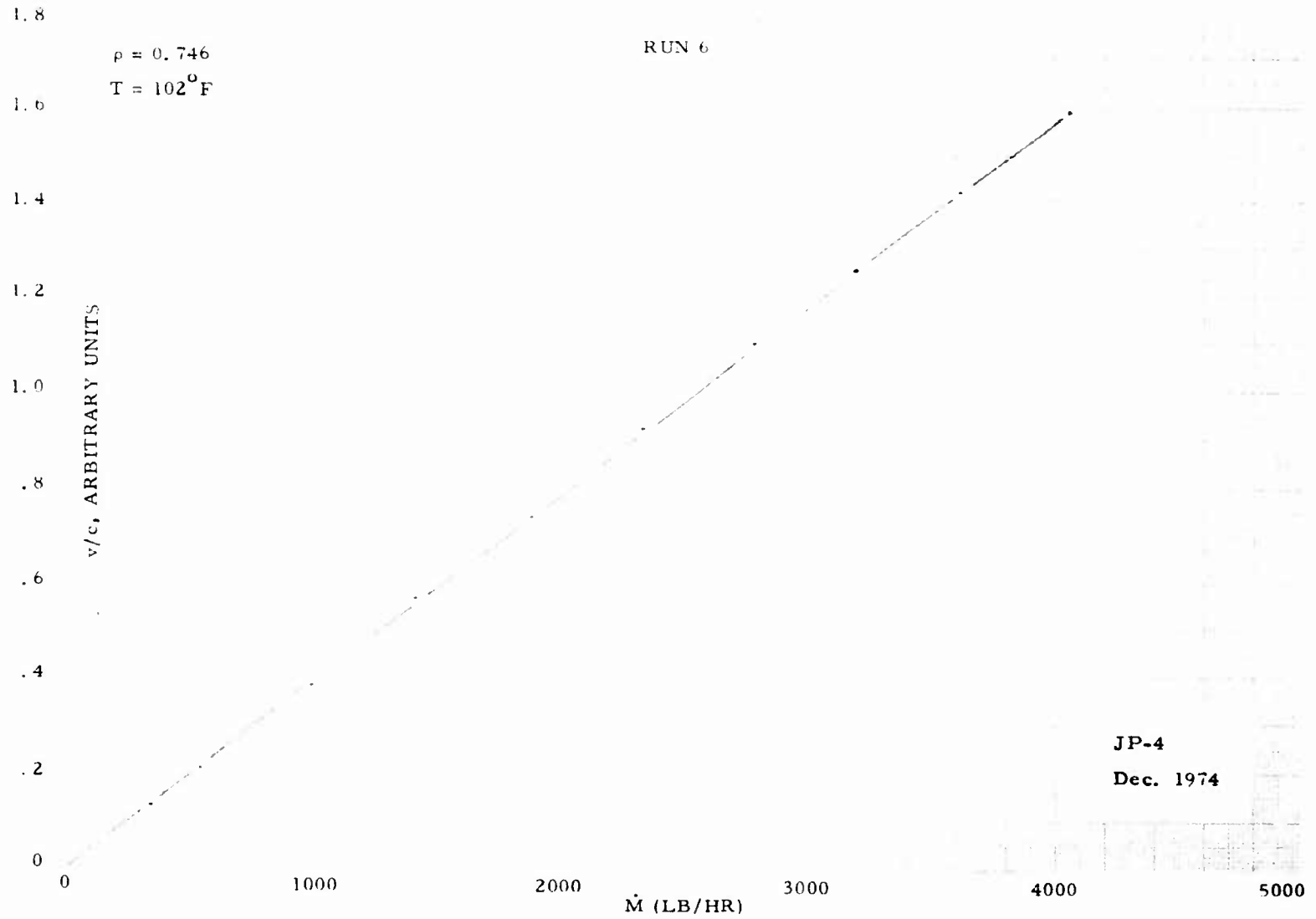

Figure A-12. v/c Versus Ṁ.

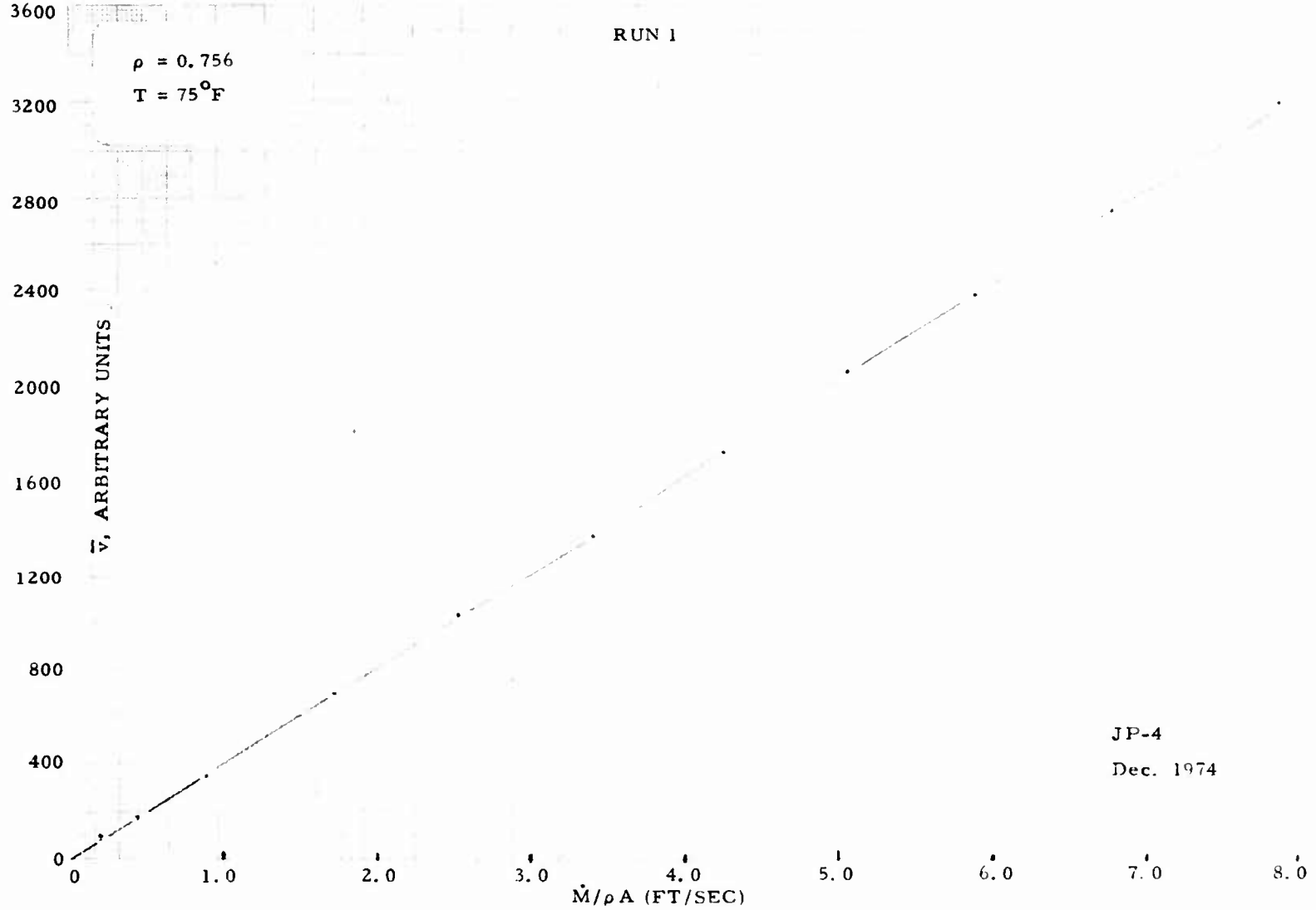

Figure A-13. $\bar{v}$ Versus $\dot{M}/\rho A$.

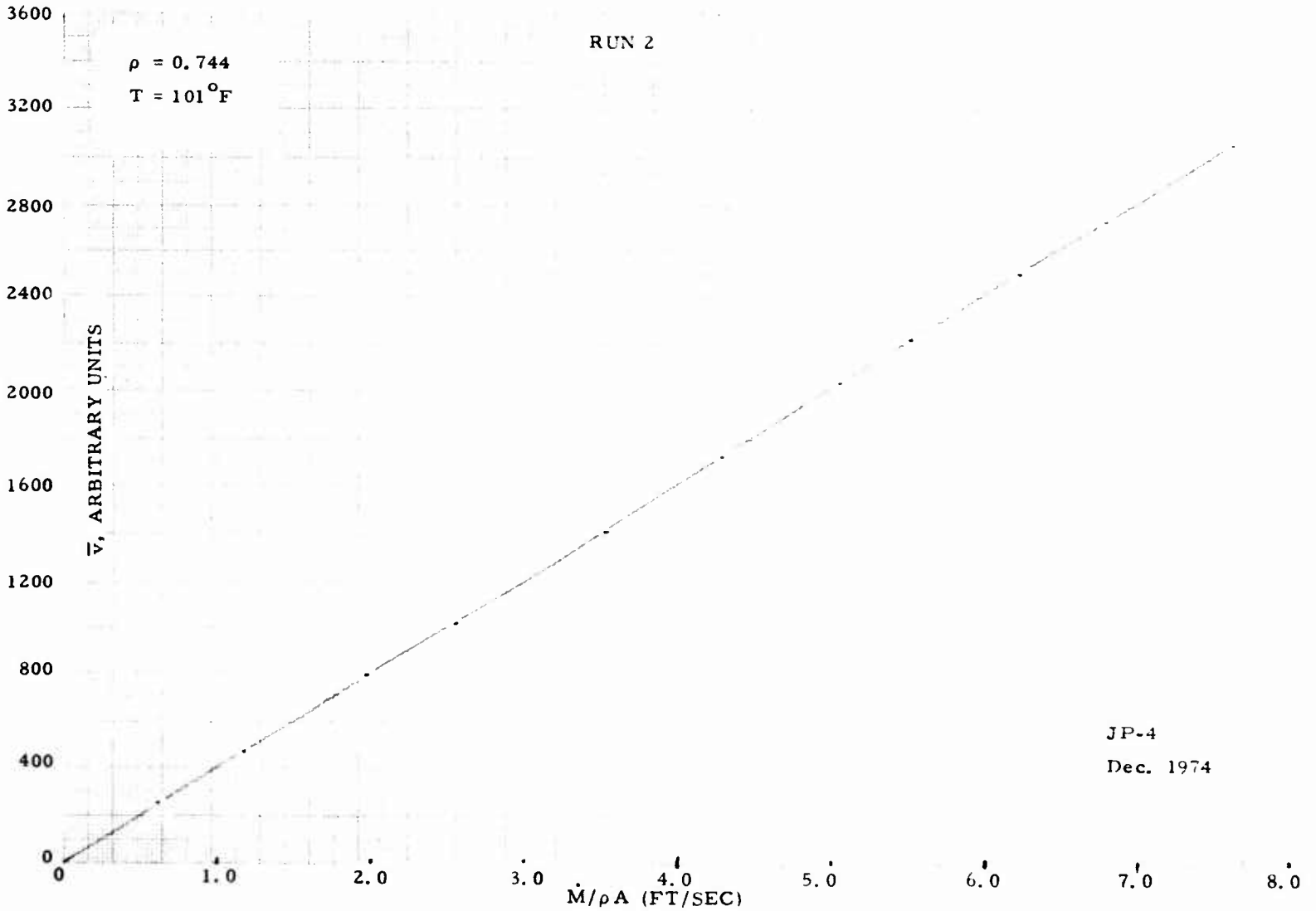

Figure A-14. $\bar{v}$ Versus $\dot{M}/\rho A$.

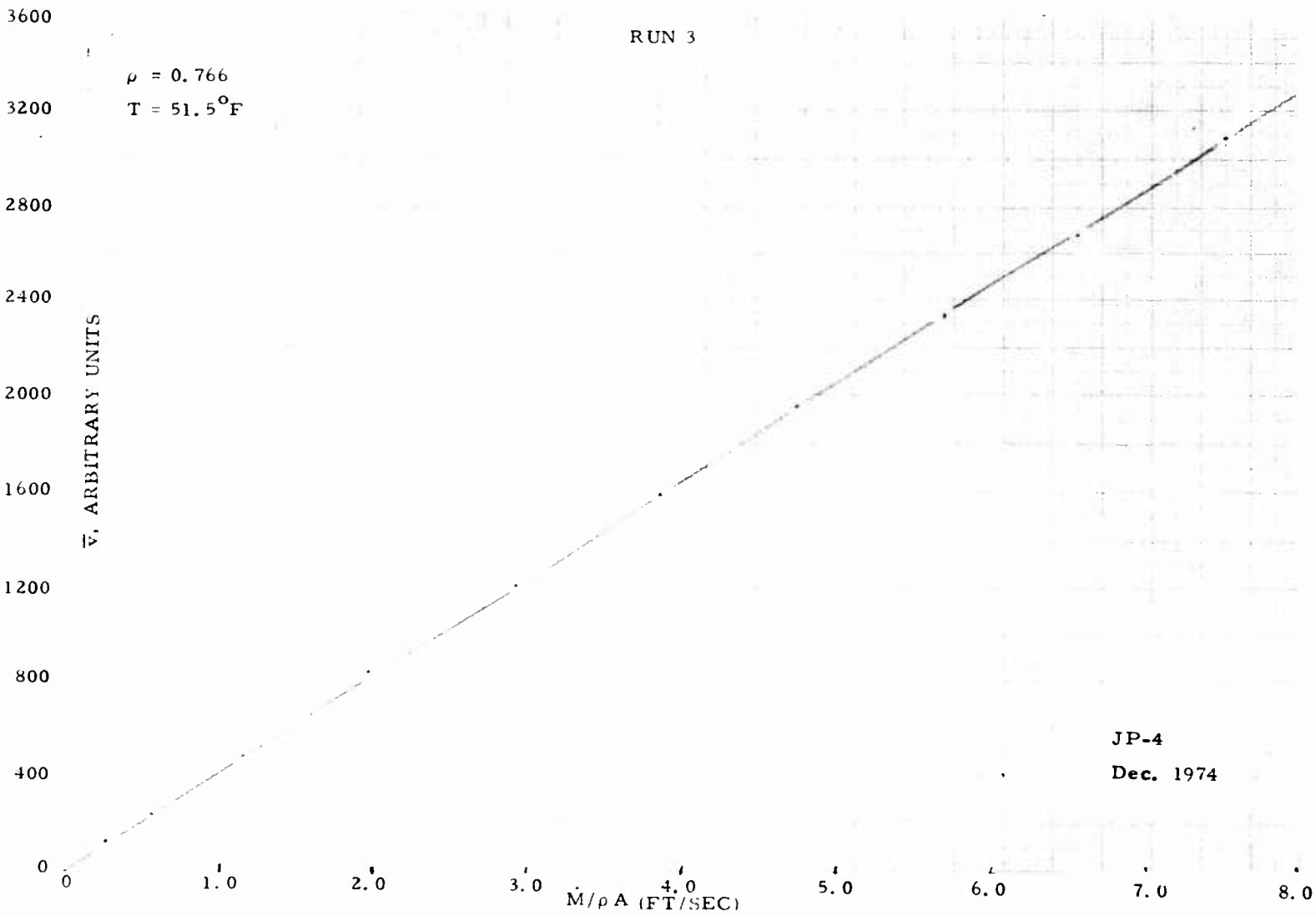

Figure A-15. $\bar{v}$ Versus $\dot{M}/\rho A$.

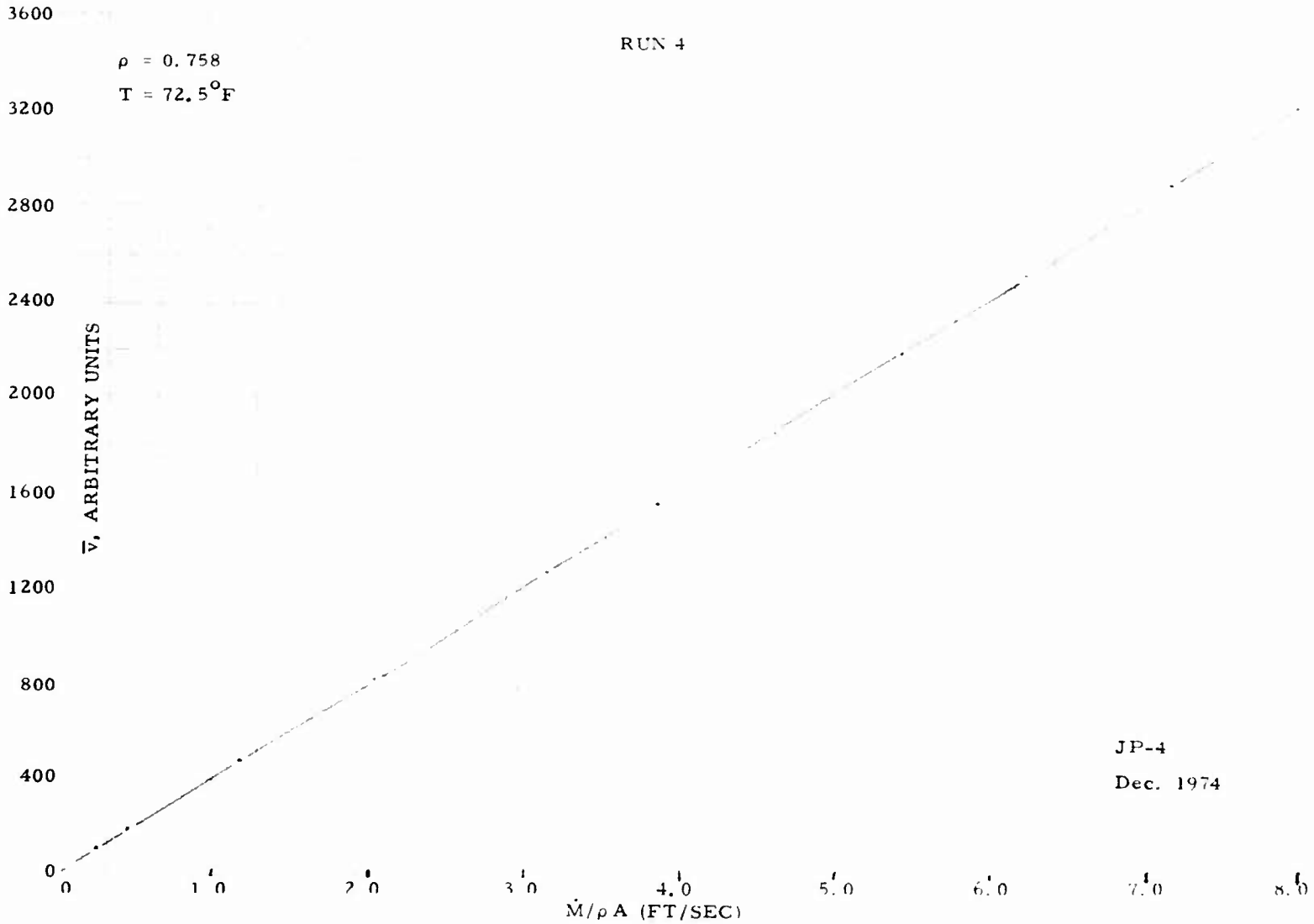

Figure A-16. $\bar{v}$ Versus $\dot{M}/\rho A$.

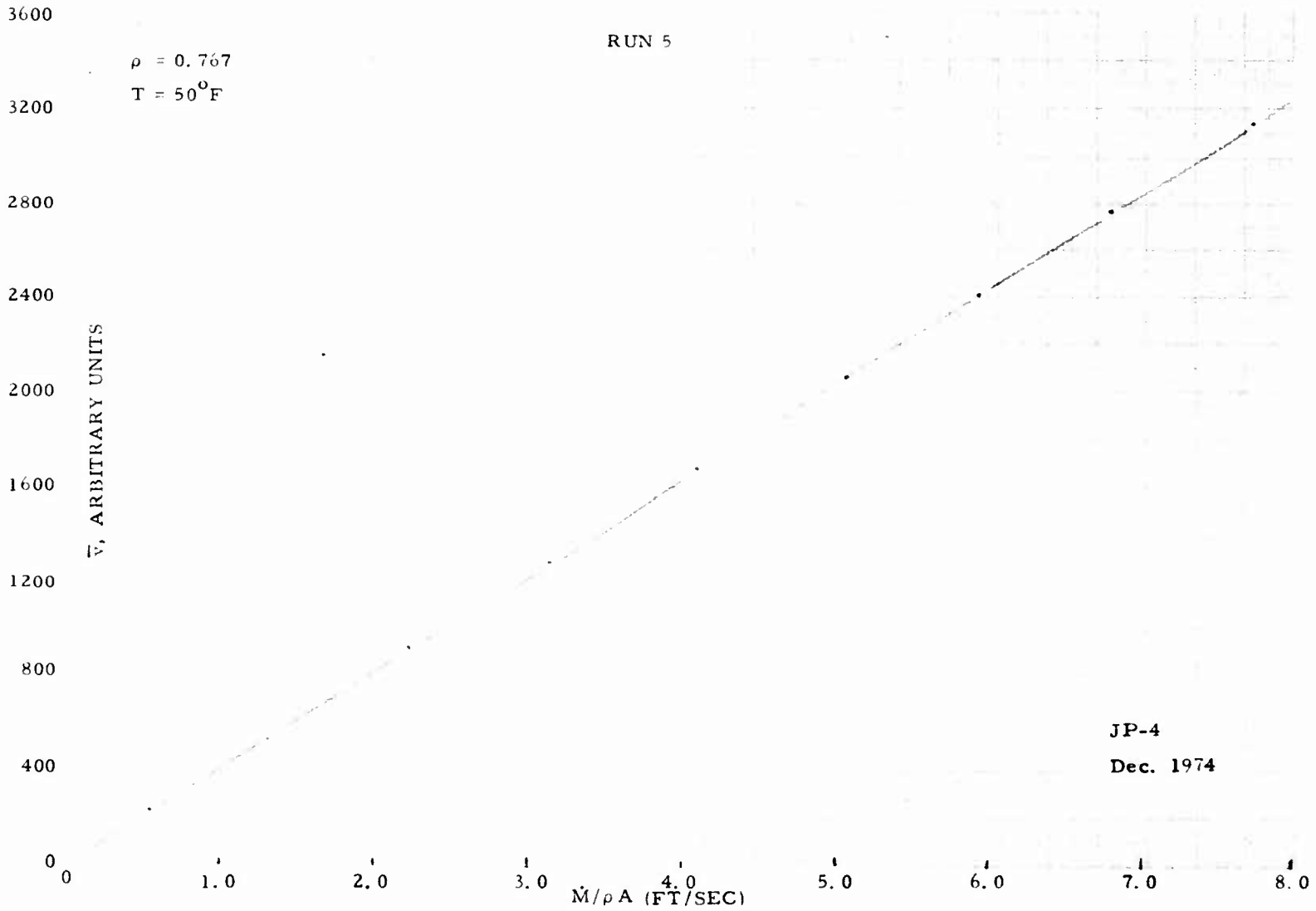

Figure A-17. $\bar{v}$ Versus $\dot{M}/\rho A$.

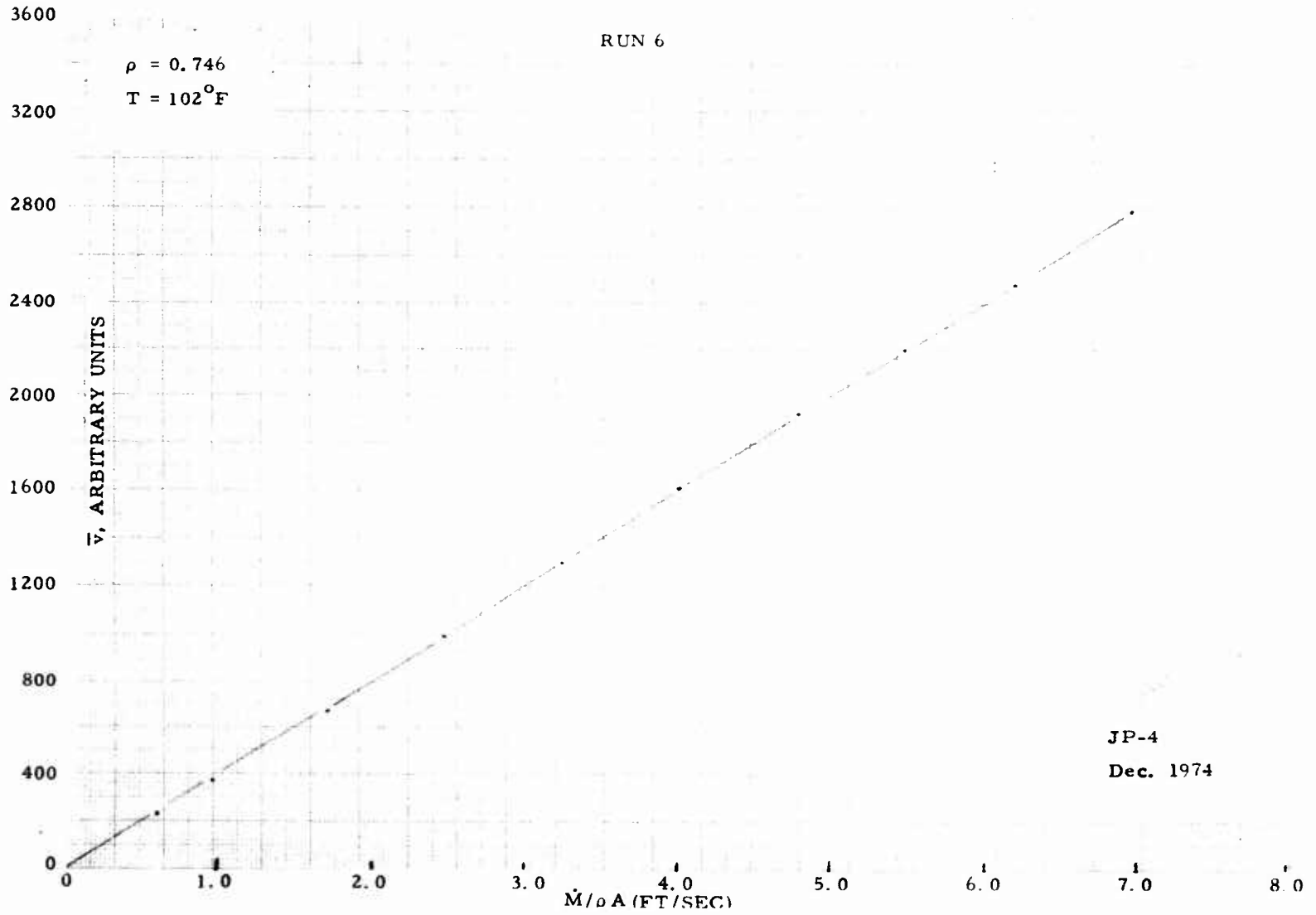

Figure A-18. $\bar{v}$ Versus $\dot{M}/\rho A$.

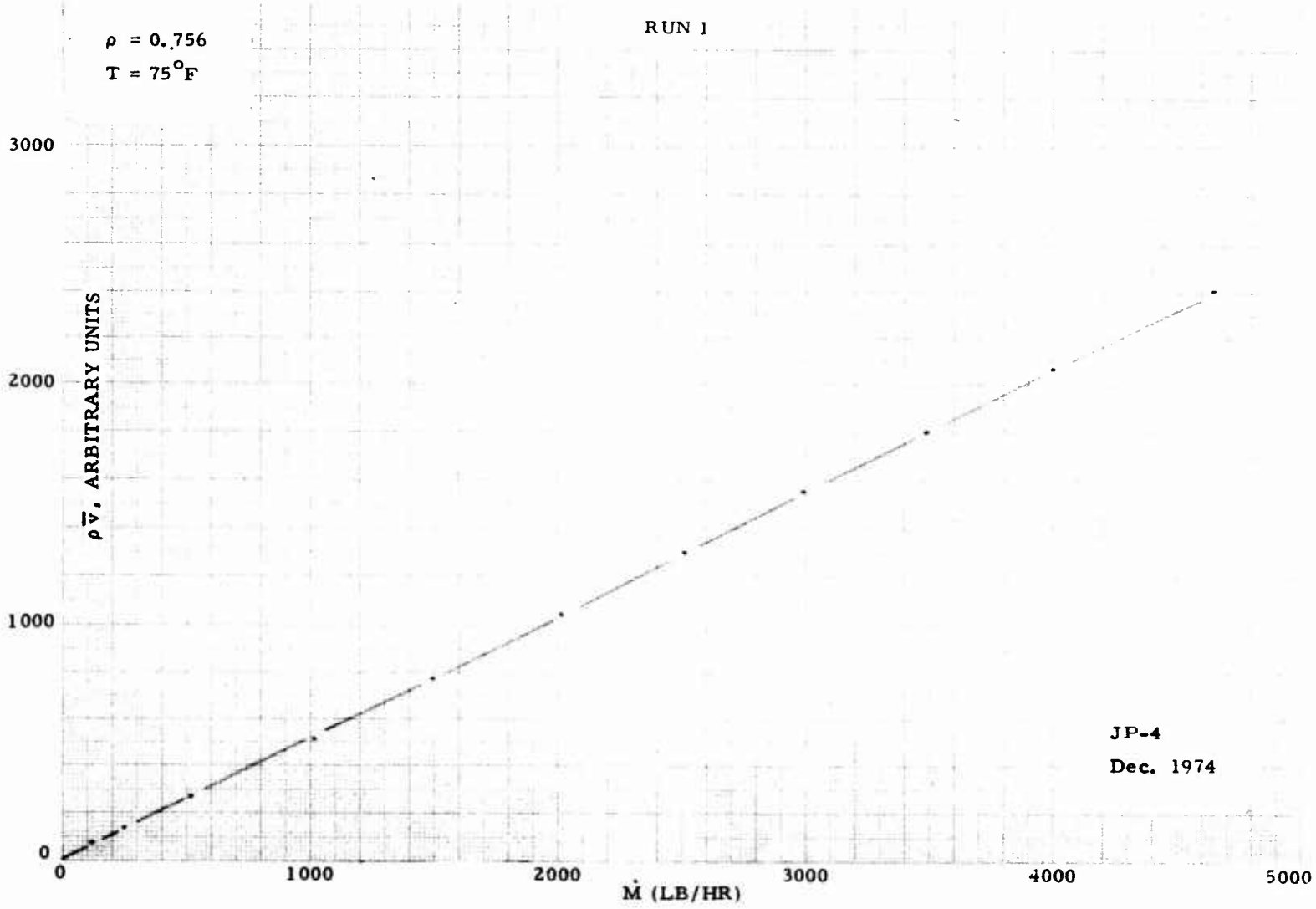

Figure A-19. $\rho \bar{v}$ Versus $\dot{M}$.

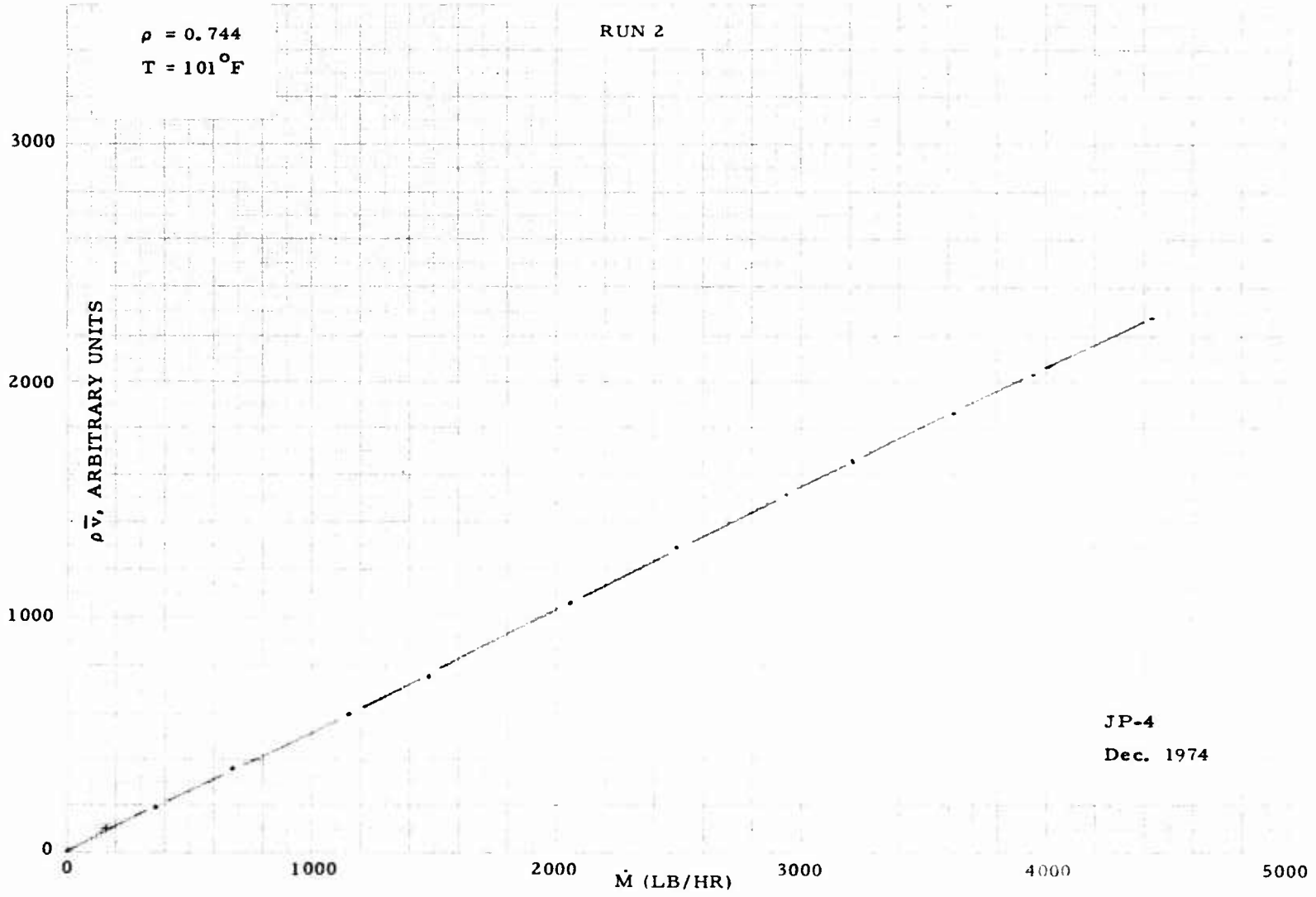

Figure A-20. $\rho \bar{v}$ Versus $\dot{M}$.

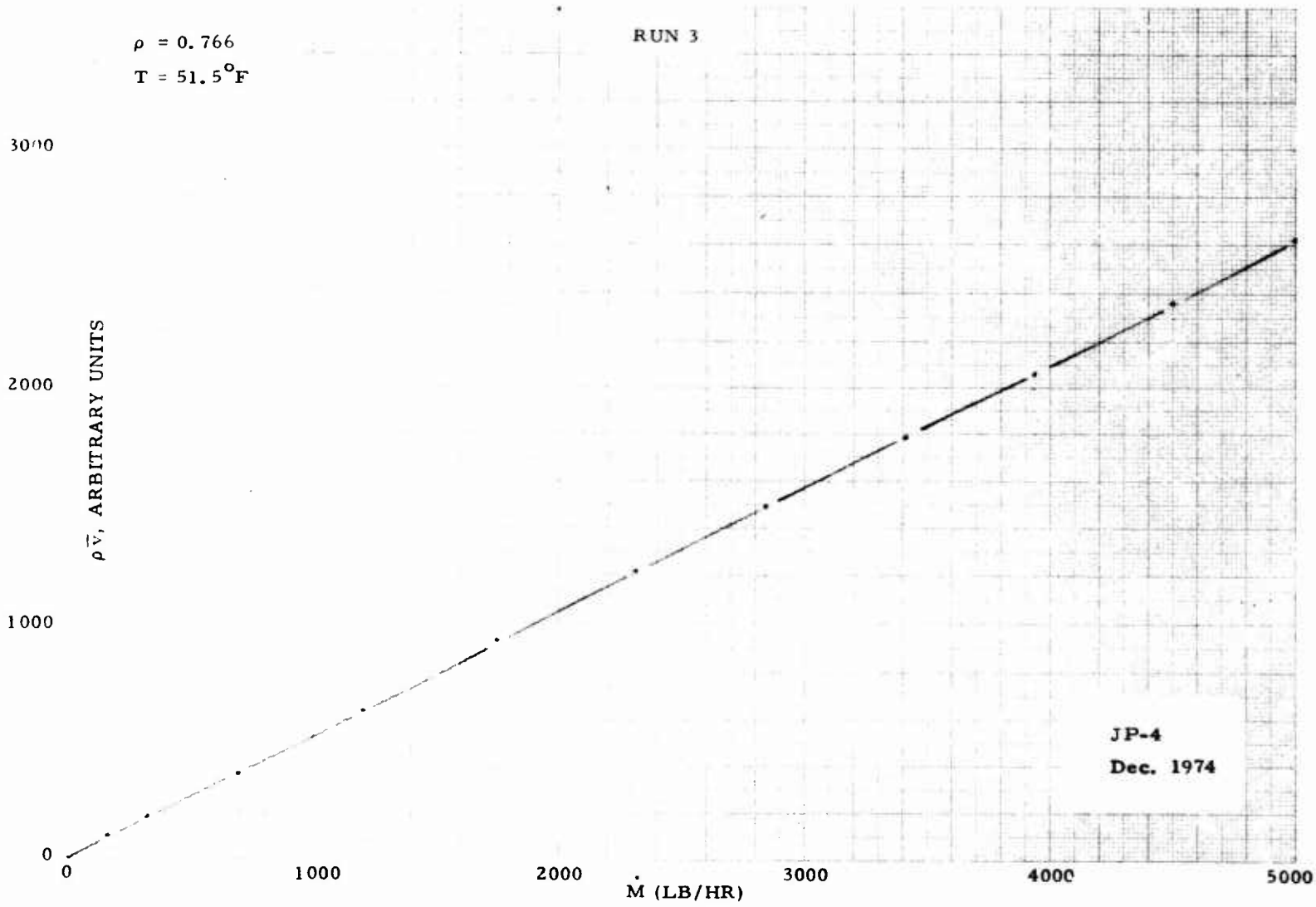

Figure A-21. $\rho \bar{v}$ Versus $\dot{M}$.

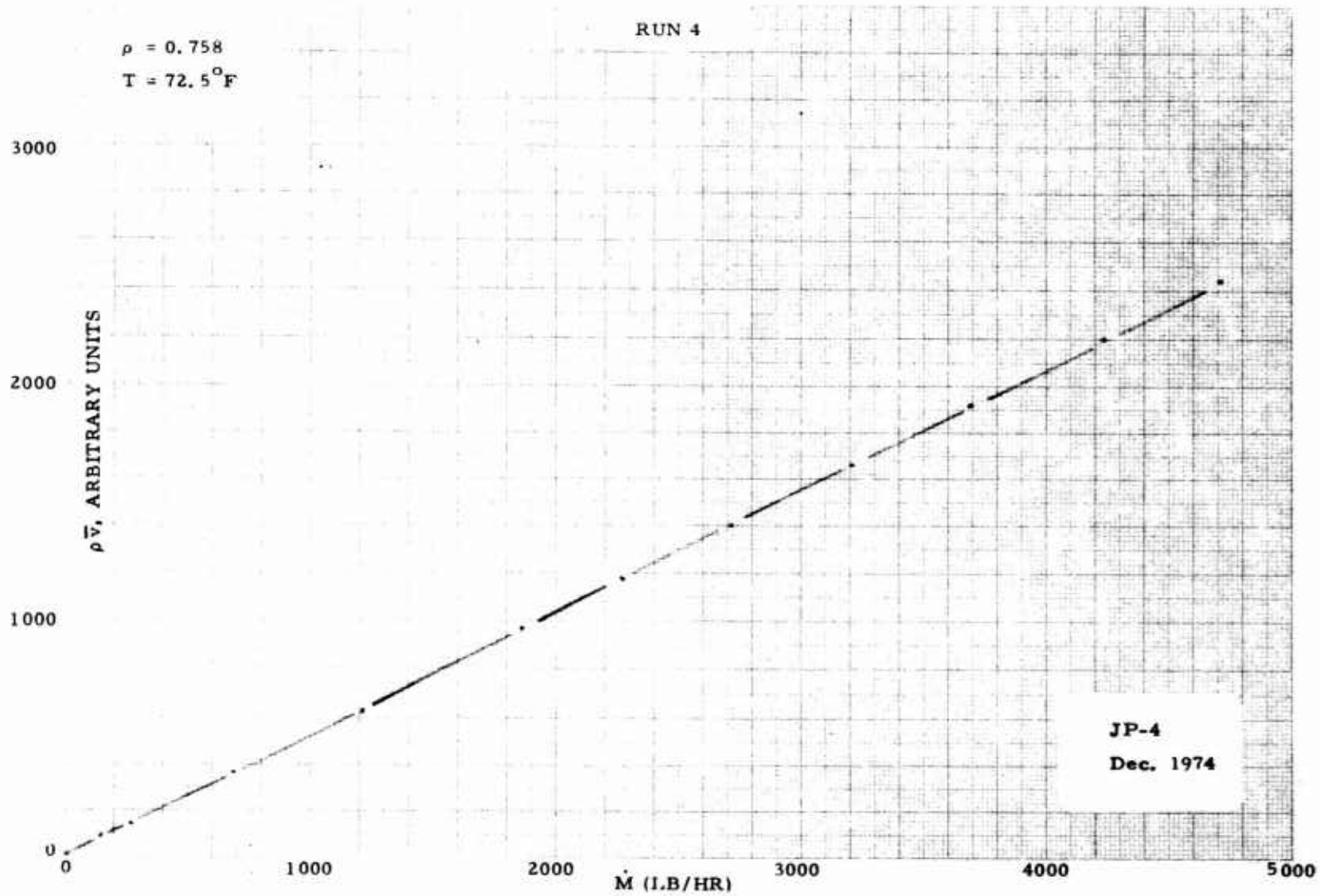

Figure A-22. $\rho \bar{v}$ Versus $\dot{M}$.

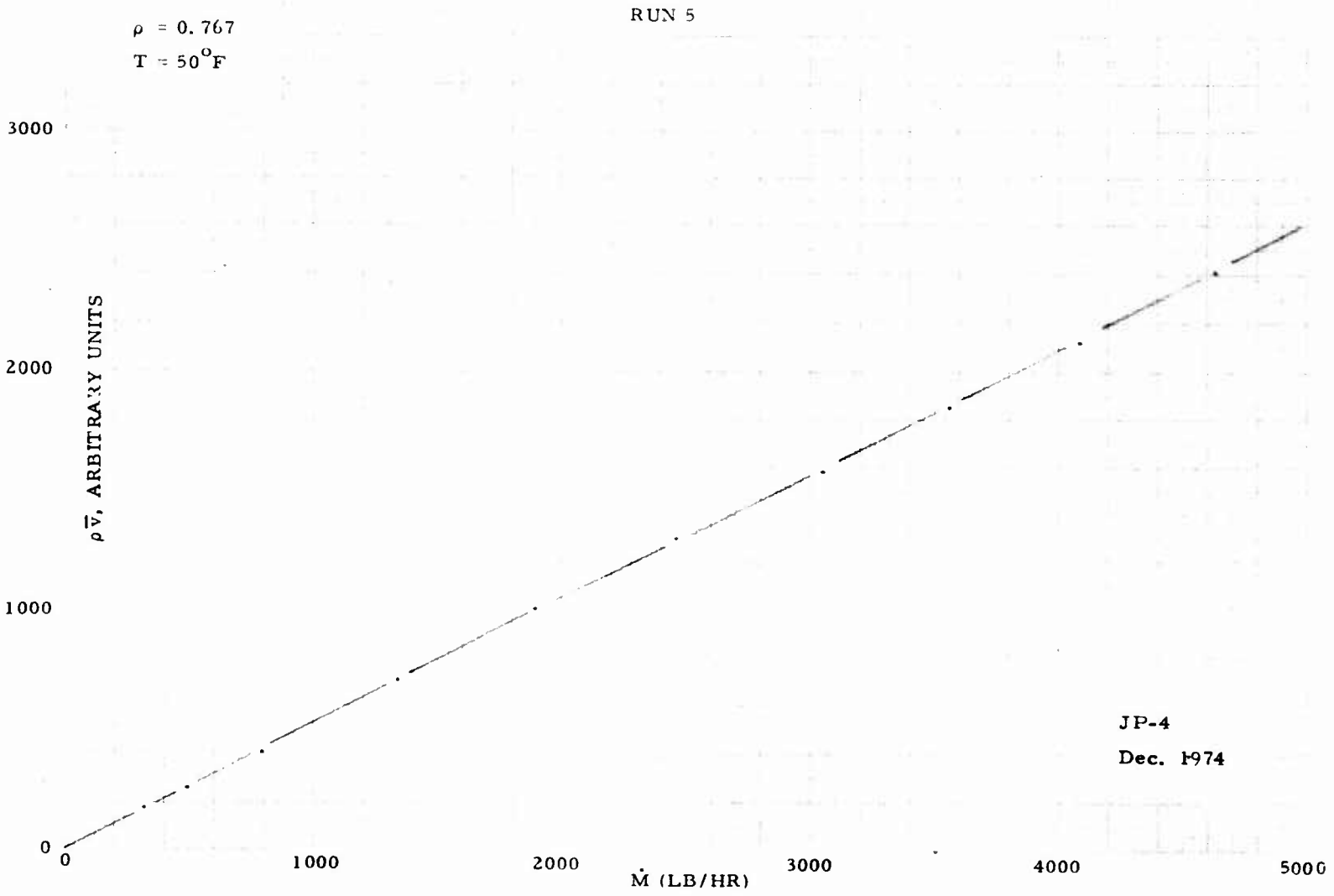

Figure A-23. $\rho \bar{v}$ Versus $\dot{M}$.

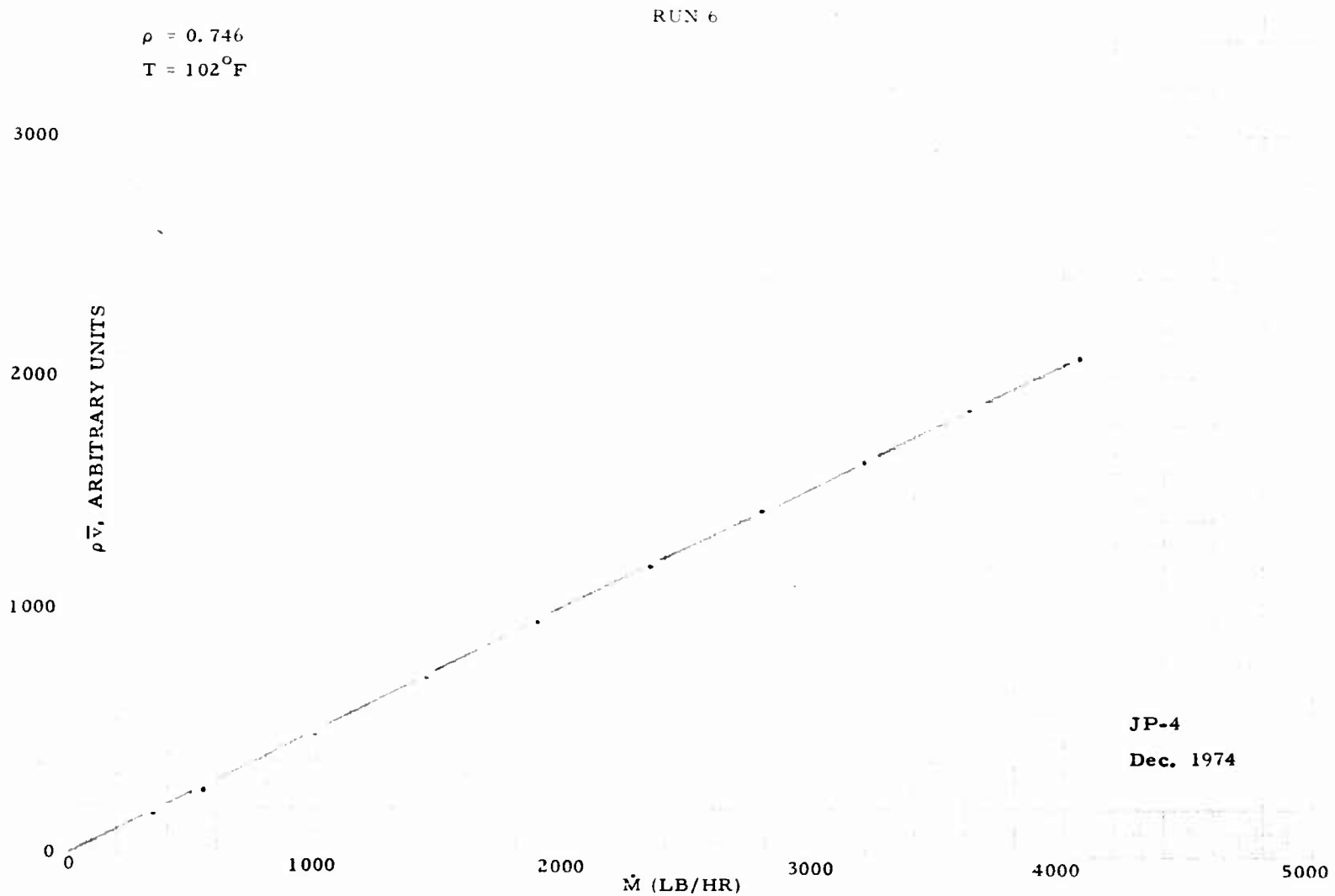

Figure A-24. $\rho \bar{v}$ Versus $\dot{M}$.

June 1974 Test Data

In the following pages we present, in tabular and graphical form, the complete test data on six separate runs, which were taken at Avco/Lycoming in June 1974. The tables are arranged in the order in which the data were taken. The graphs, however, are ordered, first, according to the measured quantity, and secondly, according to the run number. This is done for easy comparison of a given measured quantity (e.g., v/c^2, v, etc.) from run to run.

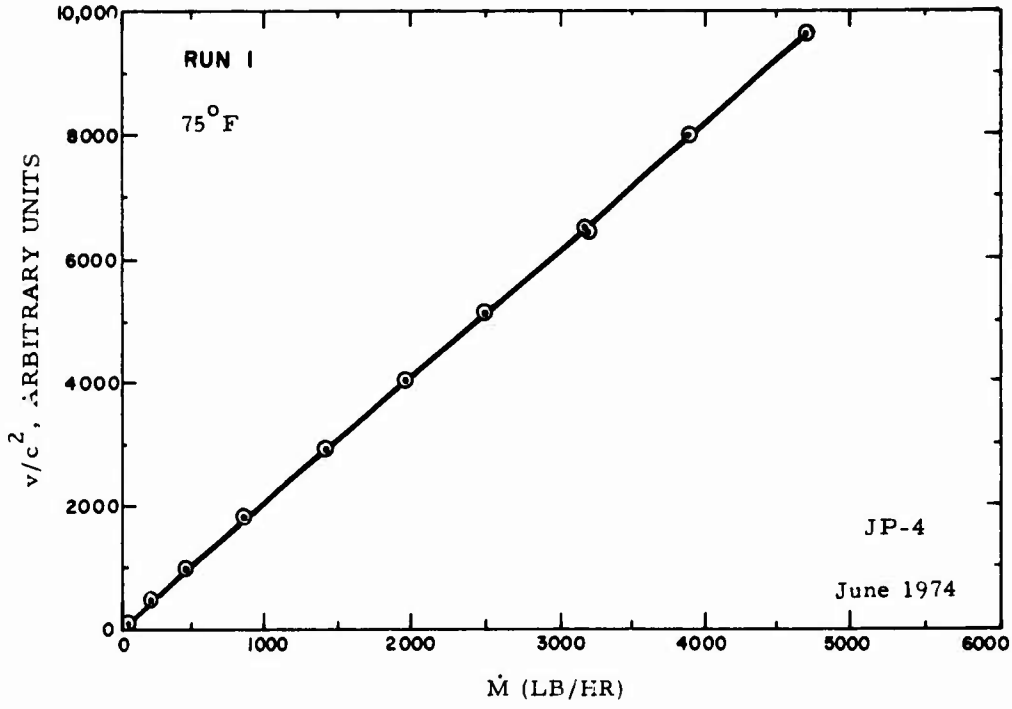

Figure A-25. v/c^2 Versus $\dot{M}$.

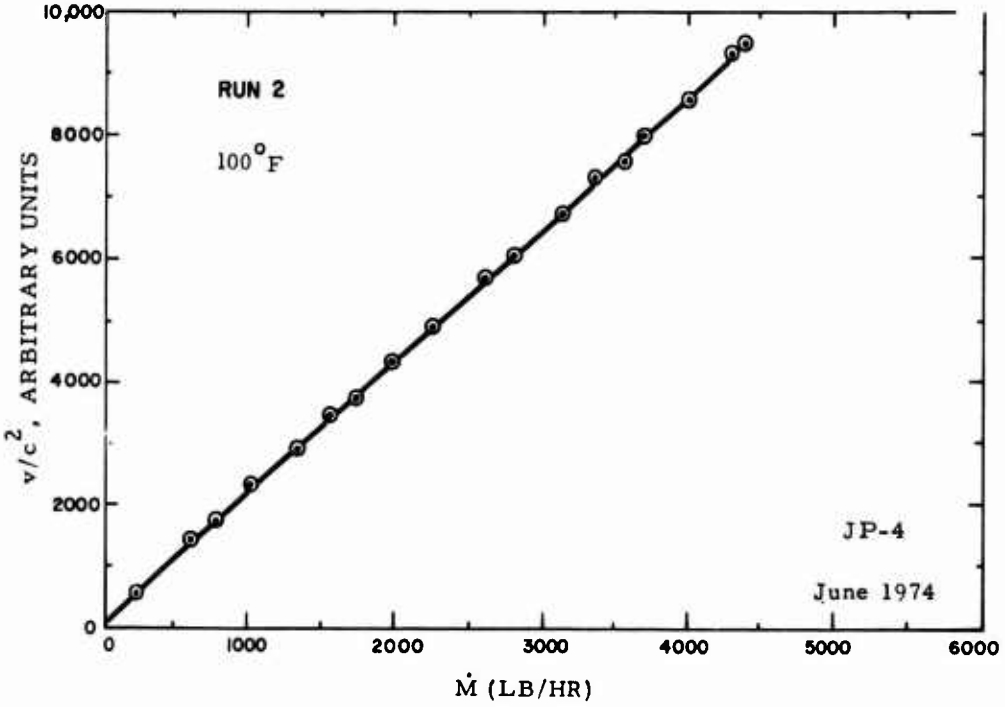

Figure A-26. v/c^2 Versus $\dot{M}$.

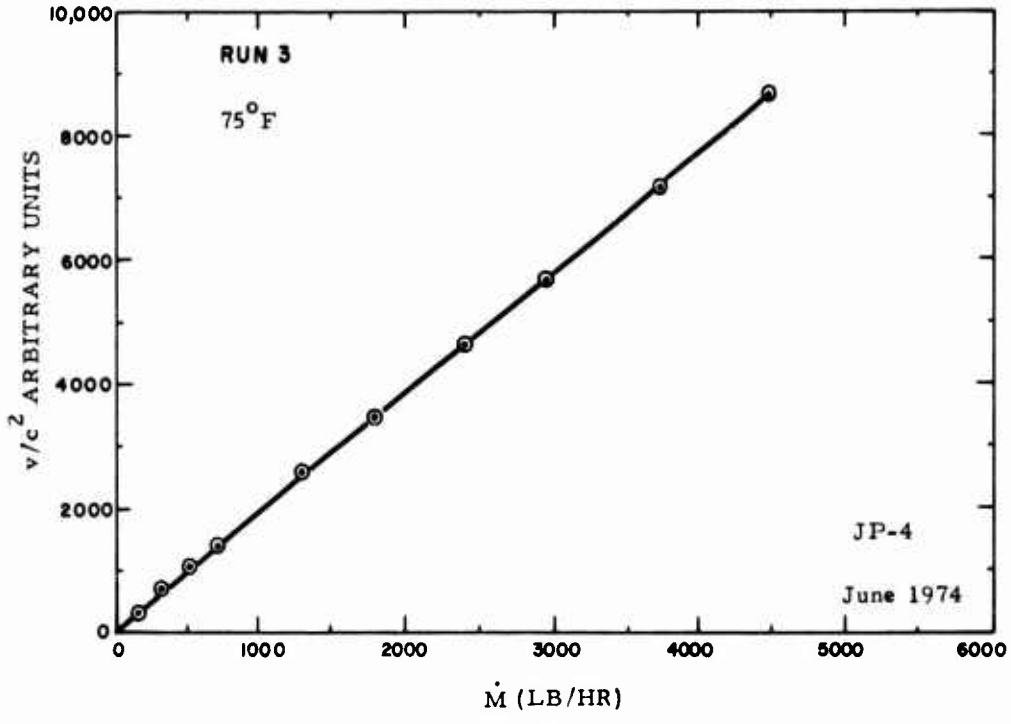

Figure A-27. v/c^2 Versus $\dot{M}$.

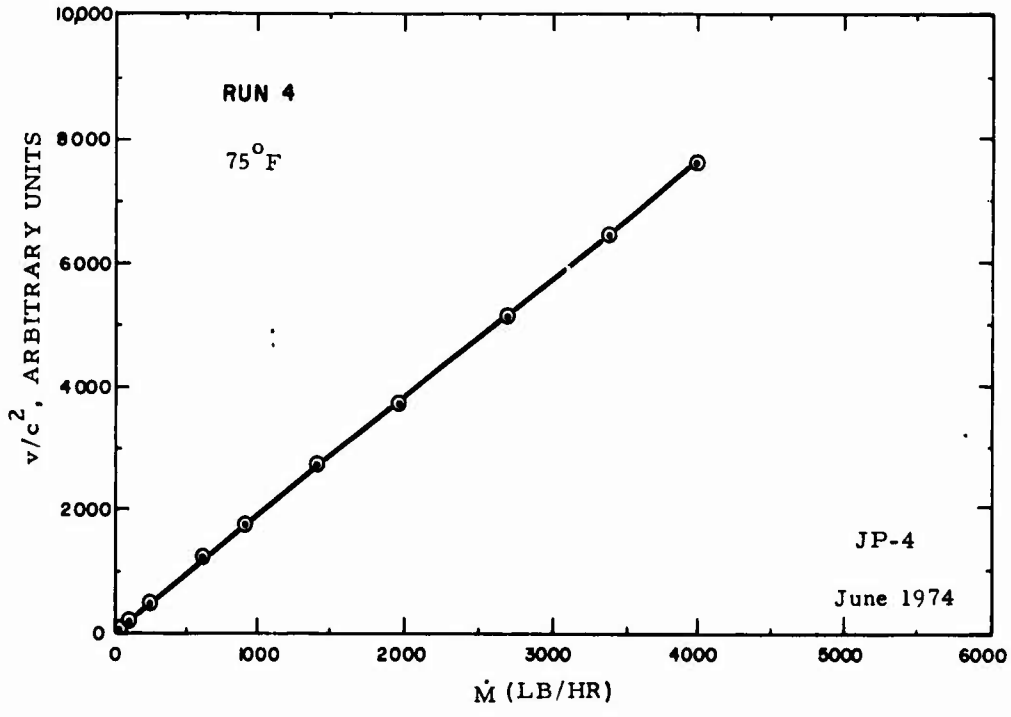

Figure A-28. v/c^2 Versus $\dot{M}$.

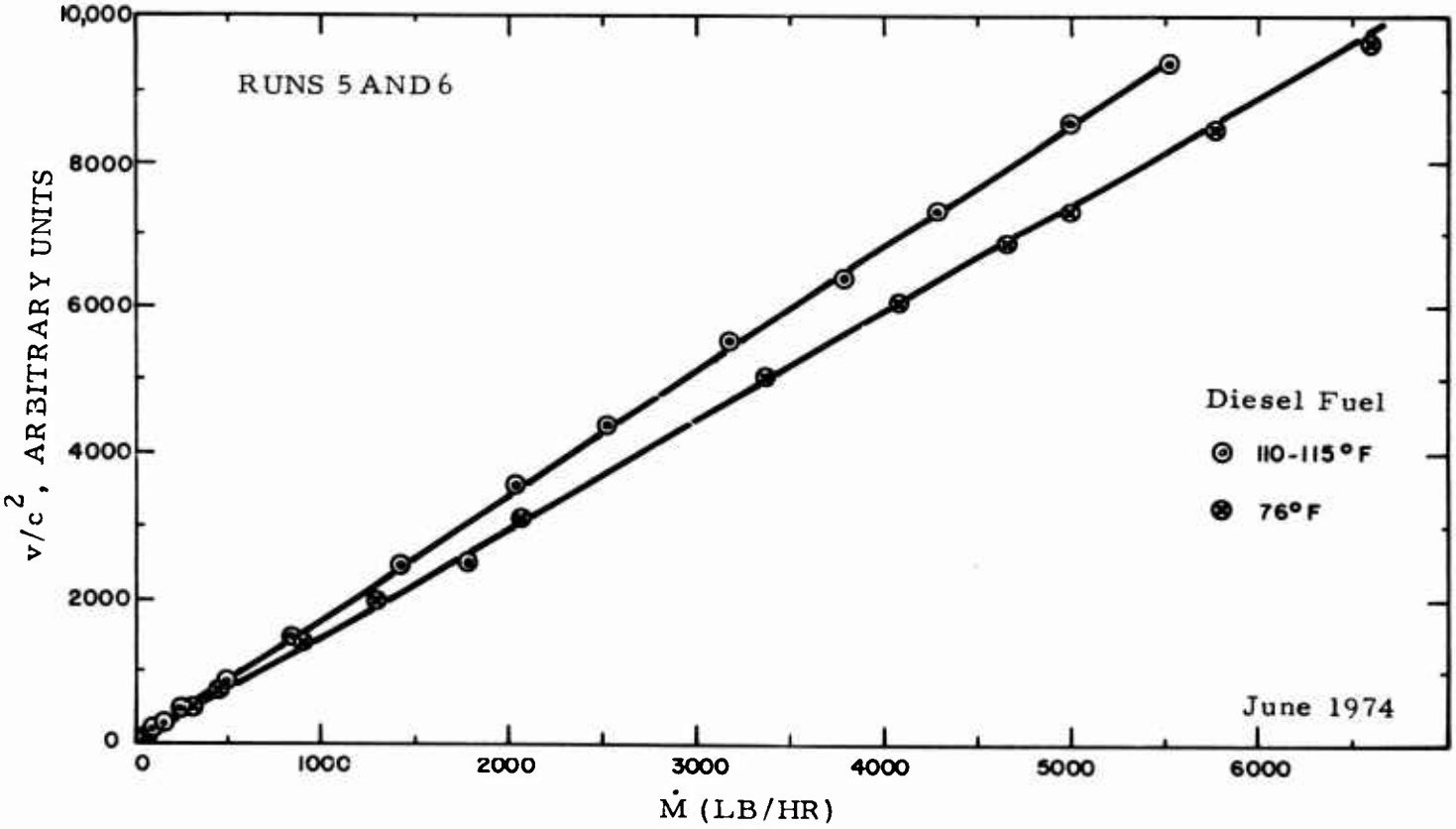

Figure A-29. v/c^2 Versus $\dot{M}$.

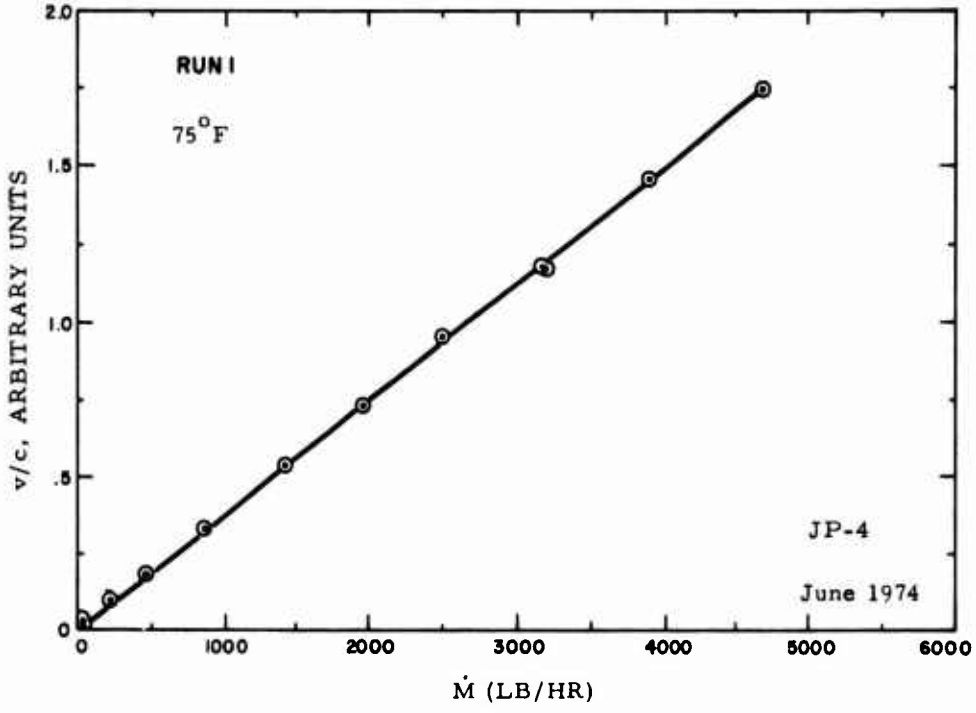

Figure A-30. v/c Versus $\dot{M}$.

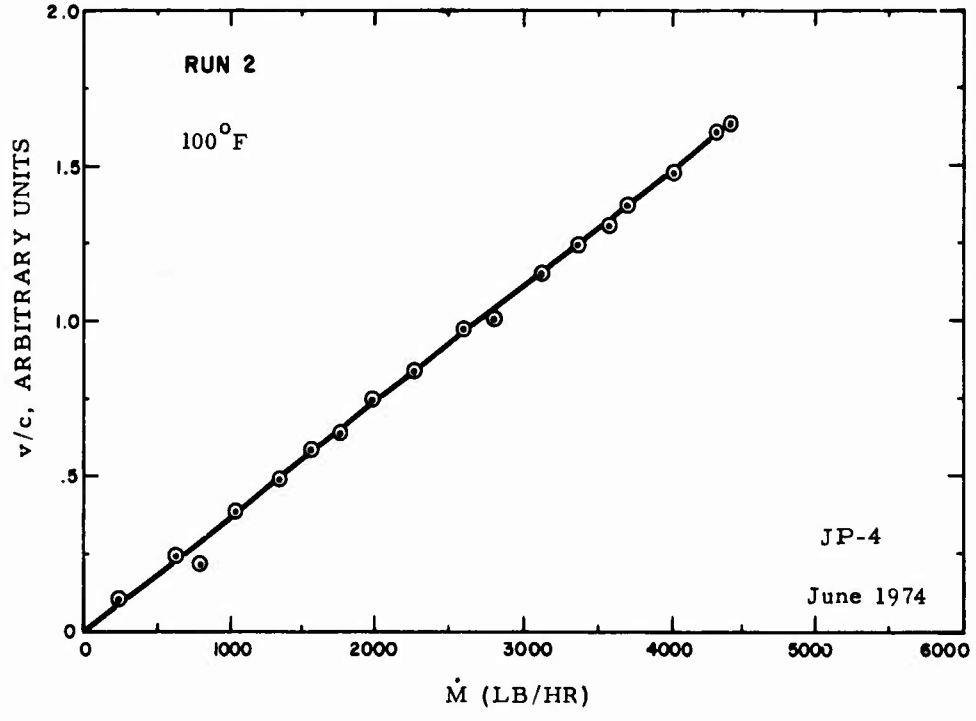

Figure A-31. v/c Versus $\dot{M}$.

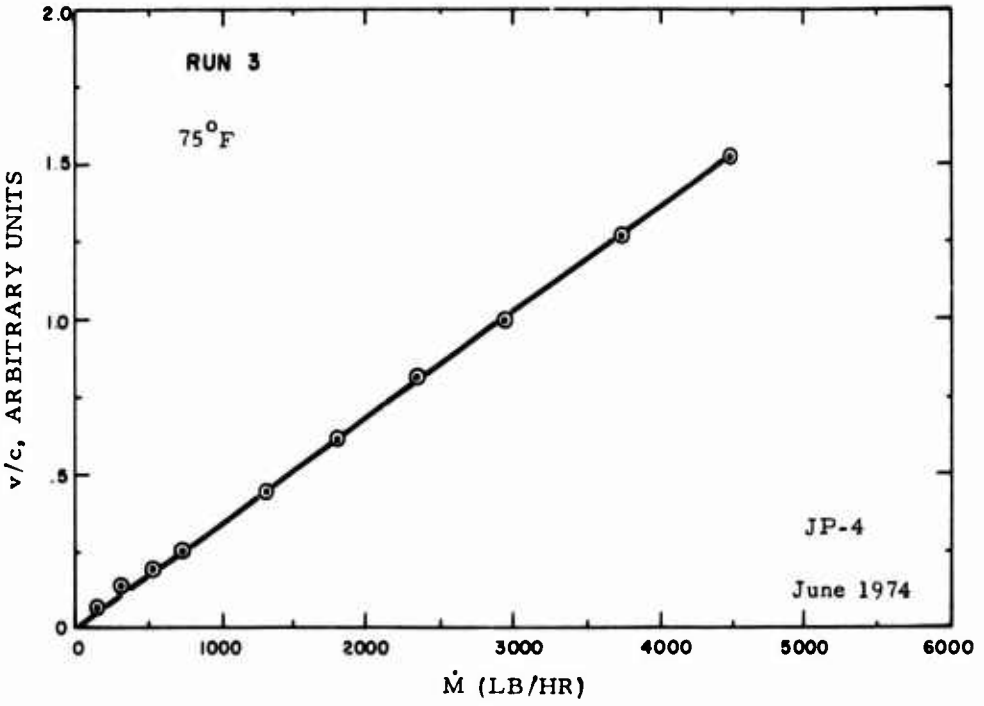

Figure A-32. v/c Versus Ṁ.

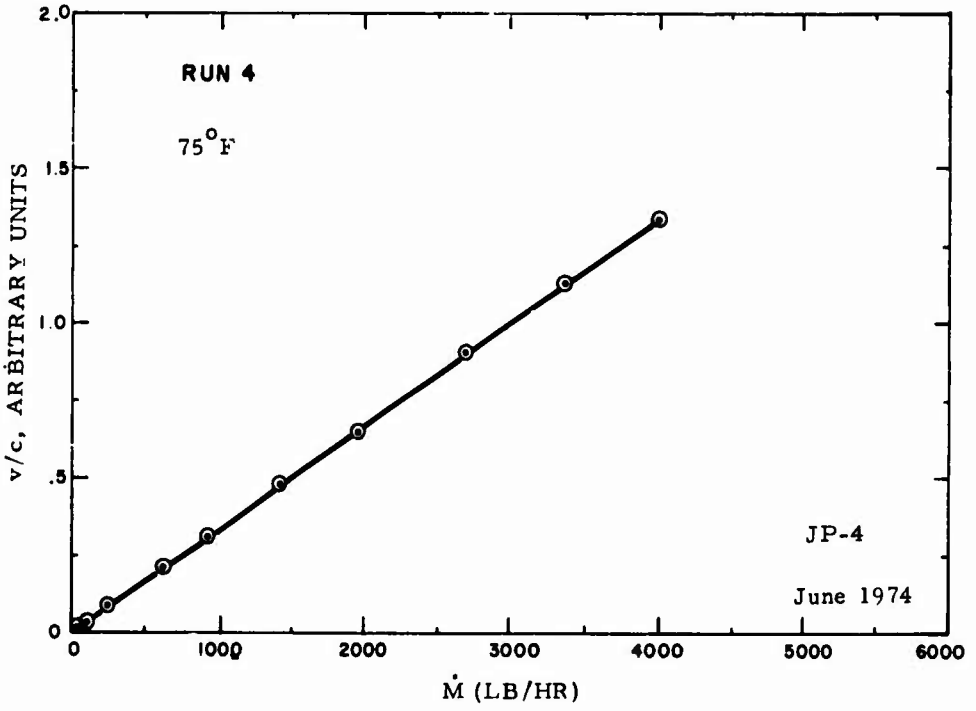

Figure A-33. v/c Versus Ṁ.

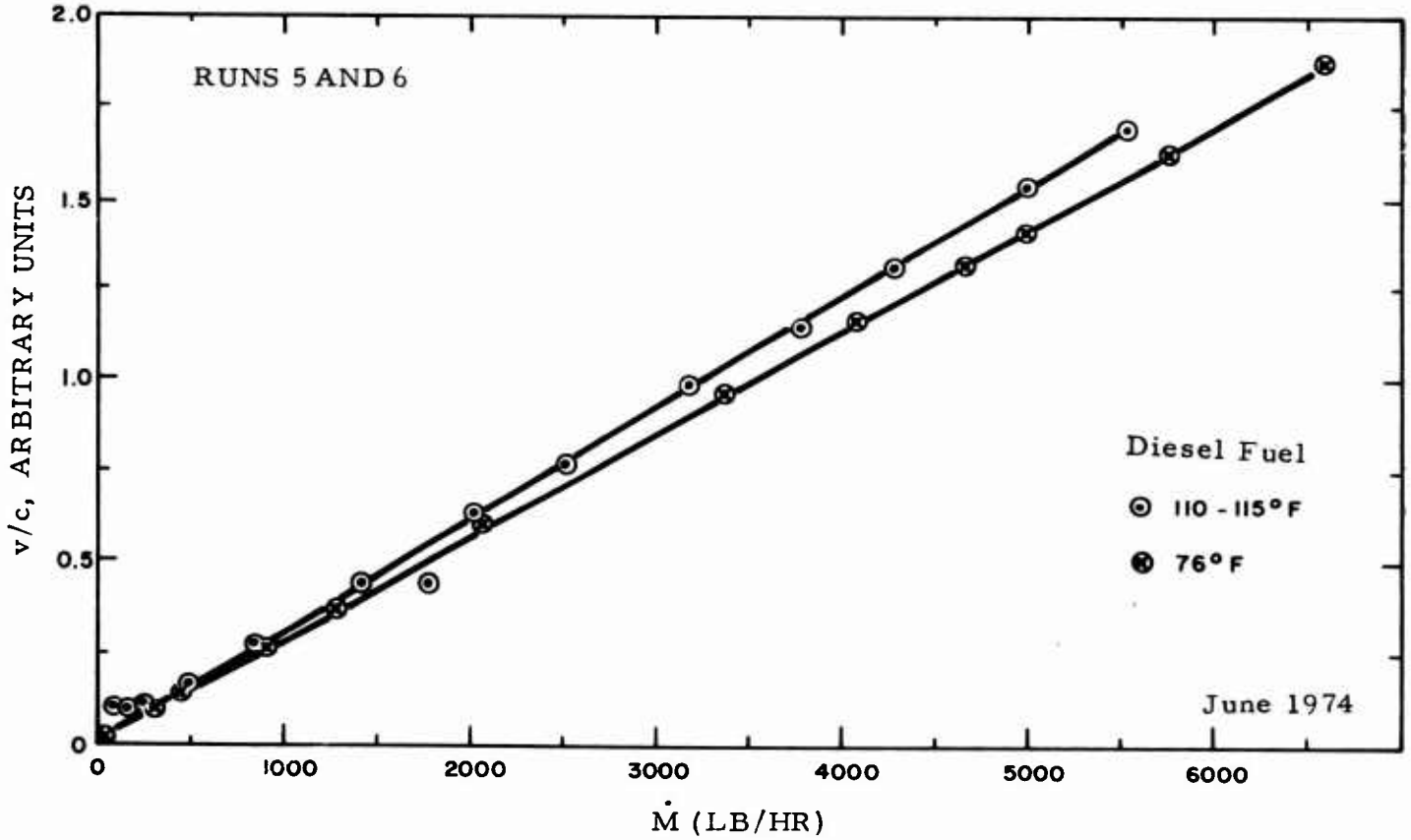

Figure A-34. v/c Versus $\dot{M}$.

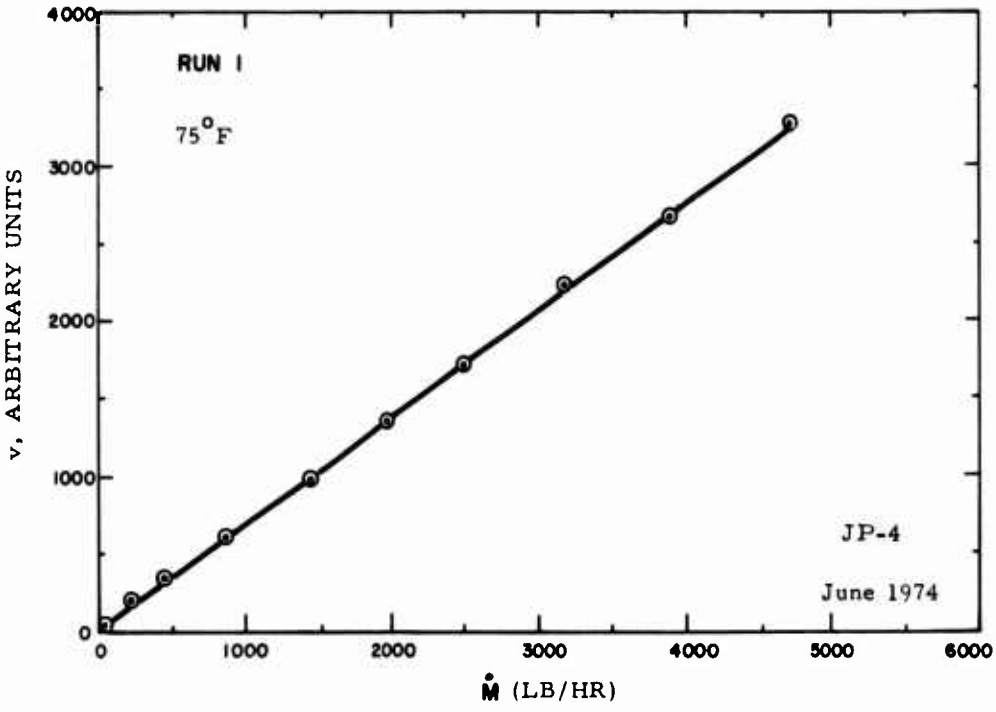

Figure A-35. v Versus $\dot{M}$.

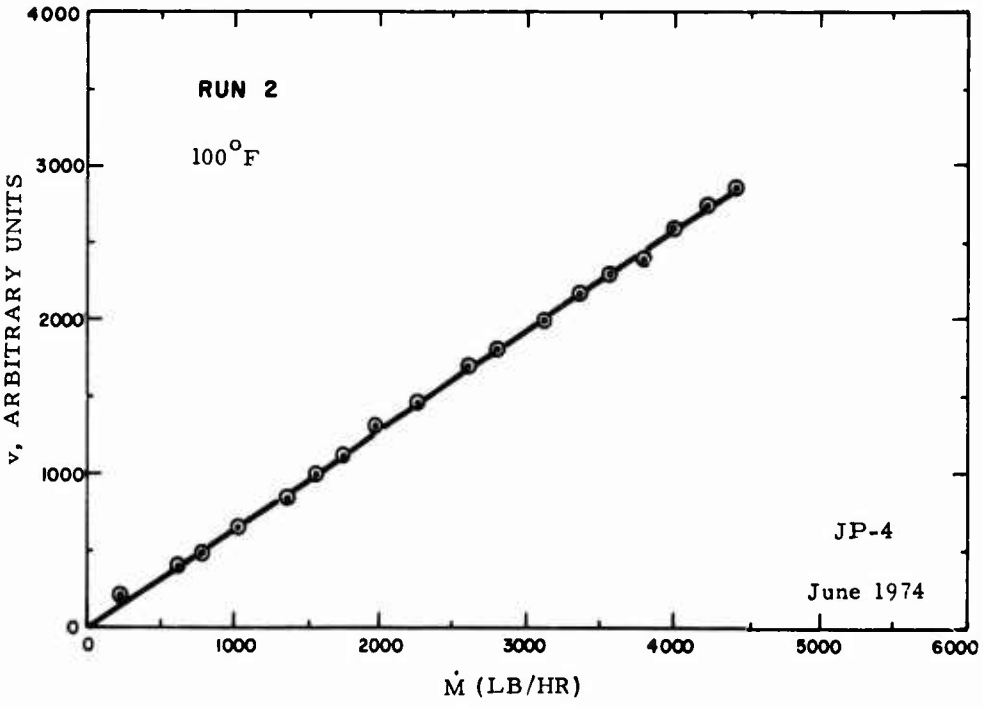

Figure A-36. v Versus $\dot{M}$.

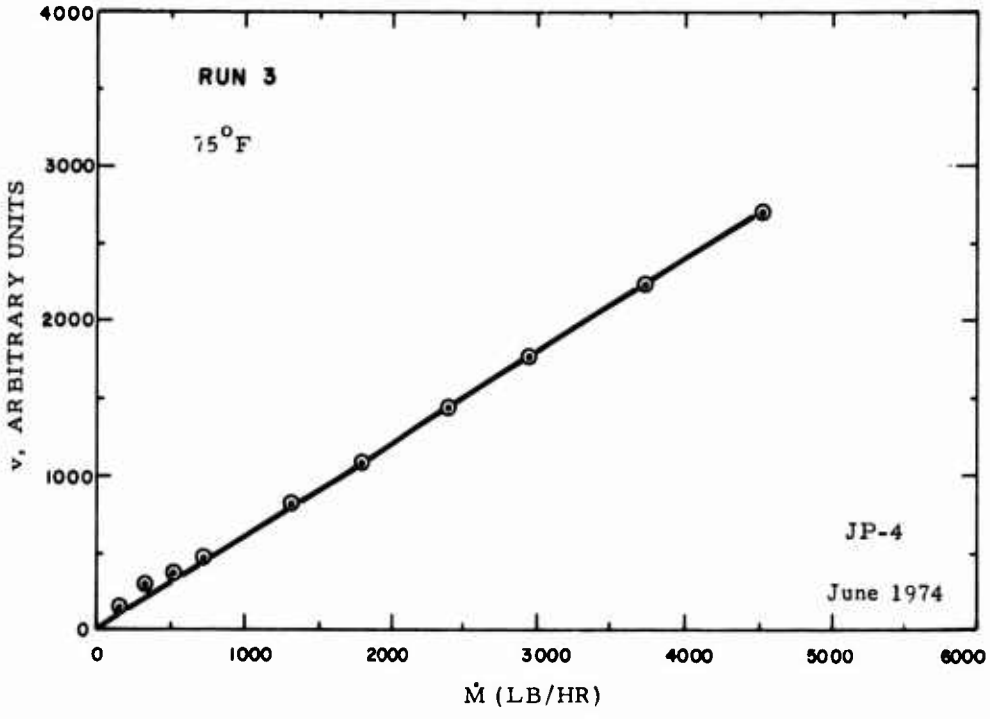

Figure A-37. v Versus Ṁ.

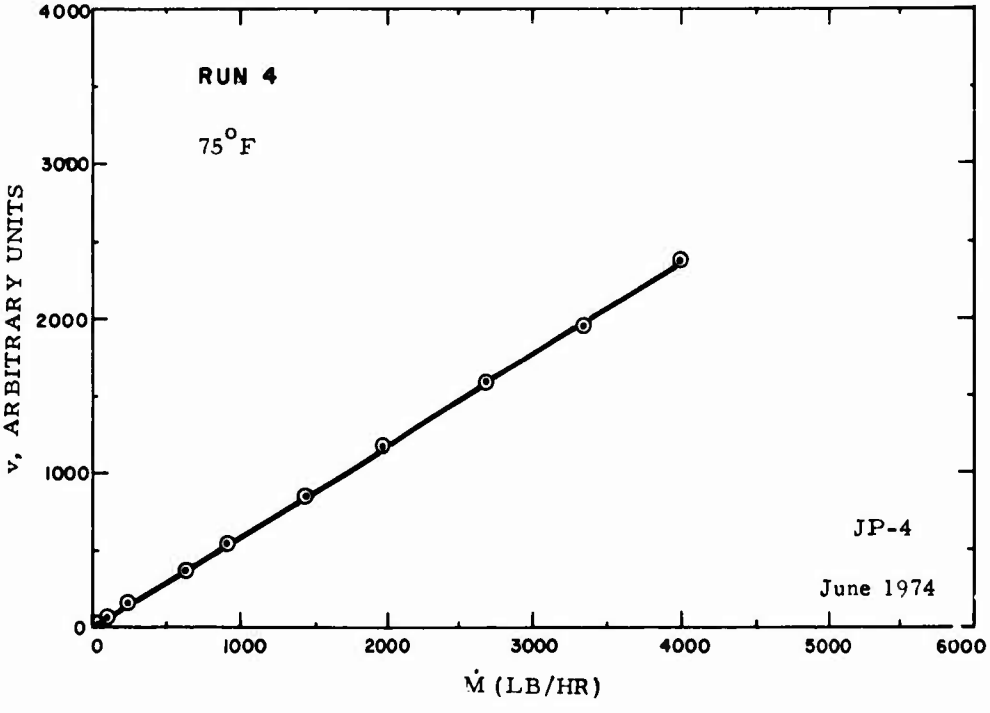

Figure A-38. v Versus Ṁ.

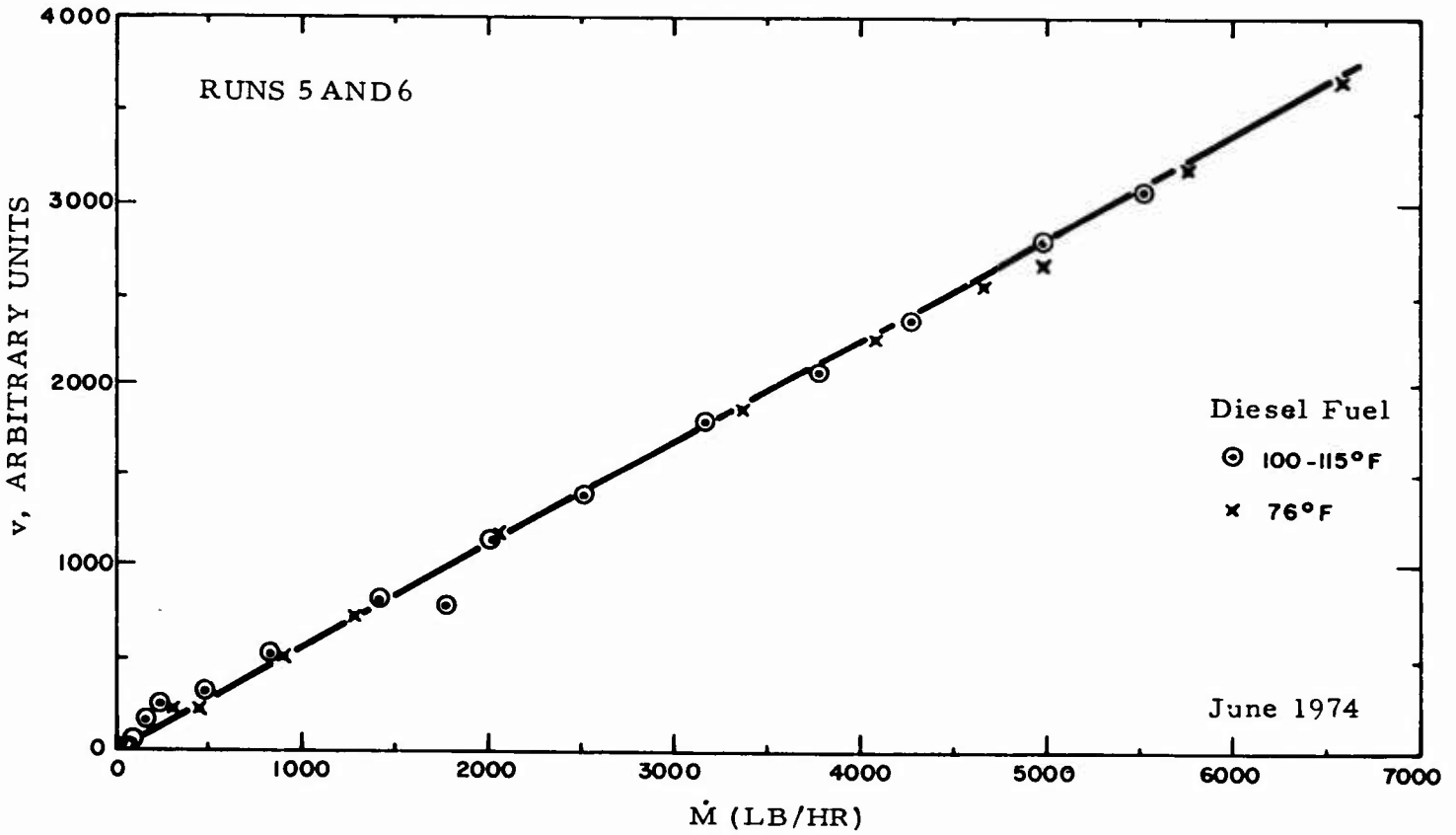

Figure A-39. v Versus $\dot{M}$.

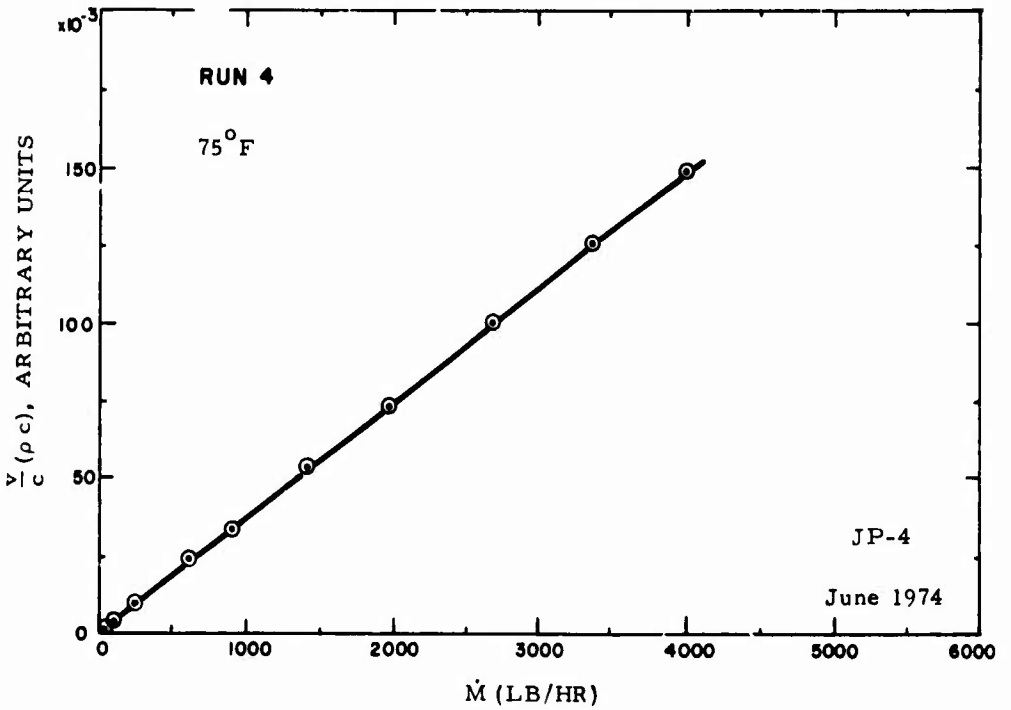

Figure A-40. $\frac{v}{c}(\rho\, c)$ Versus $\dot{M}$.

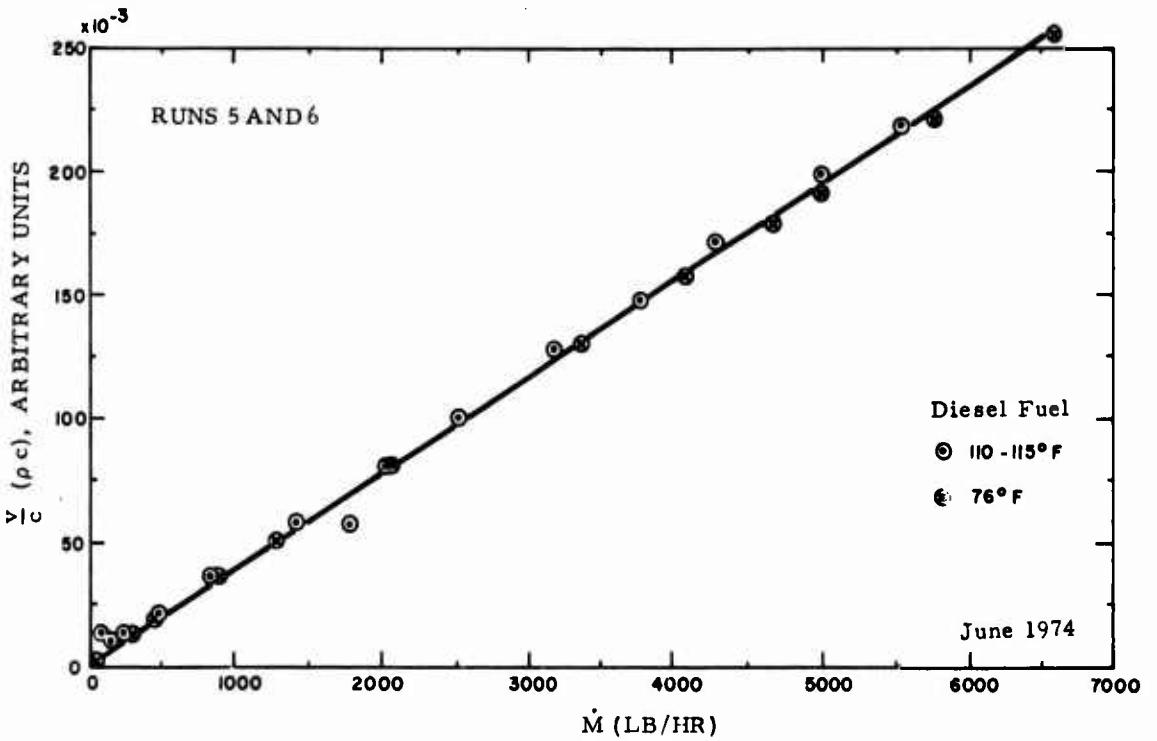

Figure A-41. $\frac{v}{c}$ $(\rho\, c)$ Versus $\dot{M}$.

APPENDIX B
AREA-AVERAGING ULTRASONIC FLOWMETERS*

BACKGROUND

This appendix relates in general to ultrasonic flowmeters and more particularly to area-average measurement of fluid flow through conduits.

In the measurement of the fluid velocity flow rates where the fluids are confined within a conduit, one nonintrusive technique which has proved to be successful in a number of applications is the use of electroacoustic transducers to generate ultrasonic waves which are transmitted diagonally across the conduit, often at 45^{o}, such that a significant component of the ultrasonic beam is transmitted in the direction parallel to the direction of flow of the fluid through the conduit. The ultrasonic modes generated at the transducers may be either longitudinal waves or shear waves, with the latter type being converted by refraction at a solid/fluid interface into longitudinal waves. The measurement of the flow velocity is made, usually, by electronic circuits which respond to the small difference in transit time between a longitudinal wave traveling diagonally downstream and one traveling diagonally upstream. The measurements may be made with waves traveling different paths or, preferably, over a common path. Also, the transit time measurements may be made sequentially on upstream and downstream transits, or, by employment of pairs of transducers, they may be made simultaneously. The determination of transit time may be accomplished by clocking the time difference between the leading edges of two video pulses or alternatively by measuring the phase shift between emitted continuous waves or bursts of continuous waves. Another technique for flow velocity measurement using ultrasonic beams involves measurement of doppler frequency shifts of scattered waves. Doppler methods, however, are presently restricted mainly to blood flow velocity measurements.

In situations where it is required to nonintrusively measure the velocity of flow of fluids in conduits, the specific measurement conditions may vary rather widely. For example, the area over which measurements are to be made may vary from less than one square millimeter in capillary tubes to several square meters in water or sewage pipes. The time during which a measurement is to be made may vary from a few milliseconds in engine control applications to one minute in chemical process plants, or even one whole day for power plant exhaust stack monitoring. The precision or accuracy requirements are usually within one percent and may be as low as one tenth of a percent. The variation in flow velocity encountered also extends over a wide range from theoretically zero

* The content and language of this appendix are based on a U. S. patent application, which has been allowed and is expected to issue in 1975.[18]

velocity at the walls of the conduit to speeds approaching or equal to the speed of sound, or even faster, in supersonic or hypersonic flow as encountered in wind tunnels. Typical liquid flows seldom exceed 3 m/s, but velocities of ~30 m/s are sometimes encountered.

In the flow of fluids in closed conduits, it is clear that the flow velocity will vary across the area of the fluid, usually being lowest near the walls of the conduit and increasing to a maximum velocity somewhere near the center. The profile of these flows will vary widely from case to case, and may include asymmetries, swirl, and reverse flow. Even in a given case, the profile is generally different for the static or dc component of flow as compared with the dynamic or ac component. For example, if one analyzes small 100-Hz oscillations superimposed upon a larger steady flow, the profile, theoretically, can be significantly flatter for the 100-Hz portion of the flow. Interrogation of the flowing fluid with an ultrasonic wave that averages over the diameter of the conduit but not over the whole area of the conduit, provides a measurement of flow velocity v_d equal to v_a/K, where v_d is the diameter averaged flow velocity, v_a is the area-averaged flow velocity and K is a constant which is less than unity, the actual value of which depends upon the flow profile. In special cases, such as laminar flow or fully developed turbulent pipe flow, K can be calculated in terms of the Reynolds number. The Reynolds number expresses the ratio of inertial to viscous forces. Numerically, this dimensionless ratio is given by the expression $Re = \rho VD/\eta$, where ρ is fluid density, V is free-stream flow velocity, D is channel width or diameter, and η is viscosity coefficient. For laminar flow of Newtonian liquids, where the Reynolds number is typically less than two thousand, the profile across the diameter is essentially parabolic in a smooth, regular, circular pipe. Under these conditions an ultrasonic flow measurement over the diameter provides a value for flow velocity v_d which is larger than the true area-average value v_a by 33% (K = 0.75, 1/K = 1.33). Accordingly, where the specific flow profile through the conduit is known, the values of the coefficient K may be utilized to convert a measurement of velocity across the diameter to the area-averaged velocity. However, in a number of circumstances, the flow profile is at best uncertain due to non-Newtonian liquids, or due to the proximity of bends, inlets, outlets, side ports or other possibly unknown perturbations or irregularities within the conduit. Thus, the reliability of the output indication, in terms of average-area velocity, can deteriorate rapidly. Even in those circumstances where the fluid type is known, e.g., JP-4, diesel fuel, etc., the value of K may not be known, particularly when temperature gradients are present, because it depends upon the value of Reynolds number Re, which can itself vary when wide temperature ranges are encountered.

The above difficulties have been recognized for some twenty years. It is not surprising, therefore, to find that in order to obtain sufficient accuracy of ultrasonic measurements under these uncertain profile conditions, several approaches have been proposed by earlier investigators.

Kritz (1955) published nomograms relating v_a to v_d in terms of Reynolds number, Fig. B-1. A graph containing this information, due to McShane (1974), is shown in Fig. B-2. Swengel (1956) originated an intrusive technique using a number of distributed points, e.g., using slender rods, or using an array of transducers, Fig. B-3. But Swengel's approach introduces three sources of error: (1) probes perturb the flow; (2) reflections lead to multipath ambiguities; (3) resonant rods or separate transducer elements are not suitable or likely to provide a wave of uniform intensity, as required for uniform weighting. Petermann (1959), although recognizing the need for area-averaging, did not describe an adequate area-weighting procedure, despite his use of multiple bounces down the pipe axis (Fig. B-4) and analysis of refractive focussing. Fisher and Spink (1972) described a multichord Gaussian approach which, for pipe diameters of about 0.2 m or larger, apparently has provided the best accuracy to date, about 0.1% (Fig. B-5) when 4 chords are used. Suzuki et al (1972) have reported on measurements in orthogonal planes, which apparently goes part way toward obtaining a better area-average than a single-path measurement (Fig. B-6), at least for large pipes, with diameters from ~0.2 m to over 1 m. See Refs. 3-7.

For area-averaging over a limited range of flow conditions, Pfau (1970) derived a preferred location, at the intersection of two profiles, where doppler measurements should be made.[8] Range-gated doppler measurements, to map out the profile, or at least segment it into, say, eight zones (Figs. B-7 and B-8), were described by Haase, Foletta and Meindl (1973).[9] Doppler measurements, however, are seldom used in industrial flowmeters, probably due to the variability of scatterers and sound speed.

In USAAMRDL TR 72-66,[1] p. 20, we suggested using a Kenics static mixer to establish an essentially flat profile, to provide, in a limited region, a situation where essentially K = 1 (Fig. B-9). (The second series of calibration tests in the present program used this type mixer.) On p. 64, Fig. 28 of TR 72-66, we showed an offset configuration similar to designs recently sold by at least one ultrasonic flowmeter manufacturer. The offset provides area-averaging but suffers from inlet and outlet perturbations and undesirable pressure drops. An earlier offset design was used by Noble (1968).[10]

Figure B-10 illustrates a nonultrasonic approach to the flow profile problem, the "Annubar," an intrusive area-averaging pitot-tube flowmeter

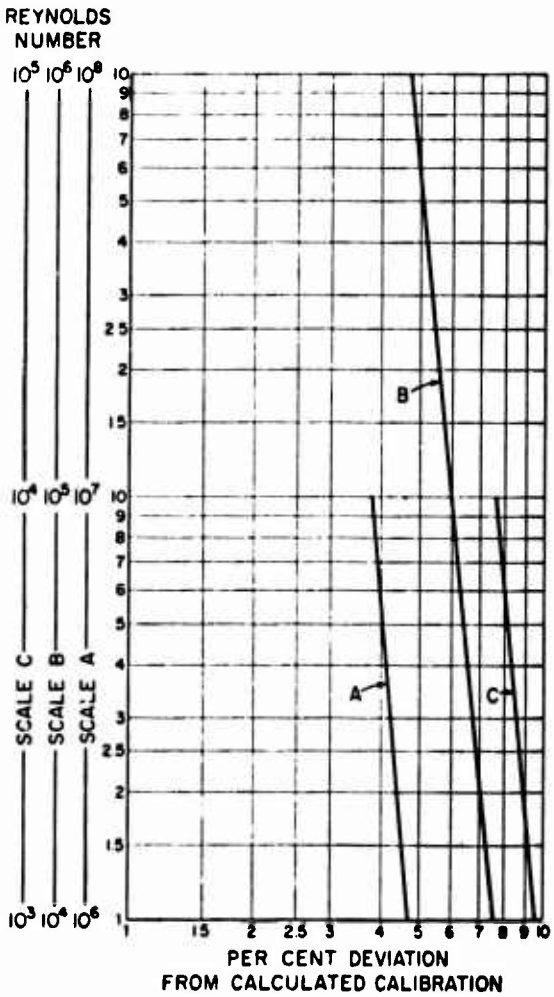

Figure B-1. Percent Deviation From Calculated Calibration Versus Reynolds Number. After Kritz (1955).

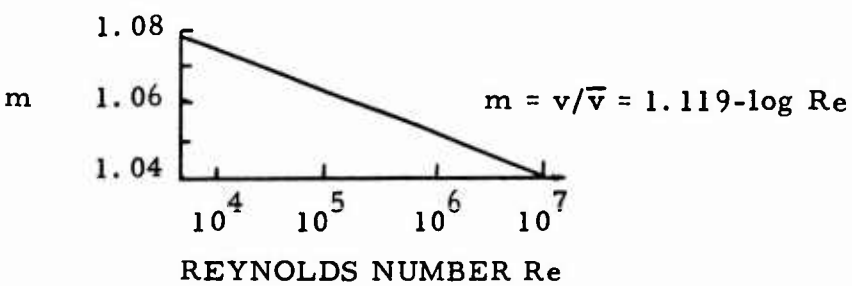

Figure B-2. Ratio of Measured Velocity to Average Velocity in a Round Pipe Versus Reynolds Number. After McShane (1974).

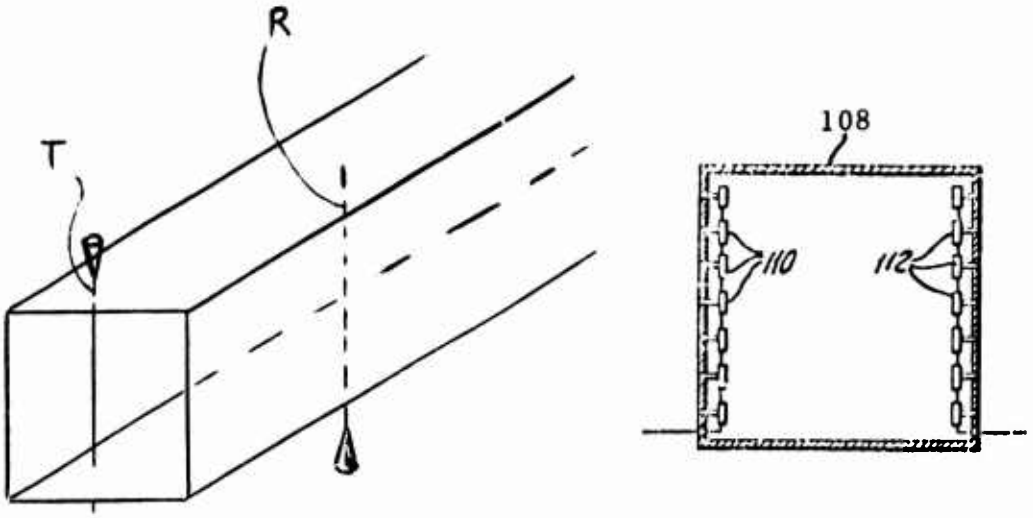

Figure B-3. Perspective View Shows Use of Slender Rods Installed Intrusively Within Duct, Intended to Provide Area-Average. End View Shows Arrays of Piezoelectric Sources (110 and 112) Intrusively Installed Within Duct (108), Intended for Same Area-Average Purpose. After Swengel (1956).

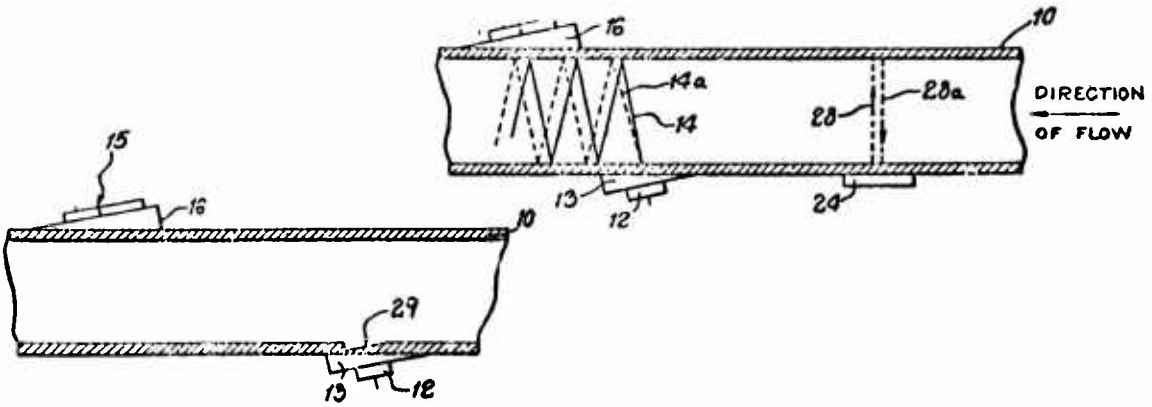

Figure B-4. Multiple Bounces Down Pipe Sample Fluid Volume Over Considerable Axial Distance, But Do Not Adequately Weight the Radial Distribution of Flow Velocity. Multiple Bounce and Transducer Configurations After Petermann (1959).

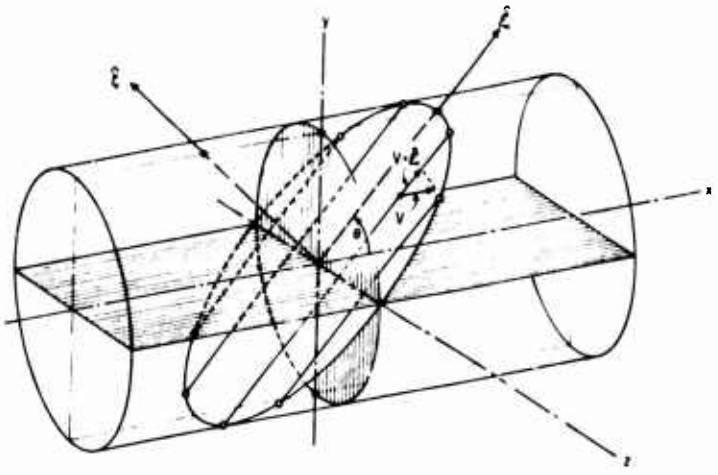

Figure B-5. Measurement Plane in Round Pipe, Illustrating Gaussian Quadrature 4-Chord Technique. After Fisher and Spink (1972).[6] Chord Locations Corresponding to Numerical Integration or Quadrature Methods of Gauss, Chebycheff and Lobatto are Given by Malone and Whirlow (1971).[32]

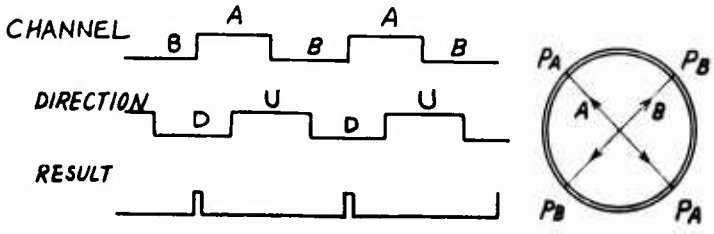

Figure B-6. Two-Channel System
D: Downstream Direction
U: Upstream Direction

This figure shows the time chart of an installation at a power station. Two pairs of probes are mounted where the sound path for each pair crosses at right angles. The flow rate is measured from the sum of two differential sing-around frequencies on two paths. The effect of slant or circular movement of flow proved to be largely improved by such a method of mounting. After Suzuki et al (1972).

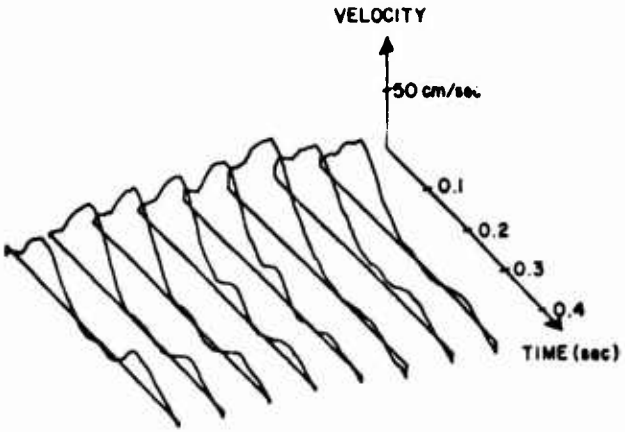

Figure B-7. Perspective View of Velocity Profile During One Cardiac Cycle in a Canine Ascending Aorta. After Haase, Foletta and Meindl (1973).

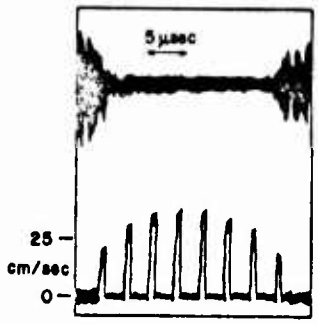

Figure B-8. Time-Average Velocity Profile in Human Ascending Aorta. After Haase, Foletta and Meindl (1974).

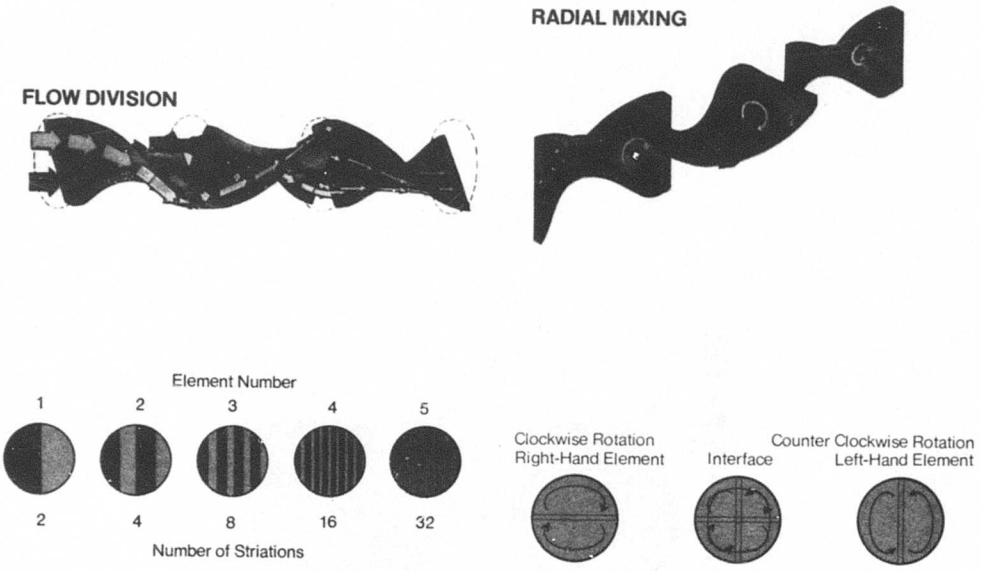

The fixed geometric design of the unit produces unique patterns of flow division and radial mixing simultaneously. In laminar flow, a processed material divides at the leading edge of each element and follows the channels created by the element shape. At each succeeding element the two channels are further divided, resulting in an exponential increase in stratification. The number of striations produced is 2^n where n is the number of elements. In either laminar or turbulent flow, rotational circulation of a processed material around its own hydraulic center in each channel of the mixer causes radial mixing of the material. All processed material is continuously and completely intermixed, resulting in virtual elimination of radial gradients in temperature, velocity and material composition. Illustrations courtesy Kenics Corporation, Lawrence, Mass.

The Kenics Static Mixer used in the December 1974 tests is identified as follows:

Serial No. 1128 — Model No. 5-10-321-00
Maximum design pressure, 3800 psi — Maximum temperature, 300°F
Dimensions:
.835 O. D. x .625 I. D. x 6" long

Figure B-9. Kenics "Static Mixer". This Unit is a Series of Fixed Helical Elements Enclosed Within a Tubular Housing.

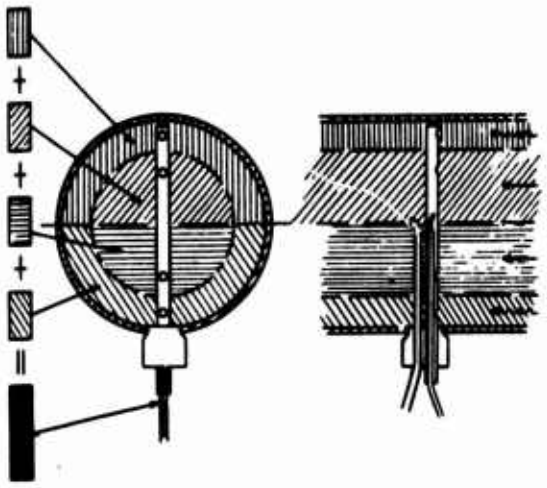

Figure B-10. Example of Flowmeter Responsive to Flow Profile.

Each annular segment of the "Annubar" primary flow element represents an area of equal cross-sectional size. Accurate detection of flow within these annular segments is achieved by large sensing ports. The various flow rates are averaged by the plenum of the upstream element. Source: Ellison Instrument Division, Dieterich Standard Corporation, Boulder, Colorado.

available from Ellison Instrument Division, Dieterich Standard Corporation, Boulder, Colorado 80302.

To further emphasize that the profile problem is generic to all fluid flowmeters, we may refer to the analyses of electromagnetic flowmeters by Bevir (1970) and by Haacke (1974).[11,12]

Turtle (1974) introduced a converging throat section, Fig. B-11, to "normalize" the velocity profile, but at the expense of the pressure drop associated with the reduced cross section.[13]

Despite the variety of the foregoing approaches, accurate measurement of area-averaged flow velocity in small conduits (diameter $\lesssim$ 1 to 3 cm) of the type of concern in this program, over the full range of flow profiles to be encountered, cannot be obtained by the methods of the other investigators cited above.

On the other hand, our area-averaging flow cell and transducer design given in USAAMRDL TR 72-66, particularly with the inclusion of improvements such as screens over the 45° transducer ports to minimize eddies in the measuring path, and a gradual transition at the inlet, provides an accurate area-average. Calibration data given elsewhere in this report show that the device is reproducible and essentially linear over wide ranges of Reynolds number. Since this desirable performance has now been demonstrated, it is appropriate to elaborate on the use of a rectilinear flow channel, in which all the fluid passing through is measured by an obliquely incident rectilinear beam, with equal area elements of flow being given equal weight by the uniform beam.

SUMMARY OF THE AREA-AVERAGING CONFIGURATIONS

Broadly speaking, in the present approach the correct weighting of the flow profile in the measurement of flow velocity across a conduit is accomplished by flowing the material through a section of conduit having a rectilinear cross section in a plane transverse to the direction of flow and interrogating the fluid with a substantially plane ultrasonic beam, itself having a rectilinear cross section, with the beam dimension and the conduit dimension along one coordinate being equal and with the beam dimension in the other direction along the other coordinate being equal to or less than the conduit dimension along the same coordinate. The measurements are preferably made in a pathlength of fluid within the very near field of the transducer generating the ultrasonic beam so that the curvature of the interrogating wave by the flow of the fluid is minimized.

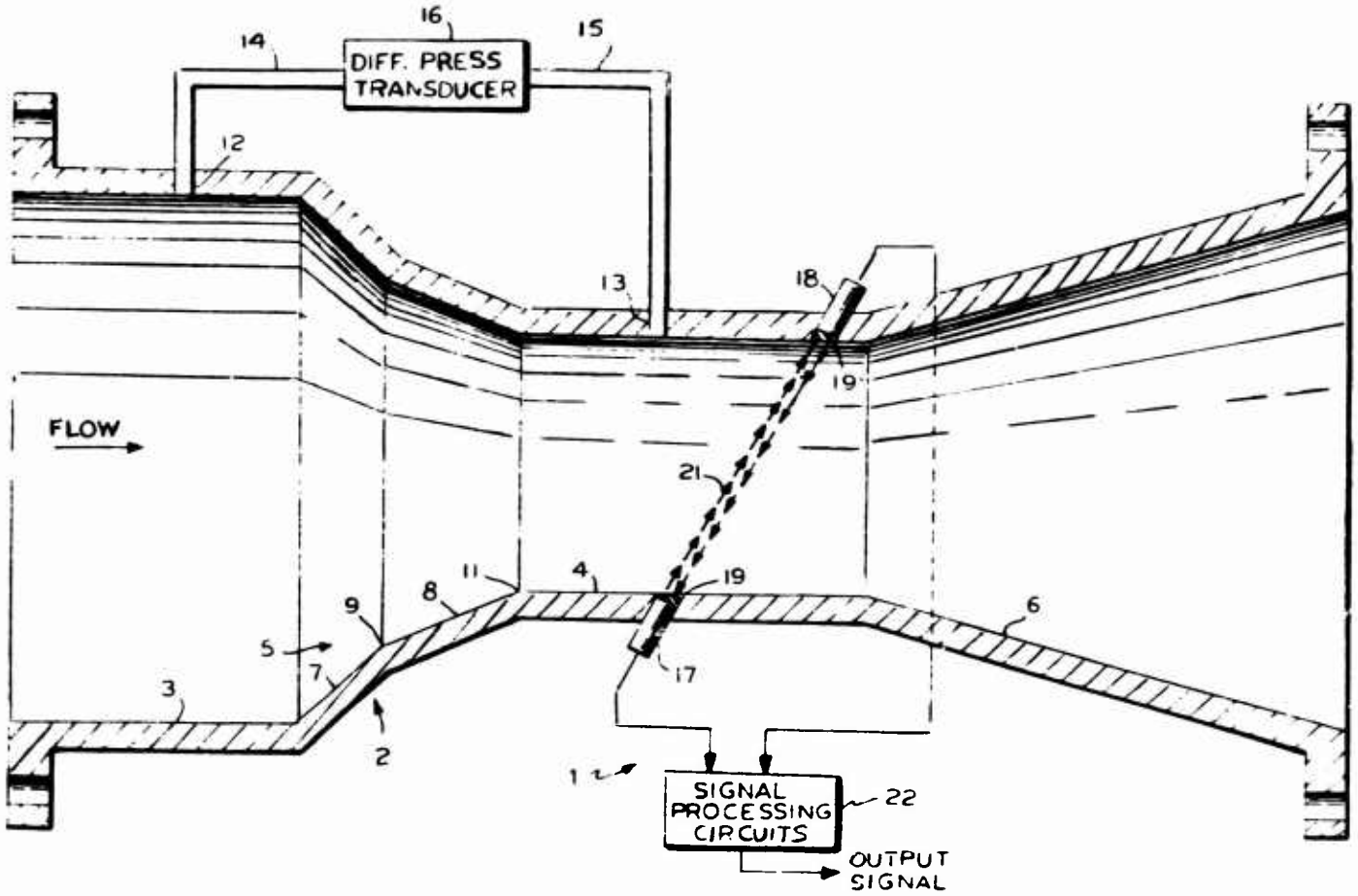

Figure B-11. Converging Throat Section "Normalizes" Flow. After Turtle (1974).

In general, the pathlength of the ultrasonic beam in the flowing fluid should not exceed d^2/λ, where d is the smaller dimension of the interrogating beam and λ is the wavelength in the fluid. Thus, in a typical situation where λ = 1 mm, if the diameter d equals 10 mm, then the pathlength should not exceed approximately 100 mm. Generally, for preferred operating conditions, the pathlength should not exceed one quarter of this distance, i.e., 25 mm long. In many situations, the rectilinear conduit, which may be either square or rectangular, is a flow cell introduced into the flow path. The flow cell assembly, then, is an entire apparatus including ultrasonic transducers mounted to produce the appropriate interrogating ultrasonic beams. These beams which bidirectionally interrogate the fluid in response to transducer energization may be given their rectilinear shape in any one of several ways. For example, piezoelectric generators and detectors may be ground to the desired shape, or a circular disk may be employed with at least one of its surfaces electroded in a rectilinear pattern. Yet another approach is to collimate generated beams of any shape by means of opposed cavities or slots having rectilinear cross sections.

By employing beams of rectilinear shape to interrogate the fluid in conduits also of rectilinear shape, all of the segments between the ceiling and the floor of the flow channel may be measured, and correct area-averaging may be provided.

DESCRIPTION OF THE DRAWINGS

Figure B-12a is an illustration in plan view of a flowmeter cell constructed in accordance with the principles of this invention. Figure B-12b is a cross-sectional view along the line bb of Fig. B-1. Figure B-12c is a cross-sectional view taken along the line cc of Fig. B-1a. Figures B-13-B-19 are cross-sectional and end views of portions of alternative embodiments of flowmeter cells constructed in accordance with the principles of this invention. Figure B-20a is an illustration of the probe of Fig. B-20 taken along the line aa. Figure B-21 is an illustration in cross-sectional view of another configuration of a flowmeter cell constructed in accordance with the principles of this invention. Figures B-22 and B-23 are illustrations in a cross-sectional view of additional embodiments of flowmeters constructed in accordance with the principles of this invention. Figures B-24 and B-25 are illustrations in a cross-sectional view of portions of flowmeter cells constructed in accordance with the principles of this invention, illustrating specific details thereof. Figure B-26 illustrates cross-polarized shear wave transducers.

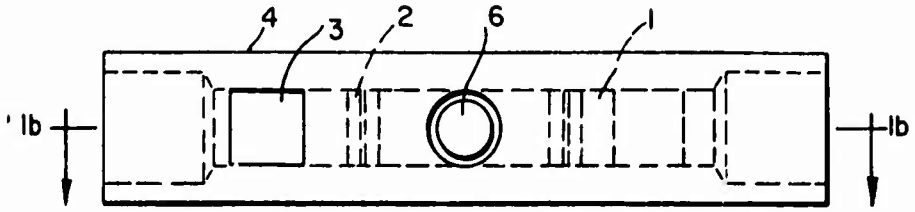

Figure B-12a. Area-Averaging Flow Cell, Top View.

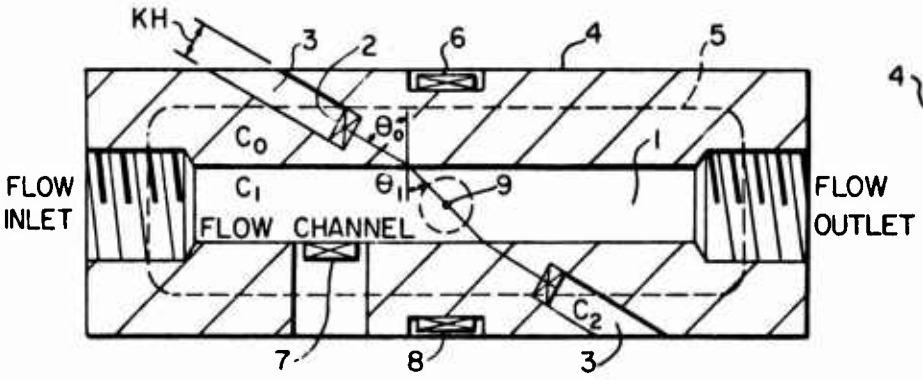

Figure B-12b. Cell Side View.

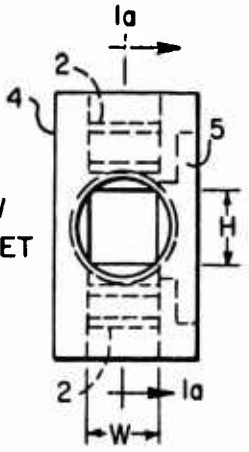

Figure B-12c. Cell End View.

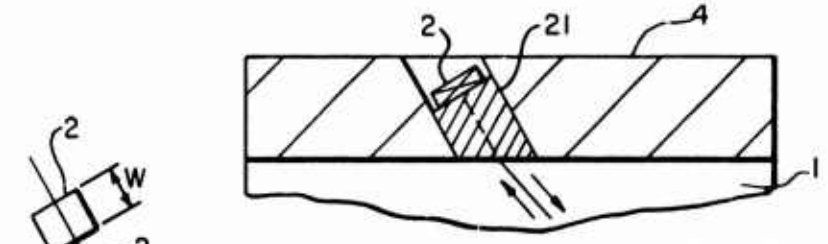

Figure B-13. Transducer Mounted on Flush Wedge.

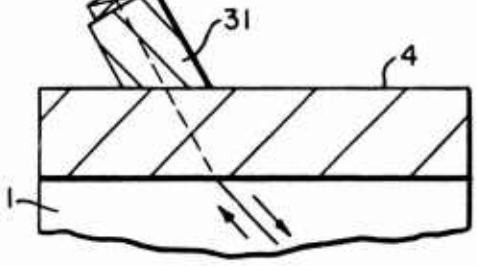

Figure B-14. Transducer Mounted on External Wedge.

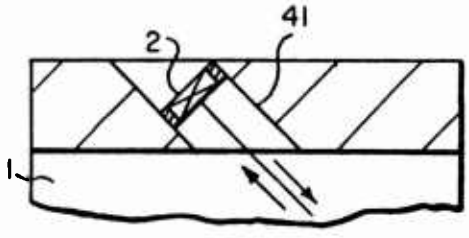

Figure B-15. Transducer in Cavity, Coupled Directly to Fluid.

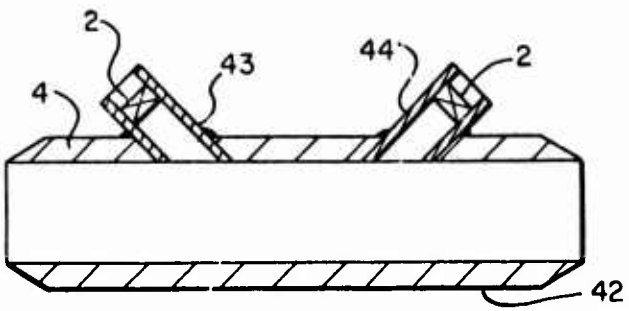

Figure B-16. Cell Used as Flow Probe in Large Conduit, Side View.

Figure B-17. Probe End View.

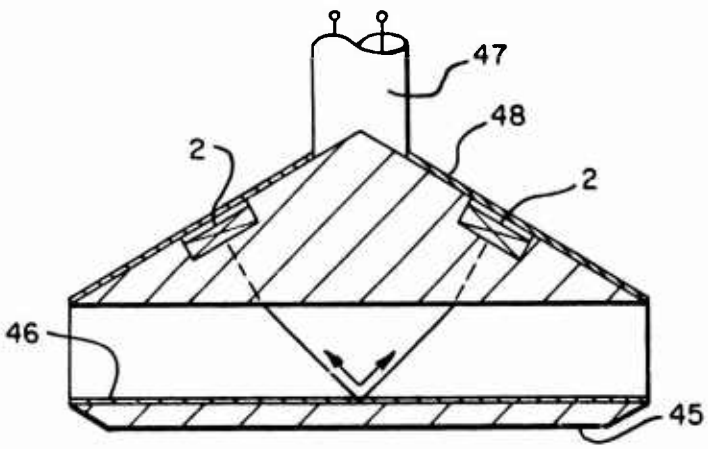

Figure B-18. Rotatable Probe for Large Conduit, Side View.

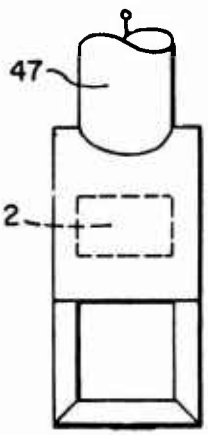

Figure B-19. Rotatable Probe End View.

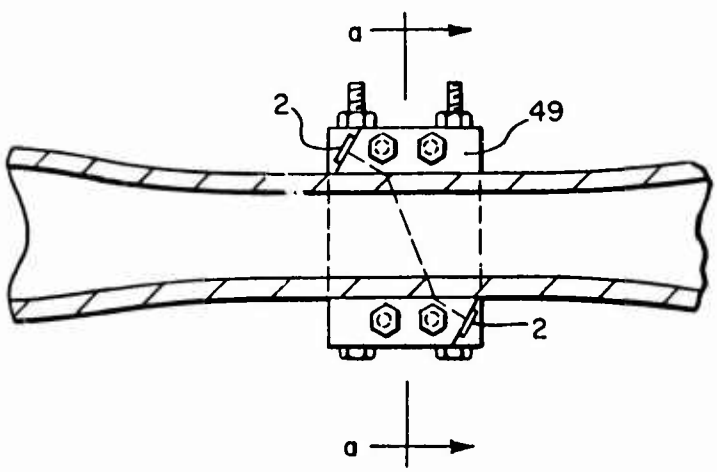

Figure B-20. Clamp-On Assembly Transforms Circular Cross Section to Square.

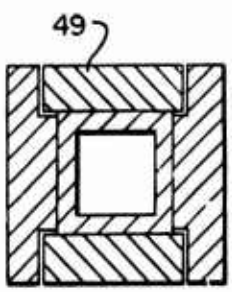

Figure B-20a. Cross Section a-a of Clamp-On Assembly.

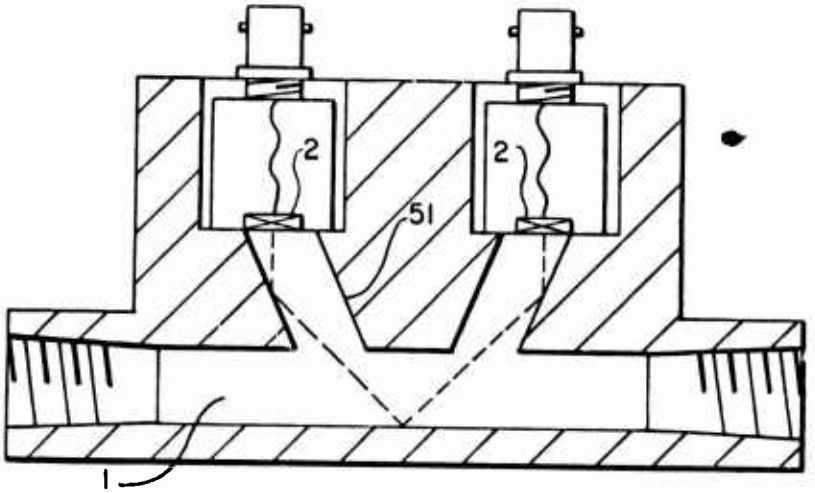

Figure B-21. Cavity Reflection Controls Oblique Interrogation.

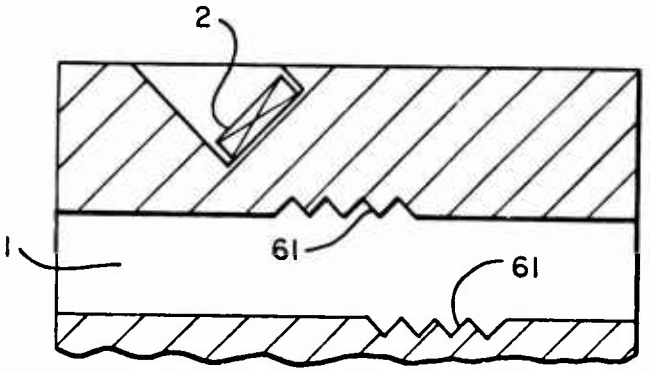

Figure B-22. Vee-Grooved Walls, Used Nonrefractively.

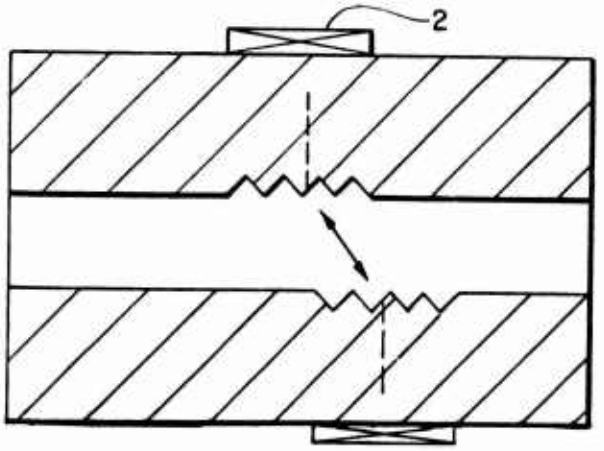

Figure B-23. Vee-Grooved Walls, Operating Refractively.

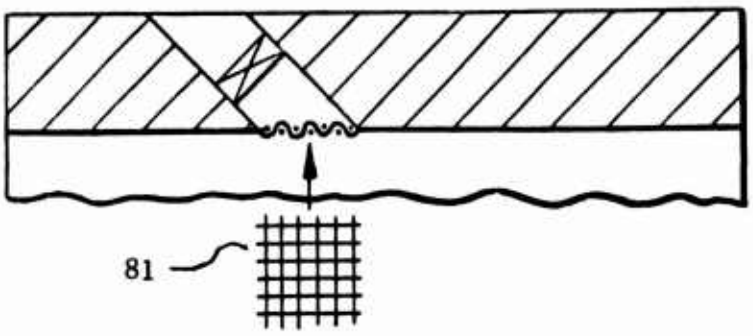

Figure B-24. Screen Over Transducer Cavity Reduces Turbulence.

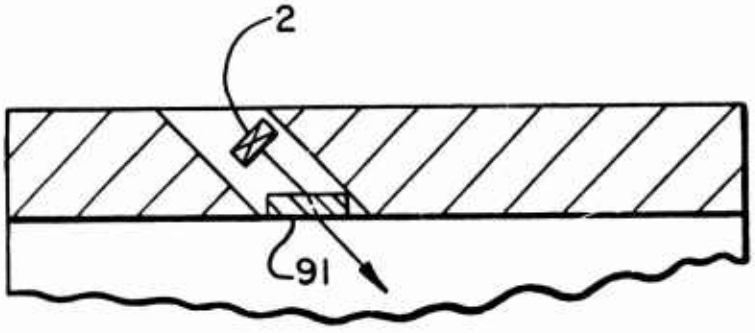

Figure B-25. Plate Installed in Cavity to Reduce Turbulence.

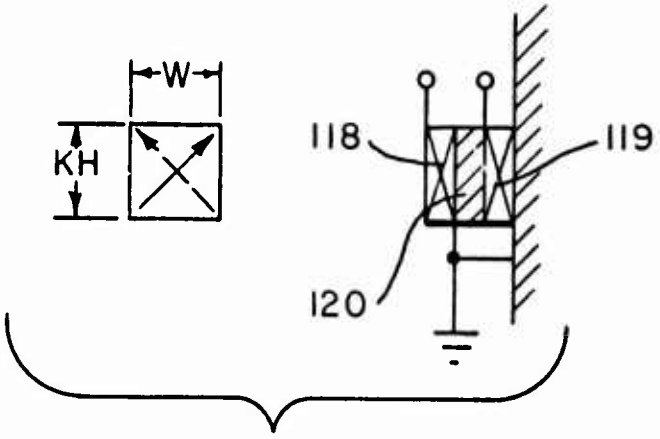

Figure B-26. Cross-Polarized Shear Wave Transducer Assembly.

DESCRIPTION OF PREFERRED EMBODIMENTS

With reference to Figs. B-12a, B-12b and B-12c, there is shown an embodiment of an ultrasonic flowmeter cell. The cell body 4 is formed out of a suitable material, such as stainless steel or aluminum. Other suitable materials include plastic, glass or many other solids. The cell contains an axial flow channel or conduit with a rectilinear cross section having a width dimension W and a height dimension H. The conduit 1 typically has a length two to ten times longer than the larger dimension of its cross section. The inlets and outlets to the flow channel 1 are shown in Fig. B-12b as threaded for connection to the line through which the fluid to be measured is flowing. Tapered fittings or flanged connections may be substituted for the threaded inlets and outlets shown, gradual transitions being preferred. Welded, brazed, soldered or epoxied fittings may also be used.

A pair of ultrasonic transducers 2 are positioned within a pair of recesses 3, with the recesses extending in a direction oblique to the axis of flow in the conduit 1. The transducers 2 generate a beam of ultrasonic waves which is characterized by a rectilinear cross section in the plane normal to the axis of propagation of the beam. The cross section of the beam has a dimension W by kH, where k has a value typically between 0.5 and 1.0. The axes of the recesses 3 are parallel to one another. The transducers 2 are arranged to launch an oblique wave in the cell body material at an angle θ_o with respect to the normal drawn to the axis of the conduit 1.

Transducers 2 may be made of any conventional piezoelectric material such as lead-zirconate-titanate, lead metaniobate, etc. The oblique waves transmitted through the cell body at angle θ_o interrogate the fluid flowing through conduit 1 at an angle θ_1, where the angles θ_o and θ_1 are related to the sound speeds c_o and c_1 in the solid and fluid, respectively, in accordance with Snell's Law: $c_o/\sin\theta_o = c_1/\sin\theta_1$. The position of transducer 2 with respect to conduit 1 will depend, therefore, on the angles θ_o and θ_1 and also on the number of times the ultrasonic beam is to transverse the fluid path. Thus, while in Fig. B-12b the beam is indicated as having a single traverse of the fluid path, by arranging for the greater separation between the two transducers along the axis of flow, a multiple traverse may be utilized, to increase the time differences for upstream and downstream waves.

The conduit within the cell 4 may be formed by being broached or electric-discharge-machined between the inlet and outlet ports. Alternatively, the conduit may be milled out and the coverplate 5 (as shown in dotted lines in Fig. B-12c) may then be attached. The coverplate 5 may be either permanently attached, such as by welding, or may be removably attached,

for example, by screws or clamps. The coverplate 5 may be formed of a transparent material such as a clear plastic so that the flow pattern and clogging or buildup of residual materials may be visually observed without the distortion of a curved lens.

The orthogonal walls of the conduit 1 enable other nonintrusive ultrasonic measurements on either a pulse-echo or through-transmission mode to be made. These measurements may include time interval measurements across the fluid perpendicular to the direction of flow to determine the sound speed, c_1, of the fluid. Additionally, the reflection coefficient at one of the walls may be measured in order to obtain ρc_1, which then allows for determination of the fluid density, ρ. The attenuation coefficient, α, of the fluid may also be measured to provide in some instances information on fluid viscosity. While such measurements can also be made in curved-wall conduits, the rectilinear conduit promotes greater accuracy.

In Fig. B-12b, transducer assemblies 6, 7 and 8 are conventional ultrasonic transducers which are positioned to perform density, sound speed and attenuation measurements. In Fig. B-12b, the transducers are illustrated as being in the same plane as the velocity measuring transducers 2. These additional transducers may, however, be located in an orthogonal plane or planes, so that the beams interrogate the same volume element of fluid at the same time that the flow velocity of that element is being interrogated. The axis of such a composite assembly would ideally intersect the flow channel 1 axis and the flow interrogation beam axis at a point 9 illustrated in Fig. B-12b.

Turning now to Fig. B-13, an alternative arrangement for positioning one of the transducer assemblies 2 is illustrated. In Fig. B-13, as in most of Figs. B-14 through B-25, only one-half of the measurement cell is shown, since in those instances the other one of the pair of transducers is identical. In the configuration of Fig. B-13, a plug 21 is inserted within the recess 3 between the transducer 2 and the fluid within the conduit 1. The plug 21 is formed of materials which will provide preferred acoustic properties such as sound speed, density and attenuation coefficient in the cell measuring region where it is undesirable to form the entire cell body 4 of a material having these specific properties. Additional materials which may be employed for this purpose include graphite, various alloys, and plastic such as polytetrafluoroethylene. In a specific example, the insert 21 is formed of acrylic plastic in which the shear wave sound speed is about 1 mm/μs, and if the fluid is water, then c_1 equals 0.5 mm/μs. If transducer 2 generates a vertically polarized (SV) shear wave at an incident angle where $\theta_o = 30^\circ$, the longitudinal wave in the water will propagate at a refracted angle θ_1 of $\sim 45^\circ$.

In Fig. B-14, the transducer 2 is mounted on a wedge 31 which is coupled to the outside surface of the cell body 4. This provides a technique for generating the oblique wave without the requirement of recessing the body of the cavity.

In Fig. B-15, a transducer assembly is illustrated in which transducer 2 is mounted within a transducer cavity 41 which extends at an oblique angle entirely through the wall of the cell 4. In this configuration the angle of incidence of a produced beam does not depend upon the ratio c_o and c_1 since the transducer is coupled to the fluid itself. In a specific example of an arrangement for a transducer in accordance with Fig. B-15, the transducer element was a piezoelectric material of circular shape, 19 mm in diameter, electroded over a rectangular area of 12.7 mm by 6.35 mm. The transducer assembly was sealed into the cavity 41 by means of an O-ring. In the specific example above, the rectilinear dimension of the conduit 1 was W = H = 12.7 mm.

In Figs. B-16 and B-17, there is illustrated a slightly modified version of Fig. B-15, in which the W by H flow channel 1 is defined by a first square or rectangular pipe 42, and the transducer channels are defined by a pair of square or rectangular pipes 43 and 44 which may be welded, brazed or epoxied at the required positions and angles, e.g., 45^{o}. For illustrative purposes, Fig. B-16 shows both transducer channels or ports on the same side of the flow channel pipe, for a double traverse. Obviously, they may be on opposite sides, as is generally intended in the other Figs. B-13-B-15. A cell assembled as in Figs. B-16 and B-17 may be useful in some instances as a probe which accurately senses, with little perturbation of the total initial profile of a large pipe or duct, all the fluid entering the cell's inlet. By mounting this probe such that its flow axis is at a suitable point such as on-axis, or off-axis at radius r, where $v(r) \approx v_a$ for the Reynolds number range of interest, a useful indication of flow may be achieved. On the other hand, either by scanning radially with one probe or by averaging the readings obtained with a number of small probes, a measure of flow velocity may be obtained in a duct or pipe which is so large that it cannot be easily interrogated nonintrusively over 100% of the total flow channel area, especially where the large channel cannot be square or rectangular.

In the type of application shown in Figs. B-16 and B-17, while the transducers are nonintrusive with respect to the small flow channel, the exterior shape and dimensions of the probe must be designed to minimize drag and more generally to minimize the pressure drop and other perturbations introduced by a small probe in a large conduit. In view of the fact that the obstructive cross section of the inlet portion of the probe can be made quite small and streamlined, and because disturbances on the

outside of the probe, downstream of the inlet, do not perturb the flow measurement, and because the orthogonal-walled W by H flow channel is itself unobstructed, this type of probe may be particularly useful in profiling and survey measurements in fluids of much larger cross section than the probe.

Another form of a probe-type cell is shown in Figs. B-18 and B-19. The major portion of the cell body 45 may be plastic, e.g., acrylic, for use with water. To increase the reflectivity of the inner surface at megahertz ultrasonic frequencies, a thin layer of higher density material 46 such as 0.1 mm thick stainless steel may be bonded to the wall opposite the transducers. The two transducers interrogate the fluid at 45°, the angle of refraction of longitudinal waves mode-converted from SV shear waves incident from the plastic at 30°. The transducers may be electrically shielded by surrounding the outer surface of the probe with additional 0.1 mm thick stainless steel, 48, grounded electrically to the electromechanical connector shield 47. This shield 47 may be a solid (inflexible) metal tube, which contains the two transducer "high" leads, and which can be used to orient the probe by rotation about its axis, to measure, for example, swirl or cross flow components, as well as axial flow velocity in a large conduit. Plastic probe bodies may also be shielded by conductive coatings, such as conductive epoxy, applied to their exterior surfaces.

A functionally equivalent construction may be built by making the major portion of the cell in Fig. B-18 out of metal or ceramic, and by inserting acrylic or other low-sound speed buffers as in the embodiment 21 of Fig. B-13.

A clamp-on flowmeter probe is shown in Figs. B-20 and B-20a appropriate to some pipes which are generally of circular cross section, but which are flexible or malleable enough so that they can be mechanically deformed by orthogonal pairs of parallel clamps 49. In the region of measurement, the originally circular pipe is constrained externally so that an essentially square or rectangular flow channel is provided. Transducers may be coupled directly to an opposing pair of flattened pipe walls, or they may be coupled or attached to one of the clamps, such that the ultrasonic beams are subsequently pressure-coupled or otherwise conventionally coupled to the opposite walls. If a circular pipe of inside radius R is deformed to a square, the length of the interior side S of the resulting square is readily calculated by equating interior "perimeters." Thus, setting $2\pi R = 4s$, then $S = \pi R/2$. This determines the required transducer or beam width, previously denoted W, as in Fig. B-14, in terms of the round pipe's interior dimension. As a numerical example,

if R = 10 mm, S = W = 15.9 mm. In other words, S is approximately 60% greater than R, or in terms of the original inside diameter 2R, S is approximately 20% less than the original inside diameter.

The combination of clamps and transducers shown in Figs. B-20 and B-20a may also be applied to originally square or rectangular thin-walled pipe, to help maintain orthogonal flat walls despite high internal fluid pressures, which tend to bow the sides of unrestrained pipe that is not sufficiently stiff by itself.

Comparing the areas A_o and A_{SQ} of the circular and square regions, respectively, it is seen that

$$A_o = \pi R^2;\ A_{SQ} = S^2 = (\pi R/2)^2;\ A_o/A_{SQ} = 4/\pi \approx 1.27 \qquad \text{(B-1)}$$

Therefore, the average flow velocity v_o in the circular region will increase by 27% to 1.27 v_o in the square region, if the fluid is incompressible. The mass flow rate, however, is the same in both regions, for any fluid confined to the conduit, whether or not the fluid is compressible, for steady-state flow.

In Fig. B-21, a cavity 51 inclined at 22.5° to the normal to the flow channel axis reflects the incident longitudinal wave beam to interrogate the fluid at 45°.

In Fig. B-22, the internal surface of the conduit 1 is subdivided into vee-grooves 61 in the regions between the transducers 2 and the fluid. This maintains propagation along a specific oblique path, and yet reduces the amount of material that must be removed near the intersection of the transducer cavity and the flow channel. Another purpose of the vee-grooves is to reduce the scale of turbulence, and to provide supports for membranes, screens or acoustic windows used as flow straighteners, as described in connection with Figs. B-24 and B-25.

Figure B-23 differs from Fig. B-22 in that the transducer launches a wave normal to the flow axis. But this wave, after impinging on the vee-grooves 61, is refracted obliquely across the fluid. When the ratio c_o/c_1 is large, as it is for metal/air interfaces, the oblique angle is relatively insensitive to changes in c_o and c_1, propagation being in a direction in air nearly normal to the vee surfaces, that is, at nearly 45° in the air. However, in Figs. B-22 and B-23, care must be exercised so that diffraction effects do not confuse the measurement.

Figures B-24 and B-25 illustrate two ways of reducing the undesirable effects of eddies, which are generated at high flow velocities. Since these eddies are not symmetrically confined to the region interrogated by the beam, their effects are not perfectly canceled by upstream and downstream interrogations, and so they produce nonlinear response. The degree of nonlinearity depends on the size and nature of the eddy compared to H. For example, small eddies will not produce departures from linearity greater than 1%, when H is sufficiently large. However, when circumstances require that interrogation be at a particular angle, and that the transducer cavity diameter be comparable to H, and if Re ranges from ~100 to ~100,000, then it is preferable to provide a means of damping or eliminating these eddies. This means should also provide a high transmission coefficient for ultrasonic energy, e.g., at least 50%, and often $\gtrsim$ 90%. In Fig. B-24, a wire cloth, or a screen mesh, 81, is used to dampen the eddies, and yet provide a high transmission coefficient. The wire cloth 81 is positioned essentially in the planes of the sidewalls of the W by H flow channel 1, i.e., a distance H apart. The wire cloth, typically made of stainless steel, may be silver brazed, soldered or epoxied in a small recess machined in the sidewall, or it may be joined to an insertable transducer assembly. A suitable mesh size for use from ~1 MHz to 5 MHz with common liquids, c ~ 1000 m/s, n < 100 centipoise, would have a mesh opening of about 1 mm, defined by wires of diameter about 0.10 to 0.25 mm. Finer meshes are preferred, provided that they do not clog, that they are strong enough, and that they do not introduce serious diffraction effects. The spaces in the wire cloth encourage thermal and compositional equilibrium to be maintained between the cavity and the flow channel. This assures that the sound beam propagates without refractive bending on passing through the screen.

The arrangement shown in Fig. B-25 illustrates an alternative to the embodiment of Fig. B-24, in that, instead of the screen, a membrane or plate 91 is used as an acoustic window. For operation essentially at a single frequency, and at a single temperature, the member 91 may be fabricated or tuned to resonance, even if its characteristic impedance is substantially different from that of the fluid (e.g., steel/water, impedance ratio ≈ 30:1). However, for interrogation of most liquids near 45°, it can be shown that plate-like window materials like plastics or graphites, because of inherent attenuation, are not particularly efficient as resonated devices. Thus, the thickness of member 91 is generally chosen based on mechanical and transmission coefficient requirements, not resonance requirements. A typical thickness would be $\lesssim$ 1 mm. For some cases the use of plastics or graphites is undesirable, but metal is allowable, sometimes as thin as 0.01 mm. As a representative example, stainless steel shim stock 0.05 mm thick is appropriate with common liquids and a frequency of about 1 MHz or less.

When the fluid is air or other low-density gas, a membrane can be used, provided the frequency is low enough. In Fig. B-25, passageways may need to be provided to assure that the fluid (c_o) is the same on both sides of member 91. Otherwise the interrogating beam will not emerge in the fluid parallel to the beam incident in the transducer cavity.

The difference in transit times between the upstream traveling beam and the downstream traveling beam provides, as discussed earlier, an indication of the flow velocity of the fluid within flow conduit 1. The upstream and downstream beams can be separated either by initiating the beams at different times so that the measurements are essentially made in rapid sequence or, preferably, by simultaneous measurements.

While electronic measuring methods can be employed using only a single transducer on either end of the measuring path, there are advantages to be obtained if two transducers are used at each end of the path. As illustrated in Fig. B-26, a pair of shear wave transducers may be orthogonally polarized with respect to one another, that is, $\pm 45^{o}$ relative to the plane of incidence. One transducer 118 is the transmitting transducer, while the other transducer 119 is the receiver transducer. The transducers 118 and 119 are separated from one another by a layer of solid material 120 having a similar, or preferably the same, characteristic acoustic impedance as the transducers themselves. For example, this intermediate may be formed of unpolarized or depolarized piezoelectric material.

In some situations the small nonuniformity of the intensity of the plane wave in the fluid may be compensated for by "shading" the transducer electrodes. For example, a small portion of the central part of the electrode may be removed, so that the corresponding part of the transducer is not activated. This would compensate for a weakened acoustic field at the edges of the beam.

To illustrate cells built in accordance with the above principles, we show exploded and assembly view photographs of the aluminum cell used in the previous contract, Figs. B-27 and B-28. In contrast to this earlier design, the more recent design, Figs. 2, 3 and 4, incorporates a screen soldered over the transducer ports (and sight ports, if present), that is, along the sidewalls of the flow channel. Another improvement aimed at reducing eddies is the welding of smooth transitions from circular pipe to the rectangular flow channel. To simplify the cell, we have taken advantage of the (v/c) (ρc) formulation and have eliminated the separate transducer previously used with the separate time intervalometer. We have also built an experimental cell of stainless steel, leaving out the ρc densitometer probe, since this probe may not always be required. When

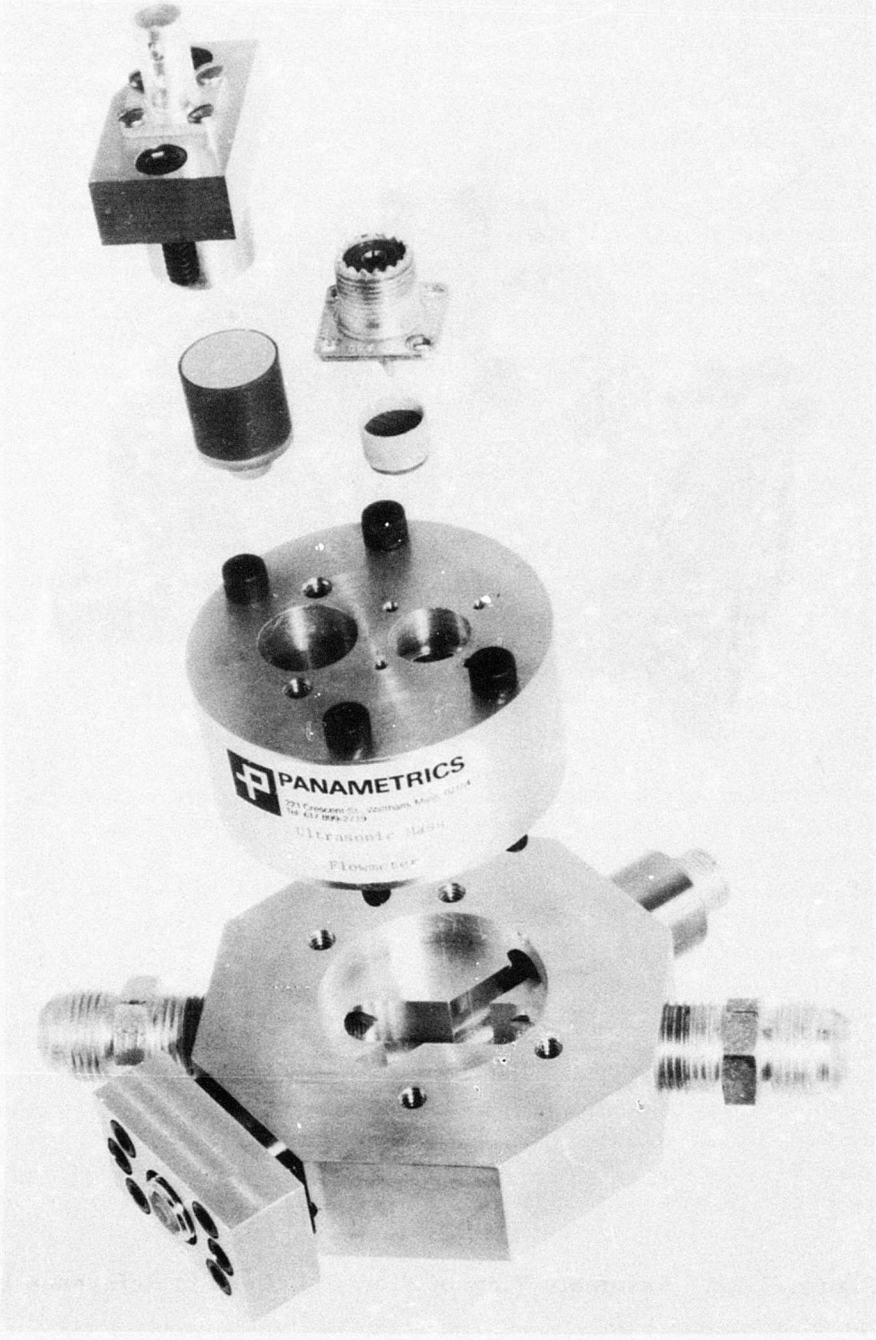

Figure B-27. Exploded View of Flow Cell Used in Reference 1.

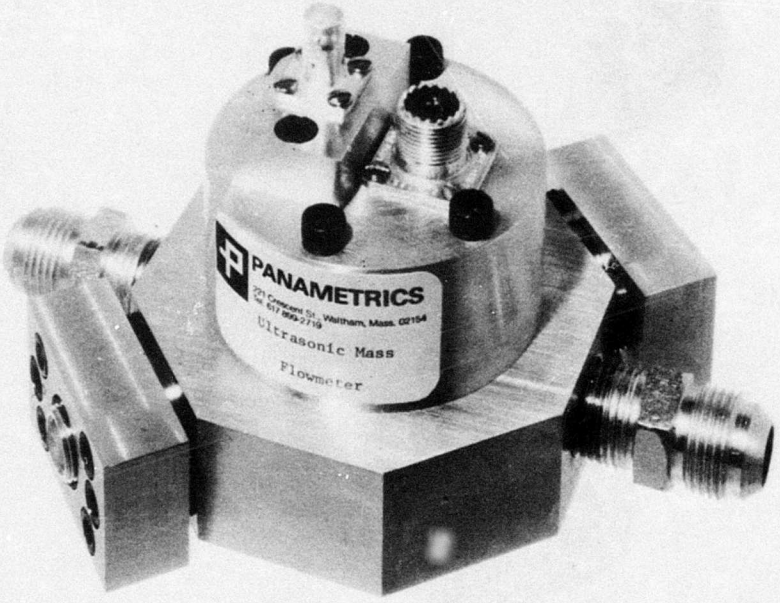

Figure B-28. Assembly View of Flow Cell Used in Reference 1.

it is required, it can be located just downstream of the v/c cell, in a standard tee fitting.

A transparent acrylic cell was also built, so that bubbles, contaminants, and flow patterns could be seen under test conditions. The cell was machined in two halves and then cemented together. The rectilinear slots were thus produced routinely, by milling the necessary channels. Circular transducer ports and inlet ports were bored after the assembly was cemented together.

To illustrate that the above concepts are applicable to fluids at high temperature, we show in Fig. B-29 a stainless steel experimental cell tested up to 300°C. Figures B-30 and B-31 show internal details of this cell, particularly the square flow channel, and the Dowtherm passageways to maintain the high temperature.

In cases where zigzag paths or area-averaging are not required, the experimental cell of Figs. B-29 to B-31 may be replaced by a simpler cell such as that shown in Fig. B-32. In Fig. B-32, the flow channel principally is comprised of standard 1-in. stainless steel pipe. The Dowtherm jacket principally is concentric 3-in. pipe. Transducer mounts are also 1-in. pipes, welded at 45°, and flanged to receive transducer holders. In one design the transducer holders are of the top hat design, fabricated of titanium because of its relatively low acoustic impedance (see Fig. E-1). The cells of Figs. B-29 and B-32 have the same flange-to-flange dimensions for the process fluid and the Dowtherm lines. But being substantially hollow, the concentric design weighs only about half as much as its solid counterpart.

A lightweight, relatively inexpensive configuration but retaining the area-averaging feature, consists of nominally 1-in. (2.54 cm) stainless steel square tubes welded together, Fig. B-33. It contains a stainless steel screen (42 mesh, 0.0055 in. wire diameter) flush with the flow tube sidewalls. Note that the transducer holder, fabricated from a standard SS 304 1-in. screwed cap fitting, contains a square hole into which a mating low-impedance window is installed. A square piezoelectric transducer, not shown, is coupled to the window. Inlet and outlet transitions are also fabricated of the standard screwed caps. Overall length of this flow cell is about 1 ft (~30 cm). Weight is about 3 lb (1.3 kg), considerably less than the flow cell of Fig. 2, which weighs some 10 lb (4.3 kg).

Readers wishing to compare the above flow cell designs with alternatives developed by other investigators, are referred to an invited ultrasonic review article recently published by one of the authors,[14] and to the references cited therein.

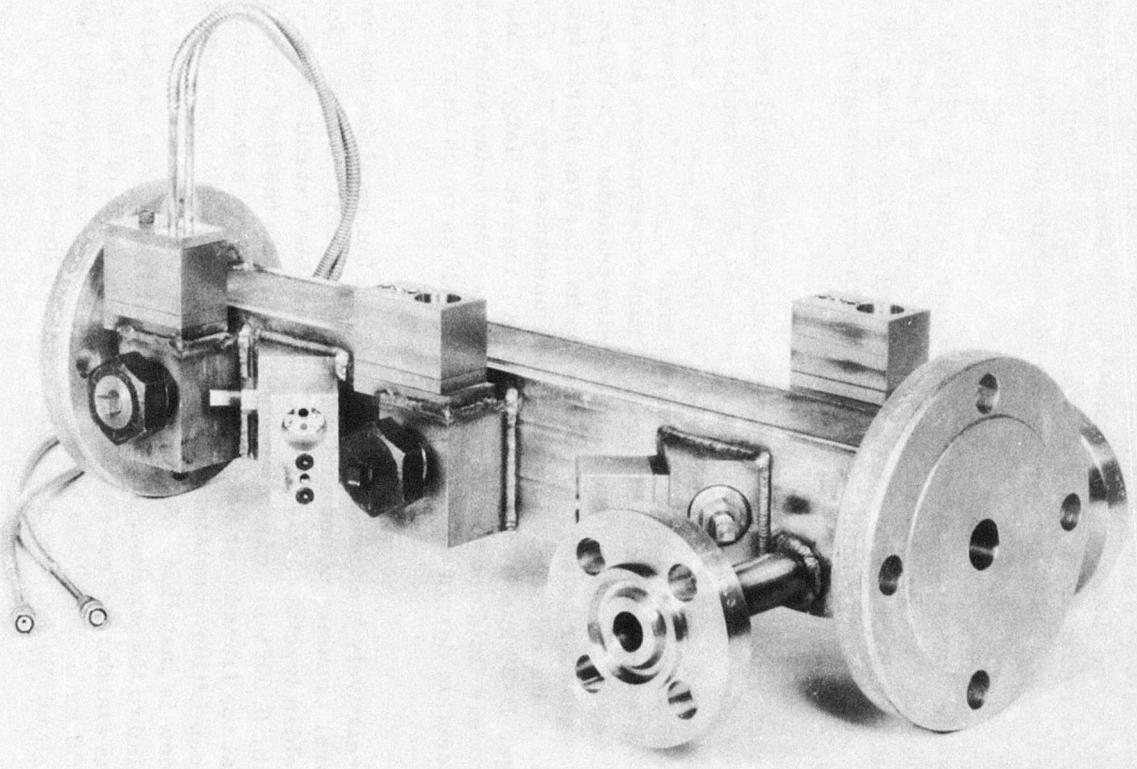

Figure B-29. Experimental Stainless Steel 304 Flowmeter Cell, Dowtherm-Jacketed, Used in Tests to Optimize Ultrasonic Frequency and Pathlength, for Two-Phase Prepolymer Flow Up to ~300°C.

Figure B-30. Exploded View of Square Flow Channel Including 45° Cavities for Short, Medium and Long Interrogation Paths.

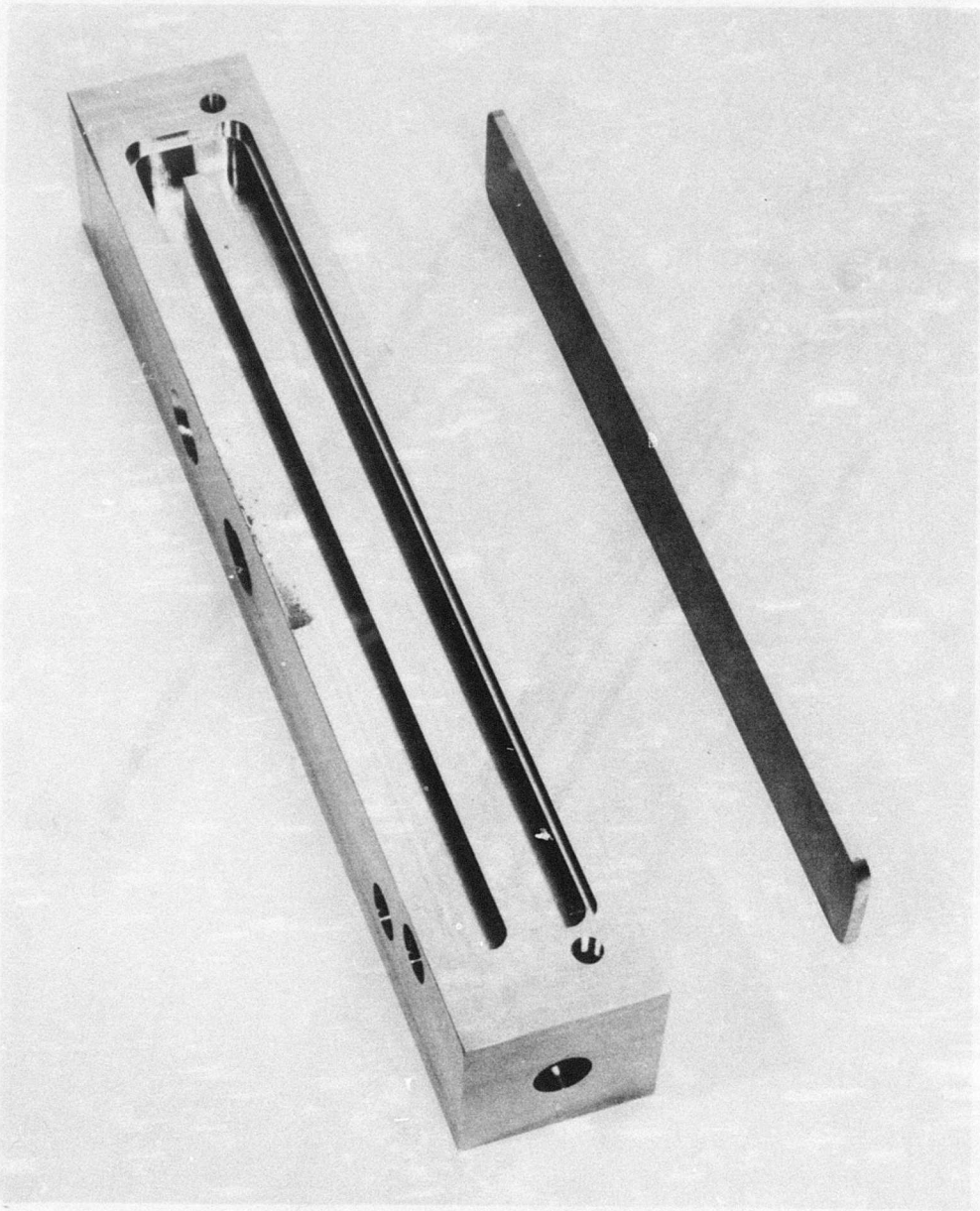

Figure B-31. Exploded View of Dowtherm Cavity, for Heating a Process Fluid Up to 300°C.

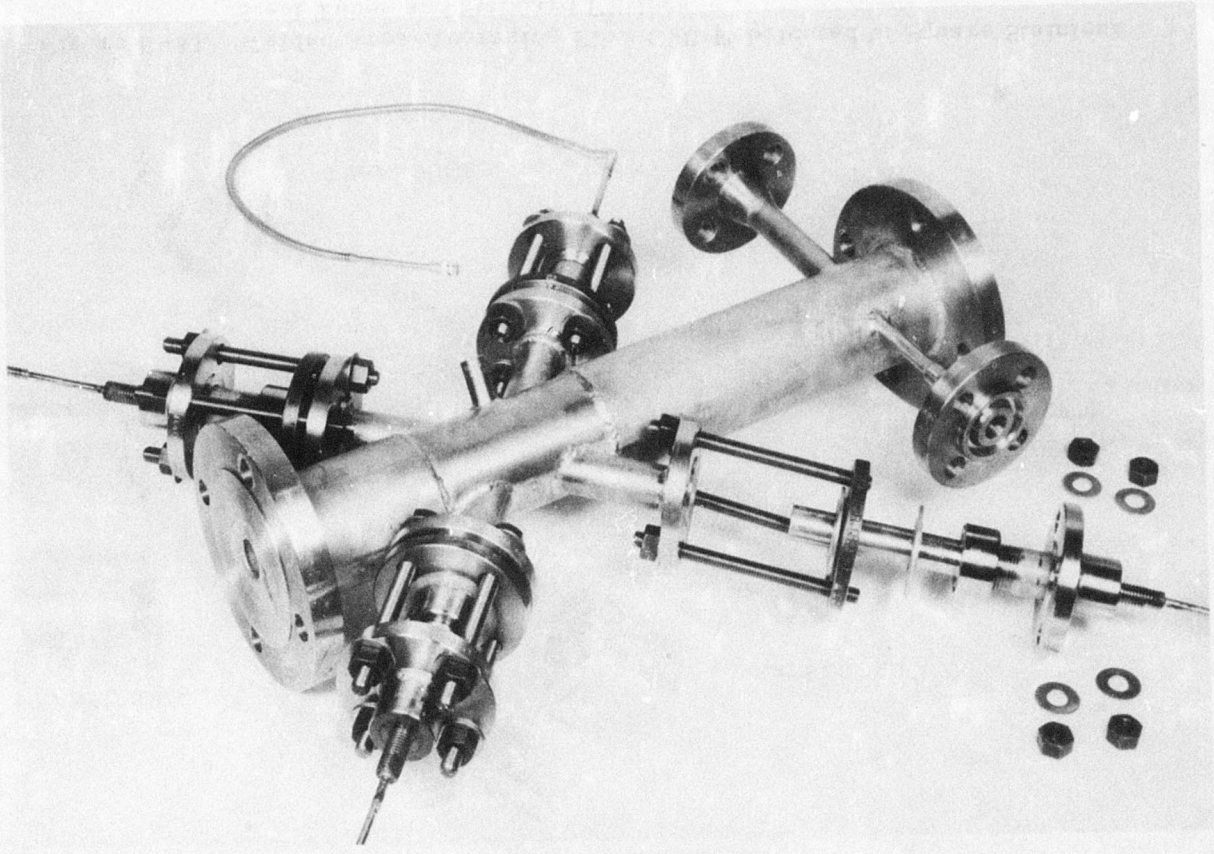

Figure B-32. Jacketed 300°C Flow Cell Fabricated With Concentrically-Welded Stainless Steel Pipe, But Not Including the Area-Averaging Feature of Figure B-29. Wetted Parts of the Transducer Holders and Windows are Made of Titanium. Flanges and Gaskets are Designed to Isolate the Transducers, Thereby Minimizing Acoustic 'Short Circuit' Through the Cell Body.

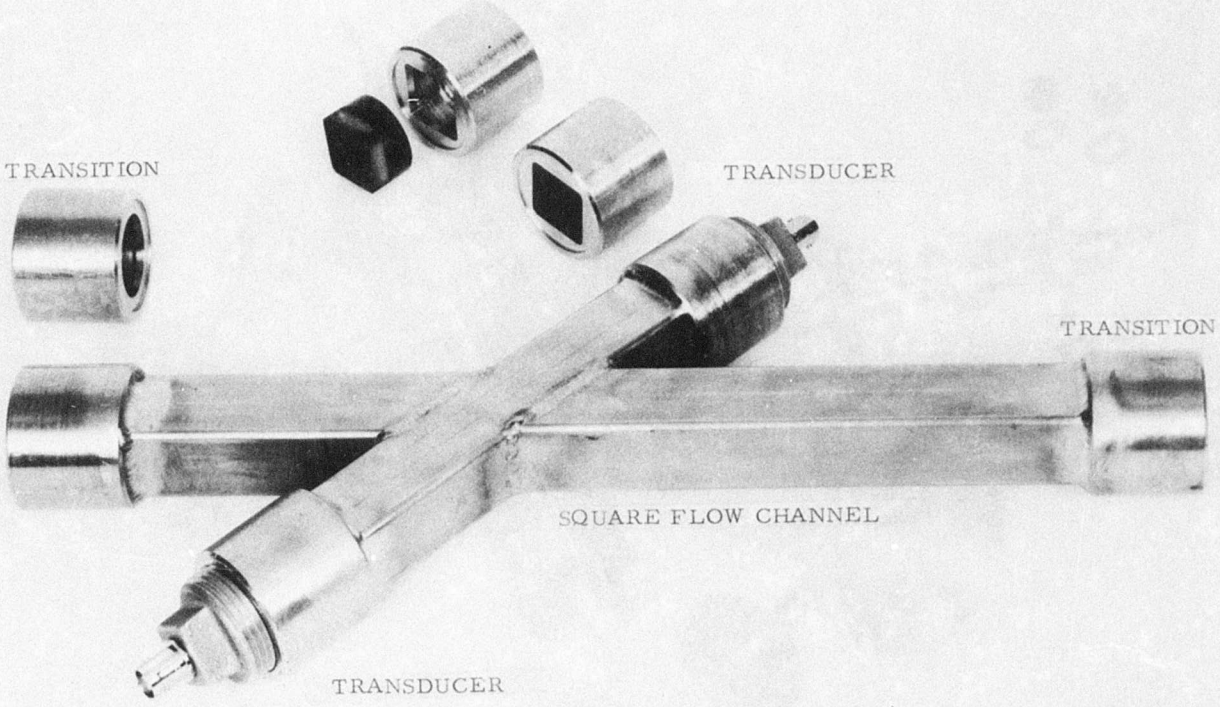

Figure B-33. Welded Area-Averaging Flow Cell Fabricated of Square Stainless Steel Tubes and Standard Fittings.

COMPARISON OF ULTRASONIC PROFILING AND AREA-AVERAGING METHODS

Alternatives. To conclude this area-averaging appendix, and to provide additional perspective, we compare the profiling potential of the transmission method (particularly where rectilinear flow is interrogated obliquely by a rectilinear beam transmitted over a full cross section of the flow channel, as used in the previous and present programs[18]) with the profiling potential of the six other ultrasonic flowmetering alternatives listed in Table B-1.

TABLE B-1. ULTRASONIC FLOWMETERING METHODS

No.	Method	Measured Parameter	Measurand
1	Transmission	Times of Flight	v, v/c or v/c^2
2	Reflection (Doppler Scatter)	Frequency Shift	v/c
3	Beam Drift	Drift Distance or Angle	v/c
4	Vortex Shedding	Shedding Frequency	v
5	Correlation	Correlation Time	v
6	Noise	Acoustic Pressure	v^n, $n > 1$
7	Hot Wire	Transit Time in Wire	Wire Temp.

The profiling comparison may be effected by commenting on or presenting cell configurations which sample or weight the flow profile so that the area-averaged value may be determined. Method 6, noise, may be omitted from further profile consideration here as it is presently limited mainly to discrete flow switch applications (on/off, threshold or leak detection) as opposed to wide-range flow measurement. This limit is due to the generated noise amplitude and spectrum responding to several factors other than v, e.g., geometry, inlet conditions, scale of turbulence, pipe roughness, etc.[18]. Profiling configurations for the remaining methods, 1 to 5, however, are compared in Fig. B-34. See also, Figs. B-35 and B-36.

Transmission Method. Let us summarize first, the principal characteristics of the rectilinear cell (Figs. 2-4, B-34a). Representative curves of constant v were obtained in 1926 by Nikuradse[19] and are reproduced in Fig. B-34a. In the present program, reference to Appendix A shows that in the JP-4 tests of December 1974, essentially linear response ($\sigma \lesssim 0.2\%$) was obtained for $\dot{M}$ from ~100 to 5000 lb/hr, or $\bar{v}$ from ~0.2 to 8 ft/s (6 to 250 cm/s). To show that this range comprises flow in the laminar, transitional and turbulent regimes, we now calculate the Reynolds numbers

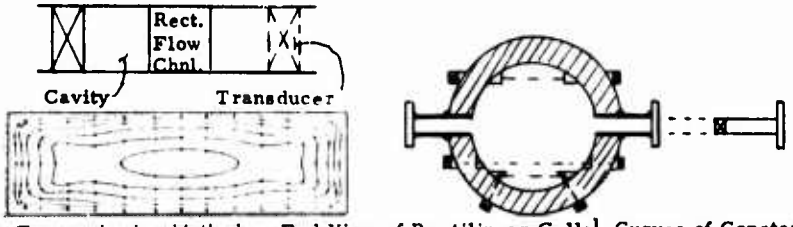

(a) Transmission Methods. End View of Rectilinear Cell;[1] Curves of Constant Velocity, After Nikuradse (1926);[2] Multichord Method Utilizing Drilled-Through Ports,[6] or Wedges, Cavities and Reflectors.

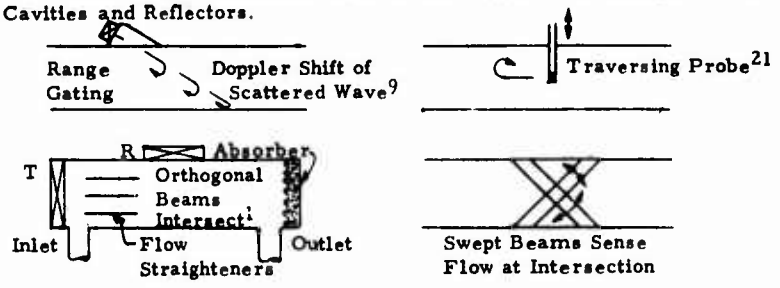

(b) Reflection Methods

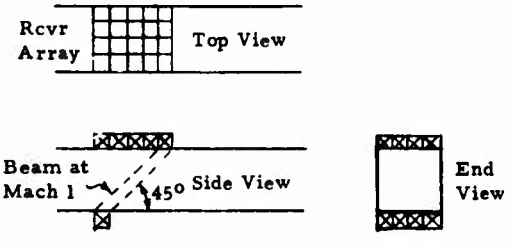

(c) Beam Drift Method

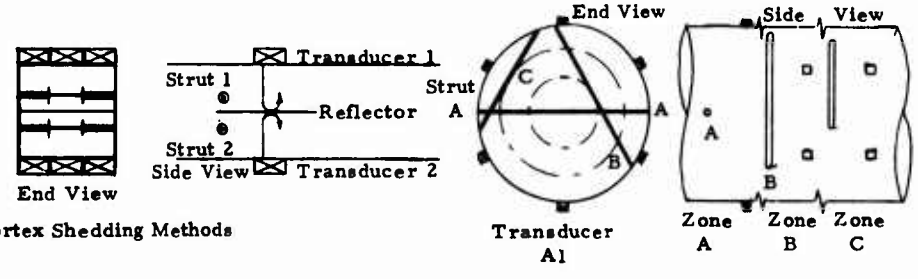

(d) Vortex Shedding Methods

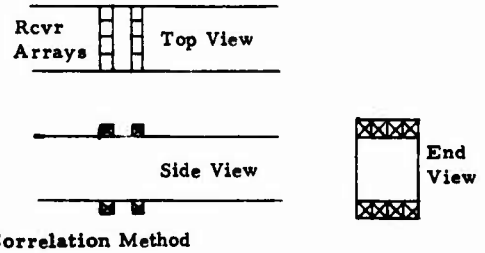

(e) Correlation Method

Figure B-34. Comparison of Ultrasonic Profiling and Area-Averaging Methods: Transmission, Reflection, Beam Drift, Vortex Shedding and Correlation. Concepts Illustrated in (a) and (b) Have Been Generally Demonstrated in the References Cited.

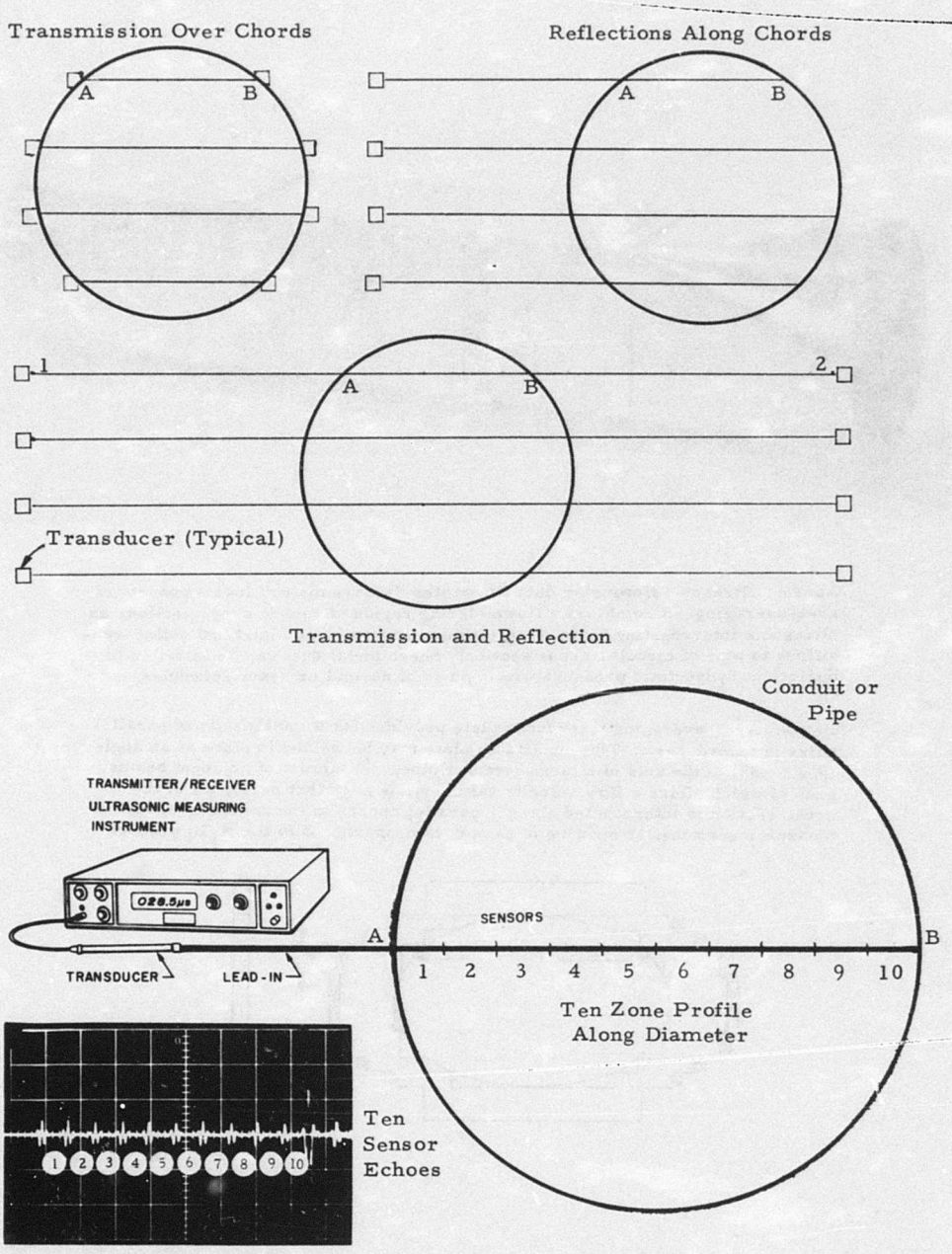

Figure B-35. Flow Profile Probe Concepts for Hot Wire Ultrasonic Anemometer. Electrical Self-Heating Connections to Terminals Such As A and B Are Not Shown.[28, 29]

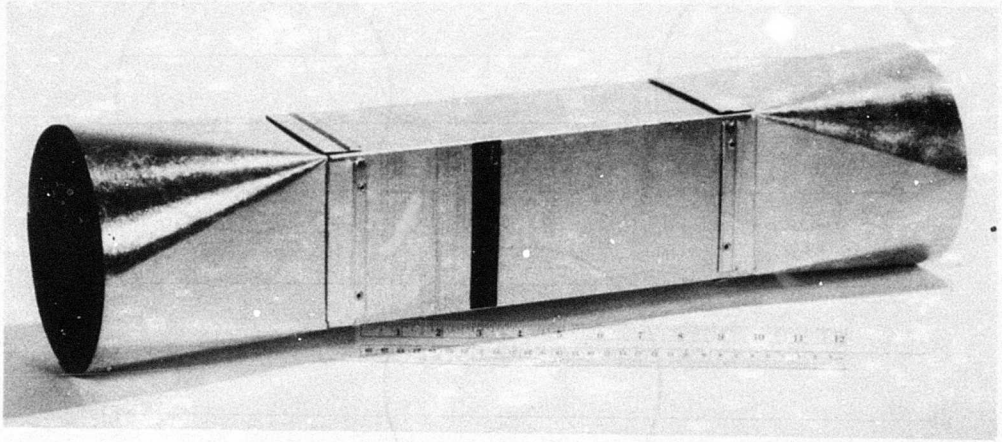

Above: Ultrasonic flowmeter duct illustrates "square meter" insert concept of area-averaging. It combines a flowmetering region of square cross section, an ultrasonic interrogating beam of rectangular envelope, and inlet and outlet transitions to pipe of circular cross section. Sheet-metal duct can be installed to operate at hydrostatic pressure within pipes of normal or heavy schedules.

Below: Area-averaging transducer plate provides for a multiplicity of parallel pairs of transducers. This insertable plate may be welded in place at an angle (e.g., 45°) to the axis of a large circular pipe. Proximity of adjacent beams, each of which yields a flow velocity value, v_i, is such that nearly all of the cross section is interrogated along i parallel chords in the generally elliptical measurement zone. Weighting of each v_i is proportional to the $W_i L_i$ product.

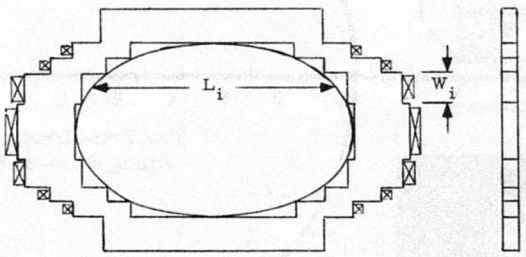

Figure B-36. Two Methods for Interrogating, Essentially the Full Cross Section of Fluid Flowing in Large Circular Conduits.

$Re = \bar{v} D_h/\nu$. The hydraulic diameter D_h for a rectangular pipe, according to Schlichting,[20] page 414, equals 4 times the area, divided by the wetted perimeter. Thus, $D_h = (4)(1)(1/2)/3$ in. = 2/3 in. = 1.7 cm for our specific cell, Fig. 2. Referring to Ref. 1, Fig. 2, $\nu \approx 0.0125$ stokes for JP-4 at 50°F, and 0.009 stokes at 100°F. Approximating these values by $\nu = 0.01$, the above area-average flow velocities $\bar{v}$ correspond to a Re range of about 800 up to about 33,000. In the lower range ($Re < 2000$) flow is clearly laminar, in mid-range ($Re > 2000$) transitional, and in the upper range, turbulent. The graphs and calculations of deviations from linearity in Appendix A, prove that with the cell of Fig. 2, for the 40:1 flow range now seen to encompass all three flow regimes, the rectilinear technique inherently provides for an area-averaging measurement without any need for subsequent profile correction by a K-factor. Again, the deviation from perfect linearity is expressed by $\sigma < 1/4\%$ of range.

The only other ultrasonic method presently known to provide comparably accurate area-averaging, is a multichord method.[6, 32] (But see also Refs. 5 and 7.) So far, this multichord method has been applied to relatively large pipes, typically of diameter > 1 ft (> 0.3 m). Referring to Fig. B-5, we note that to obtain data over chords which are sufficiently far off the pipe axis, the usual practice has been to drill ports at prescribed locations. In some instances it would be desirable to avoid penetrating the pipe, e.g., for reasons of safety. However, for the usual combinations of pipe material and fluid, and using externally-mounted transducers, the elastic properties, refraction and mode conversion phenomena prevent one from transmitting over a chord far off the pipe axis. A typical practical limit is on the order of 1/4 of the pipe radius. To avoid this limit, and at the same time obtain propagation over a path independent of refraction, Fig. B-34a suggests the use of parallel-faced internal and external wedges, or the use of internal reflectors. Where their installation and presence are allowable, such obstructions would permit one to achieve area-averaging by transmission over preferred chords without jeopardizing the pipe integrity as a penetration might. If obstructions are intolerable, internal cavities may provide an acceptable alternative.[16]

Reflection Method. Doppler methods for profiling are illustrated in Fig. B-34b, and include range-gating,[9] traversing[21] (see also Fig. B-18), and utilization of the intersection of fixed or swept beams.[1] Potential error sources, particularly for the intersecting beam methods, include nonuniform beam intensity, nonuniform distribution of scatterers, and attenuation. In all cases one assumes that the scatterers move at the local v. This assumption is known to be not generally valid for particulate scatterers in gases, and may sometimes be invalid for scatterers in liquids.

For the reflection method, as well as for Methods 3, 4 and 5 listed in Table B-1, the rectilinear flow cell concept sometimes may be incorporated to take advantage of its simpler geometry (at least regarding the ultrasonic measurements) compared to the circular pipe.

Beam Drift. This method reportedly has provided accuracy on the order of 5% for measurements of air flow in ducts.[22] It is not considered practical for liquid flow since the Mach number is so low. A schematic is given in Fig. B-34c.

Vortex Shedding. This method is usually based on the measurement of the v-dependent frequency at which vortices are shed off a single strut placed across the turbulent flow stream.[14,23] To obtain profile data, particularly for cases motivated by uncertainties in meter calibration factor, the basic concept might be expanded to include: a compound strut having several zones of differing shape or diameter; multiple struts; transducer arrays to interrogate vortices shed at different locations such as at different radii in the fluid, the response to specific locations being enhanced in some cases by focusing on the wakes of struts at said specific locations. Reflectors might be used in conjunction with pulse echo interrogation to limit each transducer to respond to only one specific wake. See Fig. B-34d, also, White, et al, and Yamasaki and Rubin (1974).[23]

Correlation. Coulthard (1973) and Ong and Beck (1974) have developed ultrasonic correlation flowmeters in the past few years.[24,25] Precisions are reported to be in the 2 to 5% range. Again, to achieve area-averaging, the rectilinear cell may be considered in view of its profile-compensating advantages compared to the usual circular pipe (Fig. B-34e).

Hot Wire Profile Probe. In contrast to Methods 1-6, wherein flow velocity is determined by measuring the speed or amplitude of sound which is generated or transmitted in the fluid itself, this last method, 7, is based on measuring sound speed in a foreign sensor, the hot wire anemometer probe. In effect, this transforms the flow profile problem to a temperature profile problem.

Hot wire anemometers are well established as flow measuring devices.[27] Means for ultrasonically measuring average temperature or temperature profile in wires which are self-heated electrically have also been established.[28,29] Average temperature in a wire can be determined by measuring the transit time over the wire, by reflection or transmission techniques, or their combination. Temperature profile in a wire can be determined by reflection techniques. Figure B-35 illustrates these techniques.

Temperature may be averaged along wires located in a plane which is perpendicular or inclined to the flow axis. In the latter case the paths could coincide with the Gaussian quadrature paths of Ref. 6. Alternatively, temperature could be profiled in one or more segmented wires located on a diameter or on chords.

In summary, ultrasonic flow profiling or area-averaging has been demonstrated for Methods 1 and 2, with accuracies better than 1% so far limited to the two transmission methods of Fig. B-34a. The use of key elements used successfully in the two transmission methods (rectilinear cell, multiple paths) might be adapted to Methods 2 to 5, but the actual potential and limitations of such adaptations are not yet known.

APPENDIX C
ρc DENSITOMETER

In USAAMRDL TR 72-66, we described the general principle of ultrasonic reflectance, or impediometry as it is sometimes called, as applied to determining the characteristic acoustic impedance ρc of aviation fuels.[1] We showed that the ideal probe material would have its own characteristic impedance Z_1 close to that of the fuel; that Z_1 would not be sensitive to temperature; and that the probe material should be readily available, machineable, rugged, impervious, and corrosion-resistant or inert relative to the fuel, including contaminants. The geometry of main interest was a cylindrical rod of stepped diameter, to provide the required echoes A and B, as in Fig. C-1.

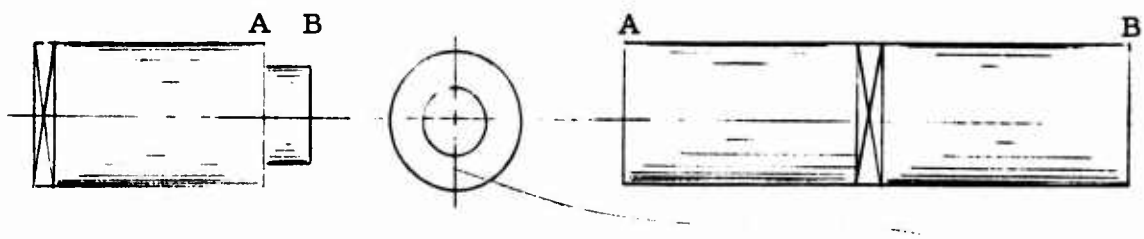

Figure C-1. ρc Probes With Stepped Diameter, and With Uniform Diameter.

The present program utilized a nearly-symmetric probe, also shown in Fig. C-1. Materials for the newer probe included fused silica and X-cut quartz. The newer probes generally were slightly larger than their predecessors, to minimize second-order interferences due to mode converted pulses generated spuriously at the sidewalls and at the ends.

Although not initially obvious, it turned out, due to practical considerations, that in order to determine the temperature-immunity of the probe, a temperature-immune echo comparator was almost mandatory. Conversely, to verify the echo comparator, a temperature-immune probe was virtually essential. In the program, an iterative procedure was followed in an attempt to yield a ρc system which was sufficiently immune to temperature, without sacrificing rangeability, linearity or other important characteristics.

As test data became available for analysis during the program, it gradually became apparent that the usual transducer bonding and probe mounting procedures were inadequate. Tests of coupling or bonding

agents such as propylene glycol (liquid), Dow resin 276V9 (viscous fluid), epoxy, electrostatic and a gold/tin eutectic solder led us to select an epoxy which is usable from -200°C to +100°C. Tests of mounts including oppositely-tapered rods, silicone-rubber-potted assemblies, epoxied-in-sleeve assemblies, and compression fittings (Conax, Swagelok) led us to select the epoxied sleeve combination. However, further test results may indicate that this selection should be revised. Accordingly, it is considered appropriate here to introduce several alternative ρc probe designs (Fig. C-2), several of which have already been fabricated (Fig. C-3). Some of these alternatives merely relieve thermal stresses at the transducer bond or simplify the mechanical mounting procedure. Others magnify the ρc sensitivity by causing the B echo to be influenced by not just 1, but 2 or 3 solid/liquid reflections before being measured. Also, the possibility of substituting a low-Z_1 rod, such as certain isopaustic glasses, graphites or possibly other materials, would offer another factor of 2 improvement in sensitivity.

The desirability of improving probe sensitivity and/or stability will be understood from the mathematical analysis given below. The analysis also implies that ρc system performance may be improved significantly by using a narrowband echo comparator approach, rather than the broader band approach embarked upon at the outset of the present program. The narrowband approach, as presently envisioned, would utilize the regeneration of continuous waves from the A and B echoes, somewhat analogous to the regeneration of continuous upstream and downstream waves which has now been successfully demonstrated in the flow velocimeter portion of this program.

Next, we present a mathematical analysis of the accuracy required in the measurement of A and B to obtain ρc within a specified fraction of 1%, assuming one uses the nearly-symmetrical probe of fused silica. This will be followed by a brief description of a proposed narrowband echo comparator, which appears capable of measuring A and B accurately enough so that ρc could be determined in the range $\pm$ 0.1 to 0.3%. Combining this ρc result with a v/c measurement of comparable accuracy, the mass flow rate $\dot{M}$ could be determined with a probable error of less than $\pm$ 0.5%.

Now we shall provide an error analysis of the ρc measurement, as a function of the measured parameters. The purpose of the analysis is to determine the accuracy to which the amplitudes of the two reflected pulses must be measured.

The ρc measurement consists of the independent measurements of the amplitudes of essentially identically-shaped 10-MHz rf pulse bursts

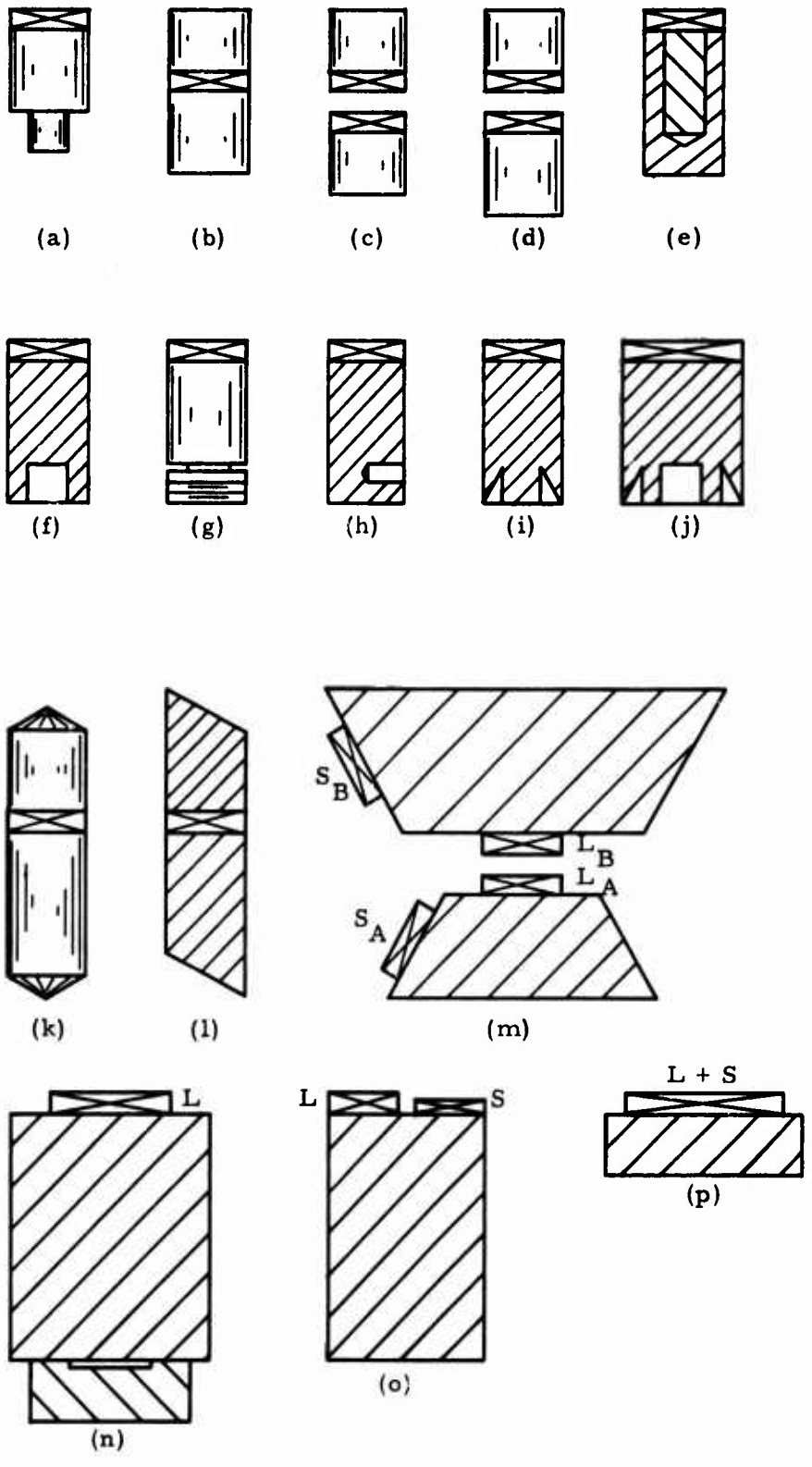

Figure C-2. Alternative Designs for ρ c Probes.

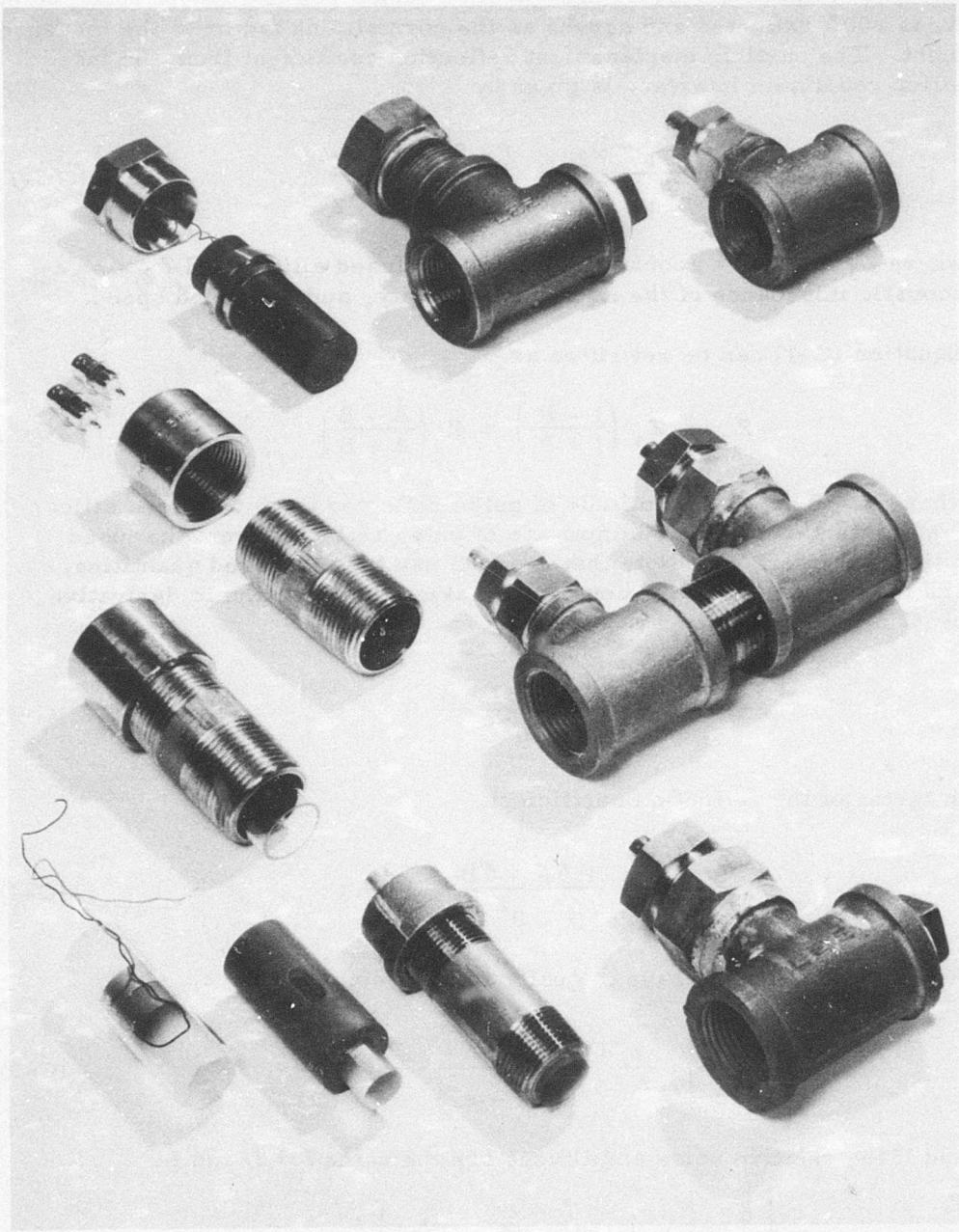

Figure C-3. Photograph of ρc Probes.

reflected from a fused silica/air interface and from a fused silica/liquid interface, where the liquid may be JP-4 fuel. The first-mentioned pulse, A, is 100% reflected and serves as the normalizing factor in the measurement. The particle displacement reflection coefficient from the fused silica rod/liquid interface is given by

$$R = \frac{Z_1 - Z_2}{Z_1 + Z_2} = \frac{\rho_1 c_1 - \rho_2 c_2}{\rho_1 c_1 + \rho_2 c_2} \tag{C-1}$$

where $Z_1 = \rho_1 c_1$ = acoustic impedance of fused silica, and $Z_2 = \rho_2 c_2$ = acoustic impedance of the liquid, ρ = density, and c = sound speed.

Equation (C-1) can be rewritten as

$$Z_2 = Z_1 \left(\frac{1 - R}{1 + R}\right) = Z_1 \left(\frac{A - B}{A + B}\right) \tag{C-2}$$

where R = B/A, B = amplitude of pulse reflected from the fused silica/liquid interface, and A = amplitude of pulse reflected from the fused silica/air interface. Note that A and B use the measured quantities, and for now we take Z_1 = constant. Taking the logarithmic derivative of (C-2),

$$\frac{\delta Z_2}{Z_2} = \frac{2B\delta A - 2A\delta B}{A^2 - B^2} \tag{C-3}$$

In terms of the reflection coefficient,

$$\frac{\delta Z_2}{Z_2} = \frac{2}{A} \frac{R\delta A - \delta B}{(1 - R^2)} \tag{C-4}$$

If the A and B pulses have mutually random noise,

$$\left|\frac{\delta Z_2}{Z_2}\right| = \frac{2}{A} \frac{R\,|\delta A| + |\delta B|}{(1 - R^2)} \tag{C-5}$$

and if the relative noise amplitudes are the same for A and B,

$$\left|\frac{\delta Z_2}{Z_2}\right| = 2\sqrt{2} \frac{R}{1 - R^2} \left|\frac{\delta A}{A}\right| \tag{C-6}$$

In the case of fused silica and JP-4, it can be shown that R = 0.86. Thus,

$$\left| \frac{\delta Z_2}{Z_2} \right| \simeq 9.3 \left| \frac{\delta A}{A} \right| \qquad \text{(C-7)}$$

In the actual measurement, A ≃ 1000 millivolts. Equation (C-7) therefore predicts that the fractional error in measuring $Z_2 = \rho_2 c_2$ is about 0.93% per millivolt of noise on the pulse amplitude. Laboratory measurements of relative ρc error vs. δ (A - B) have shown about 0.5% per millivolt, which is in reasonable agreement with the above analysis.

From the above analysis, it can be concluded that, to insure an overall ρc measurement error of less than 0.5%, the "A" and "B" measurements should each be more precise than ~0.5%. This can be accomplished if narrowband cw techniques are used and if standard precision AC voltage measuring techniques (± 0.02%) are used. This approach, which is similar in many respects to the high-frequency portion of the $(\phi_1 - \phi_2)$ measurement, is presently being investigated as an alternate and more precise means of measuring the amplitudes of the reflected waves from the fused silica/air and the fused silica/liquid interfaces.*

Along with the narrowband, reconstituted cw approach to improving the ρc determination, some improvement in probe design is anticipated. Referring again to Fig. C-2, we point out that the stepped-diameter probe (a) used in the previous contract tended to crack at the stress-raising corner. The nearly-symmetrical improvement (b) has proven to be more rugged and much better damped when fully potted, but it suffers somewhat from nonidentical crystal bond stresses when the sleeve in which it is potted expands on heating. The bond stresses due to differential thermal expansion could be eliminated by potting only one rod, but this would introduce other problems, particularly under vibratory loads. Therefore, we considered alternatives such as (c), (d), where both A and B rods could be fully potted, yet a small gap, ~1/8 in. (~3 mm), could be left between the pair of neighboring, matched crystals. Separated rods also offer more design freedom in the electronics, relative to gating and frequency selection. This separated-rod design appears relatively promising for future work with the ρc concept.

*Commercially-available instrument alternatives may also be considered. Princeton Applied Research Corporation, for example, recently introduced their Model 188 digital ratiometer (which utilizes coherent detection principles) for measuring A/B ratios.

Another group of probe alternatives is illustrated in (e) to (j), where only one bond is used, and the reference reflectors are readily fabricated in probe materials such as aluminum (subsequently anodized) or titanium. (Eliminating the reference reflector or probe, not shown, is also a possibility.)

The probes (k) and (l) provide double and triple reflections of the A and B echoes, for corresponding increases in ρc sensitivity.

Trapezoids (m) are included principally for academic interest. Potentially, these could measure viscosity (using shear wave transducers S_A and S_B) as well as ρc, leading to a determination of kinematic viscosity and Reynolds number.

At this writing, the drift in the ρc densitometer is principally due to the probe. Probe drift, in turn, is thought to be attributable mainly to the transducer/rod bond(s). Secondary sources of probe drift are attributed to minor changes in the reflectivity at the periphery of the rods, which influence the contribution of rays which strike the periphery at grazing incidence. Such secondary sources of error can be eliminated by making the rod diameter large enough to delay both mode converted and nonconverted peripherally-reflected waves beyond the time of flight of the direct waves whose end-wall reflection corresponds to the fuel ρc.

One may summarize the problems covered in the above discussion by stating that much of the difficulty in determining ρc by the reflection coefficient method stems from the fundamental difficulty of measuring the relatively small difference KA-LB between two relatively large numbers KA and LB, when $|R|$ is nearly equal to unity.

Instead of measuring the reflection coefficient, if one measures the transmission coefficient, that fundamental difficulty is avoided. However, one must avoid two new errors due to (1) attenuation in the fluid by absorption and scattering (turbulence) and (2) diffraction (beam spread).

Up to now, in this program, we have not pursued the ρc transmission approach precisely because of the computational complexity associated with eliminating the contributions of absorption, scattering and diffraction losses. However, given the present state of the art of microprocessors, plus the experimental difficulties observed with the ρc reflection approach, the transmission approach is worth considering.

Perhaps the easiest way to understand the basis for this approach is to examine the equation (C-8) for energy transmission T_e between media

of impedances Z_1 and Z_2 for plane waves at normal incidence and the corresponding graph, Fig. C-4.

$$T_e = 4 Z_1 Z_2/(Z_1 + Z_2)^2 \qquad \text{(C-8)}$$

The graph, Fig. C-4, is based on the values listed in Table C-1. Since we are concerned with transmission (see Fig. C-5) across two interfaces per path, we plot the term corresponding to T_e^2, namely, 10 log T_e^2 or 20 log T_e in dB versus the fluid impedance Z_2 for four typical materials that could be used either as buffer rods or as the flow cell structure. From Table C-1, or Fig. C-4, it will be seen that the sensitivity of 20 log T_e to Z_2 is relatively independent of probe impedance Z_1, but increases for smaller Z_2. Quantitatively, the sensitivity $(\Delta Z_2)/Z_2(\Delta dB)$ of the four quasiparallel curves in Fig. C-4 is about 1% per 0.1 dB for $Z_2 \approx 0.1$ g/cm^2-μs. This means that to determine ρc of the fluid to 1%, one needs to measure the transmitted wave amplitude to 1%. To the extent that the effect of attenuation and diffraction losses can be eliminated, this means that amplitude measurement requirements are about one order of magnitude less stringent for the transmission approach than for the reflection approach.

The diffraction loss is calculable in terms of the Seki parameter $S = \lambda z/a^2$ where $\lambda = c_2/f$, z = pathlength, and a = radius of buffer rod.[16] The attenuation loss is measurable using the differential path inherent in the rectangular cell of Fig. C-5. For this cell of dimensions 1 cm x 2 cm, each of these losses may be expected to be approximately 1 dB through suitable choice of frequency (~1 to 5 MHz) and rod diameter (~1 cm).

The ρc transmission approach, in summary, would consist of measuring two transmissions A and B, normalizing them to reference echoes A_{r1} and A_{r2} in the transmitter rods, correcting for diffraction[16] and attenuation, and finally computing T_e and then $Z_2 = \rho c$ in the fluid.

While this transmission coefficient procedure appears much more complicated than using an expression like (C-2), it will be recognized that in the transmission procedure the accurate determination of Z_2 no longer depends on the extremely precise determination of (A-B). In effect, the transmission coefficient approach exchanges computational complexity for measurement complexity. Given the capabilities of modern microprocessors, this exchange may significantly favor the transmission approach over the reflection approach within the framework of a ρc densitometer. Further, when $S << 1$, computation is simplified - see Fig. C-5.

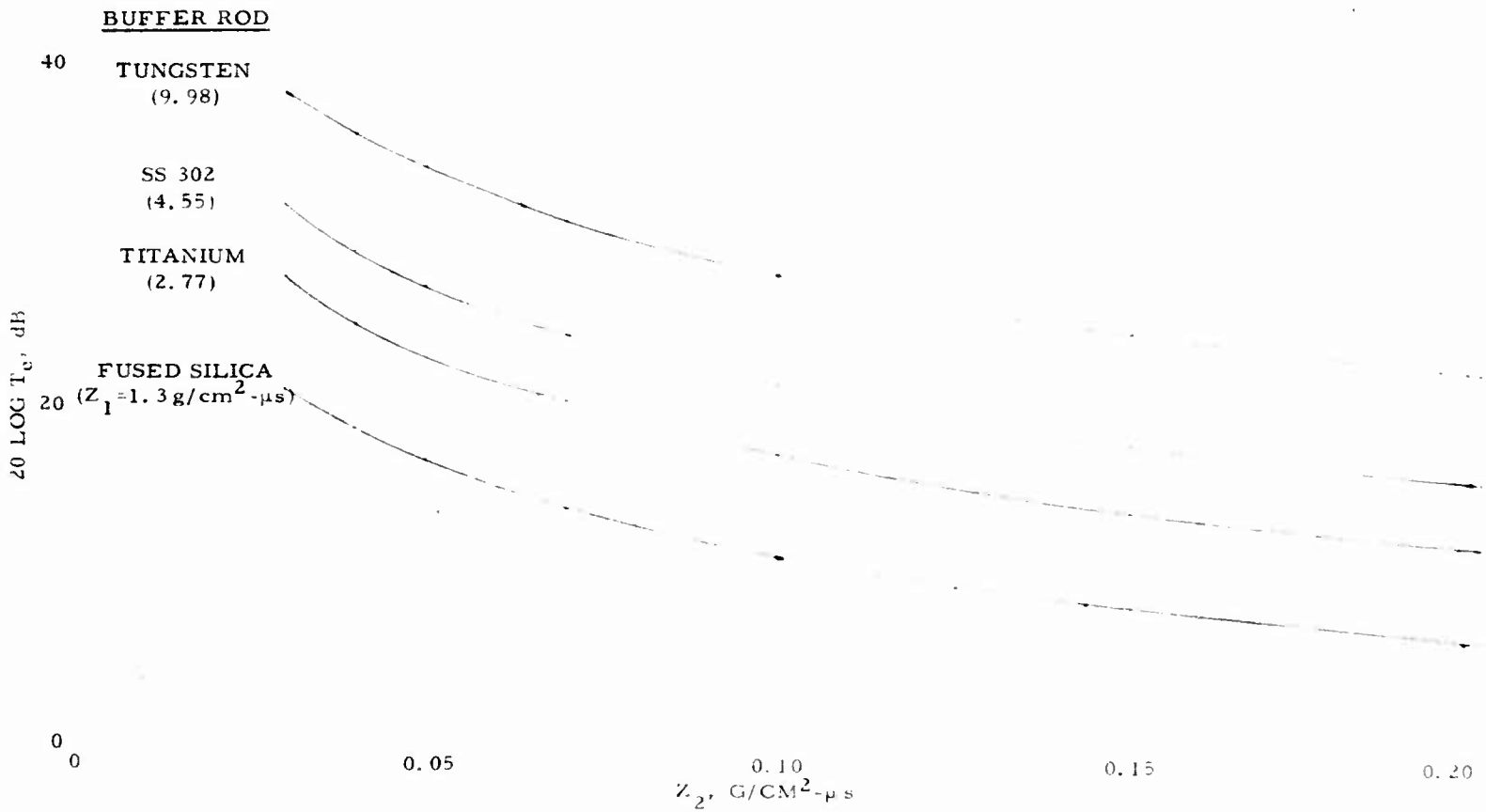

Figure C-4. Transmission Loss for Two Interfaces (Solid-Fluid-Solid) Versus Fluid Impedance Z_2, for Four Buffer Rod Materials of Different Impedances Z_1.

TABLE C-1. LOSS IN dB FOR SOLID-FLUID-SOLID TRANSMISSION PATH, ATTRIBUTABLE TO IMPEDANCE MISMATCH BETWEEN Z_1 AND Z_2

Solid	Z_1 g/cm^2-μs	Z_2 g/cm^2-μs	Loss = 20 log T_e dB
Fused Silica	1.30	0.03	21.09
		0.04	18.72
		0.05	16.91
		0.07	14.25
		0.10	11.53
		0.15	8.61
		0.20	6.70
Titanium	2.77	0.03	27.45
		0.04	25.02
		0.05	23.14
		0.07	20.34
		0.10	17.42
		0.15	14.20
		0.20	12.00
SS 302	4.55	0.03	31.73
		0.04	29.23
		0.05	27.32
		0.07	24.48
		0.10	21.50
		0.15	18.16
		0.20	15.84
Tungsten	9.98	0.03	38.45
		0.04	35.97
		0.05	34.04
		0.07	31.16
		0.10	28.12
		0.15	24.68
		0.20	22.26

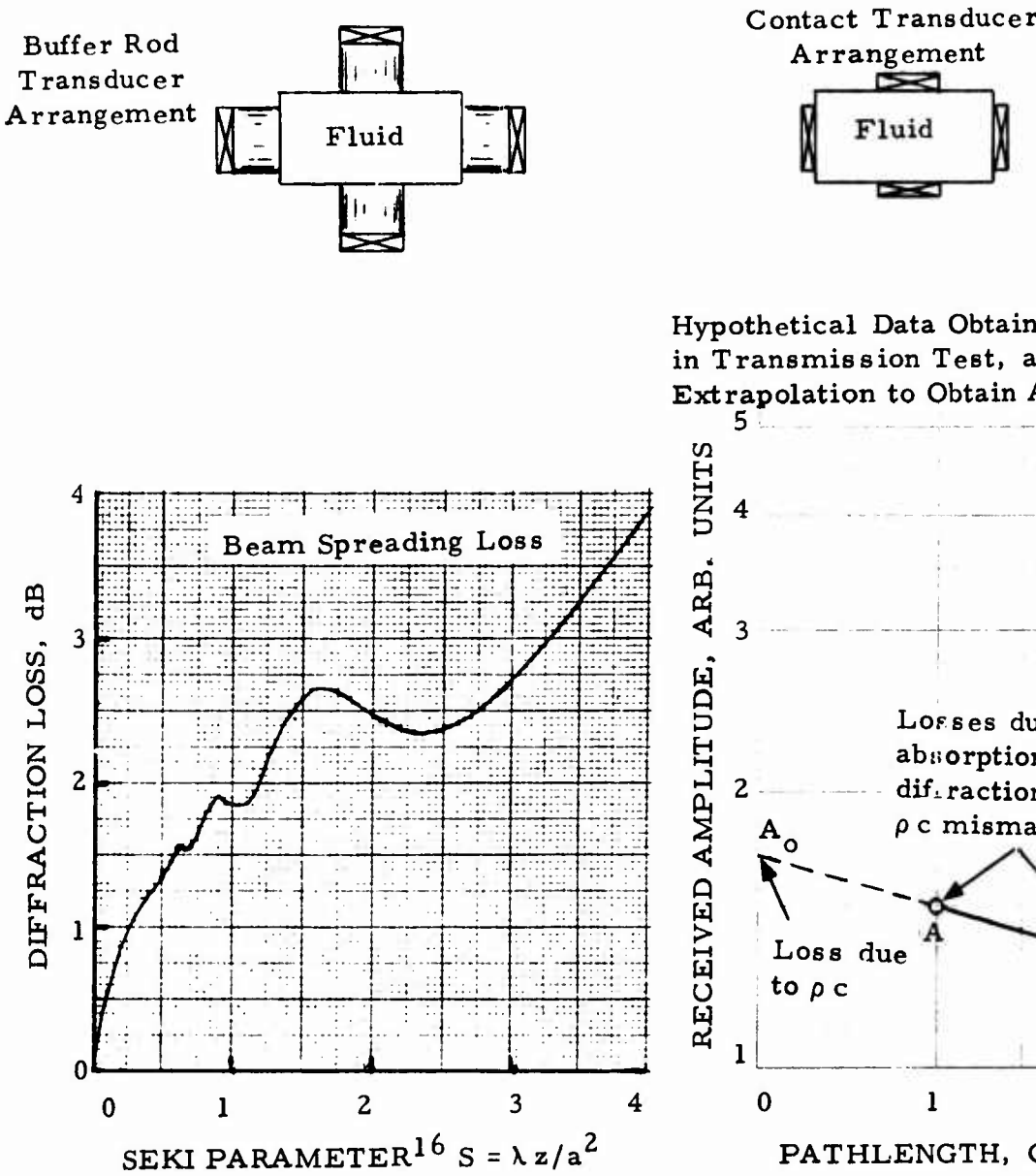

Figure C-5. Differential Path ρ c Transmission Cell. Pathlengths z_A and z_B in the fluid may be in the proportion 1:2, e.g., 1 cm x 2 cm. Received amplitudes A and B are attenuated by absorption, diffraction and mismatch losses. At 5 MHz the absorption coefficient may be ~0.1 to ~2 dB/cm. The diffraction loss for $S << 1$, is essentially proportional to pathlength. In this special case, A and B may be easily corrected (as illustrated graphically in semilog plot) for absorption plus diffraction losses, the extrapolated value A_o being ρ c-dependent: $A_o = A^2/B$.

We conclude this ρc appendix by noting that in some instances, such as operation only over a narrow temperature range, the differential path configuration of Fig. C-5 may not be necessary. The v/c transducers may suffice. That is to say, when the attenuation and beam spread are substantially constant, and if the transducer piezoelectric activity and sensitivity coefficient are also substantially constant, then the amplitude of the wave transmitted across the v/c measuring region may be interpreted in terms of the fuel impedance Z_2.

APPENDIX D
ECHO COMPARATOR

The echo comparator, Fig. D-1, consists internally of a power supply, a 10-MHz rf burst pulsed oscillator and gating circuitry, an echo comparator receiver, and output circuitry. A block diagram of the echo comparator is shown in Fig. D-2. Tracking and linearity test data are given in Figs. D-3 and D-4.

To understand the operation of the echo comparator, consider Fig. D-5, showing the nearly-symmetrical ρc probe, and broadband or video echoes A and B obtained under spike excitation. Figure D-6 shows that the spectra of A and B peak broadly below 10 MHz, and continue out at least to 10 MHz. This means that if the ρc crystal is driven with an rf burst containing, say, 10 cycles of a 10-MHz carrier, i.e., a 1μs wide burst, the echoes will closely follow the drive waveform.

The pulsed oscillator, then, drives the ρc crystal at about 10 MHz, at a prf of about 200 Hz. Probe buffers are cut to lengths L_A and L_B such that end echoes A and B arrive in 1μs time slots beginning at 10μs and 12μs after the initiation pulse. These echoes are selected by adjustable echo selectors A and B, amplified, peak detected, and finally compared in sum and difference amplifiers. Both echoes are amplified equally, but by an amount, controlled by the AGC amplifier, such that A $\approx$ 2 V. Output dc levels KA + LB and KA - LB are fed to the flow calculator via coaxial cable connections, where their quotient is formed, proportional to ρc of the fuel. K and L are manually adjusted potentiometers set such that KA = LB when probe ends A and B radiate into equal impedances, namely, dry air.

The liquid density sensed by the ρc probe may be computed from the echo comparator outputs, the probe impedance Z_1, and the sound speed c_2 in the liquid:

$$\rho = (Z_1/c_2)\,(KA - LB)/(KA + LB) \qquad \text{(D-1)}$$

An example of test data and the resulting calculation are given in Table D-1 and in the corresponding graph, Fig. D-7.

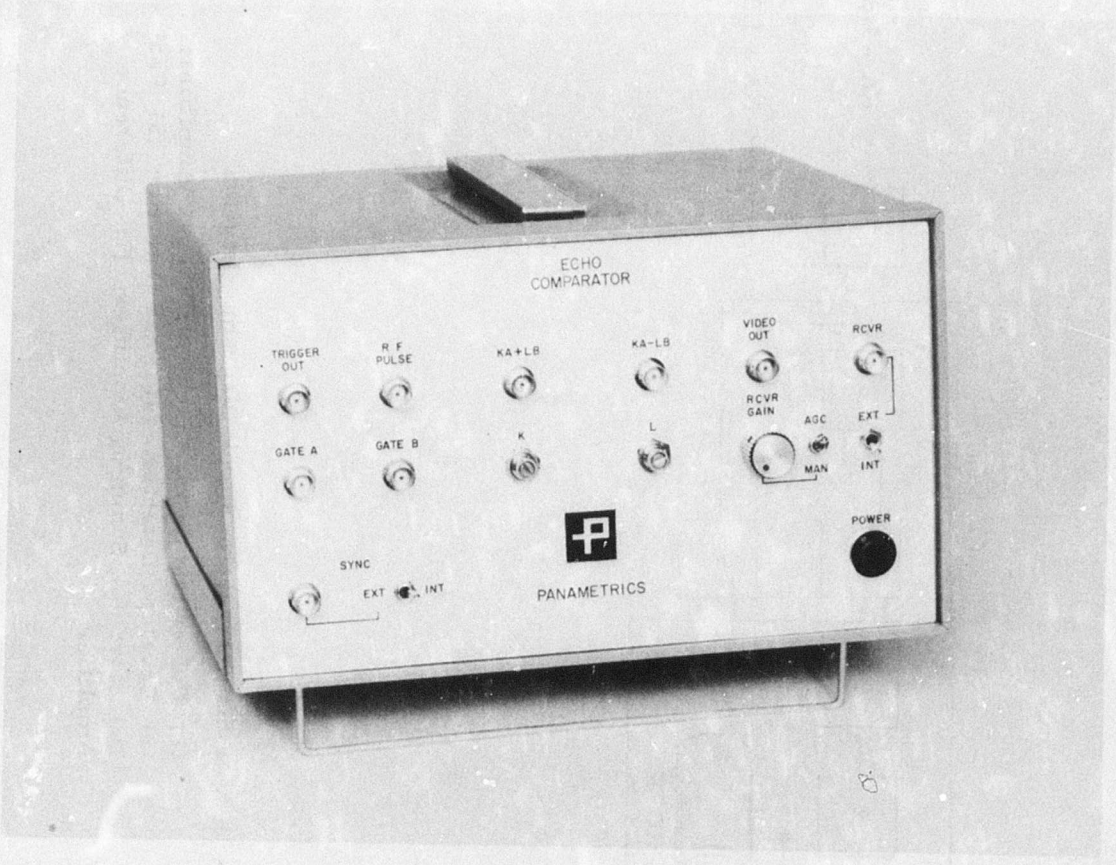

Figure D-1. Echo Comparator.

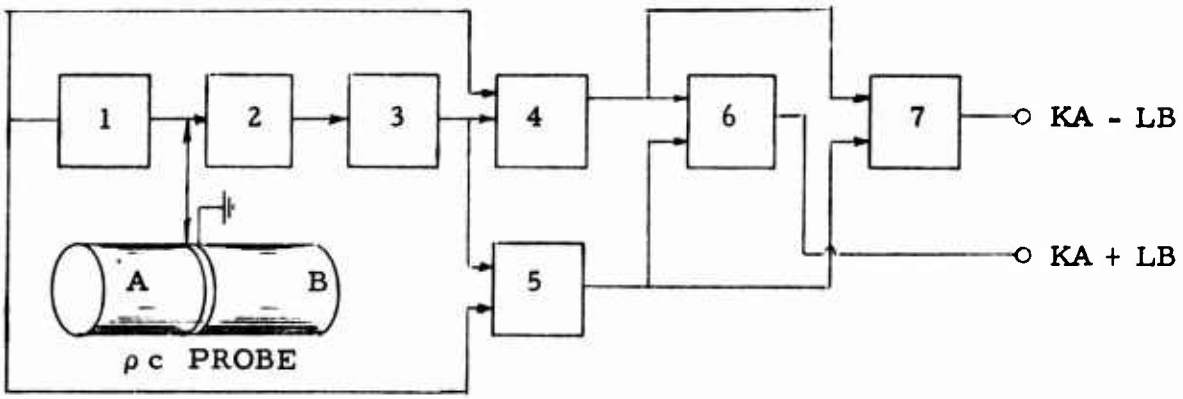

Figure D-2. Echo Comparator Block Diagram. Legend:

(1) Pulser and Gating Circuitry; (2) RF Amplifier; (3) Envelope Detector: (4) Peak Detector; (5) Peak Detector; (6) Summing Amplifier; (7) Difference Amplifier.

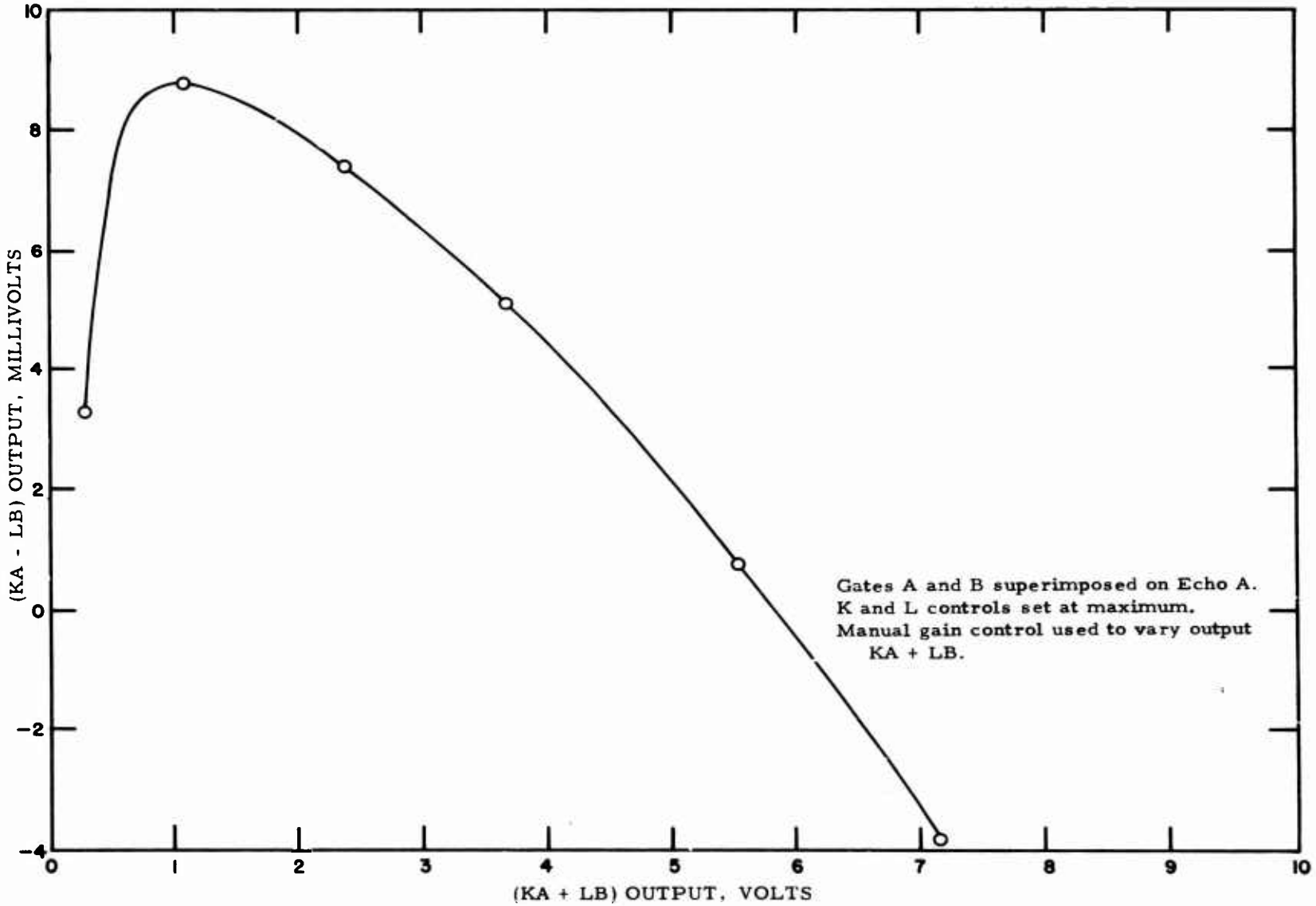

Figure D-3. Tracking of Echo Comparator - Channels A and E.

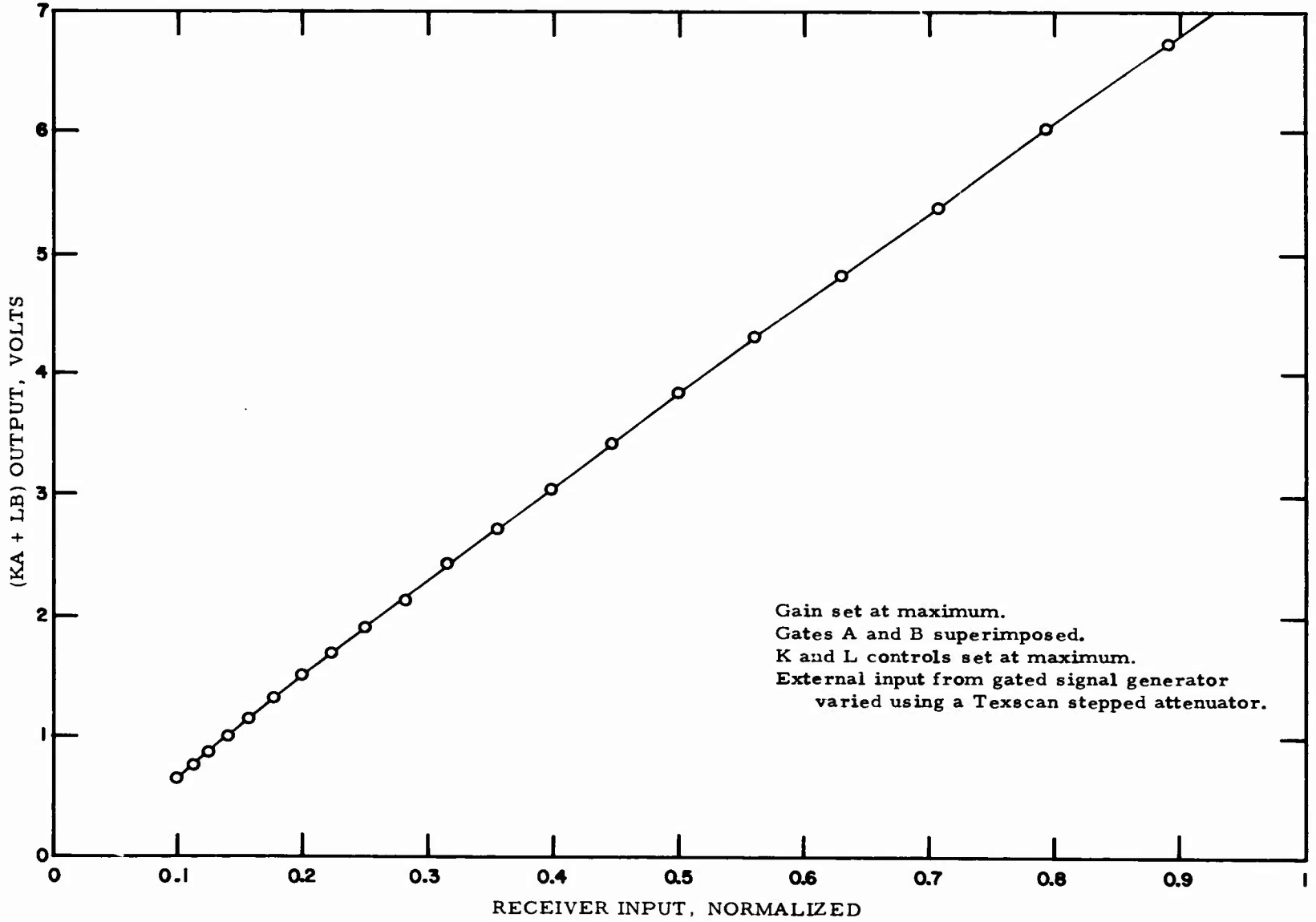

Figure D-4. Echo Comparator Receiver Linearity.

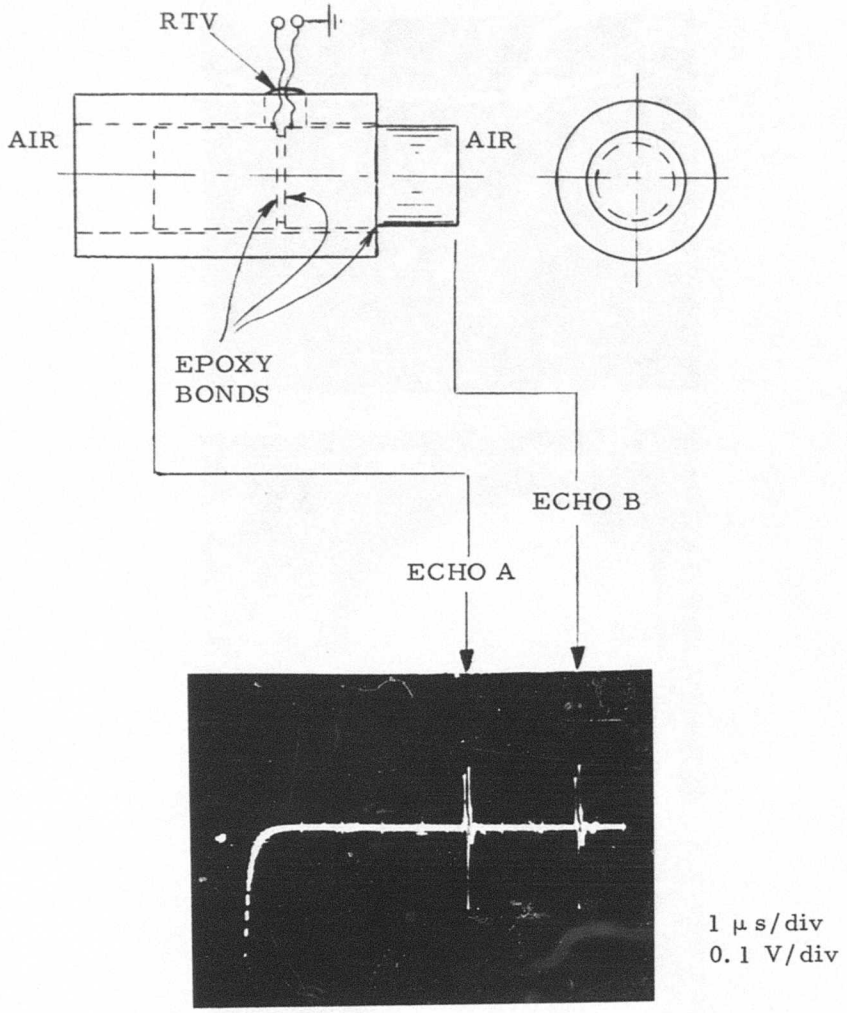

Figure D-5. Epoxy-Bonded ρ c Densitometer Probe, Using Sandwiched 10 MHz X-Cut Crystal Between Gold-Plated Fused Silica Buffer Rods. Oscillogram Showing Reference Echo A From Shorter Rod, and Echo B From Longer Rod. Echo B Decreases From the Value Shown, When It Contacts a Liquid Whose ρ c More Nearly Matches the Acoustic Impedance of Fused Silica.

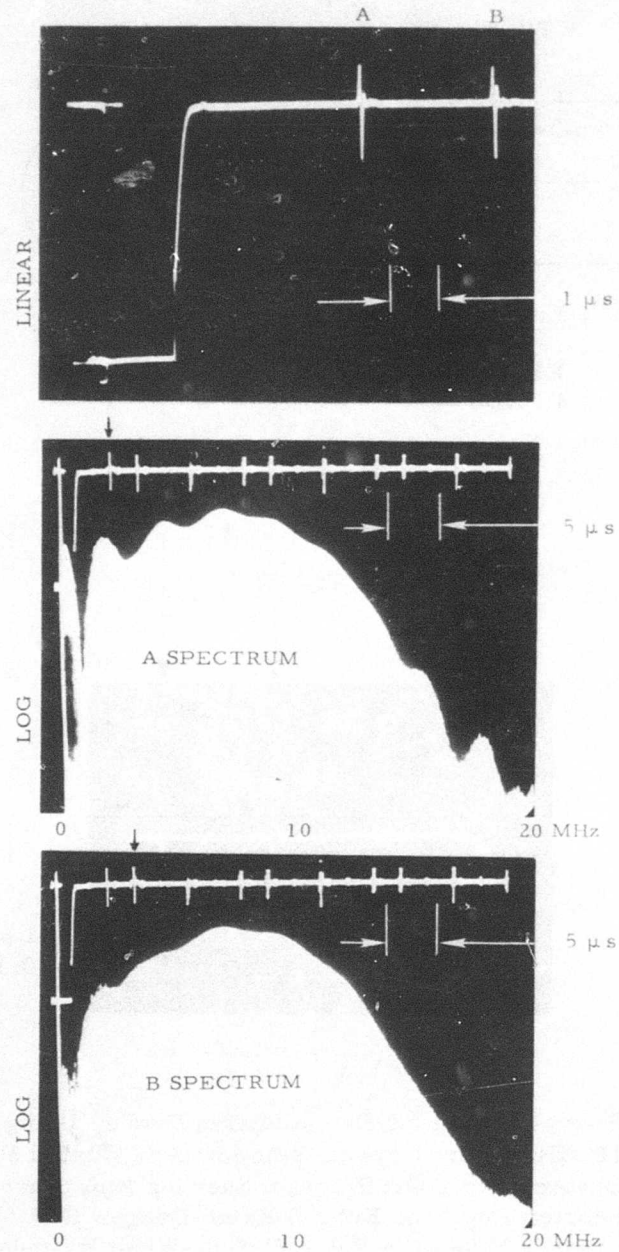

Figure D-6. Densitometer Probe Echoes A and B, in Time and Frequency Domains.

TABLE D-1. ECHO COMPARATOR TEST DATA

Liquid	ρ g/cm^3	c m/s*	KA-LB volts	KA+LB volts	Calc. ρ g/cm^3	ρ norm** g/cm^3
Acetone	.79	1172	.318	4.085	0.86	.789
Benzene	.87	1290	.380	4.015	0.95	.872
Water	.998	1500	.490	3.905	1.087	.998
Nitrobenzene	1.20	1459	.559	3.84	1.297	1.1908
Carbon Disulfide	1.26	1149	.472	3.925	1.36	1.249
Chloroiorm	1.49	986	.487	3.915	1.637	1.502
Carbon Tetrachloride	1.595	925	.479	3.92	1.715	1.575

*Corrected for test temperature, 25 to 26°C.

**Calculated value, normalized to value for water, 0.998 g/cm^3. This column may be compared with first ρ column.

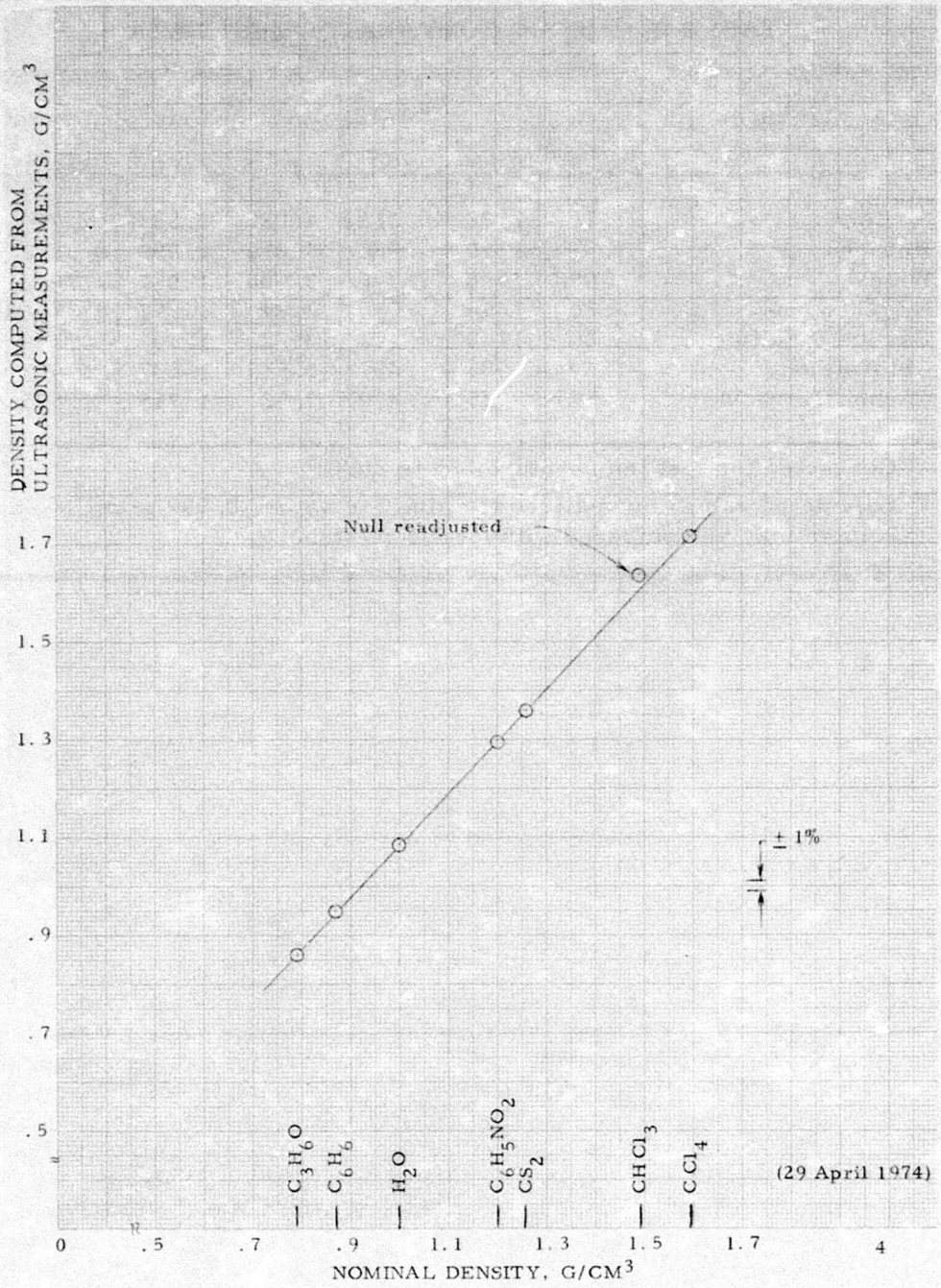

Figure D-7. Densitometer Calibration Tests.

APPENDIX E
ANALYSIS OF THERMAL EFFECTS

ACOUSTIC PROPERTIES OF FUELS - TRANSMISSION, REFRACTION

The sound speed and density of several fuels are given in Ref. 1, Figs. 1, 10 and 22. The attenuation coefficient may be estimated from data in Ref. 11 cited in Ref. 1. The temperature-dependence of these parameters may be computed or estimated from the data cited. From this data it will be evident that ρ, c and ρc of aviation fuels exhibit much larger temperature-dependences than elastic solids. Therefore, the reflection, refraction and transmission across such solid/liquid interfaces will exhibit temperature-dependences dominated by the changes in the acoustic properties of the fuel.

The application of the reflection coefficient to measuring fuel ρc has been dealt with in Appendix C. Let us deal here with transmission and refraction phenomena. The energy transmission coefficient T for plane waves at normal incidence, for propagation from medium 1 to 2, or from 2 to 1, is given by

$$T = 4 Z_1 Z_2 / (Z_1 + Z_2)^2 \qquad \text{(E-1)}$$

or

$$T = (4 Z_1/Z_2)/(Z_1/Z_2 + 1)^2 \qquad \text{(E-2)}$$

where the Z's are characteristic acoustic impedances: $Z_1 = \rho_1 c_1$, $Z_2 = \rho_2 c_2$. Equivalently, the magnitude of the transmission loss is expressed in decibel notation as

$$\text{dB loss} = 10 \log_{10} (1/T) \qquad \text{(E-3)}$$

T is determined by the impedance ratio Z_1/Z_2, as in (E-2). The ρc nomogram introduced in 1965 by one of the authors can be used in conjunction with a second graph of loss vs. Z_1/Z_2 to aid in visualizing or estimating mismatch losses. This is shown in the two graphs comprising Figs. E-1 and E-2. In the log-log ρc nomogram, Fig. E-1, note that lines of constant Z are drawn with slopes of -1, and further, that the ratio of two impedances is proportional to the linear distance between said impedance values, measured along the 45° impedance axis, which is the line of slope equal to +1. Accordingly, the mismatch from, say, steel to water, is determined by the ratio of impedance values between the

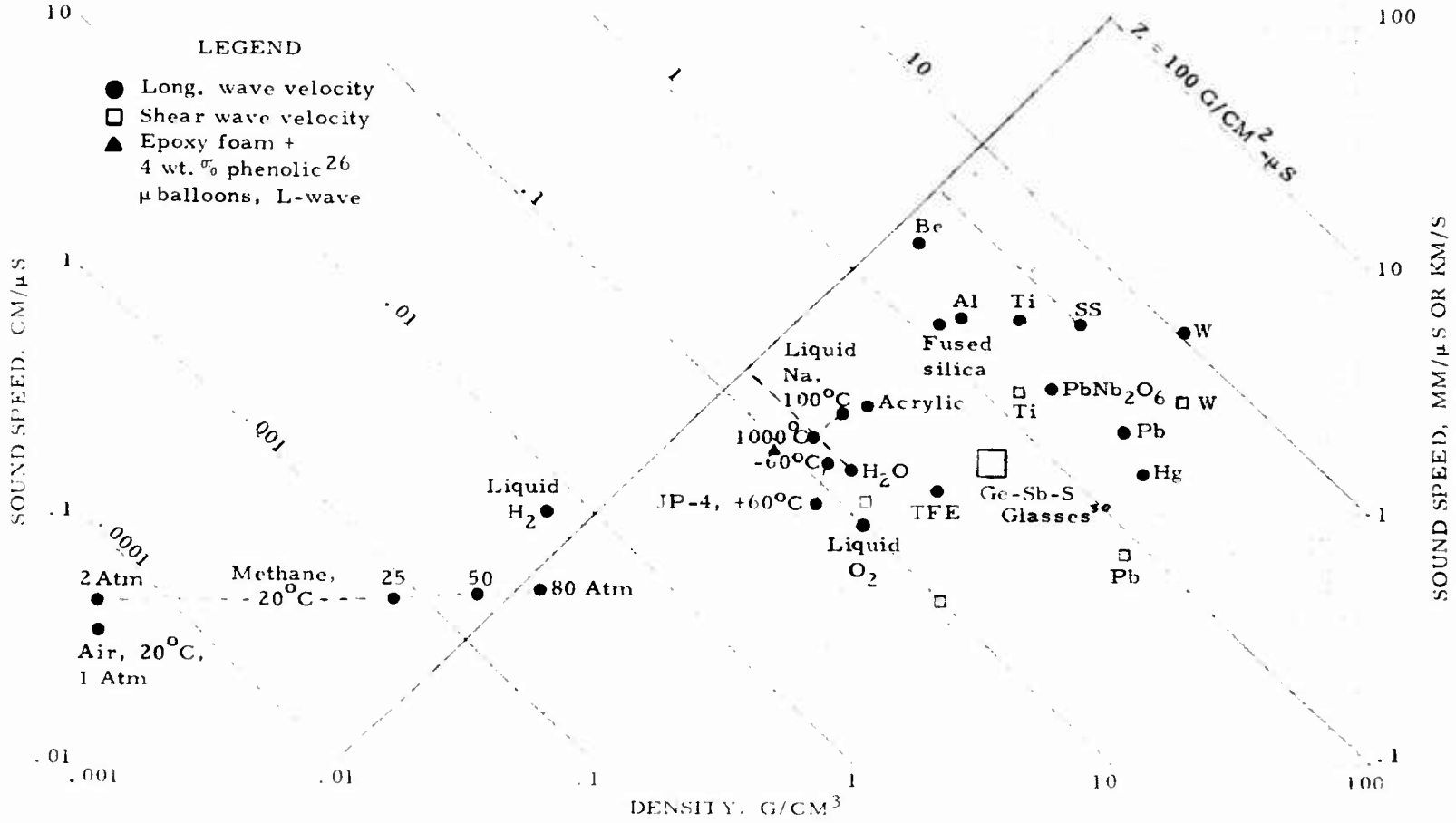

Figure E-1. Impedance Nomogram.

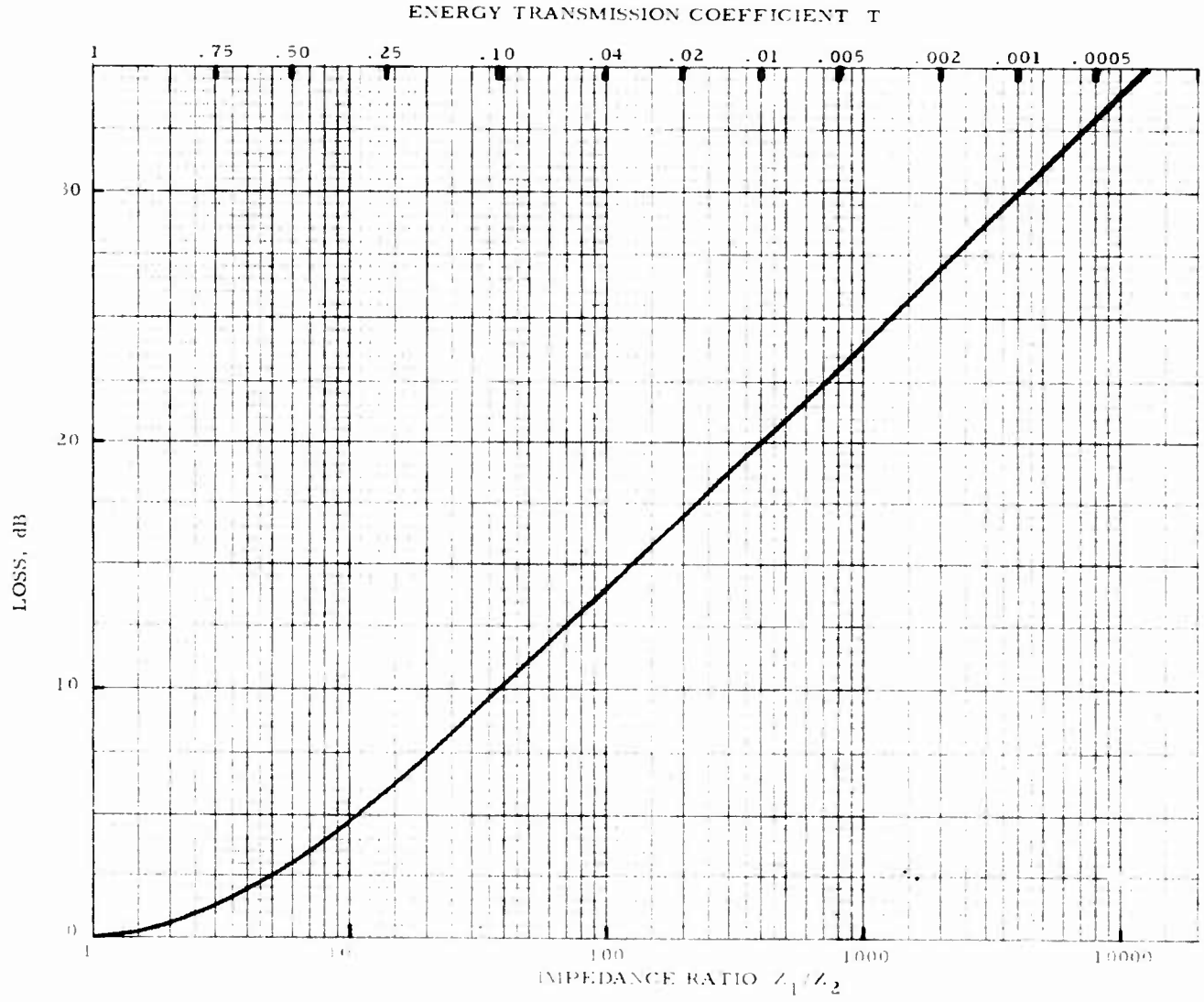

Figure E-2. Loss and Energy Transmission Coefficient Versus Impedance Ratio.

intersections of the 45° impedance axis and the two dashed iso-Z lines passing through stainless steel (SS) and water, namely, $Z_1/Z_2 \approx 4.5/0.15 = 30$. The transmission loss, Fig. E-2, is 9 dB. Over the temperature range and fuel types of interest in this contract, fuel impedance Z_2 ranges from approximately 0.05 to 0.15 g/cm^2-μs. The corresponding losses can be readily estimated for various Z_1's. Values in the loss vs. mismatch graph will be seen to correspond to the calculated values contained in Table E-1.

TABLE E-1. ENERGY TRANSMISSION COEFFICIENT T AND TRANSMISSION LOSS CALCULATED FOR PLANE WAVES AT NORMAL INCIDENCE FOR VARIOUS IMPEDANCE RATIOS

$\frac{Z_1}{Z_2}$	T	Loss dB
1	1	0
2	.89	.51
3	.75	1.25
6	.49	3.10
10	.33	4.81
14	.25	6.04
30	.12	9.04
38	.10	10.00
100	.039	14.07
200	.020	17.03
300	.013	18.78
400	.010	20.02
500	.0080	20.99
1000	.0040	23.99
2000	.0020	26.99
4000	.0010	30.00

Another way of depicting the relationship between T, Z_1 and Z_2 was given recently by Golis (1974).[33]

A useful approximation, valid to the extent that $Z_2 << Z_1$, expresses T as follows:

$$T \approx 4\, Z_2/Z_1 \qquad \text{(E-4)}$$

It can be shown that for normal incidence the sound pressure transmission coefficient expressing the ratio of pressure received at a perfectly terminated (matched backing) transducer of acoustic impedance Z_1, compared to that transmitted from an identical transducer, is also approximated by $4\ Z_2/Z_1$, if attenuation and beam spread are either negligible or compensated for. In this simplified case, the fuel characteristic impedance is directly proportional to the received amplitude, or received voltage A:

$$\rho_2 c_2 = KA\ Z_1 \tag{E-5}$$

where K is a constant that includes the transducer activity and sensitivity. This equation can be shown to apply also to transmission between appropriate buffer rods of impedance Z_1. Thus, we have a transmission coefficient impediometer or ρc densitometer.

In passing, it is interesting to note that for fluids where $Z_2 << Z_1$, if one utilized a parallel branch stilling chamber, as in Fig. 11, p. 41, in which ρc is determined by Eq. (E-5), and provided that attenuation in the fluid is either negligible or compensated for, a more sensitive transmission coefficient measurement of fuel ρc would be obtained than if the reflection coefficient method of Appendix C were attempted. Further, for gaseous fuels, by measuring c both in the freestream as well as in the parallel branch, the average freestream gas temperature T_f would be obtainable from the square of the sound speed ratio and the measured or thermostatically controlled branch temperature T_b:

$$T_f = T_b\ (c_f/c_b)^2 \tag{E-6}$$

The freestream gas impedance $(\rho c)_f$ is then given by

$$(\rho c)_f = (\rho c)_b \sqrt{T_b/T_f} = KA\ Z_1\ c_b/c_f \tag{E-7}$$

Furthermore, the mass flow rate in the freestream can be determined as the product of freestream gas impedance and Mach number:

$$\dot{M}_f = (\rho c)_f\ (v/c)_f = KA\ Z_1\ c_b\ v/c_f^2 \tag{E-8}$$

Finally, at least for a limited range of gas compositions, either the gas average molecular weight $\overline{M}$, or the $\overline{M}/\overline{\gamma}$ ratio, could be determined from

the measured c_b and temperature T_b:

$$\overline{M} = \overline{\gamma} R_o T_b / c_b^2 \quad \text{or} \quad \overline{M}/\overline{\gamma} = R_o T_b / c_b^2 \qquad \text{(E-9)}$$

where $\overline{\gamma}$ = average ratio of specific heats and R_o is the universal gas constant. From these $\overline{M}$ or $\overline{M}/\overline{\gamma}$ values, the energy content of the gaseous fuel could be computed in Btu/lb. Consequently, the rate of energy transfer in Btu/s could be metered for diagnostic or control purposes.

Refraction phenomena are of interest in this contract for two reasons. First, a flush-mounted wedge comprises one potential approach to avoiding the generation of eddies in the v measuring region of the flow cell. Second, dating back to the inception of the previous program, the possibility of measuring flow with clamp-on or externally-mounted transducers has been recognized as desirable, if it could be accomplished without sacrificing performance.

At oblique incidence, the solid/liquid transmission and mode conversion effects are more complex than at normal incidence. Having dealt with these energy partition and mode conversion problems in a recent NASA report, let us limit the present discussion simply to phenomena that are readily quantified using Snell's Law:

$$c_1 / \sin \theta_1 = c_2 / \sin \theta_2 \qquad \text{(E-10)}$$

where θ_1 = angle of incidence (in the solid), and θ_2 = refracted angle (in the fuel). The change in θ_2 caused by temperature-dependent or composition-dependent changes in c_2 are readily understood from a graph such as Fig. E-3, plotted for $\theta_1 = 45^\circ$ and for one value of c_1, namely, $c_1 = 1500$ m/s. (This is approximately the value of the shear wave velocity in ATJ graphite.)

A generally more useful graph of Snell's Law is given in Fig. E-4 for three representative values of θ_1, namely, 30°, 45°, 60°. (The interested reader will find a linearized version of this graph in Golis (1974), where the sinusoidal "distortion" of θ_1 and θ_2 axes enables the velocity ratio parameters to be plotted as straight lines.)

Of the several consequences of changing refracted angles, two of the most obvious and most important are: (1) the axially-projected path changes, and (2) the beam could miss the receiver entirely. Referring to Fig. E-5,

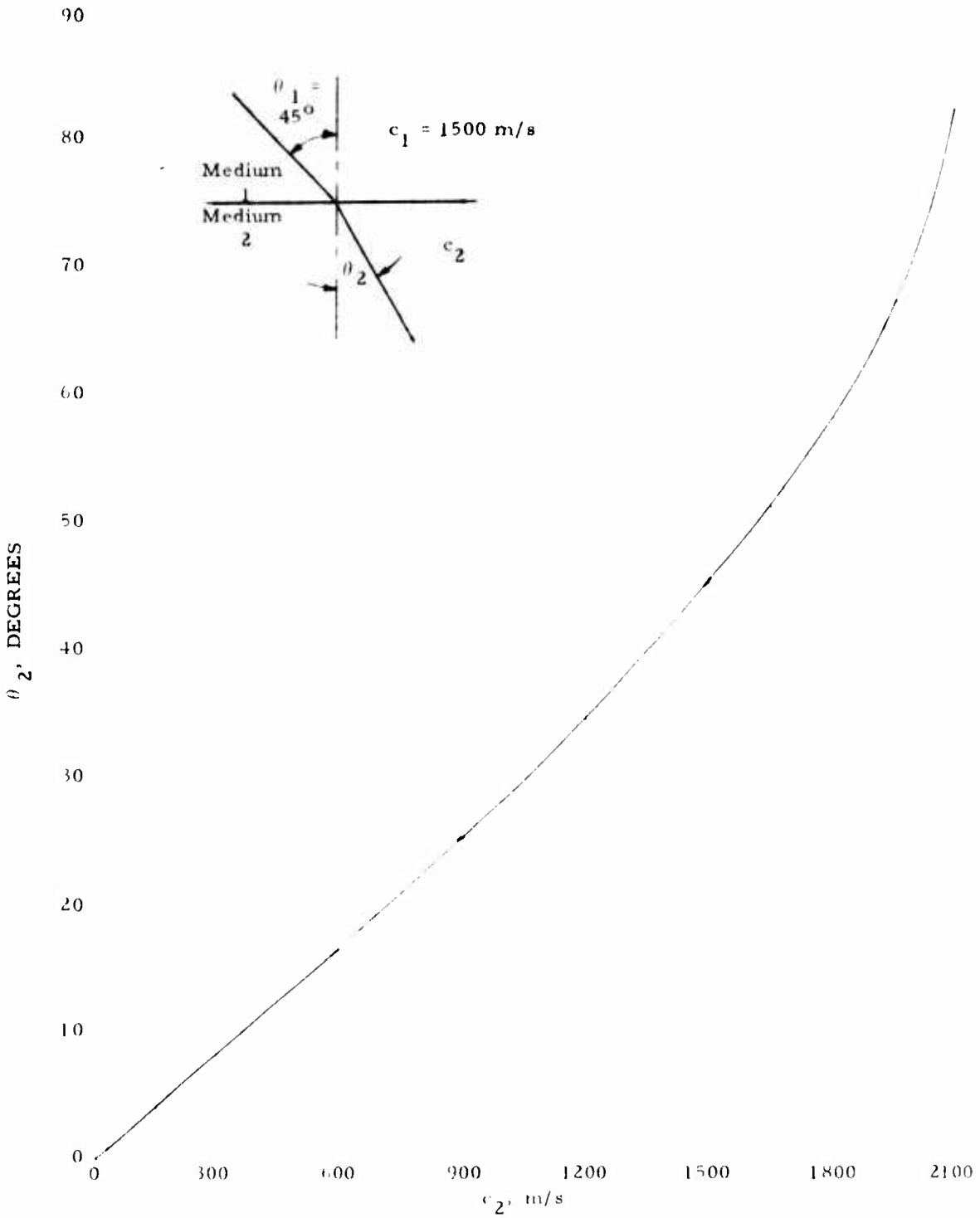

Figure E-3. Refraction Graph for $\theta_1 = 45^\circ$, $c_1 = 1500$ m/s.

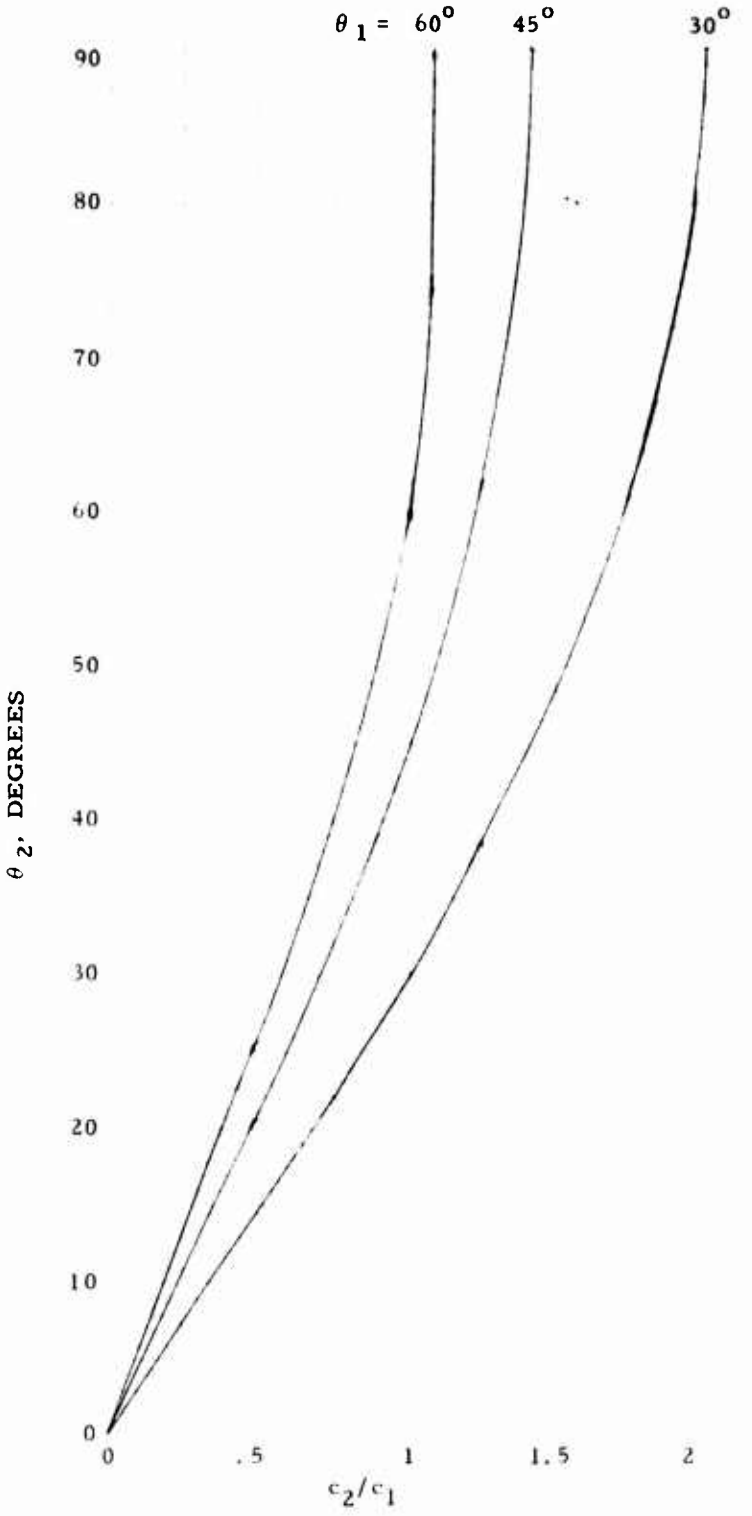

Figure E-4. Refraction Graph for θ_1 = 30, 45, 60° Versus c_2/c_1.

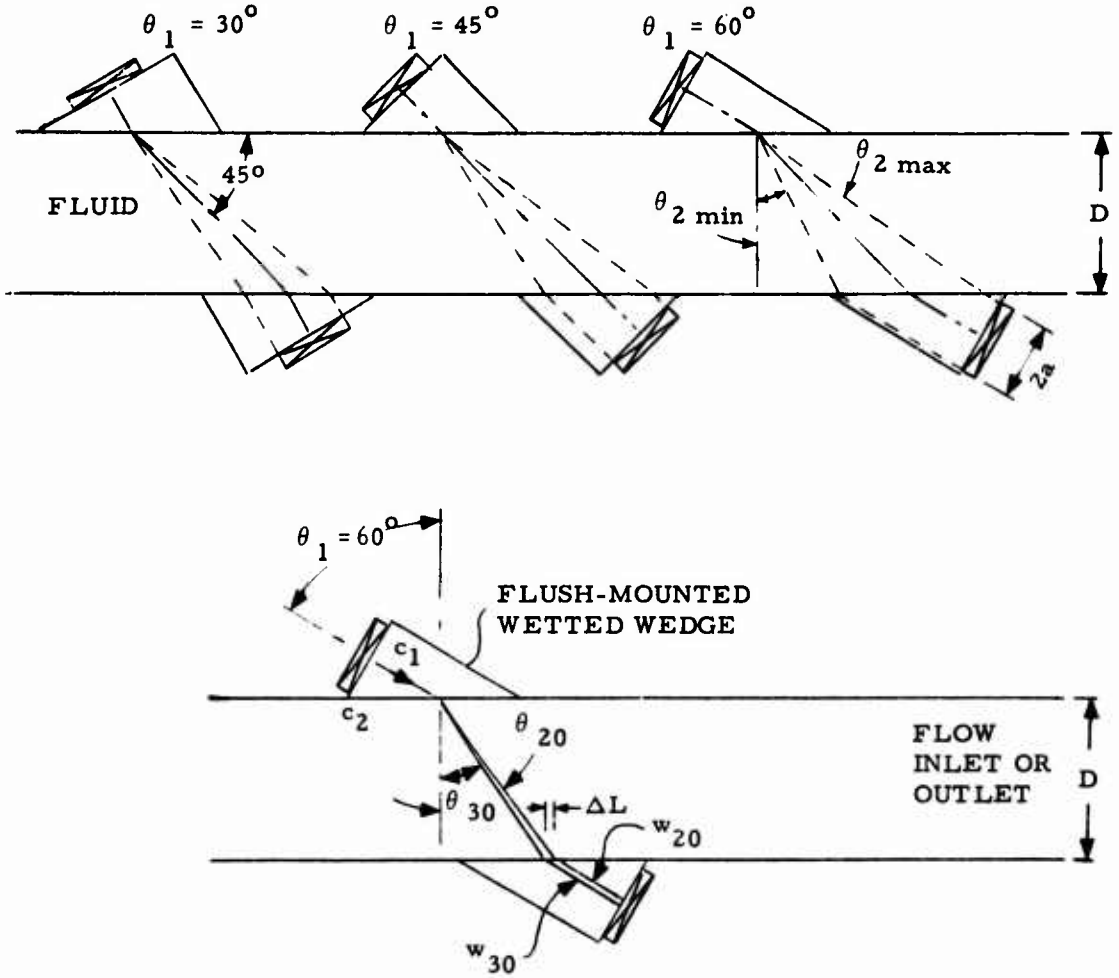

Figure E-5. Wedges Beveled for θ_1 = 30, 45, 60°. Top, Wedges Positioned for Communication Over Path at 45° to Flow Axis. Bottom, Refraction Changes for c_1 = 1500 m/s, c_2 = 980 and 1020 m/s at 30°C and 20°C, Respectively. Transducer Diameter = 2a.

the axial pathlength L is given in terms of the pipe or duct inside dimension D as

$$L = D \tan \theta_2 \qquad \text{(E-11)}$$

Note that in Fig. E-5, the centers of the wetted surfaces of the wedges are along a 45° angle to the pipe axis. However, the transducers themselves of diameter 2a may be at different angles. Under the constraint that the receiver transducer wedge intercepts at least half the beam, and under the assumptions that the beam does not spread at all, the limits on θ_2 were computed in terms of D/a for three orientations of transducers ($\theta_1 = 30^\circ, 45^\circ, 60^\circ$). By trigonometrically analyzing Fig. E-5, the limits on θ_2 are readily shown to be

$$\left.\begin{aligned} \text{limiting } \theta_2 &= 1 \pm 2\,a/\sqrt{3}\,D \quad \text{for } \theta_1 = 30^\circ \\ \text{limiting } \theta_2 &= 1 \pm a\sqrt{2}/D \quad \text{for } \theta_1 = 45^\circ \\ \text{limiting } \theta_2 &= 1 \pm 2\,a/D \quad \text{for } \theta_1 = 60^\circ \end{aligned}\right\} \qquad \text{(E-12)}$$

The calculated values in Table E-2 show that for small D/a, more latitude in θ_2 can be tolerated. The influence of θ_1 is more pronounced for small D/a. See also Fig. E-6. By combining this information with the Snell's Law graph, Fig. E-4, the required D/a can be determined in terms of the range of c_2/c_1 to be accommodated. However, data reduction must take into account the effective L - see Eq. (E-11). Except for the unique wedge/fuel case where the fractional change in c_1 per $^\circ C$ is identically equal to the fractional change in c_2 per $^\circ C$, L would change with temperature, and in any event, would change with composition, requiring compensation. For this reason, the screen is preferred over the wedge.

Referring again to Fig. E-5, the bottom part of this illustration shows explicitly the change in path due to a change in c_2. For purposes of illustration let us analyze the case where $\theta_1 = 60^\circ$; c_1 = constant = 1500 m/s; D = constant = 1 in. = 2.54 cm; and c_2 = 1000 m/s at $25^\circ C$, with a temperature coefficient of -4 m/s per $^\circ C$. The refracted angles are, therefore, θ_2 ($20^\circ C$) = 36.08°, θ_2 ($30^\circ C$) = 34.46°. The axial paths are computed by (E-11) to be: L ($20^\circ C$) = 0.729 in.; L ($30^\circ C$) = 0.686 in. The temperature-dependence of L over this range is $\Delta L/\Delta T$ = -0.43% per $^\circ C$, where ΔL = 0.043 in. = 1.1 mm corresponds to the $10^\circ C$ temperature difference.

TABLE E-2. MINIMUM AND MAXIMUM BOUNDS ON REFRACTED ANGLE θ_2, FOR NONSPREADING BEAM, SUBJECT TO CONSTRAINT THAT AT LEAST HALF THE BEAM IS INTERCEPTED, AS A FUNCTION OF D/a AND θ_1 = 30, 45 AND 60°.

$\frac{D}{a}$	$\theta_1 = 30^\circ$		$\theta_1 = 45^\circ$		$\theta_1 = 60^\circ$	
	$\theta_{2\ min}$	$\theta_{2\ max}$	$\theta_{2\ min}$	$\theta_{2\ max}$	$\theta_{2\ min}$	$\theta_{2\ max}$
1	-	65.1	-	67.5	-	71.6
2	22.9	57.6	16.3	59.6	0	63.4
3	31.6	54.2	27.9	55.8	18.4	59.0
4	35.4	52.2	32.9	53.5	26.6	56.3
5	37.6	50.9	35.7	52.1	31.0	54.5
6	38.9	50.0	37.4	51.0	33.7	53.1
7	39.9	49.4	38.6	50.2	35.5	52.1
8	40.6	48.9	39.5	49.6	36.9	51.3
9	41.1	48.5	40.1	49.2	37.9	50.7
10	41.5	48.1	40.7	48.8	38.7	50.2

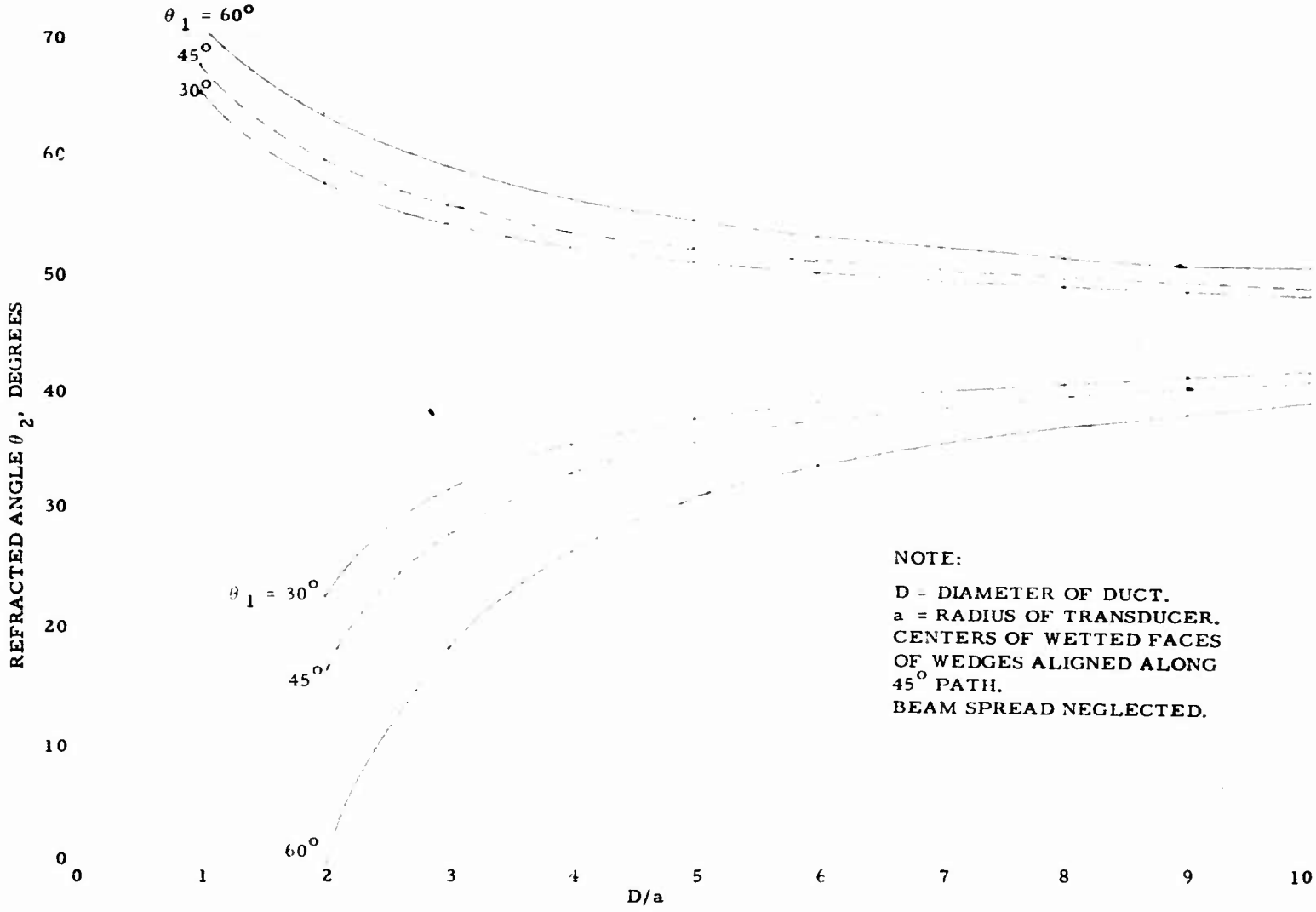

Figure E-6. Angular Bounds on Refracted θ_2, to Assure Reception of At Least Half the Beam, As a Function of D/a and θ_1. Notation: See Fig. E-5, Top.

A second consequence of refraction-induced path changes is that the pathlength in the wedges changes, too. Let us trace the central ray from the upper (transmitter) wedge to the lower (receiver) wedge. Denoting the wedge paths w_{20} = w (20°C) and w_{30} = w (30°C), it can be shown that the difference in wedge paths is $w_{30}-w_{20} = \sqrt{3}\ \Delta L/2 = 0.866\ \Delta L$, or $0.866\ \delta L$ for a 1°C change, where $\delta L \equiv 0.1\ \Delta L$.

If not compensated, the above refraction-induced changes in fluid pathlength and wedge pathlength would lead to errors in v, c, c^2, v/c and v/c^2 approximately as follows for an assumed 1°C temperature increase from, say, 25°C to 26°C.

Error in v: The phase difference $\Delta\phi$ decreases by 0.43%.

Error in c: The fluid path decreases from $\sqrt{D^2 + (L + \delta L)^2}$ to $\sqrt{D^2 + L^2}$. Numerically, the fluid path decrement, $L \cdot \delta L$, is approximately 0.0025 in. The wedge path increment is 0.0037 in. If we calculate the corresponding change in transit time $\Delta t = t_{25}-t_{26}$ = (wedge path increment)/c_1 - (fluid path decrement)/c_2, the result is $\Delta t < 1$ ns, which is a negligible fraction of the total transit time. Therefore, in the present example the errors in v, v/c and v/c^2 are dominated by the change in fluid axial path L. Percentage errors for the three terms are substantially identical, about 0.4% per °C.

To avoid thermal refraction errors associated with flush-mounted wetted wedges (which errors would obviously be unacceptable for temperature excursions much larger than 1°C) one would generally need to continuously monitor c_1 and c_2 and then compute v or related terms, taking into account the consequences of the changing c_1 and c_2. Alternatively, one can choose to avoid refraction changes by keeping θ_2 constant by means of an oblique cavity. This was our choice in the present program.

ACOUSTIC SHORT CIRCUIT

As seen from Fig. E-1, c in metals is typically about 4 to 5 times faster than in the fuels of interest. Obviously, there arises the possibility of a metal-borne wave arriving at the receiver before the fuel-borne signal. Even if the metal path were somewhat longer than the fuel path, the travel time in the metal can still be shorter than in the fuel, hence, the term, acoustic short circuit. Less obvious are the consequences of the many vibration modes that can be supported by a structure as complex as a typical flow cell. For example, suppose that a short-duration transmitted pulse is inadvertently coupled to the metal cell or pipe wall. A long pulse train will be generated because the different modes propagate at different

velocities in the metal structure. Thus, the short circuit rings on, interfering with the fuel-borne wave. In the case of an external-mount, reference to Fig. E-1 will show that the transducer-metal pipe-transducer path unfortunately tends to be well matched compared to the transducer-fuel-transducer path.

Still less obvious is the fact that even when the signal to short circuit noise ratio is high enough so that the signal is readily identified and distinguished from the short circuit noise on an oscilloscope (e.g., S/N = 10), the error in measuring flow velocity will generally be unacceptably large and temperature-dependent. We will show below, by means of a simple vector analysis, that a S/N ratio approaching 100:1 is required if short circuit errors are to be suppressed below 1%.

Referring now to the vector (or phasor) diagram, Fig. E-7, we identify a reference vector pointed "east", pairs of flow velocity signal vectors S_u and S_d representing upstream and downstream waves, and noise vectors N. Relative to the phase-measuring system described in the body of this report, full-scale flow corresponds to a phase difference of 180° between S_u and S_d.

Let us assume the S/N ratio = 10. We will consider the potential phase errors caused by collinear vectors N adding vectorially to S_u and S_d at 10% of full-scale flow, and also near full-scale flow.

At 10% of full-scale flow, S_u and S_d are symmetrically rotated $\pm 9^\circ$ from the reference vector. The small circular orbits centered on the S tips represent the allowable contributions of N. It appears reasonable, from a reciprocity argument, that N will be the same for both upstream and downstream paths. For simplicity, at the 10% of full-scale flow, we show the situation where the N vectors both point "north". The resultant wave appearing at the upstream transducer is denoted R_u, and at the downstream transducer, R_d. Intuitively, N seems to cancel. But, unfortunately, calculation of the angles involved shows that while the true angle or phase difference between S_u and S_d is 18.00°, the angle between R_u and R_d is 17.82°, the error being 1%. At lower flow velocities the error diminishes, but does not vanish except at zero flow.

At the higher flow, say, at about 94% of full scale, and with N's taken "westward", a S/N of 10 leads to an error of 7%. A S/N ratio of 100 diminishes this error source to 0.6%.

At a given moment, the angular relationship between the S's and the N's will depend on v and the sound speeds in the liquid and solid media. But these speeds depend on temperature and composition. Clearly, a rather

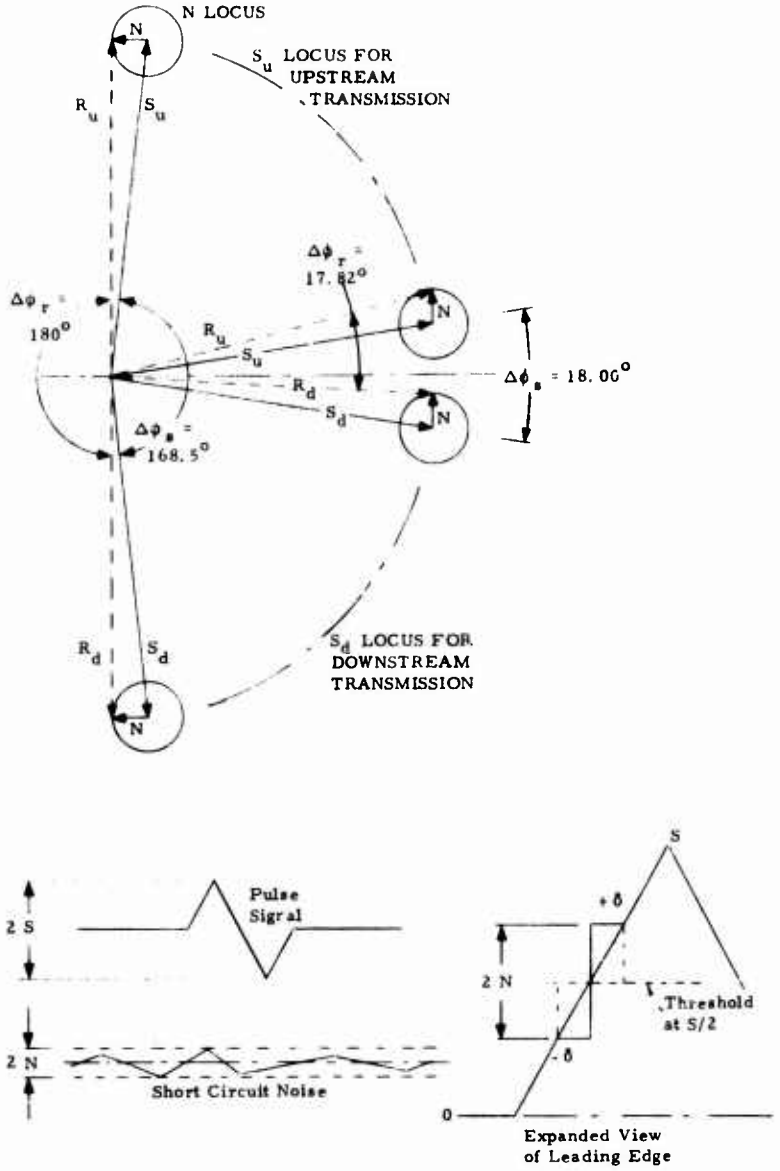

Figure E-7. Vector Diagram Showing Errors Due to Acoustic Short Circuit Noise N Adding Vectorially to Flow Velocity Signals S_u and S_d. For S/N = 10, Vectors are Drawn for Flow Velocities of 10% and About 94% of Full-Scale Flow. The Magnitude of the Resultant Percentage Error is $(|\Delta\phi_s - \Delta\phi_r|/\Delta\phi_s)(100\%)$. Three Triangular Waveforms at Bottom Show Notation for Analysis of Pulse Signals in the Presence of Interfering Acoustic Short Circuit Noise. See also: NASA CR-112313 (R), Ref. 15, pp. C-1 to C-6.

high S/N ratio is required, preferably 100:1 or higher, to assure accuracy of 1% or better over a wide range of conditions.

At the present time, ultrasonic flowmeters are also available from other manufacturers, wherein pulse techniques are used, rather than continuous waves. For the reader who may question whether the foregoing vector or phasor argument applies to the case where short circuit interferes with measuring arrival times of pulses transmitted across the fluid, we offer the following brief analysis.

Let us assume that "arrival time" is taken to be the midpoint of the leading edge. This means that attenuation effects are being eliminated by using methods such as automatic gain control, with fixed threshold, or by using a variable threshold which is continually reset to 50% of the peak received pulse amplitude, or by other means.

The received pulse waveform may have various shapes such as exponentially enveloped sine wave burst, video triplett, etc. For simplicity we treat the case of a triangular pulse. This makes it easier to explain the interfering effect of noise N upon the desired signal S.

Referring to the lower drawings in Fig. E-7, we see that corresponding to a triangular pulse of period T, amplitude S and noise of amplitude N, the threshold, set at S/2, will be reached too early, or too late, by the interval δ, where δ is the timing error. Algebraically, $\delta = \pm (T/4)/(S/N) = \pm t_r/(0.8\ S/N)$, where t_r = rise time of pulse. The maximum error in determining time differences upstream minus downstream is 2δ. In general, timing errors will vary between zero and 2δ, depending principally on the period, geometry, S/N, the materials used for the conduit and fluid, their temperature coefficients of sound speed, and the temperature range. Numerically, for T = 1 μs, δ = 25 ns if S/N = 10, and δ = 2.5 ns if S/N = 100. For T = 0.1 μs, δ's would be proportionately reduced to 2.5 ns and 0.25 ns for S/N's of 10 and 100, respectively.

It is sometimes argued that the short circuit N is a constant and therefore can be accounted for by calibration of the device. This view would appear to be supported by the definitions of repeatability and reproducibility. According to Ref. 31, these terms express the closeness of agreement among repeated measurements, approaching from the same or opposite directions, respectively, but under the same operating conditions.

But in actual practice, minor changes in temperature, composition, or dampening on the conduit interior or exterior (e.g., bubbles, scale, deposits) will influence N and/or S. Therefore, departures from calibrated performance will be observed, unless both the time (or phase)

and amplitude relationship of N and S remains constant, or unless S/N is so large that variations in S/N are negligibly small.

CELL DIMENSIONS AND INTEGRITY

Cell dimensions x increase as temperature increases by the amount ΔT according to the well-known relation

$$x = x_o (1 + \alpha \Delta T) \qquad \text{(E-13)}$$

where α is the coefficient of thermal expansion. See Fig. E-8, especially curve 2. For AISI type 304 stainless steel, $\alpha = 10.4 \times 10^{-6}$ per $^{o}F = 18.7 \times 10^{-6}$ per ^{o}C. For operation from $-65^{o}F$ to $+160^{o}F$ ($-54^{o}C$ to $+71^{o}C$) the $\alpha\Delta T$ term amounts to $(10.4 \times 10^{-6})(160 + 65) = 2.34 \times 10^{-3}$. From mid-temperature, $47.5^{o}F$, dimensions will therefore change by no more than $\pm$ 1.17 mils per inch. The flow channel area, nominally 1.000 in. x 0.500 in. = 0.500 sq in., therefore changes maximally by $\pm$ [1.0017 x .5005-.500] or $\pm$ 1.35×10^{-3} sq in. This is a fractional change of $\pm$ 0.27%.

The distance between velocimeter transducers is nominally 3 in. This distance changes by $\pm 3 \times 1.17 = \pm 3.51$ mils, or about 0.1%. The effective axial pathlength L, nominally 1 in., changes by $\pm$ 1.17 mils, or again about 0.1%.

From Eqs. (11) and (12) on page 26, one sees that the v/c formulation suppresses the effect of changing cell dimensions. But, even in the case where v is measured (to be multiplied by ρ), the dimensional changes are all well below 1%. If required, a simple temperature measurement could be used to generate the small correction term to reduce such thermal effects well below 0.1%.

Regarding cell integrity, different models of our flow cells made of AISI 304 have been subjected to temperature from cryogenic levels, $-200^{o}C$, up to $+300^{o}C$, at pressures up to several hundred psi, for periods ranging from hours to months. No structural failures have occurred. The particular flow cell most used in this program, Fig. 1, includes several welded joints, and soldered joints between the flow channel walls and the screens. The solder alloy composition was 97 Sn, 3 Ag, fluxed with a mixture of zinc and ammonium chlorides. The joint is reported to comply with Mil Standard 454B. During soldering the screens were held in position using opposed alumina wedges. Similar solder joints have been exposed to liquid nitrogen and boiling water thermal shocks with no ill effects.

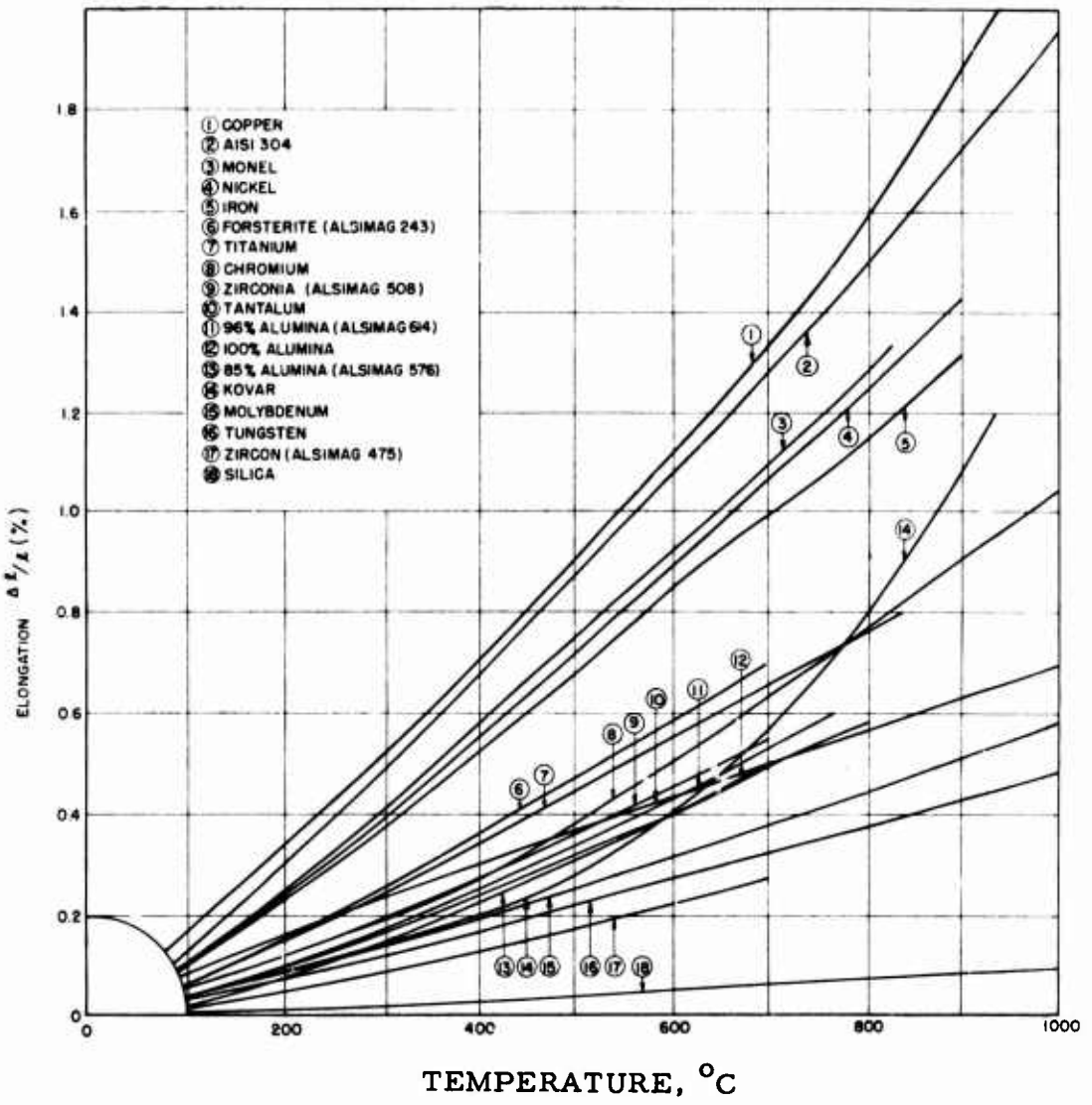

Figure E-8. Expansion Characteristics of Metals, Alloys and Ceramics. From "Materials and Techniques for Electron Tubes", by Walter H. Kohl, © 1959 by Litton Educational Pub., Inc. Reprinted by Permission of Van Nostrand Reinhold Company.

The last temperature-dependent effect to be analyzed in detail in this appendix concerns the theoretical transmission coefficient from the X-cut crystal to the SiO_2 buffer rod, across the thin epoxy bond layer. The basis for this analysis is contained in texts such as Kinsler and Fry (1962) and a similar analysis recently has been reported by Canella (1974) for liquid coupling layers.[34, 35]

The epoxy used in this analysis, Tra-Con's Type 2115, was cast into a block of approximate dimensions 1 in. x 1 in. x 3/8 in. Sound speed was measured at room temperature, liquid nitrogen temperature, and at boiling water temperature. For comparison purposes, calculations were also carried out for a common plastic, acrylic. The acrylic sound speed data of Arnold and Guenther (1966) covering 30°C to 100°C were supplemented by our measurements at 25°C and -200°C. Specimen thicknesses were measured at the temperature extremes, but the ~1% change in thickness was neglected in computing transmission coefficients, as the expansion effect is dwarfed by the changes in sound speed.

The impedance of X-cut quartz is 1.5 g/cm^2-μs; that of fused silica is 1.3 g/cm^2-μs.

Consider a sandwich model. The outer members have impedances Z_1 and Z_3. The middle layer impedance is Z_2, its thickness is ℓ, and its wave number is k. The energy transmission coefficient at normal incidence is of the form

$$T = \frac{4 Z_1 Z_3}{(Z_1 + Z_3)^2 \cos^2 k\ell + (Z_2 + Z_1 Z_3/Z_2)^2 \sin^2 k\ell} \qquad \text{(E-14)}$$

The analysis of the temperature-dependence of T at 10 MHz proceeds in two steps. First, we calculate $k\ell$ as a function of temperature: $k\ell = 2\pi 10^7 \ell/c$. Second, we calculate T, and the corresponding loss in dB, as a function of $k\ell$. Results are listed in Tables E-3 and E-4, and are plotted in Figs. E-9 and E-10. Also, from Fig. E-1, $Z_{acrylic} \approx 0.3$ g/cm^2-μs. We will use this value for Z_{epoxy}, too.

We proceed to analyze thermal effects in the bond layer as follows. To estimate ℓ, we note that the crystal and the rod ends are fine ground to an rms (root mean square)surface finish between about 8 and 16μ in. They are epoxied together under pressure, so the average bond thickness probably does not exceed twice the roughness. Therefore, ℓ is almost certainly less than 40μ in., or 1 μm. (We will neglect the thermal expansion of ℓ.) Next, from Fig. E-9, the ordinates of the bottom dashed curve,

TABLE E-3. PARAMETER $k\ell$ AT 10 MHz AS A FUNCTION OF TEMPERATURE AND THICKNESS OF ACRYLIC AND EPOXY

Material	Temp. °C	c m/s	$k\ell$ at ℓ = 1 μm (0.04 mil)	$k\ell$ at 3 μm (0.1 mil)	$k\ell$ at 10 μm (0.4 mil)
Acrylic	-200	2900	.0217	.0650	.217
"	+30	2700	.0233	.0698	.233
"	+100	2470	.0254	.0763	.254
Epoxy	-200	2890	.0217	.0652	.217
"	+25	2422	.0259	.0778	.259
"	+100	1614	.0389	.1168	.389

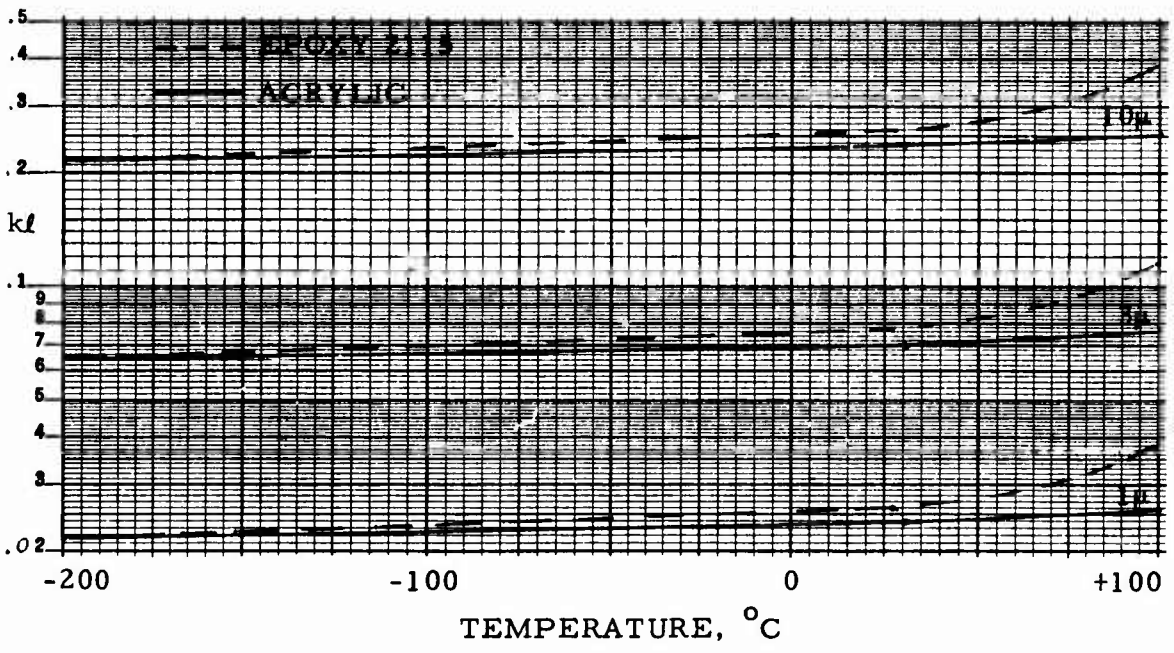

Figure E-9. Graph of Parameter $k\ell$ at 10 MHz as a Function of Temperature and Thickness of Acrylic and Epoxy.

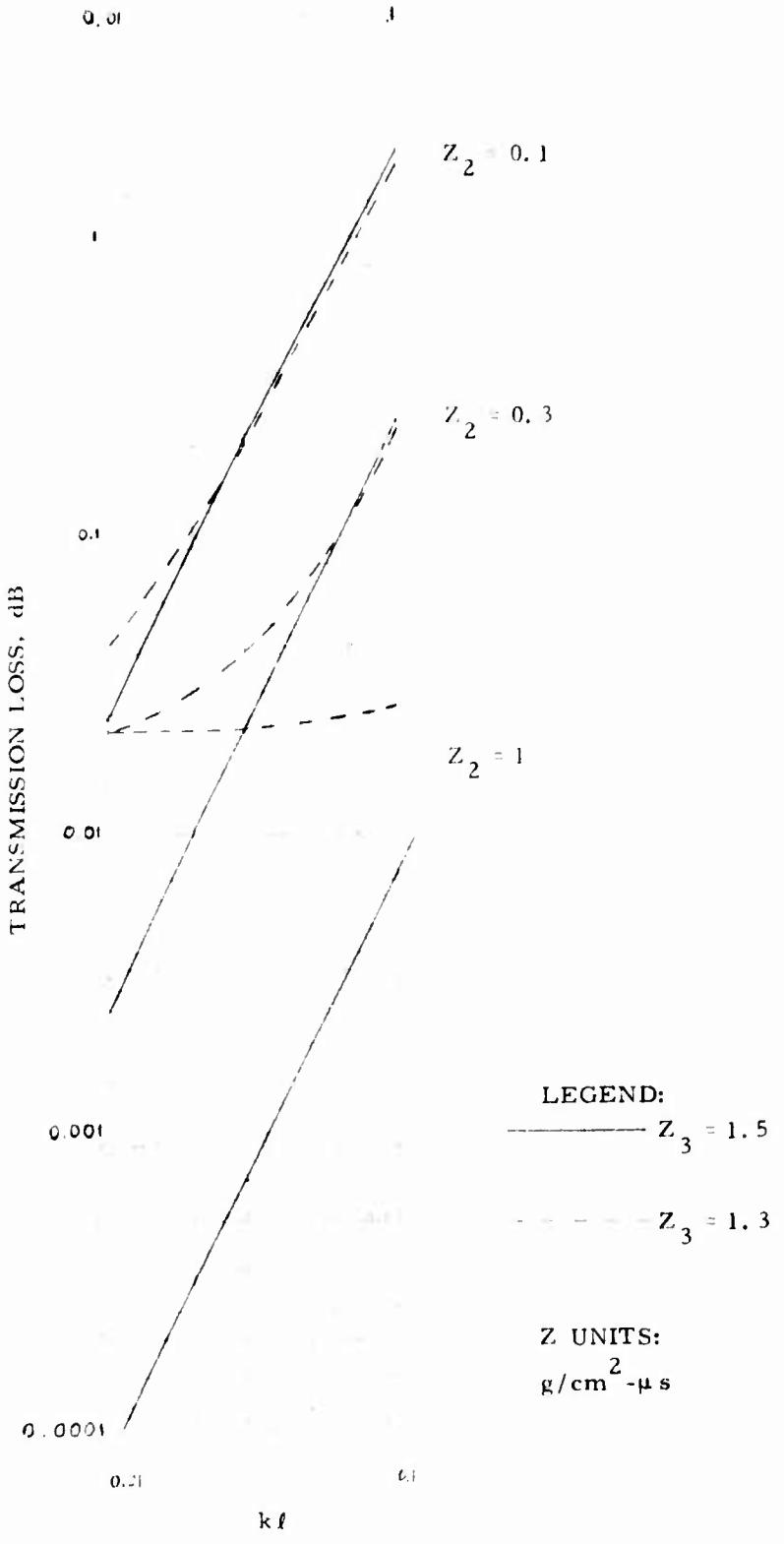

Figure E-10. Graph of Transmission Loss Versus kℓ .

TABLE E-4. ENERGY TRANSMISSION COEFFICIENT AND TRANSMISSION LOSS FOR SANDWICH MODEL OF TRANSDUCER BONDED TO ROD

Z_1	Z_3	Z_2 (grams/cm^2-microsecond)	$k\ell$ (radians)	T (energy ratio)	Loss (dB)
1.5	1.5	0.1	0.01	0.99446	0.02413
			0.03	0.95223	0.21258
			0.10	0.64282	1.91911
		0.3	0.01	0.99942	0.00252
			0.03	0.99484	0.02247
			0.10	0.94571	0.24242
		1.0	0.01	0.99998	0.00009
			0.03	0.99984	0.00069
			0.10	0.99827	0.00752
	1.3	0.1	0.01	0.99015	0.04299
			0.03	0.95371	0.20584
			0.10	0.67295	1.72017
		0.3	0.01	0.99441	0.02435
			0.03	0.99053	0.04132
			0.10	0.94859	0.22922
		1.0	0.01	0.99489	0.02225
			0.03	0.99480	0.02264
			0.10	0.99381	0.02697

from -54 to +71°C, increase from $k\ell$ = 0.028 to 0.030. Now, using Fig. E-10, the corresponding increase in transmission loss is found to be 0.004 dB for the solid middle line (X-cut quartz rod) and 0.003 dB for the dashed middle curve (fused silica rod). These computed temperature-induced increases are negligibly small, corresponding to echo amplitude changes of 0.04 and 0.03%, respectively, for temperature excursions from -54 to +71°C.

Observed thermal effects on the ρc probe in air are on the order of 0.1% per °C. We, therefore, conclude that, to the extent that the above model

is valid, the observed temperature-dependence of echo amplitude changes in the present ρc probes, is not attributable to changes in kl or sound speed in the bond layers. Mechanisms not included in the above model, such as stress or strain, possibly contribute to the observed thermal effects. Independent of the cause, if the effects are reproducible, compensation based on a temperature measurement of the ρc probe would be straightforward.

VELOCIMETER TRANSDUCERS

The velocimeter transducers are made of a modified lead metaniobate formulation, with a Curie point above 400°C. Diameter is 0.75 in. Resonant frequency is 5 MHz. We have operated such transducers, when epoxied to an ATJ graphite backing member, before, during and after cyclic immersion in liquid nitrogen and boiling water. We have also evaluated the transducer material alone in activity and sensitivity tests up to 320°C. One of the high-temperature test fixtures is shown in the photograph of Fig. E-11. Operation generally has been reliable despite these thermal dwell, cycling and shock exposures. Therefore, the velocimeter transducer assemblies are considered more than adequate for the present application.

ρc DENSITOMETER PROBE

The ρc densitometer probe consists of a mounted assembly of two cylindrical rods of fused silica, one wetted, one dry. Each rod is epoxied at its chrome-gold-metallized end to an X-cut 10-MHz crystalline quartz transducer. The quartz transducer operates piezoelectrically in its alpha phase up to 573°C. (In some experiments the rods were made of X-cut quartz, oriented transversely the same as the X-cut transducer crystal to minimize differential expansion between fused and crystalline quartz.)

The temperature coefficient relating to the X-cut quartz's frequency stability is -20×10^{-6} per °C. However, the coefficients relating to activity and sensitivity, d_{33} and g_{33}, have not been measured, to our knowledge, for this material. One purpose of the reference echo A in the ρc probe is to compensate for changes in d_{33} and g_{33} that are presumed to occur due to thermal effects or aging.

The effect of temperature on the difference in attenuation in the dry and wetted rods may be computed based on published data of the attenuation coefficient α vs. temperature (Krause et al, 1970).[17] See Fig. E-12. For the temperature range of interest, -54°C to +71°C, α decreases somewhat, as temperature increases, by about 3×10^{-4} dB/cm per °C, at 20

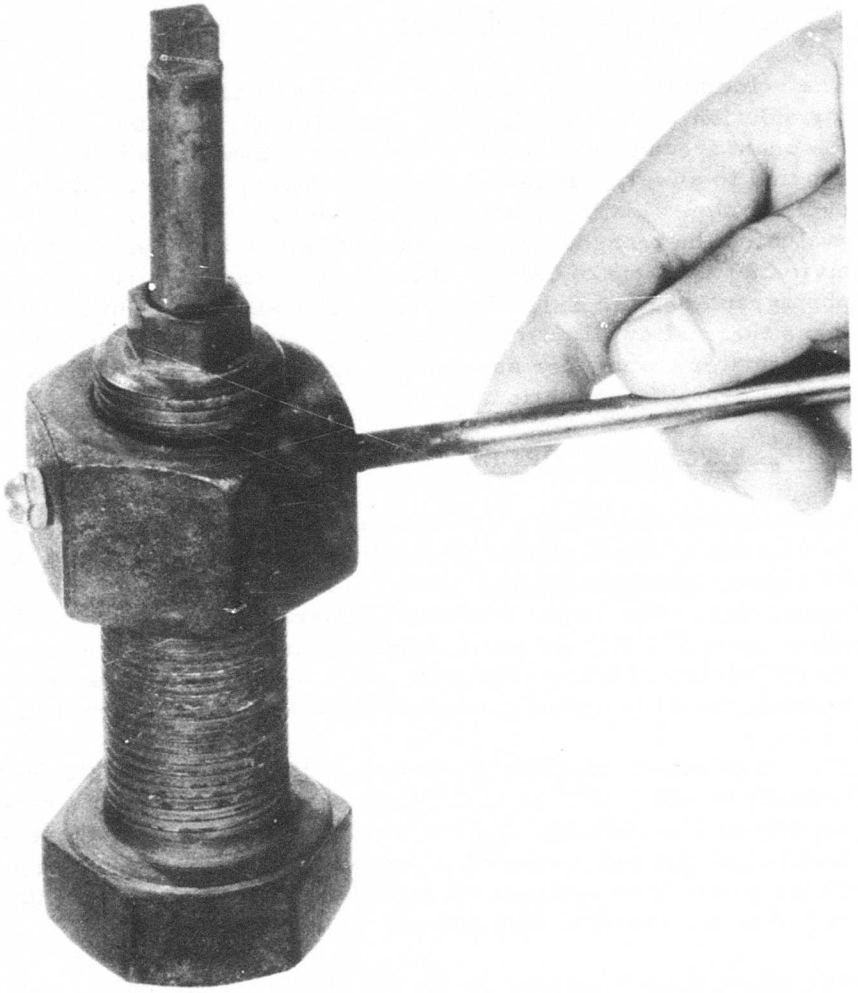

Figure E-11. Fixture for Testing Pressure-Coupled Piezoelectric Transducers at High Temperature, 300°C, and Also at Cryogenic Temperature, -200°C.

MHz. The round trip difference in rod lengths in our ρc probe is typically about 1.2 cm. Thus, for excursions of $\pm$ 62.5°C from the mid-temperature, 8.5°C, the attenuation difference at 20 MHz would not exceed $\pm$ 0.02 dB. At 10 MHz, the frequency used in the ρc probe, attenuation changes would not exceed $\pm$ 0.01 dB, or $\pm$ 0.1%, a negligibly small value. However, in the unlikely event where significant temperature differences exist between the two rods, the attenuation difference would increase somewhat. It is concluded that temperature-dependent attenuation effects in the fused silica rods do not contribute significantly to ρc errors.

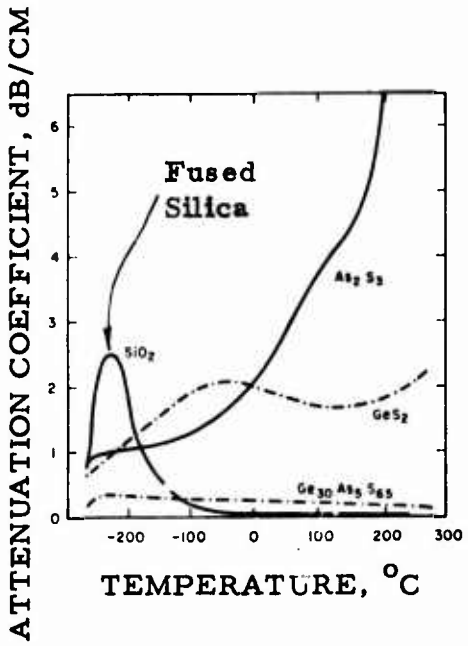

Figure E-12. 20-MHz Longitudinal Acoustic Attenuation Versus Temperature for Some Chalcogenide and Oxide Glasses, After Krause et al.[17]

LIST OF SYMBOLS

A	Echo amplitude
A_N	Zeroth order Fourier coefficient
A_o	DC term in Fourier series
a	Transducer radius
B	Echo amplitude
BCD	Binary coded decimal
c	Sound speed
D	Diameter
D_h	Hydraulic diameter
f	Frequency
H	Height dimension
K	Flow profile meter coefficient
K, L	Echo amplitude adjustment factors
k	Wave number, $2\pi/\lambda$
L	Axial pathlength
ℓ	Thickness
M, M_1, M_2	Measurements of phase shift
$\dot{M}$	Mass flow rate
$\ddot{M}$	$d\dot{M}/dt$ = time rate of change of $\dot{M}$
$\bar{M}$	Average molecular weight
N	Noise amplitude; Term in Fourier series
R	Radius; Reflection coefficient

LIST OF SYMBOLS (cont'd)

Re	Reynolds number
R_o	Universal gas constant
S	Signal; Perimeter
T	Temperature; Period
t	Time
T, T_e	Energy transmission coefficient
T_1, T_2	Time intervals downstream, upstream
V_s	Voltage signal output, Simmonds Precision densitometer
v	Flow velocity
$\bar{v}$	Area-averaged flow velocity
W	Width dimension
x	Cell dimension
Z	Acoustic characteristic impedance
α	Attenuation coefficient; Expansion coefficient
α_N	N-th order Fourier phase angle
α_1, α_2	Phase shifts in fluid
β_1, β_2	Phase shifts in Receivers 1 and 2
γ	Specific heat ratio
δ	Timing error
Δ	Difference
θ	Angle of transmission
λ	Wavelength

LIST OF SYMBOLS (cont'd)

ν	Kinematic viscosity
ρ	Density
τ	Time interval
ϕ_1, ϕ_2	Phase shifts of carrier frequency
Ψ_1, Ψ_2	Phase shifts of the fundamental modulation frequency
ω	Angular frequency